VOLUME 108 NUMBER 3

Astronomy
Astrophysics
JAN 7 1949

THE ASTROPHYSICAL JOURNAL

AN INTERNATIONAL REVIEW OF SPECTROSCOPY AND ASTRONOMICAL PHYSICS

NOVEMBER 1948

ON THE PHYSICAL AND CHEMICAL COMPOSITION OF THE SUN *Geoffrey Keller* 347
THE CONTINUOUS ABSORPTION COEFFICIENT OF THE HELIUM ATOM *Su-Shu Huang* 354
A STELLAR MODEL FOR RED GIANTS OF HIGH CENTRAL TEMPERATURE *Robert S. Richardson and Martin Schwarzschild* 373
IDEALIZED MODELS AND RECTIFIED LIGHT-CURVES FOR ECLIPSING VARIABLES *Henry Norris Russell* 388
SIX-COLOR PHOTOMETRY OF STARS. VI. THE COLORS OF EXTRAGALACTIC NEBULAE *Joel Stebbins and A. E. Whitford* 413
RELATIVE TRANSITION PROBABILITIES OF THE SWAN BANDS OF CARBON *Robert B. King* 429
AN EXTENSION OF THE SWAN SYSTEM OF THE C_2 MOLECULE *John G. Phillips* 434
THE FAR VIOLET REGION IN THE SPECTRA OF THE COOL CARBON STARS *Andrew McKellar* 453
POLYATOMIC MOLECULES IN LATE-TYPE STARS *P. Swings and A. McKellar* 458
THE ABSORPTION-LINE SPECTRA OF THE CENTRAL STARS OF THE PLANETARY NEBULAE *Lawrence H. Aller* 462
THE SPECTRUM OF GAMMA PEGASI. II *Anne B. Underhill* 476
THE BALMER SERIES IN THE SPECTRUM OF HD 45910 *Paul W. Merrill* 481
RADIAL VELOCITIES OF TWO STARS OF THE W URSAE MAJORIS CLASS *Daniel M. Popper* 490
SPECTROGRAPHIC OBSERVATIONS OF THE ECLIPSING BINARIES RZ COMAE, V 502 OPHIUCHI, RV CORVI, AND BF VIRGINIS *O. Struve and L. Gratton* 497
A SPECTROSCOPIC STUDY OF BETA AURIGAE *Burke Smith* 504
A STUDY OF THE ORBIT OF BETA AURIGAE *S. L. Piotrowski* 510
A PHOTORED STUDY OF THE ECLIPSING VARIABLE QY AQUILAE *Balfour S. Whitney* 519
ASSOCIATION OF CORONA WITH PROMINENCE *Walter Orr Roberts* 523
THE SPECTRUM OF COMET 1947n *P. Swings and Thornton Page* 526
NOTES
A NOTE ON THE SPECTRUM OF 27 CANIS MAJORIS *O. Struve and Shu-Koo Kao* 537
A NOTE ON THE SPECTRUM OF HD 698 (J. A. PEARCE'S STAR OF LARGE MASS) *O. Struve and M. Rudkjøbing* 537
ON THE SPECTRUM OF HD 193576 = V 444 CYGNI *Guido Münch* 540
NOTE ON W URSAE MAJORIS STARS *Gerard P. Kuiper* 541
A NEW BRIGHT DOUBLE STAR *Gerard P. Kuiper* 542
REVIEWS 543
INDEX 549

THE UNIVERSITY OF CHICAGO PRESS
CHICAGO, ILLINOIS, U.S.A.

November 1948 Vol. 108, No. 3

THE ASTROPHYSICAL JOURNAL

AN INTERNATIONAL REVIEW OF SPECTROSCOPY AND ASTRONOMICAL PHYSICS

Edited by

W. W. MORGAN
Managing Editor
Yerkes Observatory of the University of Chicago

S. CHANDRASEKHAR

PAUL W. MERRILL
Mount Wilson Observatory of the Carnegie Institution of Washington

HARLOW SHAPLEY
Harvard College Observatory
Cambridge, Massachusetts

N. U. MAYALL
Lick Observatory
University of California

With the Collaboration of the American Astronomical Society

Collaborating Editors:

1946-48
C. S. BEALS
Dominion Astrophysical Observatory, Victoria

LUIS E. ERRO
Astrophysical Observatory, Tonanzintla

O. C. WILSON
Mount Wilson Observatory

1947-49
LYMAN SPITZER, JR.
Princeton University Observatory

A. N. VYSSOTSKY
Leander McCormick Observatory

ALBERT E. WHITFORD
Washburn Observatory

1948-50
CECILIA H. PAYNE-GAPOSCHKIN
Harvard College Observatory

H. N. RUSSELL
Princeton University

ANDREW McKELLAR
Dominion Astrophysical Observatory, Victoria

The Astrophysical Journal is published bimonthly by the University of Chicago at the University of Chicago Press, 5750 Ellis Avenue, Chicago, Illinois, during July, September, November, January, March, and May. ¶The subscription price is $12.00 a year; the price of single copies is $3.00. Orders for service of less than a full year will be charged at the single-copy rate. ¶Postage is prepaid by the publishers on all orders from the United States and its possessions, Argentina, Bolivia, Brazil, Chile, Colombia, Costa Rica, Cuba, Dominican Republic, Ecuador, Guatemala, Haiti, Republic of Honduras, Mexico, Morocco (Spanish Zone), Nicaragua, Panama, Paraguay, Peru, Rio de Oro, El Salvador, Spain (including Balearic Islands, Canary Islands, and the Spanish Offices in Northern Africa; Andorra), Spanish Guinea, Uruguay, and Venezuela. ¶Postage is charged extra as follows: for Canada and Newfoundland, 42 cents on annual subscriptions (total $12.42); on single copies, 7 cents (total $3.07); for all other countries in the Postal Union, 96 cents on annual subscriptions (total $12.96), on single copies 16 cents (total $3.16). ¶Patrons are requested to make all remittances payable to The University of Chicago Press, in United States currency or its equivalent by postal or express money orders or bank drafts.

The following is an authorized agent:

For the British Empire, except North America and Australasia: The Cambridge University Press, Bentley House, 200 Euston Road, London, N.W. 1, England. Prices of yearly subscriptions and of single copies may be had on application.

Claims for missing numbers should be made within the month following the regular month of publication. The publishers expect to supply missing numbers free only when losses have been sustained in transit, and when the reserve stock will permit.

Business correspondence should be addressed to The University of Chicago Press, Chicago 37, Illinois.

Communications for the editors and manuscripts should be addressed to: W. W. Morgan, Editor of THE ASTROPHYSICAL JOURNAL, Yerkes Observatory, Williams Bay, Wisconsin.

Line drawings and photographs should be made by the author, and all marginal notes such as co-ordinates, wave lengths, etc., should be included in the cuts. It will not be possible to set up such material in type.

One copy of the corrected galley proof should be returned as soon as possible to the editor, Yerkes Observatory, Williams Bay, Wisconsin. Authors should take notice that the manuscript will not be sent to them with the proof.

The cable address is "Observatory, Williamsbay, Wisconsin."

The articles in this journal are indexed in the *International Index to Periodicals*, New York, N.Y.

Applications for permission to quote from this journal should be addressed to The University of Chicago Press, and will be freely granted.

Entered as second-class matter, July 31, 1940, at the Post-Office at Chicago, Ill., under the Act of March 3, 1879.
Acceptance for mailing at special rate of postage provided for in United States Postal Act of October 3, 1917, Section 1103, amended February 28, 1925.

[PRINTED IN U.S.A.]

THE ASTROPHYSICAL JOURNAL

AN INTERNATIONAL REVIEW OF SPECTROSCOPY AND ASTRONOMICAL PHYSICS

VOLUME 108 NOVEMBER 1948 NUMBER 3

ON THE PHYSICAL AND CHEMICAL COMPOSITION OF THE SUN

GEOFFREY KELLER*
Rutherfurd Observatory, Columbia University†
Received July 17, 1948

ABSTRACT

A radiative-envelope–convective-core model of the sun has been constructed on the assumption that the radiative opacity is due to oxygen. It is found that the abundances of hydrogen, helium, and heavy elements for the new model differ markedly from those obtained by M. Schwarzschild on the assumption that the opacity is due to a Russell mixture. In order to obtain an independent criterion for deciding which model is more nearly valid, the apsidal motion properties of the models have been investigated.

A comparison of the apsidal motion computed for the models with the observed apsidal motion of main-sequence binary stars indicates that the sun most nearly conforms to an intermediate model. It is found that for the intermediate model the ratio by weight of the oxygen group of elements to all the heavy elements is 0.85. The hydrogen, helium, and heavy-element abundances are 0.67, 0.29, and 0.045, respectively. These results are in good agreement with spectroscopic analyses of stellar atmospheres.

I. INTRODUCTION

It has recently been shown by M. Schwarzschild[1] that if one knows the *relative* abundances by weight in the sun of the elements heavier than helium, then the absolute abundances of hydrogen (X), helium (Y), and all the heavy elements together (Z) can be computed purely on the basis of the internal constitution. In his work Schwarzschild assumed that the relative abundances of the heavier elements are given by the Russell mixture, where the ratio by weight of the oxygen group of elements (O) to Z is equal to 0.5.

It has been pointed out by Biermann,[2] however, that the current spectroscopic estimates of the O/Z ratio in stellar atmospheres are considerably higher than those of ten years ago. Biermann realized that the adoption of an increased ratio would seriously affect the guillotine factor, and hence the whole temperature and density distribution within a radiative-envelope–convective-core model of the sun. He therefore made a number of preliminary estimates of the structure and chemical composition of the sun, using a much larger ratio, and arrived at a final estimate of $X = 0.55$, $Y = 0.11$, $Z = 0.34$, and an O/Z ratio of 0.993.

It seemed worth while to make more computations on such models by Schwarzschild's method, partly for the sake of greater precision and partly because Biermann's

* Now at Perkins Observatory, Delaware, Ohio.

† This paper is a condensation of the author's doctoral thesis.

[1] *Ap. J.*, **104**, 203, 1946.

[2] *Zs. f. Ap.*, **22**, 244, 1943.

value for Z appears inadmissibly large compared to the spectroscopic values[3] of 0.03 ± 0.015. An extreme O/Z ratio of 1.0 was assumed. On carrying out the solution, it was found that the X, Y, and Z predicted by the new model differed radically from those of both Schwarzschild and Biermann.

In view of these differences, subsidiary computations of the apsidal-motion characteristics were made for both the new model and Schwarzschild's model. A comparison of the calculated characteristics with the observed characteristics of main-sequence stars was then made, in order to decide which model is more nearly valid. It was found that the best agreement could be obtained if one employed an intermediate model with an O/Z ratio of 0.85. By means of an interpolation procedure the best values for X, Y, and Z were derived.

II. PROPERTIES OF THE OXYGEN MODEL

An important prerequisite to the construction of a model is an adequate table of guillotine factors for the assumed mixture of heavy elements. This is not at present available for mixtures rich in oxygen, but Biermann[2] gives a table of values for pure oxygen.[4] It was decided, therefore, to construct a model in which O/Z equals 1.0 and then to proceed by interpolation to a model intermediate between this and Schwarzschild's.

The method of integration followed that of Schwarzschild[1] in most details. The composition was assumed uniform throughout the star. Radiation pressure was neglected. It was further assumed that the entire energy generation from nuclear sources occurs within the convective core. The expression used for the radiative opacity is that given by Morse,[5] where $\Gamma = 4.0$, and for the guillotine factor the following empirical expression has been employed:

$$\frac{t}{\bar{g}} = 1.70 \times 10^{-6}(1+X)^{0.2}\rho^{0.2}T \,. \tag{1}$$

The fundamental differential equations for (a) hydrostatic equilibrium, (b) radiative equilibrium, and (c) the differential element of mass were written down. These were converted to dimensionless variables, giving rise to the eigenvalue C of the solution,

$$C = \frac{3\kappa_0}{4ac}\left(\frac{k}{\mu GH}\right)^{8.5}\left(\frac{1}{4\pi}\right)^{2.8}\frac{LR^{2.1}}{M^{6.7}}\,; \tag{2}$$

and the other symbols have their usual meanings.

Integration was started at the outer boundary (using a trial value of C) by analytical methods. These were supplanted by numerical procedures at about nine-tenths the radius. The conventional fitting conditions at the surface of the convective core were used to test the trial value of C.

After four trials the following results were obtained:

$$\log C = -5.5624 \,.$$

At the surface of the convective core:

$$\text{Radius} = 0.075332 \times R \,,$$

$$\text{Temperature} = 1.28494 \times \frac{\mu HGM}{kR} \,,$$

$$\text{Mass within} = 0.084403 \times M \,,$$

$$\text{Pressure} = 684.29\,\frac{GM^2}{4\pi R^4} \,,$$

$$\text{Lane-Emden variables: } \xi = 1.01272 \,,$$

$$\theta = 0.84150 \,.$$

[3] See Aller's comments, *Ap. J.*, **104**, 353, 1946.

[4] The author wishes to thank Mrs. Marjorie Hall Harrison for sending him a considerably more extensive table of the guillotine factors for oxygen.

[5] *Ap. J.*, **92**, 40, eq. (16), 1940.

At the center, in solar units:

$$\text{Temperature} = 35.29 \times 10^6 \mu \frac{M}{R}, \tag{3}$$

$$\text{Density} = 324.4 \times \frac{M}{R^3} = 229.9 \bar{\rho}. \tag{4}$$

If the numerical value for C is entered into the analytical expression (2), one has essentially the mass-luminosity law for the new model. The energy-production law is obtained by setting the integrated nuclear-energy production in the core equal to the luminosity. For this purpose the cross-sections of Bethe[6] were employed. The fraction by weight of C^{12} in the heavy-element group was taken as 0.05. The mass-luminosity and energy-production laws may be solved as simultaneous equations for X and Y. The results are

$$X = 0.97 \pm 0.10\,, \qquad Y = 0.00 \pm 0.10\,, \qquad Z = 0.03 \pm 0.03\,, \qquad \mu = 0.51\,.$$

For comparison, Schwarzschild's results for the Russell mixture model are

$$X = 0.47\,, \qquad Y = 0.41\,, \qquad Z = 0.12\,, \qquad \mu = 0.76\,.$$

The limits of error are rough estimates based on the estimated uncertainties in the opacities and capture cross-sections, without considering the most recent cross-section measurements.[6]

The high ratio of central density to mean density for the oxygen model reflects its higher central condensation. Comparison with various polytropes shows that in the region between 0.1 and 0.9 of the radius the oxygen model is very similar in density distribution to a polytrope of index $n = 3.9$. Similarly, the Russell mixture model is close to a polytrope of $n = 3.5$.

With the run of temperatures and densities predicted by the oxygen model, it is possible to compare the tabular values of the guillotine factor at various points within the sun with the values predicted by the empirical formula (1). In the region where $\log [\rho (1 + X)] > -0.3$, the error in the logarithm of the guillotine factor in no case exceeds 0.16. This is considered to be good agreement for this type of work. A final check must wait, however, for a numerical integration in which the actual tabular values of the guillotine factor are used at each step in the integration.

It can be shown that the total pressure at the center of both the oxygen and the Russell mixture models differs from that of an ideal gas by less than 10 per cent. The neglected opacity due to electron scattering is more serious, being approximately equal to that due to radiative opacity at the surface of the convective core of the oxygen model. The electron scattering is responsible for only about 15 per cent of the total opacity at the convective core for the Russell mixture model. Since these numbers are maximum rather than average values throughout the radiative envelope and since the final results for the intermediate model will involve a maximum electron-scattering effect intermediate between 100 and 15 per cent, it does not appear too serious that this factor has been neglected.

III. THE APSIDAL MOTION OF THE RUSSELL MIXTURE AND OXYGEN MODELS

The constants of apsidal motion have been calculated for both models by the methods developed by Russell,[7] Cowling,[8] and Sterne.[9] In the convective core a series expansion

[6] *Phys. Rev.*, **55**, 434, 1939; *Ap. J.*, **92**, 118, 1940. Recent results of O'Reilly and Christy (*Bull. A.P.S.*, **23**, No. 1, 11) indicate that the cross-section of C^{12} is forty times the value assumed by Bethe. The new results lead to a discrepancy with the observed abundance ratio of C^{12} and N^{14}, however. In view of the unresolved difficulties, it seems worth while to give the results of the present investigation, which was essentially complete at the time that the newer measurements were published. Should the newer values be correct, the present results would be altered greatly, but it is not possible to say how without more precise information on the relative abundances of C^{12} and N^{14}.

[7] *M.N.*, **88**, 641, 1928. [8] *M.N.*, **98**, 734, 1938. [9] *M.N.*, **99**, 451, 1939.

similar to that suggested by Motz[10] was employed. At the interface between the convective core and the radiative envelope, continuity of the tidal deformation and its first derivative was required. Integration through the envelope was performed numerically.

The result of the calculation may be expressed in terms of Sterne's coefficient k, which occurs in the expression for the ratio of the period of apsidal motion to the period of orbital motion. An alternative method, suggested by Motz,[10] is to describe the amount of apsidal motion which will be experienced by a binary system constructed from stars of a given model by giving the index of that polytrope which will exhibit the same apsidal motion under the same conditions. The latter may be termed the "effective polytropic index of the model." Values were obtained as shown in Table 1. It may be noted that the effective indices obtained in this way agree well with the effective indices obtained from a consideration of density distributions in the envelopes.

In the cases of stars for which reliable observations of the period of apsidal motion are available, it is possible to compute k and the effective index without making any assumptions with regard to the model other than that the equilibrium theory of the tides is applicable. For purposes of comparison with the theory, observational determinations of k and the effective indices have been assembled from the following sources: (*a*) Russell[11] (the formulae given by Sterne[9] connecting the orbital elements, apsidal period, and k are more accurate than those of Russell when the eccentricity is large. In such cases the values of k computed by Sterne's formulae were used); (*b*) Sterne;[12] and (*c*) Kopal.[13] Only those binaries have been employed which are considered by Russell to be most reliable. In all cases both minima have been observed.

TABLE 1

	k	Effective Polytropic Index
Russell mixture model.....	0.00585 ± 0.00002	3.5
Oxygen model.....	0.00174 ± 0.00002	3.9

The results are illustrated in Figure 1. It will be noted that five out of six of the main-sequence stars of spectral type later than B3 have effective indices >3.5, which leads one to suspect that most of these stars have a degree of central condensation intermediate between those of the Russell mixture and oxygen models. The average for all six stars is $n = 3.55$, giving equal weight to all determinations. In view of the tendency mentioned by Russell[11] for various errors of reduction to lead to too large a value of k (too small a value of n), plus what appears to be a trend toward higher n with later spectral types, $n = 3.7$ has been taken as the most probable value for the sun.

IV. THE INTERMEDIATE MODEL—COMPARISON WITH SPECTROSCOPIC ABUNDANCE DETERMINATIONS

After it was found that the effective polytropic index for the sun lies between those of the Russell mixture and oxygen models, an investigation was made to estimate the most probable composition of a model having the intermediate effective index.

To obtain the most probable composition of the heavy-element fraction, use was made of the close mathematical connection between the effective index and the slope of the curve depicting the logarithm of the guillotine factor as a function of the logarithm of the density. It was found that a curve which lay midway between those of the Russell

[10] *Ap. J.*, **94**, 253, 1941.

[11] *Ap. J.*, **90**, 641, 1939.

[12] *M.N.*, **99**, 662, 1939.

[13] *Harvard Circ.*, No. 443, 1940.

mixture and oxygen models would probably correspond to a model of index 3.7. It was then assumed that the heavy-element fraction was composed of the oxygen group in addition to Russell mixture, and the further approximation was made that the absorptive opacities of the two fractions are additive. It was found that a guillotine factor curve of the desired intermediate slope could be obtained if the fraction by weight of the oxygen group of elements was taken as 0.7, Russell mixture fraction as 0.3, or expressed differently, the oxygen-group fraction was 0.85 and the metal-group fraction 0.15. In connection with this matter it may be noted that Biermann[2] has computed the guillotine factors for several different mixtures of oxygen and magnesium + iron at a temperature of 10^7 degrees and for log $[\rho(1 + X)] = 1.41$. If one interpolates among

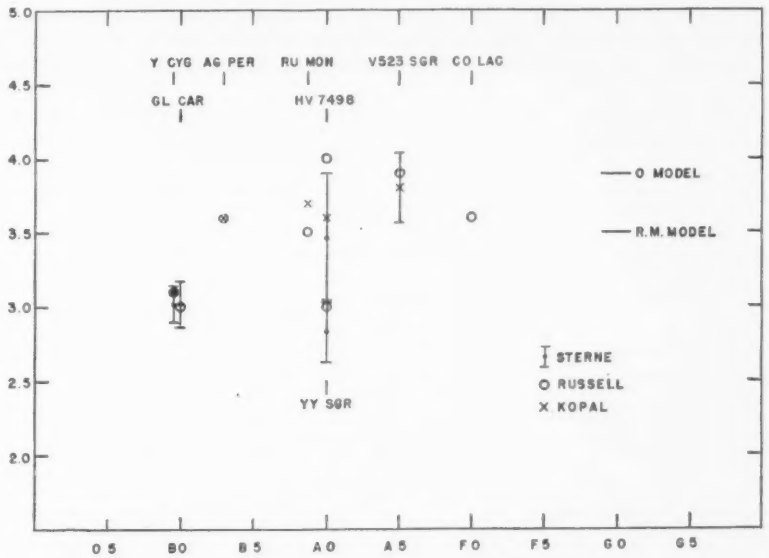

FIG. 1.—Effective polytropic indices for apsidal motion as a function of spectral class

Biermann's values, it is found that the proportions of the elements which give a logarithm of the guillotine factor halfway between those for the pure oxygen and a Russell mixture are the same as those found on the assumption that the absorptive opacities are additive.

It remained to determine the values of X and Y for the intermediate model. For this purpose approximate mass-luminosity and energy-production laws were developed in the following manner:

Equation (2) is a form of the mass-luminosity law, and in it C is a constant. In the differential equations describing a radiative-envelope–convective-core model, the quantity C first appears in the dimensionless form of the equation of radiative equilibrium. This equation may be solved for C; and, if one knows the values of the radius, pressure, temperature, and the space derivative of the temperature appearing on the right-hand side of the equation, one may calculate C. Now it has been noted that in some ways the oxygen model is similar to a polytrope of index 3.9. As a further check on the similarity, values of C were computed from the differential equation; only in this case the quantities entered on the right-hand side were appropriate to the polytrope and not to the true oxygen model. As might be expected, the resulting value of C depended upon the distance from the center of the polytrope to which the physical quantities employed in the

calculation corresponded, but the various determinations of C did not differ greatly from one another, and the average value of log C for a nine points equally spaced from 0.1 to 0.9 of the radius differed from the true value of log C by only $+0.09$. A similar computation made for the Russell mixture model in association with the polytrope $n = 3.5$ gave an average value of log C which again differed from the true one by $+0.09$. In view of these results, the value of log C for the intermediate model was computed in similar fashion from the polytrope $n = 3.7$. It is equal to -5.38. The mass-luminosity law could then be set up for the intermediate model, using in the process an empirical law for the logarithm of the guillotine factor which gives values midway between those employed for the oxygen and for Russell mixture models.

An expression which is equivalent to the energy-production law may be obtained readily from the fact that the central temperatures of all models which operate on the carbon cycle are nearly the same. For the oxygen model the central temperature is 18.0×10^6 degrees, while for the Russell mixture model the value is 19.7×10^6 degrees.

TABLE 2

FRACTIONAL ABUNDANCES BY WEIGHT

	Models			Observed	
	Russell Mixture	Intermediate	Oxygen	10 Lacertae*	Meteorites, Sun, and τ Scorpii†
Hydrogen (X)	0.47	0.67	0.97	0.74	0.56
Helium (Y)	.41	.29	.00	.24	.41
Other (Z)	.12	.045	.03	.017	.033
Oxygen group/(Z)	0.50	0.85	1.00	0.85	0.84

* Aller, *Ap. J.*, **104**, 353, 1946.

† Unsöld, *Zs. f. Ap.*, **24**, 306, 1943.

For the intermediate model a value of 18.9×10^6 degrees was adopted. An expression equivalent to equation (3) may now be set up for the intermediate model and solved for μ, provided that one has some way of estimating the numerical coefficient on the right-hand side. This coefficient is a homology invariant and is easily computed for any polytrope. Since the logarithm of its value for a polytrope of $n = 3.5$ does not differ from that for the Russell mixture model by more than ± 0.02, and the same close agreement holds between the polytrope $n = 3.9$ and the oxygen model, the value for the polytrope $n = 3.7$ was used for the intermediate model. It is equal to 29.8×10^6. When one knows μ and uses the mass-luminosity law, X, Y, and Z may be determined.

V. COMPARISON OF RESULTS WITH SPECTROSCOPIC ANALYSES

A comparison between the abundances according to the three models and the more recent determinations based on spectroscopic analysis of stellar atmospheres is given in Table 2. It is felt that the fractional abundances for the intermediate model represent the best estimates that can be made on the basis of the work described in this paper. With regard to the latter the following comments might be made:

The errors in X and Y are estimated at ± 0.10. Unsöld's values for X and Y are based largely on the data from τ Scorpii which is a B0 star. Moreover, 10 Lacertae is type Oe5. Since these bright stars would burn large percentages of their hydrogen content in times comparable to two billion years (for which reason it is now suspected that they

may be of more recent origin than the sun), an agreement in X and Y between them and the sun is not to be expected.

Unsöld[14] has made an estimate of the X/Y ratio from spectroscopic data on solar prominences, obtaining the result $X/Y = 1.25$, which is uncertain by a factor of 3 in either direction. This result is in satisfactory agreement with the predictions of the model.

The error in the Z for the intermediate model is estimated at ± 0.03; that for the oxygen group/Z ratio is $+0.05$, -0.10. All these quantities agree rather well with the observational data.

In general, it appears that the hydrogen, helium, and heavy-element abundances and the oxygen group to heavy-element abundance ratio for the sun may be determined with some accuracy from a knowledge of the mass, radius, and luminosity of the sun and the apsidal motion of the main-sequence stars. The results appear to be in good agreement with the available spectroscopic analyses of stellar atmospheres.

The author wishes to thank Dr. Martin Schwarzschild for suggesting this problem and for his generous help and encouragement, which made its completion possible.

[14] *Zs. f. Ap.*, **24**, 22, 1947.

THE CONTINUOUS ABSORPTION COEFFICIENT OF THE HELIUM ATOM

SU-SHU HUANG
Yerkes Observatory
Received August 7, 1948

ABSTRACT

In this paper the continuous absorption coefficient of *He* I beyond the series limits 504.3 A, 2600.7 A, and 3122 A (i.e., transitions from the ground state 1^1S and the two metastable states 2^3S and 2^1S to the continuum) are investigated. For the bound states, wave functions derived from the Ritz principle were used, while for the free states Coulomb wave functions with an effective charge of 1 were used. With these wave functions the continuous absorption cross-sections have been derived from the matrix elements not only of the dipole moment but also of the momentum and of the acceleration. The agreement of values derived from the momentum and the dipole moment provides a strong confirmation of the results obtained from them. However, the cross-sections derived from the acceleration are much smaller. This last circumstance is due to the fact that the main contribution to the matrix elements of the acceleration come from very near the origin, where an effective charge of 1 is unsuitable. The integrated *f*-values for the three continua have also been computed. When these *f*-values for the continua are added to the respective sums for the discrete states evaluated by other authors, we find that the *f*-sum rule is approximately satisfied. This is an additional check on our calculation.

I. INTRODUCTION

The continuous absorption coefficient of *He* I in its ground state 1^1S ($1s^2$ configuration) was first computed by Wheeler[1] in his theory of the dispersion of helium; it was later derived independently by Vinti.[2] The former used Hylleraas' wave function[3] for the ground state, and the latter used a less elaborate wave function derived by Eckart;[4] and both authors made use of the hydrogenic approximation for the wave functions for the continuum. A similar method was also used by Jen[5] in an early investigation on the continuous absorption coefficient of the negative hydrogen ion. No computation has so far been made regarding the absorption cross-sections from two metastable states, 2^3S and 2^1S (1s2s configuration). Recently Romberg[6] gave a general treatment of the matrix elements of the dipole moment for the s–p transition on the basis of the hydrogenic approximation. By expressing the solution of the wave function in the Coulomb field in the form of a complex integral in the manner suggested by Hylleraas,[7] Romberg assumes nonintegral values of the principal quantum number, thus allowing empirically for the Rydberg correction; but so far no numerical results have been published. We should also mention that Goldberg[8] has made an estimate of the *f*-values for these continua from the known values of *f* for the line transitions.

Recently Chandrasekhar,[9] in a series of papers devoted to the continuous absorption coefficient of negative hydrogen, has shown how the cross-sections derived from the matrix elements not only of the dipole moment but also of the momentum and of the acceleration can be a guide in deciding the reliability of the derived cross-sections; and it would appear from his investigations that the cross-section derived from the

[1] *Phys. Rev.*, **43**, 258, 1933.
[2] *Phys. Rev.*, **44**, 524, 1933.
[3] *Zs. f. Phys.*, **54**, 347, 1929.
[4] *Phys. Rev.*, **36**, 878, 1930.
[5] *Phys. Rev.*, **43**, 540, 1933.
[6] *Phys. Rev.*, **71**, 706, 1947.
[7] *Arch. f. Math. og Natv.*, **48**, No. 4, 57, 1945.
[8] *Ap. J.*, **90**, 414, 1939.
[9] *Ap. J.*, **100**, 176, 1944; **102**, 223, 395, 1945; S. Chandrasekhar and F. H. Breen, *Ap. J.*, **104**, 430, 1946.

matrix element of the momentum is, perhaps, the most reliable. Following this idea, in the present investigation we shall evaluate the three types of matrix elements for each of the three states mentioned before and compare them.

For the ground state of *He* we shall use Hylleraas' wave function[9] with six parameters; for the two other states, starting from wave functions of the forms given by Hylleraas and Undheim,[10] we have solved for the constants according to the Ritz principle. Wave functions thus obtained predict for the energies of the 2^3S and 2^1S states the values $-0.35040\ Rh$ and $-0.28975\ Rh$, respectively; these values are to be compared with the corresponding experimental values, $-0.35043\ Rh$ and $-0.29191\ Rh$. For the free state we shall use Coulomb wave functions with an effective charge of 1. With the bound state very well represented, it remains to be seen to what extent the approximation of the Coulomb field is a good one. For the sake of comparison and completeness the cross-sections from the ground state derived from the matrix elements of the dipole moment have also been recomputed.

II. THE WAVE FUNCTION OF THE FREE STATE

The Schrödinger equation for two electrons (distinguished by 1 and 2) in the field of a fixed nucleus is

$$\nabla_1^2\Psi+\nabla_2^2\Psi+\left[E+2\left(\frac{Z_0}{r_1}+\frac{Z_0}{r_2}-\frac{1}{r_{12}}\right)\right]\Psi=0\,, \tag{1}$$

if we measure distance and energy in the units of the Bohr radius and Rh, respectively. Evidently, the nuclear charge Z_0 in the present case is 2. Assume that the 1s electron is not appreciably disturbed by the free electron ejected by the ionization process from the atom, so that the interaction term enters only into the potential function of the free electron; then we can separate the variables of the two electrons thus:

$$\Psi=\Psi_0(1)\Phi(2) \qquad \text{and} \qquad E=E_0+\epsilon\,, \tag{2}$$

where

$$\Psi_0(1)=\pi^{-1/2}Z_0^{3/2}\,e^{-Z_0r_1}=2^{3/2}\pi^{-1/2}\,e^{-2r_1} \tag{3}$$

denotes the wave function belonging to energy level E_0 of the 1s electron in the field of the singly ionized atom, and $\Phi(2)$, the solution of the differential equation,

$$\nabla_2^2\Phi(2)+\left[\epsilon+2\left(\frac{Z_0}{r_2}-\frac{1}{r_{12}}\right)\right]\Phi(2)=0\,, \tag{4}$$

is the continuous wave function for the free electron with the energy ϵ.

The approximation that we shall introduce is to replace the expression inside the parenthesis by Z/r_2; Z is therefore a sort of effective nuclear charge with respect to the free electron. In our later calculations we shall put Z equal to 1, i.e., assume that the screening of the inner electron is complete. The solution of equation (4) thus simplified is well known: its angular part is $P_l^m(\cos\theta)e^{im\phi}$, while the radial part, $R_{\epsilon,\,l}(r)$, satisfies the differential equation:

$$\frac{d^2(rR)}{dr^2}+\left[\epsilon+\frac{2Z}{r}-\frac{l(l+1)}{r^2}\right](rR)=0\,, \tag{5}$$

with the integral value of l (for convenience we shall suppress the subscript 2).

As was shown by Schrödinger,[11] the solution of equation (5) with positive eigen-

[10] *Zs. f. Phys.*, **65**, 759, 1930.

[11] *Ann. d. Phys.*, **79**, 361, 1926; L. Schlesinger, *Einführung in die Theorie der gewöhnlichen Differentialgleichungen auf funktionentheoretischer Grundlage* (3d ed.; Berlin, 1922), pp. 260–266.

values of ϵ can be expressed by a Laplace contour integral, which can, in turn, be transformed into the form

$$-2iR_{\epsilon,\,l}(r) = r^l \int_{-i\sqrt{\epsilon}}^{+i\sqrt{\epsilon}} e^{xr}(x+i\sqrt{\epsilon})^{l+iZ/\sqrt{\epsilon}}(x-i\sqrt{\epsilon})^{l-iZ/\sqrt{\epsilon}}dx\,. \tag{6}$$

The normalization of the wave function for the continuous state in the manner of

$$\int_\infty d\tau \Phi^*_{\epsilon_2} \int_{\epsilon_1}^{\epsilon_1+\Delta\epsilon} \Phi_\epsilon d\epsilon = 1 \qquad \text{or} \qquad 0\,, \tag{7}$$

according as ϵ_2 lies between ϵ_1 and $\epsilon_1 + \Delta\epsilon$ or not, has been worked out by Fues.[12] With the normalization thus defined, we can finally express the wave function in the continuous state as follows:

$$\Phi_{\epsilon,\,l,\,m}(r,\,\theta,\,\phi) = \left[\frac{1}{2\pi}\,\frac{(2l+1)}{2}\,\frac{(l-m)!}{(l+m)!}\right]^{1/2} P_l^m(\cos\theta)\, e^{im\phi}$$
$$\times\left[\frac{e^{2\pi Z/\sqrt{\epsilon}}-1}{2\pi^2 Z\prod_{\mu=1}^{l}\left(1+\frac{Z^2}{\mu^2\epsilon}\right)}\right]^{1/2} \frac{e^{\pi Z/\sqrt{\epsilon}}}{(2\sqrt{\epsilon})^l\,\Gamma(l+1)} R_{\epsilon,\,l}(r)\,. \tag{8}$$

Hence $\Psi_0(1)\Phi_{\epsilon,\,l,\,m}(2)$ is a particular solution of equation (1) with certain appropriate approximations. The complete wave function for the free state can therefore be written in the form

$$\Psi_{\epsilon,\,l,\,m} = \frac{1}{\sqrt{2}}\left[\Psi_0(1)\Phi_{\epsilon,\,l,\,m}(2) \pm \Psi_0(2)\Phi_{\epsilon,\,l,\,m}(1)\right], \tag{9}$$

where the plus or the minus sign is to be associated with the symmetrical (singlet) or the antisymmetrical (triplet) state, respectively. For the sake of brevity, we shall write equation (9) as

$$\Psi_{\epsilon,\,l,\,m} = \Phi(1,\,2) \pm \Phi(2,\,1)\,. \tag{10}$$

III. THE WAVE FUNCTIONS FOR THE BOUND STATES

After making some conversion both for the co-ordinate system and for the unit, we can express the Hylleraas' wave function for the ground state in the following form:

$$\Psi(1^1\mathrm{S}) = C_1\, e^{-\alpha(r_1+r_2)}\left[c_0 + c_1\alpha r_{12} + c_2\alpha^2(r_2-r_1)^2\right.$$
$$\left. + c_3\alpha(r_1+r_2) + c_4\alpha^2(r_1+r_2)^2 + c_5\alpha^2 r_{12}^2\right]. \tag{11}$$

We shall similarly express the wave functions for two metastable states in the form

$$\Psi(2^3\mathrm{S}) = C_2(\Psi_1-\Psi_2)\,; \qquad \Psi(1^1\mathrm{S}) = C_3(\Psi_1+\Psi_2)\,, \tag{12}$$

where

$$\Psi_1 = \tfrac{1}{2}\, e^{-ar_1-br_2}\left[c_1 + c_2\alpha(r_1+r_2) + c_3\alpha(r_2-r_1)\right.$$
$$\left. + c_4\alpha r_{12} + c_5\alpha^2 r_{12}(r_1+r_2) + c_6\alpha^2 r_{12}(r_2-r_1)\right], \tag{13}$$

and

$$\Psi_2 = \tfrac{1}{2}\, e^{-br_1-ar_2}\left[c_1 + c_2\alpha(r_1+r_2) - c_3\alpha(r_2-r_1)\right.$$
$$\left. + c_4\alpha r_{12} + c_5\alpha^2 r_{12}(r_1+r_2) - c_6\alpha^2 r_{12}(r_2-r_1)\right]. \tag{14}$$

[12] *Ann. d. Phys.*, **81**, 281, 1926.

The constants in the wave functions (12)–(14) have been determined and are given in Table 1, which also includes Hylleraas' values for the ground state. The normalization factor can be obtained in the process of determining the constants.

In what follows we shall use the well-known expansion for r_{12}:

$$r_{12} = \hat{r} \sum_{\nu=0}^{\infty} \left(\frac{x^2}{2\nu+3} - \frac{1}{2\nu-1} \right) x^{\nu} P_{\nu}(\cos\Theta), \tag{15}$$

where

$$P_{\nu}(\cos\Theta) = \sum_{\mu=-\nu}^{\nu} \frac{(\nu-|\mu|)!}{(\nu+|\mu|)!} P_{\nu}^{\mu}(\cos\theta_1) P_{\nu}^{\mu}(\cos\theta_2)\, e^{i\mu(\phi_1-\phi_2)} \tag{16}$$

and

$$\cos\Theta = \cos\theta_1 \cos\theta_2 + \sin\theta_1 \sin\theta_2 \cos(\phi_1-\phi_2) \tag{17}$$

while

$$\begin{aligned} &\hat{r} = r_1, \qquad x = \frac{r_2}{r_1} \qquad \text{if} \qquad r_1 > r_2; \\ &\hat{r} = r_2, \qquad x = \frac{r_1}{r_2} \qquad \text{if} \qquad r_2 > r_1. \end{aligned} \tag{18}$$

TABLE 1

CONSTANTS ASSOCIATED WITH WAVE FUNCTIONS OF BOUND STATES

State	1^1S	2^3S	2^1S
Normalization constant	$C_1 = 1.3843$	$C_2 = 0.16346$	$C_3 = 0.4073$
a	1.82	2.704	2.702
a		2.096	2.094
b		0.6085	0.6080
c_0	1		
c_1	0.1944	1	1
c_2	0.0388	−0.2865	−0.13575
c_3	−0.0554	−0.2842	−0.13599
c_4	0.0100	−0.07978	0.05316
c_5	−0.0096	−0.007053	−0.006629
c_6		0.011718	0.0009538

IV. THE CONTINUOUS ABSORPTION COEFFICIENT

As is well known, the transition probability is closely related with the matrix element of the dipole moment, or is equivalent to the matrix element of the momentum or the acceleration. In the evaluation with the exact solution of wave equations for both the initial and the final state, these three matrix elements are connected exactly in the following manner:

$$\begin{aligned} (b|x_1+x_2|f) &= \frac{2}{E_f-E_b}\left(b\left| \frac{\partial}{\partial x_1} + \frac{\partial}{\partial x_2} \right| f \right) \\ &= \frac{4}{(E_f-E_b)^2}\left(b\left| \frac{\partial V}{\partial x_1} + \frac{\partial V}{\partial x_2} \right| f \right), \end{aligned} \tag{19}$$

where E_f and E_b denote, respectively, the energy in the free state f and in the bound state b. Similar formulae hold for the two other components. Unfortunately, in most

cases neither of the wave functions used is exact, the three expressions (19) no longer being equal. As we have already stated, Chandrasekhar's investigation[13] on this point in the context of the negative hydrogen led him to believe that the cross-section derived from the matrix element of the momentum is the most reliable one. Proceeding now to the computation of these three kinds of matrix elements, we shall denote the total sum of the squares of the amplitude of the matrix elements of the dipole moment, the momentum, and the acceleration by M_d^2, M_m^2, and M_a^2, respectively, i.e.,

$$M_d^2 = \sum_{l,\,m} [(b\,|\,x_1+x_2\,|\,f)^2+(b\,|\,y_1+y_2\,|\,f)^2+(b\,|\,z_1+z_2\,|\,f)^2]\,, \tag{20}$$

$$M_m^2 = \frac{4}{(E_f-E_b)^2}\sum_{l,\,m}\left[\left(b\left|\frac{\partial}{\partial x_1}+\frac{\partial}{\partial x_2}\right|f\right)^2+\left(b\left|\frac{\partial}{\partial y_1}+\frac{\partial}{\partial y_2}\right|f\right)^2 + \left(b\left|\frac{\partial}{\partial z_1}+\frac{\partial}{\partial z_2}\right|f\right)^2\right], \tag{21}$$

and

$$M_a^2 = \frac{16}{(E_f-E_b)^4}\sum_{l,\,m}\left[\left(b\left|\frac{x_1}{r_1^3}+\frac{x_2}{r_2^3}\right|f\right)^2+\left(b\left|\frac{y_1}{r_1^3}+\frac{y_2}{r_2^3}\right|f\right)^2+\left(b\left|\frac{z_1}{r_1^3}+\frac{z_2}{r_2^3}\right|f\right)^2\right]. \tag{22}$$

In writing equation (22), we have assumed that the acceleration is that in an inverse-square field. From these expressions we can see that the contribution to M_d^2 comes from regions of the configuration space relatively more distant than those which contribute to M_m^2. Similarly, contribution to M_a^2 arises principally from very close to the nucleus.

On account of the particular normalization used in equation (7) the differential f-value, i.e., df/dE, for the transitions to the continuum is given by

$$\frac{df}{dE} = \tfrac{1}{3}EM^2\,. \tag{23}$$

In this expression E is the energy of the incident quanta in units of Rh, and M^2 represents M_d^2, M_m^2, or M_a^2 as the case may be. The atomic absorption coefficient α for the continuum is accordingly given by

$$\alpha = \frac{\pi e^2}{Rmc}\left[\frac{df}{dE}\right]. \tag{24}$$

V. THE COMPUTATION OF CROSS-SECTIONS FOR THE GROUND STATE

If we use wave functions given in equations (9) and (11), and carry out the integration expressed in equations (20)–(22) over the angular part, we obtain the following results:

$$M_d^2 = \gamma_1 I_d^2\,, \qquad M_m^2 = \gamma_1 I_m^2\,, \qquad \text{and} \qquad M_a^2 = \gamma_1 I_a^2\,, \tag{25}$$

where

$$\gamma_1 = \frac{128}{9}\,\frac{C_1^2}{Z(Z^2+\epsilon)(1-e^{-2\pi Z/\sqrt{\epsilon}})} \tag{26}$$

[13] *Ap. J.*, **102**, 223, 1945.

and

$$I_d = (1 - e^{2\pi Z/\sqrt{\epsilon}}) \int_0^\infty \int_0^\infty e^{-(a+2)r_1 - ar_2} R(r_2)\, r_1^2 r_2^2$$
$$\times \{3 r_2 [c_0 + c_2 a^2 (r_2 - r_1)^2 + c_3 a (r_1 + r_2) + c_4 a^2 (r_1 + r_2)^2 \quad (27)$$
$$+ c_5 a^2 (\tfrac{1}{3} r_1^2 + r_2^2)] + c_1 a \hat{r} [r_1 (\tfrac{1}{5} x^3 - x) + r_2 (x^2 + 3)]\} \, dr_1 dr_2 ;$$

$$I_m = (1 - e^{2\pi Z/\sqrt{\epsilon}}) \int_0^\infty \int_0^\infty e^{-(a+2)r_1 - ar_2} r_1^2 r_2^2$$
$$\times \left\{ 3 \left(\frac{dR(r_2)}{dr_2} + 2 \frac{R(r_2)}{r_2} \right) [c_0 + c_2 a^2 (r_2 - r_1)^2 + c_3 a (r_1 + r_2) \right. \quad (28)$$
$$+ c_4 a^2 (r_1 + r_2)^2 + c_5 a^2 (r_1^2 + r_2^2)] + 4 c_5 a^2 r_1 r_2 R(r_2)$$
$$\left. + c_1 a \hat{r} \left[(x^2 + 3) \left(\frac{dR(r_2)}{dr_2} + 2 \frac{R(r_2)}{r_2} \right) - 2 (\tfrac{1}{5} x^3 - x) R(r_2) \right] \right\} dr_1 dr_2 ;$$

and

$$I_a = (1 - e^{2\pi Z/\sqrt{\epsilon}}) \int_0^\infty \int_0^\infty e^{-(a+2)r_1 - ar_2} R(r_2)$$
$$\times \{3 r_1^2 [c_0 + c_2 a^2 (r_2 - r_1)^2 + c_3 a (r_1 + r_2) + c_4 a^2 (r_1 + r_2)^2 \quad (29)$$
$$+ c_5 a^2 (r_1^2 + r_2^2)] - 2 c_5 a^2 r_1 r_2^3 + c_1 a \hat{r} [r_2^2 (\tfrac{1}{5} x^3 - x) + r_1^2 (x^2 + 3)]\} \, dr_1 dr_2 .$$

As the integral I_d has already been worked out by Wheeler, we simply give the result below, with certain rearrangement in the final expression. Letting

$$L_n(\epsilon, \sigma) = (\sigma^2 + \epsilon)^{-n} e^{-(2Z/\sqrt{\epsilon}) \tan^{-1}(\sqrt{\epsilon}/\sigma)} , \quad (30)$$

we have

$$I_d = A_0 (a + Z) L_0(\epsilon, a) + A_3 Z (Z^2 + \epsilon)(2a - Z) L_3(\epsilon, a)$$
$$+ A_4 Z (Z^2 + \epsilon)[5a(a - Z) + (Z^2 - \epsilon)] L_4(\epsilon, a)$$
$$+ A_5 Z (Z^2 + \epsilon)[30a^3 - 45Za^2 + 18(Z^2 - \epsilon)a + Z(7\epsilon - 2Z^2)] L_5(\epsilon, a) \quad (31)$$
$$+ B_0 (a + Z) L_0(\epsilon, 2a + 2) + B_1 Z (2a + 2 + Z) L_1(\epsilon, 2a + 2)$$
$$+ B_2 Z (Z^2 + \epsilon) L_2(\epsilon, 2a + 2) + B_3 Z (Z^2 + \epsilon)(4a + 4 - Z) L_3(\epsilon, 2a + 2),$$

where

$$A_0 = \frac{288\pi c_1 a}{(a+2)^7} = 0.02697 ,$$
$$A_3 = 96\pi \left[\frac{c_0}{(a+2)^3} + \frac{3 c_3 a}{(a+2)^4} + \frac{4(3c_2 + 3c_4 + c_5) a^2}{(a+2)^5} \right] = 5.654 ,$$
$$A_4 = 192\pi \left[\frac{(c_1 + c_3) a}{(a+2)^3} + \frac{6(c_4 - c_2) a^2}{(a+2)^4} \right] = 1.1170 , \quad (32)$$
$$A_5 = 192\pi \frac{(c_2 + c_4 + c_5) a^2}{(a+2)^3} = 1.4051 ;$$
$$B_0 = -A_0 = -0.02697 , \qquad B_1 = 2(a+2) A_0 = 0.2060 ,$$
$$B_2 = -(a+2) B_1 = -0.7869 , \qquad B_3 = \tfrac{1}{3}(a+2) B_2 = -1.0017 .$$

The evaluation of the integral I_m requires some lengthy, though straightforward transformations. Thus, one of the integrals which we have to evaluate is

$$\int_0^\infty \int_0^\infty e^{-(\alpha+2)r_1-\alpha r_2}\hat{r}(x^2+3)\frac{dR(r_2)}{dr_2}\, r_1^2 r_2^2 dr_1 dr_2 .$$

In order to carry out the integration, we first re-write it in the following form:

$$\begin{aligned}
&\int_0^\infty e^{-\alpha r_2}\frac{dR(r_2)}{dr_2}\, r_2 dr_2 \int_0^{r_2} e^{-(\alpha+2)r_1} r_1^4 dr_1 \\
&+3\int_0^\infty e^{-\alpha r_2}\frac{dR(r_2)}{dr_2}\, r_2^3 dr_2 \int_0^{r_2} e^{-(\alpha+2)r_1} r_1^2 dr_1 \\
&+\int_0^\infty e^{-\alpha r_2}\frac{dR(r_2)}{dr_2}\, r_2^4 dr_2 \int_{r_2}^\infty e^{-(\alpha+2)r_1} r_1 dr_1 \\
&+3\int_0^\infty e^{-\alpha r_2}\frac{dR(r_2)}{dr_2}\, r_2^2 dr_2 \int_{r_2}^\infty e^{-(\alpha+2)r_1} r_1^3 dr_1 .
\end{aligned}$$

By use of the following relations:

$$\begin{aligned}
\int_0^\infty e^{-\alpha r}\frac{dR(r)}{dr}\, r^m dr \int_0^r e^{-\beta x} x^n dx &= \alpha\int_0^\infty e^{-\alpha r} R(r)\, r^m dr \int_0^r e^{-\beta x} x^n dx \\
&- m\int_0^\infty e^{-\alpha r} R(r)\, r^{m-1} dr \int_0^r e^{-\beta x} x^n dx - \int_0^\infty e^{-(\alpha+\beta)r} R(r)\, r^{m+n} dr
\end{aligned}$$

and

$$\begin{aligned}
\int_0^\infty e^{-\alpha r}\frac{dR(r)}{dr}\, r^m dr \int_r^\infty e^{-\beta x} x^n dx &= \alpha\int_0^\infty e^{-\alpha r} R(r)\, r^m dr \int_r^\infty e^{-\beta x} x^n dx \\
&- m\int_0^\infty e^{-\alpha r} R(r)\, r^{m-1} dr \int_r^\infty e^{-\beta x} x^n dx + \int_0^\infty e^{-(\alpha+\beta)r} R(r)\, r^{m+n} dr ,
\end{aligned}$$

which can be easily established through integration by part, we could put these four integrals equal to the sum of eight integrals:

$$\begin{aligned}
&+\alpha\int_0^\infty e^{-\alpha r_2} R(r_2)\, r_2 dr_2 \int_0^{r_2} e^{-(\alpha+2)r_1} r_1^4 dr_1 , \\
&-\int_0^\infty e^{-\alpha r_2} R(r_2)\, dr_2 \int_0^{r_2} e^{-(\alpha+2)r_1} r_1^4 dr_1 , \\
&+3\alpha\int_0^\infty e^{-\alpha r_2} R(r_2)\, r_2^3 dr_2 \int_0^{r_2} e^{-(\alpha+2)r_1} r_1^2 dr_1 , \\
&-9\int_0^\infty e^{-\alpha r_2} R(r_2)\, r_2^2 dr_2 \int_0^{r_2} e^{-(\alpha+2)r_1} r_1^2 dr_1 , \\
&+\alpha\int_0^\infty e^{-\alpha r_2} R(r_2)\, r_2^4 dr_2 \int_{r_2}^\infty e^{-(\alpha+2)r_1} r_1 dr_1 , \\
&-4\int_0^\infty e^{-\alpha r_2} R(r_2)\, r_2^3 dr_2 \int_{r_2}^\infty e^{-(\alpha+2)r_1} r_1 dr_1 , \\
&+3\alpha\int_0^\infty e^{-\alpha r_2} R(r_2)\, r_2^2 dr_2 \int_{r_2}^\infty e^{-(\alpha+2)r_1} r_1^3 dr_1 , \\
&-6\int_0^\infty e^{-\alpha r_2} R(r_2)\, r_2 dr_2 \int_{r_2}^\infty e^{-(\alpha+2)r_1} r_1^3 dr_1 .
\end{aligned}$$

After the integration over r_1 has been effected by successive integration by part several times, each of these integrals can be reduced to a linear combination of terms of the following standard form:

$$J_n = \int_0^\infty e^{-\beta r} R(r)\, r^n dr . \tag{33}$$

Similar processes of reduction can be applied to the other integrals occurring in I_m. Fortunately, every integral in I_m can be reduced to a sum of J_n, with n taking integral values from -1 onward.

In computing the integral J_n given in equation (33), we first invert the order of integration. The integration over r can be effected, and we have

$$J_n = \frac{(-1)^{n+1}(n+1)!}{2i} \int_{-i\sqrt{\epsilon}}^{+i\sqrt{\epsilon}} \frac{(x+i\sqrt{\epsilon})^{1+iZ/\sqrt{\epsilon}}(x-i\sqrt{\epsilon})^{1-iZ/\sqrt{\epsilon}}}{(x-\beta)^{n+2}}\, dx . \tag{34}$$

By modifying the contour of this complex integral to pass around the barrier line connecting the two branch points $x = \pm i\sqrt{\epsilon}$ in the positive sense, we get a factor of $1 - e^{2\pi Z/\sqrt{\epsilon}}$; then, taking the contour around the poles $x = \beta$ and $x = \infty$ in the negative sense, we obtain

$$J_n = \frac{(-1)^n (n+1)!\pi}{1 - e^{2\pi Z/\sqrt{\epsilon}}} [\Re(\beta) + \Re(\infty)] \tag{35}$$

where $\Re(\beta)$ and $\Re(\infty)$ represent the residue of the integrand in equation (34) at $x = \beta$ and $x = \infty$, respectively. The evaluation of the residues follows the standard procedure. This process is essentially that used by Fues[12] and Sugiura,[14] except that here we also have to evaluate the residue at infinity for some of the integrals. As in the case of I_d, the total contributions due to the residues at infinity cancel out.

The final result of the calculation is

$$\begin{aligned} I_m = {} & C_0(Z-2)L_0(\epsilon, a) + C_1 Z(a+Z)L_1(\epsilon, a) + C_2 Z(Z^2+\epsilon)L_2(\epsilon, a) \\ & + C_3 Z(Z^2+\epsilon)(2a-Z)L_3(\epsilon, a) + C_4 Z(Z^2+\epsilon)[5a(a-Z) + (Z^2-\epsilon)]L_4(\epsilon, a) \\ & + D_0(Z-2)L_0(\epsilon, 2a+2) + D_1 Z(2a+2+Z)L_1(\epsilon, 2a+2) \\ & + D_2 Z(Z^2+\epsilon)L_2(\epsilon, 2a+2), \end{aligned} \tag{36}$$

where

$$C_0 = \frac{48\pi c_1 a^2}{(a+2)^6} = 0.03125 , \qquad C_1 = -2(a+2)C_0 = -0.2388 ,$$

$$\begin{aligned} C_2 &= 48\pi \left[\frac{(c_0 - c_3)a}{(a+2)^3} - \frac{(c_1 - 6c_2 - 3c_3 + 6c_4)a^2}{(a+2)^4} + \frac{12(c_2 + c_4 + c_5)a^3}{(a+2)^5} \right] \\ &= 5.282 , \end{aligned}$$

$$\begin{aligned} C_3 &= 96\pi \left[\frac{\{(c_1 + c_3) - 2(c_2 + c_4 + c_5)\}a^2}{(a+2)^3} + \frac{6(c_4 - c_2)a^3 + 4c_5 a^2}{(a+2)^4} \right] \\ &= -0.5688 , \end{aligned} \tag{37}$$

$$C_4 = 192\pi \frac{(c_2 + c_4 + c_5)a^3}{(a+2)^3} = 2.557 ; \qquad D_0 = -C_0 = -0.03125 ,$$

$$D_1 = 4(a+2)C_0 = 0.4775 , \qquad D_2 = -\tfrac{1}{2}(a+2)D_1 = -0.9120 .$$

[14] *Sci. Papers Inst. Phys. and Chem. Res.* (Tokyo), **11**, No. 193, 1, 1929.

The computation of I_a proceeds along similar lines, except that, in the first place, the total contribution due to residues at infinity do not cancel, and, in the second place, there is an integral that cannot be expressed in closed algebraic form; consequently, we have additional terms. The final expression is

$$\begin{aligned} I_a = {} & E_{-1}L_{-1}(\epsilon, a) + E_0(a+Z)L_0(\epsilon, a) + E_1[(a^2+\epsilon) + 2Z(a+Z)]L_1(\epsilon, a) \\ & + E_2Z(Z^2+\epsilon)L_2(\epsilon, a) + E_3Z(Z^2+\epsilon)(2a-Z)L_3(\epsilon, a) + F_{-1}L_{-1}(\epsilon, 2a+2) \\ & + F_0(2a+2+Z)L_0(\epsilon, 2a+2) + F_1[4(a+1)^2+\epsilon+2Z(2a+2+Z)] \\ & \times L_1(\epsilon, 2a+2) + F_2Z(Z^2+\epsilon)L_2(\epsilon, 2a+2) + F_3Z(Z^2+\epsilon)(4a+4-Z) \\ & \times L_3(\epsilon, 2a+2) + G_1Z + G_2 - F_{-1}(3a^2+8a+4) - \tfrac{1}{6}F_0(15Z+11a+12) \\ & + 4F_1 + G_3Z(Z^2+\epsilon)\int_{2a+2}^{\infty} \frac{5y(y-Z)+Z^2-\epsilon}{(y-a)^2} L_4(\epsilon, y)\,dy . \end{aligned} \tag{38}$$

where

$$\begin{aligned} E_{-1} &= -\frac{24\pi c_1 a}{(a+2)^5} = -0.03279, \\ E_0 &= 12\pi\left[\frac{c_0}{(a+2)^3} + \frac{(c_1+15c_3)a}{5(a+2)^4} + \frac{12(c_2+c_4+c_5)a^2}{(a+2)^5}\right] = 0.1075, \\ E_1 &= -12\pi\left[\frac{(c_1+c_3)a}{(a+2)^3} + \frac{6(c_4-c_2)a^2}{(a+2)^4}\right] = -0.06980, \\ E_2 &= 8\pi\left[-\frac{c_1 a}{(a+2)^2} + \frac{6(c_2+c_4+c_5)a^2}{(a+2)^3}\right] = -0.2581, \\ E_3 &= -\frac{32\pi c_5 a^2}{(a+2)^2} = 0.2191; \qquad F_{-1} = -E_{-1} = 0.03279; \\ F_0 &= \tfrac{3}{5}(a+2)E_{-1} = -0.07515, \qquad F_1 = -\tfrac{1}{6}(a+2)F_0 = 0.04786, \\ F_2 &= \tfrac{4}{3}(a+2)F_1 = 0.2437, \qquad F_3 = -(a+2)F_2 = -0.9309; \\ G_1 &= 12\pi\left[\frac{c_0}{(a+2)^3} + \frac{3c_3 a}{(a+2)^4} + \frac{12(c_2+c_4+c_5)a^2}{(a+2)^5}\right] = 0.6950, \\ G_2 &= 12\pi\left[\frac{(c_3-c_0)a}{(a+2)^3} + \frac{\{6(c_4-c_2)-3c_3\}a^2}{(a+2)^4} - \frac{12(c_2+c_4+c_5)a^3}{(a+2)^5}\right] \\ &= -1.4342, \\ G_3 &= \tfrac{32}{5}\pi c_1 a(a+2) = 27.17. \end{aligned} \tag{39}$$

These expressions can now be evaluated by substituting the values of the various constants given in the first column of Table 1. At the same time, we shall set $Z = 1$. The results are finally given in Table 2 and illustrated in Figure 1.

Both from Table 2 and from Figure 1 we can easily see that the results derived from the matrix elements of the dipole moment and of the momentum are practically the same except near the series limit. Wheeler[1] has pointed out that, for $\epsilon = 0.01$, the dipole moment calculated on the basis of the Hartree field is about 5 per cent greater than

TABLE 2

RESULTS OF CALCULATIONS FOR THE GROUND STATE

WAVE LENGTH IN A.U.	K.E. OF FREE ELECTRON IN *Rh* UNIT	ELECTRON NUMBER df/dE DERIVED FROM			CONTINUOUS ATOMIC ABSORPTION COEFFICIENT IN 10^{-18} CM^2 DERIVED FROM		
		Dipole Moment	Momentum	Acc.	Dipole Moment	Momentum	Acc.
504.3	0	0.9297	0.9701	0.2427	7.456	7.780	1.9465
460	0.1740	.8131	.8329	.2067	6.521	6.680	1.6577
420	0.3627	.6983	.7063	.17287	5.600	5.665	1.3864
380	0.5911	.5806	.5835	.14247	4.656	4.680	1.1426
340	0.8732	.4646	.4646	.11222	3.726	3.726	0.9000
300	1.2306	.3544	.3547	.08455	2.842	2.845	0.6781
260	1.6979	.2578	.2585	.06093	2.068	2.073	0.4887
220	2.335	.17487	.17573	.04088	1.4025	1.4094	0.3279
180	3.256	.10851	.10903	.02488	0.8703	0.8744	0.19954
140	4.702	.05924	.05872	.013042	0.4751	0.4709	0.10460
100	7.306	.02616	.02478	.005313	0.2098	0.19874	0.04261
60	13.381	.007331	.006224	.0012745	0.05879	0.04992	0.010221
20	43.76	0.000374	0.000241	0.0000478	0.00300	0.00194	0.000383
Integrated f-value for the continuum		1.504	1.495				

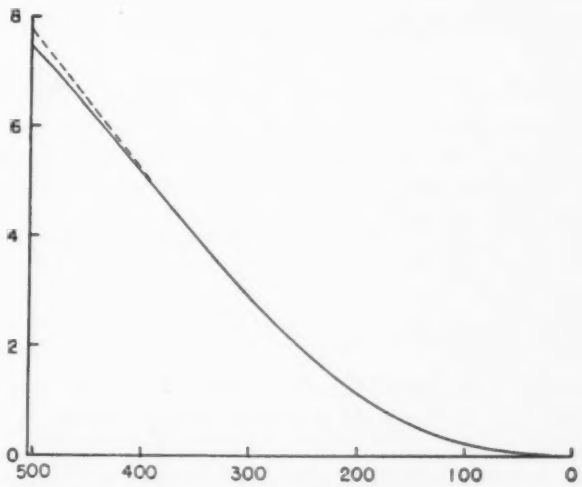

FIG. 1.—The continuous atomic absorption coefficient in units of 10^{-18} cm^2 is plotted against the corresponding wave length in A.U. for the ground state. The full line represents the result derived from the matrix element of the dipole moment, while the broken line represents that of the momentum.

that from the Coulomb field. This also confirms the theory that the matrix element of momentum gives a more reliable result for the cross-section.

However, it will be noticed that the cross-sections derived from the acceleration are much too small, compared with those derived from the momentum and the dipole moment. This is not surprising when it is realized that the main contribution to the acceleration integral comes from near the origin and that here an effective charge of 1 is evidently unsuitable. Later computation on the two metastable states confirms this point, so that we may conclude that the matrix element of the acceleration cannot be used in the present case with the approximation of a Coulomb field. It is reasonable to suppose that the cross-sections derived from the three kinds of matrix elements will be in better agreement when the calculations are repeated with Hartree fields.

VI. THE COMPUTATION OF CROSS-SECTIONS FOR THE METASTABLE STATES

Owing to the similarity between the wave functions of these two states, we shall consider these two cases together. The matrix elements in the present case can be derived from equations (9) and (12), exactly as in the case of the ground state. Hence, as in equation (25), we have

$$M_d^2 = \gamma_2 I_d^2 , \qquad M_m^2 = \gamma_2 I_m^2 , \qquad M_a^2 = \gamma_2 I_a^2 , \tag{40}$$

where

$$\gamma_2 = \frac{32}{9} \frac{\pi^2 C_i^2}{Z(Z^2+\epsilon)(1 - e^{-2\pi Z/\sqrt{\epsilon}})} , \tag{41}$$

with $C_i = C_2$ for the 2^3S state and $C_i = C_3$ for the 2^1S state.

The evaluation of the various matrix elements is much more tedious than in the case of the ground state, as the wave function for the bound state is of a much more complicated form. For example, for the z component of the dipole moment we first calculate

$$\int\int \Psi_1^*(z_1 + z_2)\Phi(1, 2)\, d\tau_1 d\tau_2 \tag{42}$$

and get the result,

$$\int\int \Psi_1^*(z_1 + z_2)\Phi(2, 1)\, d\tau_1 d\tau_2 , \tag{43}$$

from the final expression (42) by interchanging a and b and changing the signs before the coefficients c_3 and c_6. Twice the value obtained from subtraction (for the orthostate) or addition (for the parastate) of expressions (42) and (43) gives the total value of the z component of the matrix element of the dipole moment.

A similar process can be carried out for the matrix element of the momentum and the acceleration. Omitting all the details of these rather elaborate calculations, we shall give only the final results.

All the following equations (eqs. [44]–[55]) are valid for both the metastable states. Thus for the integral of the dipole moment we have:

$$\begin{aligned}
I_d = {} & 2A_0(b+Z)L_0(\epsilon, b) - 2A_1[(b^2+\epsilon) + 2Z(b+Z)]L_1(\epsilon, b) \\
& + 16A_3Z(Z^2+\epsilon)(2b-Z)L_3(\epsilon, b) + 32A_4Z(Z^2+\epsilon)[5b(b-Z) + (Z^2-\epsilon)] \\
& \times L_4(\epsilon, b) + 32A_5Z(Z^2+\epsilon)[30b^3 - 45Zb^2 + 18(Z^2-\epsilon)b + Z(7\epsilon - 2Z^2)] \\
& \times L_5(\epsilon, b) - 2B_0(a+Z)L_0(\epsilon, a) + 2B_1[(a^2+\epsilon) + 2Z(a+Z)]L_1(\epsilon, a) \\
& - 16B_3Z(Z^2+\epsilon)(2a-Z)L_3(\epsilon, a) - 32B_4Z(Z^2+\epsilon)[5a(a-Z) + (Z^2-\epsilon)] \\
& \times L_4(\epsilon, a) - 32B_5Z(Z^2+\epsilon)[30a^3 - 45Za^2 + 18(Z^2-\epsilon)a + Z(7\epsilon - 2Z^2)] \\
& \times L_5(\epsilon, a) + 2C_0(a+b+2+Z)L_0(\epsilon, a+b+2) - 2C_1[(a+b+2)^2 \\
& + \epsilon + 2Z(a+b+2+Z)]L_1(\epsilon, a+b+2) + 8C_2Z(Z^2+\epsilon)L_2(\epsilon, a+b+2) \\
& + 16C_3Z(Z^2+\epsilon)[2(a+b+2) - Z]L_3(\epsilon, a+b+2) + 32C_4Z(Z^2+\epsilon) \\
& \times [5(a+b+2)(a+b+2-Z) + (Z^2-\epsilon)]L_4(\epsilon, a+b+2),
\end{aligned} \tag{44}$$

where

$$A_0=\frac{144c_4a}{(a+2)^7}+\frac{1008(c_5-c_6)a^2}{(a+2)^8},\qquad A_1=\frac{144(c_5+c_6)a^2}{(a+2)^7},$$

$$A_3=\frac{6c_1}{(a+2)^3}+\frac{18(c_2-c_3)a}{(a+2)^4},$$

$$A_4=\frac{6(c_2+c_3+c_4)a}{(a+2)^3}+\frac{18(c_5-c_6)a^2}{(a+2)^4},\qquad A_5=\frac{6(c_5+c_6)a^2}{(a+2)^3};$$

$$B_0=\pm\left[\frac{144c_4a}{(b+2)^7}+\frac{1008(c_5+c_6)a^2}{(b+2)^8}\right],\qquad B_1=\pm\frac{144(c_5-c_6)a^2}{(b+2)^7},$$

$$B_3=\pm\left[\frac{6c_1}{(b+2)^3}+\frac{18(c_2+c_3)a}{(b+2)^4}\right],$$

$$B_4=\pm\left[\frac{6(c_2-c_3+c_4)a}{(b+2)^3}+\frac{18(c_5+c_6)a^2}{(b+2)^4}\right],\qquad B_5=\pm\frac{6(c_5-c_6)a^2}{(b+2)^3};\tag{45}$$

$$C_0=B_0-A_0,$$

$$C_1=\pm\left[\frac{144c_4a}{(b+2)^6}+\frac{288(4c_5+3c_6)a^2}{(b+2)^7}\right]-\left[\frac{144c_4a}{(a+2)^6}+\frac{288(4c_5-3c_6)a^2}{(a+2)^7}\right],$$

$$C_2=\pm\left[\frac{72c_4a}{(b+2)^5}+\frac{72(9c_5+5c_6)a^2}{(b+2)^6}\right]-\left[\frac{72c_4a}{(a+2)^5}+\frac{72(9c_5-5c_6)a^2}{(a+2)^6}\right],$$

$$C_3=\pm\left[\frac{12c_4a}{(b+2)^4}+\frac{48(4c_5+c_6)a^2}{(b+2)^5}\right]-\left[\frac{12c_4a}{(a+2)^4}+\frac{48(4c_5-c_6)a^2}{(a+2)^5}\right],$$

$$C_4=\pm\frac{24c_5a^2}{(b+2)^4}-\frac{24c_5a^2}{(a+2)^4}.$$

In these and all the following equations the upper signs are always to be associated with the 2^3S state, while the lower signs are to be associated with the 2^1S state.

From an even longer calculation we can get

$$\begin{aligned}I_m=&\,2D_0(b+Z)L_0(\epsilon,b)-2D_1[(b^2+\epsilon)+2Z(b+Z)]L_1(\epsilon,b)\\&+8D_2Z(Z^2+\epsilon)L_2(\epsilon,b)+16D_3Z(Z^2+\epsilon)(2b-Z)L_3(\epsilon,b)+32D_4Z(Z^2+\epsilon)\\&\times[5b(b-Z)+(Z^2-\epsilon)]L_4(\epsilon,b)-2E_0(a+Z)L_0(\epsilon,a)+2E_1[(a^2+\epsilon)\\&+2Z(a+Z)]L_1(\epsilon,a)-8E_2Z(Z^2+\epsilon)L_2(\epsilon,a)-16E_3Z(Z^2+\epsilon)(2a-Z)\\&\times L_3(\epsilon,a)-32E_4Z(Z^2+\epsilon)[5a(a-Z)+(Z^2-\epsilon)]L_4(\epsilon,a)+2F_0\\&\times(a+b+2+Z)L_0(\epsilon,a+b+2)-2F_1[(a+b+2)^2+\epsilon+2Z\\&\times(a+b+2+Z)]L_1(\epsilon,a+b+2)+8F_2Z(Z^2+\epsilon)L_2(\epsilon,a+b+2)\\&+16F_3Z(Z^2+\epsilon)[2(a+b+2)-Z]L_3(\epsilon,a+b+2).\end{aligned}\tag{46}$$

The constants occurring in equation (46) are given below:

$$D_0=\frac{24ac_4a}{(a+2)^6}+\frac{(120a-48)(c_5-c_6)a^2}{(a+2)^7},$$

$$D_1=\frac{24bc_4a}{(a+2)^5}+\frac{24\{5b(c_5-c_6)-2(c_5+c_6)\}a^2}{(a+2)^6},$$

$$D_2=\frac{6\{bc_1-(c_2+c_3)a\}}{(a+2)^3}+\frac{6\{3b(c_2-c_3)-ac_4\}a}{(a+2)^4}$$
$$+\frac{6\{4b(c_5+c_6)+(2-3a)(c_5-c_6)\}a^2}{(a+2)^5},$$

$$D_3=\frac{6b(c_2+c_3+c_4)a}{(a+2)^3}+\frac{6\{3b(c_5-c_6)-2(a+1)(c_5+c_6)\}a^2}{(a+2)^4},$$

$$D_4=\frac{6b(c_5+c_6)a^2}{(a+2)^3};$$

$$E_0=\pm\left[\frac{24bc_4a}{(b+2)^6}+\frac{(120b-48)(c_5+c_6)a^2}{(b+2)^7}\right],$$

$$E_1=\pm\left[\frac{24ac_4a}{(b+2)^5}+\frac{24\{5a(c_5+c_6)-2(c_5-c_6)\}a^2}{(b+2)^6}\right],$$

$$E_2=\pm\left[\frac{6\{ac_1-(c_2-c_3)a\}}{(b+2)^3}+\frac{6\{3a(c_2+c_3)-bc_4\}a}{(b+2)^4}\right.$$
$$\left.+\frac{6\{4a(c_5-c_6)+(2-3b)(c_5+c_6)\}a^2}{(b+2)^5}\right], \tag{47}$$

$$E_3=\pm\left[\frac{6a(c_2-c_3+c_4)a}{(b+2)^3}+\frac{6\{3a(c_5+c_6)-2(b+1)(c_5-c_6)\}a^2}{(b+2)^4}\right],$$

$$E_4=\pm\frac{6a(c_5-c_6)a^2}{(b+2)^3};$$

$$F_0=E_0-D_0,$$

$$F_1=\left[-\frac{24(a+b)c_4a}{(a+2)^5}+\frac{\{96c_5-120(a+b)(c_5-c_6)\}a^2}{(a+2)^6}\right]$$
$$\mp\left[-\frac{24(a+b)c_4a}{(b+2)^5}+\frac{\{96c_5-120(a+b)(c_5+c_6)\}a^2}{(b+2)^6}\right],$$

$$F_2=\left[-\frac{6(a+b)c_4a}{(a+2)^4}+\frac{6\{4c_5-(3a+4b)(c_5+c_6)-(7a+8b)(c_5-c_6)\}a^2}{(a+2)^5}\right]$$
$$\mp\left[-\frac{6(a+b)c_4a}{(b+2)^4}+\frac{6\{4c_5-(3b+4a)(c_5-c_6)-(7b+8a)(c_5+c_6)\}a^2}{(b+2)^5}\right],$$

$$F_3=\pm\frac{12(a+b)c_5a^2}{(b+2)^4}-\frac{12(a+b)c_5a^2}{(a+2)^4}.$$

It is easy to show that, as in the case of the ground state, the sum of residues at infinity of the integrals vanish for both I_d and I_m. However, this is not the case for I_a, and the final expression consists of three groups of terms: the first group comes from the residues at finite points; the second group comes from residues at infinity; and the third group consists of those terms which require numerical integrations. Thus

$$I_a = I_a^{(1)} + I_a^{(2)} + I_a^{(3)}, \tag{48}$$

where

$$\begin{aligned} I_a^{(1)} = {} & -G_{-1}L_{-1}(\epsilon, b) + 2G_0(b+Z)L_0(\epsilon, b) - 2G_1[(b^2+\epsilon) + 2Z(b+Z)] \\ & \times L_1(\epsilon, b) + 8G_2Z(Z^2+\epsilon)L_2(\epsilon, b) + 16G_3Z(Z^2+\epsilon)(2b-Z)L_3(\epsilon, b) \\ & + H_{-1}L_{-1}(\epsilon, a) - 2H_0(a+Z)L_0(\epsilon, a) + 2H_1[(a^2+\epsilon) + 2Z(a+Z)] \\ & \times L_1(\epsilon, a) - 8H_2Z(Z^2+\epsilon)L_2(\epsilon, a) - 16H_3Z(Z^2+\epsilon)(2a-Z)L_3(\epsilon, a) \\ & - K_{-1}L_{-1}(\epsilon, a+b+2) + 2K_0(a+b+2+Z)L_0(\epsilon, a+b+2) - 2K_1 \\ & \times [(a+b+2)^2+\epsilon+2Z(a+b+2+Z)]L_1(\epsilon, a+b+2) + 8K_2Z(Z^2+\epsilon) \\ & \times L_2(\epsilon, a+b+2) + 16K_3Z(Z^2+\epsilon)[2(a+b+2)-Z]L_3(\epsilon, a+b+2) \\ & + 32K_4Z(Z^2+\epsilon)[5(a+b+2)(a+b+2-Z) + (Z^2-\epsilon)]L_4(\epsilon, a+b+2); \end{aligned} \tag{49}$$

$$\begin{aligned} I_a^{(2)} = {} & G_{-1}[2(a+2)Z - (a+b+2)^2 + b^2] - H_{-1}[2(b+2)Z - (a+b+2)^2 \\ & + a^2] + 2G_0(Z-b) - 2H_0(Z-a) + 2K_0[Z - (a+b+2)] \\ & + 2(G_1 - H_1 + K_1); \end{aligned} \tag{50}$$

and

$$\begin{aligned} I_a^{(3)} = {} & \frac{32c_4aZ(Z^2+\epsilon)}{5}[(a+2)\mathfrak{I}_1(\epsilon; a+b+2, b) \mp (b+2)\mathfrak{I}_1(\epsilon; a+b+2, a)] \\ & + \frac{32a^2Z(Z^2+\epsilon)}{5}[(c_5+c_6)(a+2)\mathfrak{I}_2(\epsilon; a+b+2, b) \\ & \mp (c_5-c_6)(b+2)\mathfrak{I}_2(\epsilon; a+b+2, a)] \\ & + \frac{32a^2Z(Z^2+\epsilon)}{5}[(c_5-c_6)\mathfrak{I}_3(\epsilon; a+b+2, b) \mp (c_5+c_6)\mathfrak{I}_3(\epsilon; a+b+2, a)], \end{aligned} \tag{51}$$

while $\mathfrak{I}_1$, $\mathfrak{I}_2$, and $\mathfrak{I}_3$ are defined as

$$\mathfrak{I}_1(\epsilon; \lambda, \rho) = \int_\lambda^\infty \frac{dy}{(y-\rho)^2}[5y(y-Z) + (Z^2-\epsilon)]L_4(\epsilon, y), \tag{52}$$

$$\mathfrak{I}_2(\epsilon; \lambda, \rho) = \int_\lambda^\infty \frac{dy}{(y-\rho)^2}[30y^3 - 45Zy^2 + 18(Z^2-\epsilon)y + Z(7\epsilon - 2Z)]L_5(\epsilon, y), \tag{53}$$

and

$$\mathfrak{I}_3(\epsilon; \lambda, \rho) = \int_\lambda^\infty \frac{dy}{(y-\rho)}[30y^3 - 45Zy^2 + 18(Z^2-\epsilon)y + Z(7\epsilon - 2Z)]L_5(\epsilon, y). \tag{54}$$

The constants occurring in these expressions are given below:

$$G_{-1}=\frac{24c_4a}{(a+2)^5}+\frac{120(c_5-c_6)a^2}{(a+2)^6},$$

$$G_0=\frac{6c_1}{(a+2)^3}+\frac{6\{15(c_2-c_3)+c_4\}a}{5(a+2)^4}+\frac{(144c_5+96c_6)a^2}{5(a+2)^5},$$

$$G_1=\frac{6(c_2+c_3+c_4)a}{(a+2)^3}+\frac{(96c_5-84c_6)a^2}{5(a+2)^4},$$

$$G_2=-\frac{c_4a}{(a+2)^2}+\frac{4(c_5+2c_6)a^2}{(a+2)^3},\qquad G_3=-\frac{(c_5+c_6)a^2}{(a+2)^2};$$

$$H_{-1}=\pm\left[\frac{24c_4a}{(b+2)^5}+\frac{120(c_5+c_6)a^2}{(b+2)^6}\right],$$

$$H_0=\pm\left[\frac{6c_1}{(b+2)^3}+\frac{6\{15(c_2+c_3)+c_4\}a}{5(b+2)^4}+\frac{(144c_5-96c_6)a^2}{5(b+2)^5}\right],$$

$$H_1=\pm\left[\frac{6(c_2-c_3+c_4)a}{(b+2)^3}+\frac{(96c_5+84c_6)a^2}{5(b+2)^4}\right],$$

$$H_2=\pm\left[-\frac{c_4a}{(b+2)^2}+\frac{4(c_5-2c_6)a^2}{(b+2)^3}\right],\qquad H_3=\mp\frac{(c_5-c_6)a^2}{(b+2)^2};\tag{55}$$

$$K_{-1}=H_{-1}-G_{-1},$$

$$K_0=\pm\frac{1}{5}\left[\frac{36c_4a}{(b+2)^4}+\frac{(384c_5+144c_6)a^2}{(b+2)^5}\right]$$
$$-\frac{1}{5}\left[\frac{36c_4a}{(a+2)^4}+\frac{(384c_5-144c_6)a^2}{(a+2)^5}\right],$$

$$K_1=\pm\frac{6}{5}\left[\frac{c_4a}{(b+2)^3}+\frac{3(5c_5+c_6)a^2}{(b+2)^4}\right]$$
$$-\frac{6}{5}\left[\frac{c_4a}{(a+2)^3}+\frac{3(5c_5-c_6)a^2}{(a+2)^4}\right],$$

$$K_2=\pm\frac{2}{5}\left[-\frac{c_4a}{(b+2)^2}+\frac{2(2c_5-c_6)a^2}{(b+2)^3}\right]$$
$$-\frac{2}{5}\left[-\frac{c_4a}{(a+2)^2}+\frac{2(2c_5+c_6)a^2}{(a+2)^3}\right],$$

$$K_3=\pm\frac{1}{5}\left[\frac{c_4a}{(b+2)}-\frac{(3c_5-c_6)a^2}{(b+2)^2}\right]-\frac{1}{5}\left[\frac{c_4a}{(a+2)}-\frac{(3c_5+c_6)a^2}{(a+2)^2}\right],$$

$$K_4=\pm\frac{2c_5a^2}{5(b+2)}-\frac{2c_5a^2}{5(a+2)}.$$

Although the expressions are very similar for these two states, the numerical values are, of course, different. The constants to be used for the 2^3S state are given in the second column of Table 1, and those for the 2^1S state are given in the third column. Substituting

these values of constants in expressions (45), (47), and (55), we can compute the numerical values for various coefficients of equations (44), (46), and (48). These numerical values are given for both states in Table 3.

TABLE 3

NUMERICAL VALUES OF CONSTANTS OCCURRING IN EXPRESSIONS FOR THREE KINDS OF MATRIX ELEMENTS

	2^3S	2^1S		2^3S	2^1S		2^3S	2^1S
A_0	−0.003352	+0.0003660	B_0	−0.02175	−0.005691	C_0	−0.018398	−0.006057
A_1	+ .0002540	− .0003096	B_1	− .02405	+ .009716	C_1	− .06731	− .006308
						C_2	− .10967	+ .004194
A_3	+ .08691	+ .08748	B_3	− .2620	− .05246	C_3	− .08249	+ .03922
A_4	− .16236	− .05519	B_4	− .06175	− .03268	C_4	− .02234	+ .02926
A_5	+ .002979	− .003623	B_5	− .04640	+ .018727			
D_0	− .003742	+ .0009495	E_0	− .008960	− .005402	F_0	− .005218	− .006352
D_1	− .005202	+ .0013870	E_1	− .04168	− .03519	F_1	− .04453	− .05455
D_2	+ .2008	+ .11168	E_2	− .5869	− .07487	F_2	− .07556	+ .009621
D_3	− .10330	− .02808	E_3	− .07220	− .09154	F_3	− .03021	+ .03952
D_4	+ .0018128	− .002203	E_4	− .09726	+ .03921			
G_{-1}	− .007979	+ .0015864	H_{-1}	− .02987	− .012770	K_{-1}	− .02189	− .014356
G_0	+ .08613	+ .08700	H_0	− .2935	− .04352	K_0	− .03481	+ .006512
G_1	− .16222	− .05537	H_1	− .06531	− .03125	K_1	− .019810	+ .009257
G_2	+ .019830	− .010579	H_2	− .018547	+ .03518	K_2	− .000770	+ .017603
G_3	−0.002034	+0.002472	H_3	+0.02017	−0.008140	K_3	+0.000234	− .02416
						K_4	−0.002874	+0.012155

The final results for the cross-sections and the electron number are given in Tables 4 and 5 and illustrated in Figures 2 and 3, respectively, for these two states. For reasons already given, we shall not present the calculation for the acceleration integral.

TABLE 4

RESULTS OF CALCULATIONS FOR THE 2^3S STATE

WAVE LENGTH IN A.U.	K.E. OF FREE ELECTRON IN *Rh* UNIT	ELECTRON NUMBER df/dE DERIVED FROM		CONTINUOUS ATOMIC ABSORPTION COEFFICIENT IN 10^{-18}CM^2 DERIVED FROM	
		Dipole Moment	Momentum	Dipole Moment	Momentum
2600.7	0	0.3694	0.3309	2.963	2.654
1737.8	0.1740	.2973	.2678	2.384	2.148
1277.9	0.3627	.2030	.18897	1.6281	1.5155
967.9	0.5911	.13179	.12489	1.0570	1.0016
744.8	0.8732	.08357	.08080	0.6702	0.6480
576.4	1.2306	.05172	.04585	0.4148	0.3677
445.0	1.6979	.03131	.02759	0.2511	0.2213
339.3	2.335	.018009	.015627	0.14443	0.12533
252.7	3.256	.009643	.008102	0.07734	0.06498
180.38	4.702	.004545	.003650	0.03645	0.02927
119.02	7.306	.0016459	.0012795	0.013200	0.010262
66.37	13.381	.0003939	.0002614	0.003159	0.002096
20.66	43.76	0.00001479	0.000007896	0.0001186	0.00006333
Integrated f-value for the continuum		0.265	0.238		

TABLE 5

RESULTS OF CALCULATIONS FOR THE 2^1S STATE

WAVE LENGTH IN A.U.	K.E. OF FREE ELECTRON IN *Rh* UNIT	ELECTRON NUMBER df/dE DERIVED FROM		CONTINUOUS ATOMIC ABSORPTION COEFFICIENT IN 10^{-18} CM^2 DERIVED FROM	
		Dipole Moment	Momentum	Dipole Moment	Momentum
3122	0.	1.2780	1.3344	10.250	10.702
1955.9	0.1740	0.5996	0.6034	4.809	4.839
1392.1	0.3627	0.3044	0.3116	2.441	2.499
1032.0	0.5911	0.15949	0.16877	1.2791	1.3535
782.1	0.8732	0.08529	0.09365	0.6840	0.7511
598.5	1.2306	0.04611	0.05226	0.3698	0.4191
458.0	1.6979	0.02504	0.02896	0.2008	0.2323
346.9	2.335	0.013396	0.015502	0.10744	0.12433
256.8	3.256	0.006838	0.007720	0.05484	0.06191
182.47	4.702	0.003162	0.003398	0.02536	0.02725
119.94	7.306	0.0011758	0.0011753	0.009430	0.009430
66.65	13.381	0.0002622	0.0002400	0.002103	0.0019248
20.69	43.76	0.00000959	0.00000745	0.0000769	0.0000597
Integrated f-value for the continuum		0.398	0.407		

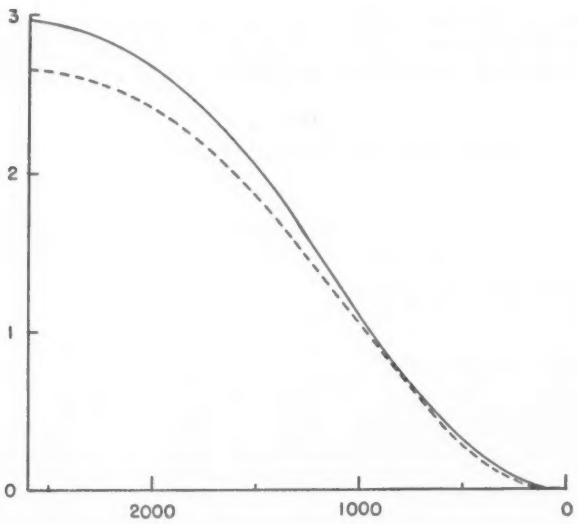

FIG. 2.—The continuous atomic absorption coefficient in units of 10^{-18} cm^2 is plotted against the corresponding wave length in A.U. for the 2^2S state. The full line represents the result derived from the matrix element of the dipole moment, while the broken line represents that of the momentum.

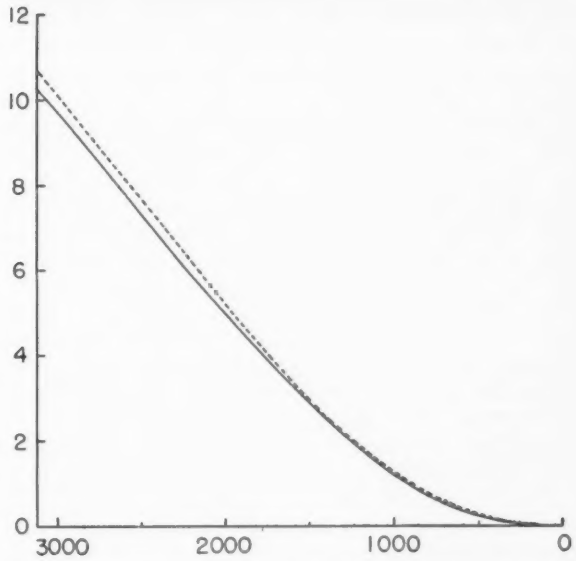

FIG. 3.—The continuous atomic absorption coefficient in units of 10^{-18} cm^2 is plotted against the corresponding wave length in A.U. for the 2^1S state. The full line represents the result derived from the matrix element of the dipole moment, while the broken line represents that of the momentum.

TABLE 6

THE f-VALUES FOR DISCRETE TRANSITIONS

	1^1S–n^1P	2^3S–n^3P	2^1S–n^1P
$n=2$	0.3555	0.5592	0.3918
3	0.0722	0.0520	0.1499
4	0.0282	0.0307	0.0618
5	0.0144	0.0129	0.0245
6	0.0082	0.0067	0.0123
$\sum_{n=7}^{\infty} f_n$ (estimated)	0.028	0.044	0.030
$\sum_{n=2}^{\infty} f_n$	0.507	0.706	0.670
Double jump	0.04		
f-value for continuum	1.504 (dipole) 1.495 (momen.)	0.265 (dipole) 0.238 (momen.)	0.398 (dipole) 0.407 (momen.)
Sum	2.05 (dipole) 2.04 (momen.)	0.97 (dipole) 0.94 (momen.)	1.07 (dipole) 1.08 (momen.)

VII. THE f-SUM RULE[15] AND SOME RELATED REMARKS

Finally, we shall consider the sum rule of Reiche, Kuhn, and Thomas. The total f-values for the three continua have been found by numerical integrations. They are given in the corresponding tables (2, 4, and 5). These values can be used to check the f-sum rules. The f-values for the discrete transitions have been computed by Hylleraas,[16] Goldberg,[8] and Vinti,[17] and it is expected that more systematic results will soon be given by Romberg.[6] Although the values for the individual lines obtained by these authors disagree, the total f-value for the discrete states, as evaluated by them, almost agree. Here we shall take Hylleraas' results for comparison. His results are given in Table 6. The f-value of the double jump from the ground state in this table is taken from Vinti's work.[17] The total f-values for the discrete states in these three cases have been estimated by applying the $1/n^3$ rule[18] to the computed values. When the f-values found in this paper for the continua are added to the respective sums for the discrete states, we find that the f-sum rule is approximately satisfied. For the ground state, the integrated f-value for the continuum is found to be 1.58 by Wheeler,[1] and 1.55 by Vinti.[2] For the two metastable states, the estimated f-values for the continuum are obtained by Goldberg[8] by extending the expression for the discrete f-value to the continuum according to the method given by Menzel and Pekeris.[19] Goldberg's values are 0.163 for the 2^3S state and 0.297 for the 2^1S state; these have to be contrasted with the values 0.27 and 0.40, respectively, obtained in the present investigation. Hence our results fulfil the f-sum rule more closely.

Summarizing, we can conclude that the wave functions derived from the Ritz principle for bound states and the hydrogenic wave function for the free state represent a good model for a great part of the configuration space. We conclude this from the agreement of the cross-sections derived from matrix elements of the dipole moment and of the momentum. The hydrogenic approximation for the free state, as seen from the failure of the acceleration integral, evidently cannot be applied to the region very near to the nucleus.

I wish to express my sincere thanks to Professor S. Chandrasekhar for his suggestion of this problem and also for his guidance.

[15] W. Kuhn, *Zs. f. Phys.*, **33**, 408, 1925.

[16] *Zs. f. Phys.*, **106**, 395, 1937.

[17] *Phys. Rev.*, **42**, 632, 1932.

[18] D. R. Hartree, *Proc. Cambridge Phil. Soc.*, **24**, 426, 1928.

[19] *M.N.*, **96**, 77, 1935.

A STELLAR MODEL FOR RED GIANTS OF HIGH CENTRAL TEMPERATURE

ROBERT S. RICHARDSON AND MARTIN SCHWARZSCHILD
Mount Wilson and Palomar Observatories
and Princeton University Observatory
Received August 10, 1948

ABSTRACT

The assumption is made that the turbulence in the convective core of a red giant emits acoustical noise of such strength that the entire energy flux is carried solely by the noise through the layers surrounding the core. According to this assumption, a stellar model is computed which consists of a convective core, an isothermal zone, and a radiative envelope. It is found that a star built according to this model may have a central temperature high enough for the carbon cycle to operate and have simultaneously a radius as large as that of the biggest red giant.

I. INTRODUCTION

In the theory of stellar structure the red giants present the following problem: Any stellar model based on the classical equilibrium conditions can be made to fit a late-type giant in mass and radius. But the central temperature thus derived comes out so low that no known process can convert hydrogen into heavier elements at a sufficient rate to produce the high luminosity of a giant.

To avoid this difficulty, one might assume that the red giants use not hydrogen but other light elements, such as lithium, for their basic fuel.[1] For such elements nuclear processes are known which give a high rate of energy production even at rather low temperatures. But if these elements are used instead of hydrogen as basic fuel, a giant has a total store of energy sufficient only for a short life. The assumption of a short life for red giants appears to be in discordance with their large number in our galaxy in general and in the globular clusters in particular. On the other hand, it seems unlikely that unknown processes exist which can convert hydrogen into heavier elements at high rates at low temperatures.

Therefore, one is led to assume that the models based on the classic equilibrium conditions do not apply to the red giants. Hence one might search for a new physical mechanism which would change basically one of the equilibrium conditions in at least a portion of a red giant. In this investigation a model is constructed under the assumption that the classic hydrostatic equilibrium condition holds throughout a red giant but that the thermal equilibrium, which in classic models is either radiative or convective, is isothermal throughout a certain zone in a red giant. The physical reason for this assumption is described in the following section.

II. POSSIBLE EXISTENCE OF NOISE ZONE

Nuclear processes, such as the carbon cycle, are so highly temperature dependent that the energy source in a star must be strongly concentrated toward the center. This produces a high energy flux per square centimeter, which, in turn, leads to thermal instability and turbulence. Therefore, the core of a star is generally believed to be in convective, rather than radiative, equilibrium.

The turbulence in the core will produce a field of compression waves, each individual wave being essentially caused by the acceleration or deceleration of a turbulent element. Although these acoustical waves travel in random directions, the preferential direction

[1] G. Gamow and E. Teller, *Phys. Rev.*, **55**, 791, 1939.

will be outward, since the basic force driving the turbulence is directed outward. Each wave progresses with the velocity of sound, carrying its mechanical energy with it. Hence the field of noise consisting of the sum of all the compression waves will present a net flux of energy outward. Under favorable circumstances the turbulence might produce so much noise that its mechanical energy flux is of the same order as the total energy flux produced by the nuclear processes. Under such conditions, the energy transport by noise cannot be neglected in comparison with radiative or convective transport.

The essential assumption made in this investigation is that the turbulence in the convective core of a red giant produces so much noise that, at a certain critical distance from the center, the energy flux of the noise is equal to the rate of nuclear energy production. For the layers just outside this critical distance the above assumption leads to an isothermal condition. If the temperature gradient in these layers were not zero, radiative or even convective energy transport would occur in addition to the noise flux, so that the total energy flux would differ from the energy production. This, in turn, would lead to temperature changes and to a general resettling of the interior of the star until isothermal conditions were established in the noise zone. In the isothermal layer no turbulence can exist because of lack of any driving force, and hence no additional noise will be emitted. Therefore, the noise flux remains constant until, farther out, the noise starts to be dissipated into thermal energy. There radiation will take over and transport the energy to the surface.

Thus the essential assumption here made leads to a model consisting of three parts: (1) a central convective core, in which the energy transport is by convection and the temperature gradient is adiabatic; (2) an isothermal zone, in which the noise provides the energy flux and the temperature gradient is zero; and, finally, (3) a radiative envelope in which the energy transport is by radiation and the temperature gradient is governed by the radiation transfer law. The transition from the adiabatic to the isothermal temperature gradient will probably be rather sharp, since, as long as convection has to carry any part of the energy flux, the temperature gradient must be nearly adiabatic. On the other hand, the transition from the isothermal to the radiative temperature gradient may actually be fairly gradual, since the noise dissipation may occur in a layer of appreciable depth. However, the simplifying assumption of a sharp transition does not appear likely to distort essential features of the model.

It is difficult to decide at present whether the basic assumption discussed above is physically tenable. If the noise is to carry the entire energy flux in the isothermal zone, the acoustic velocity oscillations of the material must be of the order of 0.01 km/sec. This may appear small compared with the thermal velocity and the sound velocity, which are approximately 200 km/sec. But, even to produce noise of such small velocity oscillation, the turbulent velocities would probably have to be of the order of 3 km/sec. (This estimate is based on the assumption that the noise emission of a turbulent element is comparable to that of an oscillating solid sphere.) On the other hand, the usual considerations regarding the turbulence in convective cores predict turbulent velocities only of the order of 0.3 km/sec.

This discrepancy is too small to be taken as a proof against the basic assumption made in this investigation, since the theory of turbulence applied to the stellar interior is still very uncertain. However, the above considerations show that the assumption of an isothermal noise zone is at present speculative and that the model based on this assumption will have to be checked by a detailed comparison of its characteristics with the observable features of red giants.

III. CONSTRUCTION OF MODEL

According to the discussion of the preceding section, the model to be computed consists of a convective core, an isothermal zone, and a radiative envelope. To simplify the computations, the following approximations are used: (*a*) The chemical composition is

constant throughout the star; (*b*) radiation pressure and degeneracy are negligible; (*c*) in the convective core, $\gamma = \frac{5}{3}$; (*d*) in the radiative envelope the absorption coefficient is given by a simple power law representing approximately the absorption coefficient of the Russell mixture; and (*e*) the entire energy generation from nuclear sources occurs within the convective core.

In the convective core the equilibrium conditions correspond to the polytropic equation of index 1.5. For this equation the particular solution, which has no singularity at the center, is available in tabular form.[2] For the radiative envelope and the isothermal zone, the necessary solutions had to be derived by numerical integration.

The integrations were performed in terms of nondimensional variables. The definition of these variables and the differential equations used are tabulated in the appendix. The differential equations of the radiative envelope in their nondimensional form have a one-parameter family of solutions. The same is true for the isothermal zone. To obtain a reasonable representation of all possible cases, four particular solutions were derived for the radiative envelope and two for the isothermal zone. These solutions are given in Tables 1 and 2. The integrations were performed with one more decimal place than is reproduced in the tables. The inner parts of the solutions for the radiative envelope were computed with steps half as large as those given in Table 1.

To assemble a consistent solution for the complete star, the solutions of the three parts of the star must be fitted together, so that all the physical variables are continuous at the two interfaces.

It is convenient for the fitting process to introduce the homology-invariant quantities U and V, defined in the Appendix.[3] For any particular solution these quantities are definite functions of the distance from the center. Hence in the U-V plane each particular solution is represented by a curve, as shown in Figure 1. U-V–curves were drawn corresponding to five solutions for radiative envelopes (four from Table 1 and one computed earlier for a main-sequence model[4]), three solutions for isothermal zones (two from Table 2 and one for an isothermal core computed by Wares[5]), and the solution for the convective core. Since U and V are direct functions of the physical variables, they must also be continuous at the interfaces. The assembled solution for a complete star is represented by a continuous curve in the U-V plane. In particular a solution for the model here considered is represented by a curve that starts at the point corresponding to the center ($U = 3$, $V = 0$), follows the convective solution, switches at an arbitrary point to an isothermal solution, follows this curve, switches at an arbitrary point to a radiative solution, and follows this curve out to the surface.

The arbitrariness in the choice of the two transition points does not reflect an actual physical freedom. It is caused solely by the present lack of knowledge regarding the conditions which determine the point where the noise flux takes over the energy transport and which govern the distance through which the noise can pass without dissipation.

As long as the two limits of the noise zone cannot be determined by physical considerations, the model here considered has a two-parameter family of solutions. This family of solutions may be represented fairly well by six individual complete solutions, which may be assembled from the curves shown in Figure 1. (Cases with very narrow noise zones have not been included here, since they would hardly differ much from main-sequence models.) The first four cases all use the same isothermal solution (with $\xi_1 = 2.0$), but each involves a different one of the four new radiative solutions. For the re-

[2] Brit. Assoc. for the Advancement of Science, *Math. Tables*, Vol. 2 (1932).

[3] Cf. Chandrasekhar, *An Introduction to the Study of Stellar Structure* (Chicago: University of Chicago Press, 1938) chap. iv.

[4] M. Schwarzschild, *Ap. J.*, **104** 203, 1946.

[5] We are greatly indebted to Drs. Chandrasekhar and Wares for making this integration available to us.

TABLE 1

INTEGRATIONS FOR RADIATIVE ENVELOPE

$\log(\frac{1}{x}-1)$	-Log q	$-\frac{d \log q}{d \log(\frac{1}{x}-1)}$	Log t	$\frac{d \log t}{d \log(\frac{1}{x}-1)}$	Log p	$\frac{d \log p}{d \log(\frac{1}{x}-1)}$	U	V
				Log C = -4.0				
-1.00	0.00000	0.0000	-1.67342	1.0000	-5.98806	4.7143	0.0000	51.857
-0.95	.00000	.0000	-1.62342	1.0000	-5.75234	4.7143	.0000	46.730
- .90	.00000	.0000	-1.57342	1.0000	-5.51663	4.7143	.0000	42.161
- .85	.00000	.0000	-1.52342	1.0000	-5.28091	4.7143	.0002	38.089
- .80	.00000	.0000	-1.47342	1.0000	-5.04520	4.7143	.0001	34.459
- .75	.00000	.0000	-1.42342	1.0000	-4.80949	4.7142	.0003	31.224
- .70	.00001	.0001	-1.37342	1.0000	-4.57378	4.7142	.0004	28.341
- .65	.00001	.0001	-1.32342	1.0000	-4.33807	4.7142	.0005	25.772
- .60	.00002	.0002	-1.27342	1.0000	-4.10236	4.7141	.0008	23.482
- .55	.00003	.0002	-1.22342	1.0000	-3.86665	4.7141	.0011	21.440
- .50	.00004	.0004	-1.17342	1.0000	-3.63095	4.7139	.0015	19.621
- .45	.00006	.0006	-1.12342	1.0000	-3.39526	4.7137	.0021	17.999
- .40	.00010	.0009	-1.07343	0.9999	-3.15959	4.7133	.0030	16.553
- .35	.00015	.0013	-1.02344	.9998	-2.92393	4.7128	.0041	15.264
- .30	.00023	.0019	-0.97345	.9997	-2.68831	4.7121	.0057	14.114
- .25	.00035	.0028	- .92347	.9996	-2.45273	4.7111	.0078	13.089
- .20	.00052	.0040	- .87350	.9994	-2.21721	4.7095	.0104	12.174
- .15	.00076	.0058	- .82354	.9990	-1.98179	4.7073	.0139	11.357
- .10	.00111	.0082	- .77360	.9986	-1.74649	4.7042	.0185	10.626
- .05	.00159	.0114	- .72368	.9979	-1.51139	4.6999	.0242	9.9732
.00	.00226	.0157	- .67380	.9971	-1.27654	4.6939	.0314	9.3878
+ .05	.00318	.0213	- .62398	.9959	-1.04203	4.6859	.0402	8.8621
+ .10	.00442	.0285	- .57422	.9943	-0.80799	4.6752	.0512	8.3888
+ .15	.00607	.0377	- .52455	.9922	-0.57457	4.6611	.0644	7.9609
+ .20	.00823	.0491	- .47501	.9895	-0.34195	4.6428	.0802	7.5722
+ .25	.01102	.0633	- .42562	.9859	-0.11038	4.6195	.0988	7.2172
+ .30	.01460	.0804	- .37643	.9813	+0.11989	4.5902	.1207	6.8908
+ .35	.01912	.1008	- .32750	.9757	+0.34853	4.5539	.1459	6.5880
+ .40	.02475	.1249	- .27889	.9687	+0.57515	4.5096	.1746	6.3049
+ .45	.03168	.1528	- .23066	.9603	+0.79933	4.4564	.2070	6.0375
+ .50	.04009	.1846	- .18289	.9501	+1.02062	4.3934	.2430	5.7826
+ .55	.05020	.2203	- .13567	.9382	+1.23849	4.3199	.2824	5.5373
+ .60	.06219	.2597	- .08909	.9244	+1.45242	4.2356	.3249	5.2995
+ .65	.07622	.3023	- .04326	.9087	+1.66187	4.1404	.3700	5.0672
+ .70	.09246	.3475	+ .00174	.8910	+1.86628	4.0347	.4168	4.8396
+ .75	.11100	.3945	+ .04581	.8715	+2.06516	3.9191	.4646	4.6160
+ .80	.13192	.4421	+ .08887	.8503	+2.25805	3.7951	.5122	4.3965
+ .85	.15521	.4891	+ .13082	.8277	+2.44456	3.6641	.5582	4.1817
+ .90	.18080	.5340	+ .17161	.8040	+2.62439	3.5285	.6013	3.9727
+0.95	.20855	.5754	+ .21120	.7994	+2.79736	3.3904	.6400	3.7708
+1.00	.23824	.6117	+ .24955	.7545	+2.96343	3.2524	.6729	3.5776
+1.05	.26961	.6416	+ .28665	.7296	+3.12265	3.1170	.6988	3.3948
+1.10	.30228	.6641	+ .32252	.7052	+3.27522	2.9867	.7168	3.2240
+1.15	.33588	.6781	+ .35719	.6817	+3.42144	2.8638	.7261	3.0665
+1.20	.36995	.6834	+ .39071	.6593	+3.56175	2.7501	.7265	2.9236
+1.25	.40408	.6800	+ .42314	.6384	+3.69663	2.6472	.7183	2.7961
+1.30	.43782	.6683	+ .45458	.6192	+3.82667	2.5563	.7018	2.6844
+1.35	.47078	.6490	+ .48510	.6021	+3.95247	2.4781	.6780	2.5888
+1.40	.50261	.6233	+ .51482	.5870	+4.07470	2.4131	.6480	2.5092
+1.45	.53302	.5924	+ .54384	.5740	+4.19400	2.3612	.6134	2.4450
+1.50	.56179	.5578	+ .57227	.5634	+4.31104	2.3224	.5755	2.3959
+1.55	.58876	.5208	+ .60022	.5550	+4.42645	2.2963	.5355	2.3610
+1.60	.61385	.4826	+ .62780	.5487	+4.54086	2.2822	.4950	2.3395
+1.65	.63705	.4450	+ .65512	.5446	+4.65485	2.2792	.4549	2.3302
+1.70	.65837	.4081	+ .68230	.5426	+4.76897	2.2874	.4162	2.3330
+1.75	.67788	.3729	+ .70942	.5426	+4.88375	2.3051	.3796	2.3461
+1.80	.69570	.3400	+ .73659	.5444	+4.99964	2.3320	.3454	2.3689
+1.85	.71192	.3096	+ .76389	.5481	+5.11708	2.3669	.3139	2.4004
+1.90	.72670	.2818	+ .79143	.5535	+5.23645	2.4092	.2854	2.4395
+1.95	.74015	.2568	+ .81927	.5604	+5.35811	2.4580	.2597	2.4856
+2.00	.75242	.2344	+ .84749	.5686	+5.48235	2.5124	.2366	2.5375
+2.05	.76364	.2146	+ .87615	.5782	+5.60943	2.5716	.2167	2.5946
+2.10	.77392	.1970	+ .90533	.5888	+5.73957	2.6348	.1985	2.6558
+2.15	.78337	.1816	+ .93506	.6004	+5.87296	2.7013	.1828	2.7204
+2.20	0.79211	0.1681	+0.96538	0.6127	+6.00974	2.7702	0.1691	2.7877

TABLE 1 (continued)

$\text{Log}(\frac{1}{x}-1)$	-Log q	$-\frac{d \log q}{d \log(\frac{1}{x}-1)}$	Log t	$\frac{d \log t}{d \log(\frac{1}{x}-1)}$	Log p	$\frac{d \log p}{d \log(\frac{1}{x}-1)}$		V
			Log C = -4.0 (continued)					
+2.25	0.80021	0.1564	+0.99634	0.6257	+6.15001	2.8409	0.1572	2.8569
2.30	.80777	.1462	1.02796	.6391	6.29385	2.9126	.1469	2.9272
2.35	.81485	.1374	1.06026	.6529	6.44128	2.9846	.1380	2.9979
2.40	.82153	.1299	1.09325	.6668	6.59230	3.0564	.1304	3.0686
2.45	.82786	.1235	1.12694	.6807	6.74691	3.1275	.1240	3.1386
2.50	.83390	.1181	1.16131	.6945	6.90503	3.1973	.1184	3.2074
2.55	.83969	.1135	1.19638	.7080	7.06661	3.2654	.1138	3.2746
2.60	.84527	.1097	1.23212	.7213	7.23154	3.3314	.1100	3.3397
2.65	.85068	.1066	1.26850	.7342	7.39970	3.3948	.1069	3.4024
2.70	.85595	.1042	1.30553	.7466	7.57097	3.4556	.1044	3.4625
2.75	.86111	.1024	1.34316	.7585	7.74521	3.5135	.1025	3.5197
2.80	.86619	.1010	1.38136	.7698	7.92227	3.5682	.1012	3.5739
2.85	.87122	.1002	1.42012	.7805	8.10198	3.6196	.1003	3.6248
2.90	.87621	.0997	1.45940	.7905	8.28418	3.6677	.0998	3.6723
2.95	.88120	.0997	1.49916	.7998	8.46869	3.7123	.0998	3.7165
+3.00	0.88619	0.1001	+1.53937	0.8086	+8.65536	3.7535	0.1002	3.7572
			Log C = -4.3					
-1.00	0.00000	0.0000	-1.67342	1.0000	-5.81663	4.7143	0.0000	51.857
-0.95	.00000	.0000	-1.62342	1.0000	-5.58091	4.7143	.0000	46.730
- .90	.00000	.0000	-1.57342	1.0000	-5.34520	4.7143	.0002	42.161
- .85	.00000	.0000	-1.52342	1.0000	-5.10949	4.7143	.0002	38.089
- .80	.00000	.0000	-1.47342	1.0000	-4.87377	4.7143	.0003	34.459
- .75	.00001	.0001	-1.42342	1.0000	-4.63806	4.7142	.0004	31.224
- .70	.00001	.0001	-1.37342	1.0000	-4.40235	4.7142	.0005	28.341
- .65	.00002	.0001	-1.32342	1.0000	-4.16664	4.7142	.0008	25.772
- .60	.00002	.0002	-1.27342	1.0000	-3.93094	4.7141	.0011	23.481
- .55	.00004	.0004	-1.22342	0.9999	-3.69525	4.7139	.0016	21.440
- .50	.00006	.0005	-1.17343	.9999	-3.45956	4.7137	.0022	19.620
- .45	.00010	.0008	-1.12343	.9999	-3.22390	4.7135	.0032	17.998
- .40	.00015	.0013	-1.07344	.9998	-2.98824	4.7130	.0044	16.552
- .35	.00023	.0019	-1.02345	.9997	-2.75260	4.7123	.0062	15.262
- .30	.00034	.0028	-0.97347	.9996	-2.51701	4.7114	.0085	14.112
- .25	.00052	.0041	- .92350	.9995	-2.28147	4.7099	.0115	13.086
- .20	.00077	.0060	- .87353	.9991	-2.04603	4.7077	.0155	12.169
- .15	.00113	.0086	- .82359	.9987	-1.81072	4.7044	.0208	11.350
- .10	.00165	.0121	- .77367	.9980	-1.57560	4.6992	.0278	10.615
- .05	.00237	.0169	- .72379	.9970	-1.34079	4.6927	.0359	9.9581
.00	.00336	.0233	- .67397	.9958	-1.10637	4.6839	.0466	9.3678
+ .05	.00473	.0316	- .62423	.9940	-0.87245	4.6720	.0597	8.8359
+ .10	.00656	.0422	- .57459	.9916	-0.63923	4.6562	.0758	8.3548
+ .15	.00900	.0559	- .52509	.9885	-0.40692	4.6356	.0954	7.9173
+ .20	.01220	.0728	- .47576	.9845	-0.17578	4.6086	.1188	7.5165
+ .25	.01635	.0937	- .42667	.9792	+0.05382	4.5743	.1464	7.1466
+ .30	.02164	.1189	- .37787	.9726	+0.28149	4.5314	.1785	6.8024
+ .35	.02832	.1490	- .32944	.9644	+0.50679	4.4784	.2155	6.4789
+ .40	.03662	.1841	- .28147	.9543	+0.72916	4.4143	.2574	6.1717
+ .45	.04682	.2246	- .23406	.9422	+0.94801	4.3378	.3042	5.8769
+ .50	.05917	.2703	- .18731	.9277	+1.16271	4.2476	.3558	5.5909
+ .55	.07393	.3210	- .14134	.9108	+1.37256	4.1439	.4115	5.3118
+ .60	.09134	.3760	- .09628	.8916	+1.57688	4.0266	.4704	5.0380
+ .65	.11159	.4344	- .05224	.8699	+1.77500	3.8962	.5316	4.7685
+ .70	.13481	.4948	- .00933	.8460	+1.96630	3.7542	.5935	4.5033
+ .75	.16107	.5555	+ .03233	.8203	+2.15025	3.6025	.6543	4.2431
+ .80	.19033	.6145	+ .07266	.7929	+2.32643	3.4436	.7119	3.9894
+ .85	.22246	.6697	+ .11159	.7644	+2.49454	3.2806	.7643	3.7440
+ .90	.25720	.7188	+ .14907	.7353	+2.65448	3.1169	.8093	3.5093
+0.95	.29420	.7597	+ .18510	.7061	+2.80628	2.9560	.8450	3.2876
+1.00	.33300	.7906	+ .21968	.6774	+2.95018	2.8010	.8696	3.0811
+1.05	.37306	.8099	+ .25285	.6496	+3.08654	2.6552	.8821	2.8918
+1.10	.41378	.8170	+ .28466	.6234	+3.21589	2.5209	.8819	2.7212
+1.15	.45455	.8117	+ .31520	.5990	+3.33886	2.4002	.8691	2.5701
+1.20	.49475	.7944	+ .34458	.5767	+3.45616	2.2944	.8445	2.4392
+1.25	.53381	.7664	+ .37291	.5568	+3.56857	2.2044	.8095	2.3283
+1.30	.57123	.7292	+ .40029	.5394	+3.67687	2.1305	.7658	2.2373
+1.35	.60661	.6850	+ .42688	.5245	+3.78188	2.0726	.7156	2.1652
+1.40	.63965	.6360	+ .45278	.5123	+3.88439	2.0303	.6613	2.1112
+1.45	0.67017	0.5843	+0.47814	0.5027	+3.98516	2.0030	0.6050	2.0741

TABLE 1 (continued)

$\text{Log}(\frac{1}{x}-1)$	-Log q	$-\frac{d \log q}{d \log(\frac{1}{x}-1)}$	Log t	$\frac{d \log t}{d \log(\frac{1}{x}-1)}$	Log p	$\frac{d \log p}{d \log(\frac{1}{x}-1)}$	U	V
				Log C = -4.3 (continued)				
+1.50	0.69807	0.5319	+0.50308	0.4956	+4.08493	1.9900	0.5487	2.0529
1.55	.72338	.4806	.52774	.4911	4.18438	1.9902	.4941	2.0462
1.60	.74617	.4315	.55223	.4889	4.28415	2.0026	.4424	2.0529
1.65	.76659	.3858	.57666	.4891	4.38483	2.0265	.3944	2.0719
1.70	.78481	.3438	.60117	.4914	4.48697	2.0608	.3507	2.1019
1.75	.80104	.3060	.62584	.4958	4.59106	2.1044	.3114	2.1418
1.80	.81548	.2722	.65078	.5023	4.69755	2.1564	.2766	2.1906
1.85	.82833	.2425	.67610	.5106	4.80684	2.2160	.2459	2.2473
1.90	.83979	.2165	.70187	.5206	4.91927	2.2822	.2192	2.3109
1.95	.85004	.1939	.72818	.5320	5.03515	2.3539	.1961	2.3803
2.00	.85923	.1744	.75509	.5448	5.15474	2.4304	.1762	2.4547
2.05	.86753	.1577	.78268	.5587	5.27826	2.5107	.1591	2.5331
2.10	.87504	.1433	.81098	.5737	5.40587	2.5940	.1444	2.6146
2.15	.88189	.1310	.84006	.5894	5.53770	2.6795	.1319	2.6984
2.20	.88817	.1205	.86994	.6058	5.67384	2.7663	.1213	2.7837
2.25	.89397	.1117	.90064	.6225	5.81433	2.8536	.1123	2.8696
2.30	.89936	.1042	.93219	.6395	5.95919	2.9407	.1047	2.9554
2.35	.90440	.0978	.96459	.6565	6.10839	3.0270	.0983	3.0405
2.40	.90915	.0925	0.99784	.6734	6.26186	3.1118	.0928	3.1242
2.45	.91366	.0881	1.03192	.6901	6.41953	3.1946	.0884	3.2059
2.50	.91798	.0845	1.06684	.7063	6.58127	3.2748	.0848	3.2852
2.55	.92212	.0816	1.10255	.7221	6.74696	3.3522	.0818	3.3616
2.60	.92614	.0793	1.13904	.7373	6.91641	3.4263	.0795	3.4349
2.65	.93006	.0775	1.17627	.7519	7.08951	3.4968	.0777	3.5046
2.70	.93390	.0763	1.21421	.7658	7.26603	3.5636	.0764	3.5707
2.75	.93769	.0754	1.25283	.7789	7.44580	3.6264	.0756	3.6329
2.80	.94145	.0750	1.29208	.7912	7.62860	3.6853	.0751	3.6911
2.85	.94520	.0750	1.33193	.8027	7.81425	3.7400	.0751	3.7452
2.90	.94896	.0753	1.37234	.8134	8.00253	3.7906	.0754	3.7954
2.95	.95274	.0759	1.41326	.8233	8.19324	3.8372	.0760	3.8420
+3.00	0.95656	0.0770	+1.45465	0.8323	+8.38618	3.8797	0.0771	3.8836
				Log C = -4.6				
-1.00	0.00000	0.0000	-1.67342	1.0000	-5.64520	4.7143	0.0000	51.857
-0.95	.00000	.0000	-1.62342	1.0000	-5.40949	4.7143	.0002	46.730
- .90	.00000	.0000	-1.57342	1.0000	-5.17377	4.7143	.0002	42.161
- .85	.00000	.0000	-1.52342	1.0000	-4.93806	4.7143	.0003	38.089
- .80	.00000	.0001	-1.47342	1.0000	-4.70235	4.7142	.0004	34.459
- .75	.00001	.0001	-1.42342	1.0000	-4.46664	4.7142	.0005	31.224
- .70	.00001	.0001	-1.37342	1.0000	-4.23093	4.7142	.0008	28.341
- .65	.00002	.0002	-1.32342	1.0000	-3.99522	4.7141	.0013	25.771
- .60	.00004	.0003	-1.27342	1.0000	-3.75952	4.7140	.0017	23.481
- .55	.00006	.0005	-1.22342	1.0000	-3.52383	4.7137	.0024	21.439
- .50	.00009	.0008	-1.17343	0.9999	-3.28815	4.7134	.0033	19.618
- .45	.00014	.0012	-1.12343	.9998	-3.05249	4.7130	.0047	17.996
- .40	.00022	.0019	-1.07345	.9997	-2.81686	4.7123	.0066	16.549
- .35	.00033	.0028	-1.02346	.9996	-2.58127	4.7112	.0091	15.258
- .30	.00051	.0042	-0.97349	.9994	-2.34575	4.7096	.0126	14.106
- .25	.00076	.0061	- .92353	.9990	-2.11033	4.7072	.0171	13.078
- .20	.00114	.0089	- .87359	.9985	-1.87505	4.7038	.0231	12.159
- .15	.00167	.0127	- .82368	.9979	-1.63997	4.6990	.0307	11.336
- .10	.00244	.0180	- .77381	.9969	-1.40518	4.6921	.0407	10.599
- .05	.00351	.0251	- .72400	.9955	-1.17080	4.6826	.0533	9.9366
.00	.00498	.0345	- .67426	.9937	-0.93698	4.6696	.0690	9.3392
+ .05	.00700	.0469	- .62464	.9910	-0.70392	4.6520	.0887	8.7981
+ .10	.00973	.0627	- .57517	.9876	-0.47188	4.6285	.1125	8.3051
+ .15	.01335	.0828	- .52591	.9830	-0.24118	4.5979	.1414	7.8529
+ .20	.01809	.1079	- .47690	.9770	-0.01224	4.5583	.1760	7.4344
+ .25	.02423	.1386	- .42823	.9693	+0.21447	4.5081	.2166	7.0432
+ .30	.03206	.1757	- .38000	.9596	+0.43837	4.4456	.2638	6.6737
+ .35	.04192	.2195	- .33230	.9477	+0.65880	4.3690	.3176	6.3206
+ .40	.05414	.2706	- .28526	.9332	+0.87502	4.2769	.3783	5.9795
+ .45	.06909	.3287	- .23902	.9159	+1.08621	4.1681	.4454	5.6470
+ .50	.08712	.3936	- .19372	.8956	+1.29154	4.0421	.5181	5.3203
+ .55	.10855	.4644	- .14951	.8724	+1.49014	3.8991	.5952	4.9980
+ .60	.13363	.5396	- .10653	.8462	+1.68118	3.7403	.6751	4.6798
+ .65	.16254	.6172	- .06493	.8175	+1.86395	3.5676	.7554	4.3663
+ .70	.19535	.6949	- .02482	.7865	+2.03778	3.3843	.8335	4.0595
+ .75	.23198	.7695	+ .01370	.7538	+2.20226	3.1939	.9064	3.7619
+ .80	.27220	.8380	+ .05055	.7201	+2.35713	3.0009	0.9708	3.4765
+ .85	.31561	.8969	+ .08570	.6862	+2.50238	2.8099	1.0236	3.2068
+ .90	.36168	.9435	+ .11917	.6525	+2.63822	2.6252	1.0623	2.9556
+ .95	0.40971	0.9752	+0.15097	0.6200	+2.76507	2.4509	1.0846	2.7259

TABLE 1 (continued)

$\text{Log}(\frac{1}{x}-1)$	- Log q	$\frac{d \log q}{d \log(\frac{1}{x}-1)}$	Log t	$\frac{d \log t}{d \log(\frac{1}{x}-1)}$	Log p	$\frac{d \log p}{d \log(\frac{1}{x}-1)}$	U	V
				Log C = -4.6 (continued)				
+1.00	0.45891	0.9901	+0.18119	0.5891	+2.88354	2.2904	1.0891	2.5194
1.05	.50842	.9876	.20992	.5603	2.99438	2.1462	1.0756	2.3374
1.10	.55737	.9678	.23727	.5340	3.09846	2.0200	1.0446	2.1805
1.15	.60493	.9320	.26337	.5106	3.19670	1.9130	0.9980	2.0484
1.20	.65034	.8826	.28837	.4900	3.29007	1.8251	.9383	1.9403
1.25	.69301	.8224	.31242	.4724	3.37953	1.7562	.8686	1.8550
1.30	.73246	.7548	.33566	.4578	3.46600	1.7056	.7927	1.7911
1.35	.76842	.6834	.35824	.4461	3.55038	1.6724	.7139	1.7471
1.40	.80078	.6112	.38032	.4372	3.63351	1.6554	.6355	1.7213
1.45	.82958	.5410	.40202	.4312	3.71617	1.6535	.5602	1.7122
1.50	.85495	.4748	.42348	.4278	3.79909	1.6656	.4898	1.7182
1.55	.87715	.4140	.44484	.4270	3.88294	1.6905	.4256	1.7381
1.60	.89645	.3593	.46622	.4286	3.96834	1.7272	.3684	1.7705
1.65	.91319	.3110	.48774	.4326	4.05584	1.7745	.3180	1.8142
1.70	.92766	.2690	.50952	.4390	4.14595	1.8316	.2744	1.8681
1.75	.94018	.2328	.53167	.4472	4.23914	1.8973	.2370	1.9311
1.80	.95103	.2020	.55428	.4577	4.33582	1.9710	.2052	2.0022
1.85	.96046	.1758	.57747	.4699	4.43635	2.0515	.1783	2.0805
1.90	.96868	.1537	.60131	.4839	4.54107	2.1380	.1557	2.1650
1.95	.97589	.1352	.62588	.4994	4.65024	2.2296	.1367	2.2546
2.00	.98224	.1196	.65127	.5163	4.76410	2.3253	.1208	2.3486
2.05	.98789	.1066	.67753	.5343	4.88283	2.4242	.1076	2.4458
2.10	.99294	.0957	.70472	.5532	5.00656	2.5255	.0965	2.5455
2.15	0.99749	.0866	.73286	.5728	5.13540	2.6281	.0873	2.6467
2.20	1.00163	.0791	.76200	.5928	5.26938	2.7313	.0796	2.7486
2.25	1.00542	.0728	.79215	.6131	5.40852	2.8342	.0732	2.8501
2.30	1.00892	.0676	.82331	.6334	5.55274	2.9360	.0679	2.9508
2.35	1.01219	.0632	.85549	.6536	5.70205	3.0362	.0635	3.0497
2.40	1.01526	.0597	.88867	.6735	5.85631	3.1338	.0599	3.1463
2.45	1.01818	.0568	.92283	.6930	6.01538	3.2284	.0570	3.2399
2.50	1.02096	.0545	.95796	.7118	6.17910	3.3196	.0547	3.3301
2.55	1.02364	.0527	0.99400	.7299	6.34728	3 4070	.0529	3.4166
2.60	1.02624	.0514	1.03093	.7472	6.51972	3.4901	.0515	3.4988
2.65	1.02878	.0504	1.06870	.7636	6.69621	3.5688	.0505	3.5768
2.70	1.03128	.0498	1.10728	.7791	6.87652	3.6428	.0499	3.6501
2.75	1.03376	.0495	1.14660	.7938	7.06042	3.7122	.0496	3.7188
2.80	1.03624	.0495	1.18663	.8073	7.24766	3.7769	.0496	3.7829
2.85	1.03872	.0498	1.22732	.8200	7.43802	3.8367	.0498	3.8421
2.90	1.04122	.0503	1.26862	.8317	7.63126	3.8919	.0504	3.8968
2.95	1.04376	.0512	1.31048	.8425	7.82713	3.9424	.0512	3.9468
+3.00	1.04634	0.0522	+1.35285	0.8524	+8.02542	3.9884	0.0522	3.9924
				Log C = -4.9				
-1.00	0.00000	0.0000	-1.67342	1.0000	-5.47377	4.7143	0.0002	51.857
-0.95	.00000	.0000	1.62342	1.0000	-5.23806	4.7143	.0002	46.730
- .90	.00000	.0000	1.57342	1.0000	-5.00234	4.7143	.0002	42.161
- .85	.00000	.0000	1.52342	1.0000	-4.76663	4.7142	.0004	38.088
- .80	.00001	.0001	1.47342	1.0000	-4.53092	4.7142	.0006	34.459
- .75	.00001	.0001	1.42342	1.0000	-4.29521	4.7142	.0008	31.224
- .70	.00002	.0002	1.37342	1.0000	-4.05950	4.7141	.0012	28.341
- .65	.00003	.0003	1.32342	1.0000	-3.82380	4.7140	.0016	25.771
- .60	.00005	.0005	1.27342	1.0000	-3.58811	4.7138	.0025	23.480
- .55	.00009	.0008	1.22343	0.9999	-3.35243	4.7135	.0035	21.438
- .50	.00013	.0012	1.17344	.9999	-3.11676	4.7130	.0050	19.617
- .45	.00021	.0018	1.12344	.9998	-2.88113	4.7123	.0070	17.994
- .40	.00032	.0028	1.07346	.9996	-2.64554	4.7113	.0098	16.545
- .35	.00050	.0042	1.02349	.9994	-2.41001	4.7097	.0136	15.253
- .30	.00076	.0062	0.97352	.9990	-2.17458	4.7073	.0186	14.100
- .25	.00113	.0091	.92359	.9986	-1.93930	4.7093	.0253	13.069
- .20	.00169	.0132	.87367	.9980	-1.70418	4.6988	.0342	12.146
- .15	.00248	.0189	.82380	.9969	-1.46941	4.6915	.0456	11.318
- .10	.00361	.0267	.77398	.9953	-1.23507	4.6813	.0604	10.575
- .05	.00520	.0372	.72426	.9934	-1.00134	4.6673	.0790	9.9041
.00	.00740	.0512	.67466	.9906	-0.76843	4.6480	.1024	9.2960
+ .05	.01040	.0695	.62523	.9867	-0.53666	4.6220	.1314	8.7414
+ .10	.01443	.0930	.57601	.9817	-0.30638	4.5875	.1669	8.2316
+ .15	.01980	.1227	.52709	.9749	-0.07808	4.5425	.2096	7.7584
+ .20	.02682	.1597	.47856	.9662	+0.14766	4.4847	.2604	7.3143
+ .25	.03590	.2048	.43052	.9550	+0.37014	4.4118	.3200	6.8927
+ .30	.04746	.2590	.38310	.9411	+0.58855	4.3216	.3889	6.4875
+ .35	.06196	.3228	.33646	.9240	+0.80197	4.2120	.4670	6.0935
+ .40	.07990	.3962	.29076	.9035	+1.00941	4.0819	.5539	5.7069
+0.45	0.10173	0.4788	-0.24617	0.8794	+1.20980	3.9304	0.6487	5.3249

TABLE 1 (continued)

$\log(\frac{1}{x}-1)$	$-\log q$	$\frac{d \log q}{d \log(\frac{1}{x}-1)}$	$\log t$	$\frac{d \log t}{d \log(\frac{1}{x}-1)}$	$\log p$	$\frac{d \log p}{d \log(\frac{1}{x}-1)}$	U	V
			Log C = -4.9 (continued)					
+0.50	0.12791	0.5696	-0.20287	0.8517	+1.40210	3.7581	0.7497	4.9465
.55	.15879	.6665	- .16106	.8204	1.58529	3.5667	.8544	4.5719
.60	.19461	.7668	- .12088	.7862	1.75851	3.3594	0.9594	4.2033
.65	.23546	.8670	- .08248	.7495	1.92105	3.1406	1.0612	3.8433
.70	.28125	0.9630	- .04596	.7109	2.07246	2.9155	1.1551	3.4972
.75	.33163	1.0502	- .01139	.6720	2.21258	2.6900	1.2370	3.1683
.80	.38605	1.1241	+ .02122	.6330	2.34155	2.4702	1.3023	2.8617
.85	.44375	1.1805	+ .05192	.5948	2.45977	2.2612	1.3473	2.5806
.90	.50375	1.2160	+ .08074	.5585	2.56792	2.0679	1.3691	2.3282
0.95	.56498	1.2283	+ .10781	.5245	2.66687	1.8933	1.3661	2.1057
1.00	.62619	1.2162	+ .13325	.4935	2.75761	1.7400	1.3378	1.9144
1.05	.68620	1.1801	+ .15721	.4656	2.84124	1.6091	1.2853	1.7525
1.10	.74385	1.1223	+ .17986	.4409	2.91889	1.5007	1.2114	1.6199
1.15	.79813	1.0462	+ .20136	.4196	2.99167	1.4142	1.1203	1.5143
1.20	.84824	0.9565	+ .22188	.4016	3.06066	1.3486	1.0169	1.4337
1.25	.89365	.8588	+ .24157	.3868	3.12686	1.3025	0.9071	1.3758
1.30	.93407	.7581	+ .26060	.3750	3.19121	1.2745	.7961	1.3383
1.35	0.96948	.6592	+ .27912	.3662	3.25458	1.2630	.6887	1.3194
1.40	1.00008	.5659	+ .29726	.3601	3.31776	1.2666	.5884	1.3171
1.45	1.02621	.4808	+ .31517	.3567	3.38148	1.2842	.4978	1.3297
1.50	1.04832	.4052	+ .33297	.3558	3.44639	1.3144	.4180	1.3559
1.55	1.06689	.3395	+ .35079	.3574	3.51311	1.3562	.3491	1.3945
1.60	1.08243	.2836	+ .36875	.3614	3.58219	1.4087	.2908	1.4441
1.65	1.09540	.2367	+ .38696	.3676	3.65414	1.4711	.2420	1.5040
1.70	1.10623	.1976	+ .40554	.3761	3.72945	1.5425	.2016	1.5733
1.75	1.11528	.1654	+ .42460	.3867	3.80853	1.6222	.1684	1.6511
1.80	1.12287	.1390	+ .44424	.3994	3.89180	1.7096	.1412	1.7367
1.85	1.12928	.1175	+ .46457	.4140	3.97960	1.8036	.1191	1.8291
1.90	1.13470	.0999	+ .48568	.4305	4.07226	1.9038	.1012	1.9278
1.95	1.13932	.0856	+ .50765	.4486	4.17007	2.0092	.0865	2.0318
2.00	1.14331	.0739	+ .53057	.4682	4.27326	2.1191	.0750	2.1403
2.05	1.14676	.0644	+ .55450	.4892	4.38202	2.2323	.0650	2.2522
2.10	1.14978	.0566	+ .57950	.5112	4.49652	2.3400	.0571	2.3667
2.15	1.15245	.0503	+ .60562	.5339	4.61686	2.4656	.0506	2.4831
2.20	1.15483	.0451	+ .63290	.5573	4.74309	2.5839	.0454	2.6002
2.25	1.15697	.0408	+ .66135	.5810	4.87524	2.7019	.0411	2.7171
2.30	1.15893	.0374	+ .69099	.6047	5.01326	2.8189	.0376	2.8330
2.35	1.16069	.0345	+ .72181	.6282	5.15709	2.9340	.0347	2.9471
2.40	1.16236	.0322	+ .75380	.6514	5.30663	3.0465	.0324	3.0592
2.45	1.16402	.0304	+ .78695	.6742	5.46170	3.1557	.0305	3.1669
2.50	1.16549	.0289	+ .82120	.6960	5.62212	3.2607	.0290	3.2710
2.55	1.16690	.0278	+ .85653	.7171	5.78769	3.3618	.0278	3.3712
2.60	1.16827	.0269	+ .89289	.7372	5.95821	3.4581	.0270	3.4668
2.65	1.16959	.0262	+ .93024	.7564	6.13342	3.5495	.0263	3.5575
2.70	1.17089	.0258	+0.96852	.7746	6.31303	3.6357	.0259	3.6430
2.75	1.17217	.0256	+1.00768	.7916	6.49686	3.7166	.0256	3.7232
2.80	1.17345	.0256	+1.04766	.8077	6.68460	3.7922	.0256	3.7982
2.85	1.17473	.0257	+1.08842	.8225	6.87599	3.8624	.0257	3.8678
2.90	1.17603	.0260	+1.12989	.8363	7.07075	3.9272	.0260	3.9321
2.95	1.17734	.0264	+1.17202	.8490	7.26863	3.9869	.0265	3.9914
3.00	1.17868	.0270	+1.21476	.8606	7.46936	4.0416	.0270	4.0457
3.05	1.18005	.0277	+1.25807	.8712	7.67271	4.0916	.0277	4.0952
3.10	1.18145	.0286	+1.30187	.8809	7.87844	4.1369	.0286	4.1402
3.15	1.18291	.0297	+1.34614	.8897	8.08632	4.1778	.0297	4.1807
3.20	1.18442	.0308	+1.39083	.8976	8.29614	4.2145	.0308	4.2172
3.25	1.18600	.0322	+1.43589	.9047	8.50771	4.2473	.0322	4.2497
3.30	1.18764	.0335	+1.48128	.9110	8.72081	4.2764	.0335	4.2785
3.35	1.18936	.0352	+1.52698	.9166	8.93529	4.3020	.0352	4.3039
3.40	1.19116	.0371	+1.57294	.9215	9.15095	4.3242	.0371	4.3259
3.45	1.19306	.0390	+1.61912	.9258	9.36765	4.3433	.0390	4.3448
3.50	1.19506	.0412	+1.66551	.9295	9.58524	4.3596	.0412	4.3610
3.55	1.19718	.0436	+1.71206	.9326	9.80356	4.3729	.0436	4.3741
3.60	1.19942	.0460	+1.75876	.9350	10.02248	4.3835	.0460	4.3846
3.65	1.20179	.0487	+1.80557	.9371	10.24188	4.3918	.0487	4.3928
3.70	1.20429	.0515	+1.85246	.9388	10.46163	4.3979	.0515	4.3988
3.75	1.20695	.0548	+1.89943	.9399	10.68163	4.4016	.0548	4.4024
3.80	1.20978	.0582	+1.94645	.9407	10.90176	4.4033	.0582	4.4040
3.85	1.21278	.0620	+1.99349	.9410	11.12192	4.4028	.0620	4.4034
3.90	1.21597	.0657	+2.04054	.9409	11.34201	4.4004	.0657	4.4009
3.95	1.21936	.0698	+2.08757	.9404	11.56193	4.3961	.0698	4.3966
4.00	1.22295	0.0741	+2.13458	0.9397	11.78159	4.3901	0.0741	4.3905

TABLE 2

INTEGRATIONS FOR ISOTHERMAL ZONE

χ	ψ	$\frac{d\psi}{d\chi}$	U	V
		$\xi_1 = 2.0$		
0.380	-0.0314	9.82	1.916	3.730
.375	+0.0183	10.06	1.850	3.774
.370	.0692	10.31	1.786	3.815
.365	.1214	10.56	1.725	3.854
.360	.1748	10.81	1.664	3.892
.355	.2295	11.06	1.606	3.926
.350	.2855	11.31	1.550	3.959
.345	.3426	11.56	1.496	3.988
.340	.4011	11.81	1.442	4.016
.335	.4608	12.06	1.391	4.040
.330	.5217	12.31	1.341	4.063
.325	.5839	12.56	1.294	4.082
.320	.6473	12.81	1.247	4.100
.315	.7120	13.06	1.202	4.114
.310	.7779	13.31	1.158	4.126
.305	.8451	13.56	1.117	4.135
.300	.9135	13.81	1.076	4.142
.295	0.9831	14.05	1.037	4.146
.290	1.0540	14.30	0.999	4.147
.285	1.1261	14.55	.963	4.146
.280	1.1995	14.79	.928	4.142
.275	1.2741	15.04	.894	4.135
.270	1.3499	15.28	.862	4.126
.265	1.4269	15.53	.831	4.114
.260	1.5051	15.77	.801	4.100
.255	1.5846	16.01	.772	4.083
.250	1.6652	16.25	.745	4.063
.245	1.7471	16.50	.718	4.042
.240	1.8302	16.74	.693	4.017
.235	1.9145	16.98	.669	3.990
.230	2.0000	17.22	.646	3.961
.225	2.0867	17.46	.624	3.929
.220	2.1746	17.70	.603	3.895
.215	2.2637	17.95	.583	3.859
.210	2.3541	18.19	.564	3.820
.205	2.4457	18.44	.546	3.779
.200	2.5385	18.68	.528	3.737
.195	2.6325	18.93	.512	3.691
.190	2.7278	19.18	.497	3.644
.185	2.8243	19.43	.482	3.595
.180	2.9221	19.69	.469	3.544
.175	3.0211	19.94	.456	3.490
.170	3.1215	20.21	.444	3.435
.165	3.2232	20.47	.433	3.378
.160	3.3262	20.74	.423	3.319
.155	3.4306	21.02	.414	3.258
.150	3.5364	21.30	.405	3.195
.145	3.6437	21.59	.397	3.131
.140	3.7524	21.89	.391	3.065
.135	3.8626	22.21	.385	2.998
.130	3.9745	22.53	.380	2.929
.125	4.0879	22.86	.376	2.858
.120	4.2031	23.22	.373	2.786
.115	4.3201	23.58	.371	2.712
.110	4.4390	23.98	.370	2.637
.105	4.5599	24.39	.371	2.561
.100	4.6830	24.84	.372	2.484
.095	4.8084	25.32	.376	2.405
.090	4.9362	25.84	.381	2.326
.085	5.0668	26.42	.388	2.246
.0800	5.2005	27.06	.398	2.164
.0775	5.2686	27.40	.403	2.124
.0750	5.3375	27.77	.410	2.083
.0725	5.4074	28.16	.418	2.042
.0700	5.4784	28.59	.426	2.001
.0675	5.5504	29.04	.435	1.960
.0650	5.6236	29.52	.446	1.919
.0625	5.6980	30.05	.457	1.878
.0600	5.7739	30.62	.470	1.837
0.0575	+5.8512	31.24	0.484	1.796
0.0550	+5.9301	31.94	0.500	1.756
.0525	6.0109	32.70	.518	1.717
.0500	6.0937	33.56	.538	1.678
.0475	6.1788	34.52	.560	1.640
.0450	6.2664	35.60	.585	1.602
.0425	6.3569	36.84	.613	1.566
.0400	6.4507	38.27	.645	1.531
.0375	6.5484	39.94	.680	1.498
.0350	6.6507	41.92	.719	1.467
.0325	6.7584	44.29	.764	1.439
.0300	6.8726	47.18	.813	1.415
.0275	6.9948	50.76	.868	1.396
.0250	7.1272	55.30	.929	1.382
.0225	7.2725	61.20	0.996	1.377
0.0200	+7.4349	69.12	1.067	1.382
		$\xi_1 = 2.7$		
0.340	-0.2221	25.38	1.252	8.631
.335	-0.0940	25.84	1.131	8.655
.330	+0.0362	26.26	1.022	8.664
.325	.1685	26.65	0.924	8.661
.320	.3026	27.01	.835	8.644
.315	.4386	27.35	.754	8.616
.310	.5761	27.67	.682	8.577
.305	.7152	27.96	.616	8.528
.300	.8557	28.23	.558	8.470
.295	0.9975	28.49	.504	8.403
.290	1.1405	28.72	.456	8.328
.285	1.2847	28.94	.413	8.247
.280	1.4299	29.14	.374	8.159
.275	1.5760	29.33	.339	8.065
.270	1.7231	29.50	.307	7.965
.265	1.8710	29.66	.279	7.860
.260	2.0197	29.81	.253	7.752
.255	2.1691	29.95	.230	7.638
.250	2.3192	30.09	.209	7.522
.245	2.4700	30.21	.190	7.400
.240	2.6213	30.32	.173	7.277
.235	2.7731	30.43	.158	7.150
.230	2.9255	30.52	.144	7.021
.225	3.0784	30.62	.132	6.889
.220	3.2317	30.70	.120	6.755
.215	3.3854	30.79	.111	6.619
.210	3.5396	30.86	.102	6.481
.205	3.6940	30.94	.093	6.342
.200	3.8489	31.00	.086	6.201
.195	4.0041	31.07	.079	6.058
.190	4.1596	31.13	.073	5.915
.185	4.3154	31.19	.068	5.770
.180	4.4715	31.24	.063	5.624
.175	4.6278	31.30	.058	5.477
.170	4.7844	31.35	.054	5.329
.165	4.9413	31.40	.051	5.181
.160	5.0984	31.44	.047	5.031
.155	5.2558	31.49	.044	4.881
.150	5.4133	31.54	.042	4.730
.145	5.5711	31.58	.040	4.579
.140	5.7291	31.62	.037	4.427
.135	5.8874	31.66	.036	4.275
.130	6.0458	31.71	.034	4.122
.125	6.2044	31.75	.033	3.968
.120	6.3633	31.79	.031	3.815
.115	6.5223	31.83	.030	3.661
.110	6.6816	31.88	.030	3.506
.105	6.8411	31.92	.029	3.351
.100	7.0008	31.96	.029	3.196
.095	7.1607	32.01	.028	3.041
.090	7.3209	32.06	.028	2.885
.085	7.4813	32.11	.029	2.730
.080	7.6420	32.17	.029	2.573
.075	7.8030	32.23	.030	2.417
0.070	+7.9643	32.30	0.031	2.261

TABLE 3

MATHEMATICAL QUANTITIES CHARACTERIZING SIX REPRESENTATIVE CASES OF MODELS WITH NOISE ZONES

Case	1	2	3	4	5	6
Log C	-4.9	-4.6	-4.3	-4.0	-4.9	-4.9
ξ_1	2.0				2.7	
θ_1	0.49594				0.24966	
χ_1	0.37683				0.33138	
ψ_1	0.0				0.0	
$(-d\psi/d\chi)_1$	9.9751				26.142	
U_2	0.924	0.520	0.414	0.380	0.0288	0.0361
V_2	1.383	1.714	2.062	2.346	3.292	4.316
χ_2	0.0252	0.0523	0.0738	0.0913	0.1031	0.1363
ψ_2	7.116	6.017	5.372	4.903	6.902	5.846
$(-d\psi/d\chi)_2$	54.89	32.76	27.96	25.70	31.94	31.65
z_2	1.242	1.478	1.629	1.750	2.510	3.374
$100x_2$	5.41	3.22	2.30	1.75	0.308	0.0422
$-\log q_2$	0.8871	0.8444	0.7583	0.6779	1.1657	1.1902
$\log t_2$	0.2387	0.4143	0.5664	0.7094	0.8282	1.5490
$\log p_2$	3.1171	3.7634	4.3424	4.8837	5.6549	9.0387
$100x_1$	0.362	0.446	0.449	0.423	0.0959	0.0174
$\log p_1$	6.2076	6.3764	6.6756	7.0130	8.6523	11.5776
$-\log q_1$	1.6277	1.3608	1.2060	1.0889	1.2526	1.2733
$\log t_c$	0.5432	0.7188	0.8710	1.0140	1.4308	2.1517
$\log p_c$	6.9690	7.1378	7.4370	7.7744	10.1590	13.0843

TABLE 4

PHYSICAL CHARACTERISTICS OF MODELS WITH NOISE ZONES. SIX REPRESENTATIVE CASES APPLIED TO STARS OF TEN TIMES THE SOLAR MASS, A CENTRAL TEMPERATURE OF 30 MILLION DEGREES, AND COMPOSED OF 50 PER CENT HYDROGEN, 40 PER CENT HELIUM AND 10 PER CENT RUSSELL MIXTURE.

Case	1	2	3	4	5	6
$R/R_\odot$	19.9	29.8	42.4	58.9	153.7	808.3
$r_1/R_\odot$	0.072	0.133	0.190	0.249	0.147	0.140
$r_2/R_\odot$	1.077	0.959	0.972	1.028	0.474	0.341
$M_{r1}/M_\odot$	0.236	0.436	0.622	0.815	0.559	0.533
$M_{r2}/M_\odot$	1.297	1.431	1.745	2.100	0.683	0.645
$T_1=T_2$	$15x10^6$	$15x10^6$	$15x10^6$	$15x10^6$	$7.5x10^6$	$7.5x10^6$
$\log \bar{\rho}$	-2.748	-3.275	-3.731	-4.160	-5.411	-7.573
$\log \rho_c$	3.201	2.667	2.358	2.123	2.840	2.882
$\log \rho_1$	2.744	2.210	1.901	1.666	1.936	1.978
$\log \rho_2$	-0.347	-0.403	-0.432	-0.463	-1.061	-0.561
$\log(L/L_\odot)$	4.76	4.84	4.95	5.07	3.65	2.75
$\log \kappa_2$	-1.23	-1.27	-1.30	-1.32	-0.72	-0.35

In Tables 3 and 4 the subscript c denotes the center of the star. The subscript 1 denotes the inner interface between the convective core and the isothermal noise zone. The subscript 2 denotes the outer interface between the noise zone and the radiative envelope.

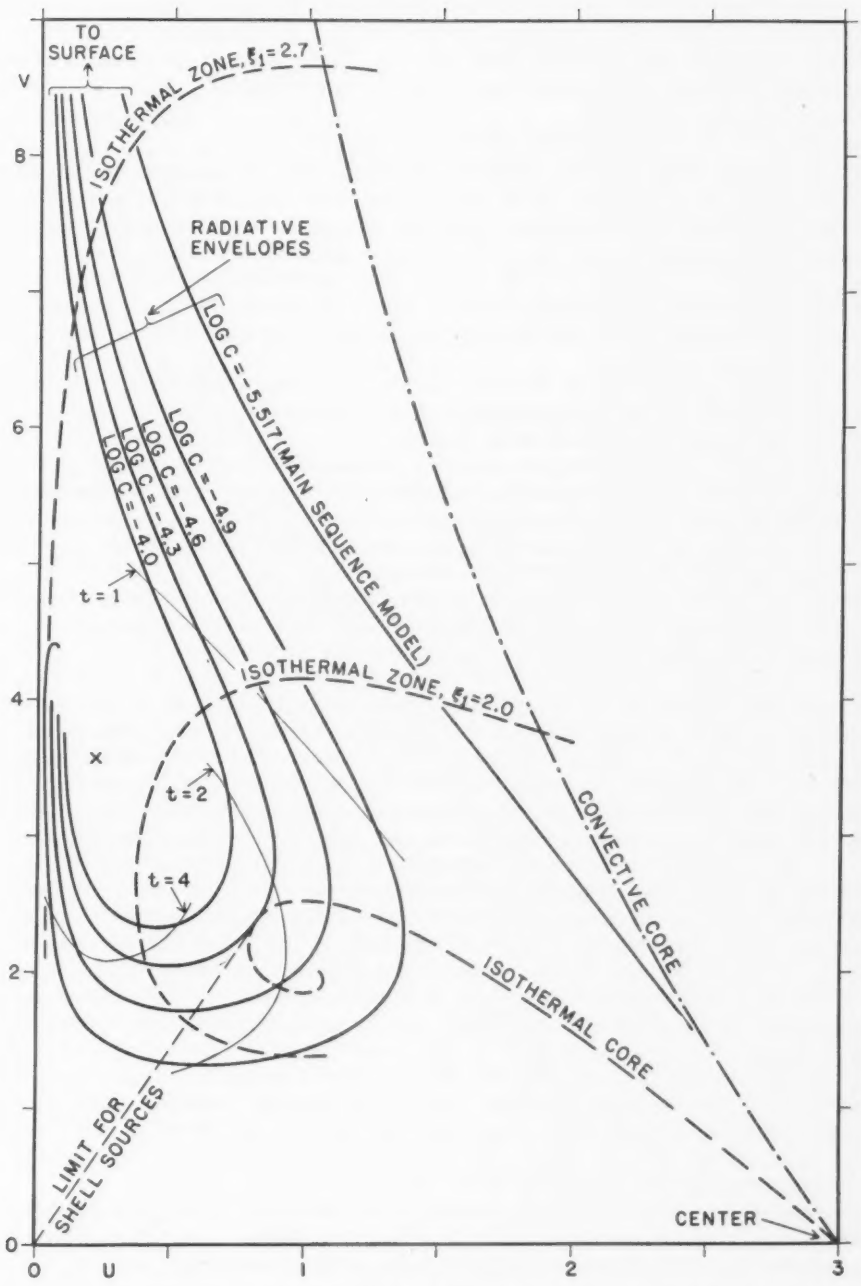

Fig. 1.—Representation of the integrations in terms of the homology invariants U and V

maining cases the other isothermal solution was used (with $\xi_1 = 2.7$) and the radiative solution with $\log C = -4.9$. Since the corresponding U-V–curves have two intersections (not counting the third near the main-sequence model), two different cases (Nos. 5 and 6) could be constructed from them. For all six cases, Table 3 gives the values of the nondimensional variables at the center and at the two interfaces.

IV. PHYSICAL CHARACTERISTICS OF MODEL

Thus far the model has been constructed entirely in terms of nondimensional variables. To facilitate inspection of the model and comparison with observed stars, it is convenient to apply the model to a star of definite mass and chemical composition. For the purpose, we have chosen a mass ten times the solar mass and a composition of 50 per cent hydrogen, 40 per cent helium, and 10 per cent heavier elements. This composition corresponds to a mean molecular weight of 0.74 (the following results do not depend greatly on the assumed composition, since the molecular weight in most stars will certainly lie between 0.5 and 1.0).

Furthermore, in accordance with the discussion in the introduction, a central temperature of 30,000,000° has been assumed, a value high enough for the carbon cycle to give the required energy production in giants.

With the values chosen for the mass, the mean molecular weight, and the central temperature, all nondimensional quantities can be transformed into the corresponding physical quantities with the help of the equations by which the nondimensional quantities were defined. The results of this transformation are given in Table 4 for the six representative cases described in the preceding section.

The first line of Table 4 contains the main results. *It shows that the model here discussed can give radii as large as those of late-type giants even if the model is adjusted to a central temperature high enough for the carbon cycle to operate.* As a secondary result, it may be noted that the mass inside the convective core (M_{r_1}) is of the order of half a solar mass, the radius of the core (r_1) of the order of a seventh of a solar radius, and the central density of the order of several hundred grams per cubic centimeter. Hence it appears that the convective core of the present model is similar to that of main-sequence giants.

The question arises concerning how the introduction of the noise zone can increase the stellar radius so greatly without appreciably affecting the convective core. This might be understood as follows: Just outside the convective core the pressure gradient is about the same in both main-sequence and noise-zone models. This pressure gradient in main-sequence models is partially accounted for by the temperature gradient; whereas in the noise-zone model it must be accounted for by the density gradient alone. Hence, a steep decrease of density is found in the noise zone, as shown by Table 4 ($\rho_1/\rho_2 = 100$–1000). Consequently, the density and hence the opacity per cubic centimeter ($\kappa\rho$) is low at the inner boundary of the radiative envelope of the noise-zone model. Therefore, the radiative temperature gradient is low in the envelope, thus giving a high temperature for a long distance. This, in turn, leads to a low pressure gradient according to the hydrostatic equation and to a large extent of the envelope.

The next to the last line of Table 4 gives the resulting luminosities for the six representative cases. For the first four cases, the luminosities correspond to rather high absolute magnitudes. Lower luminosities would have been obtained if integrations for radiative envelopes with lower C-values had been used.

The last line of Table 4 gives the absorption coefficient for the Russell mixture at the inner boundary of the radiative envelope. Since the values found are, in all cases but one, smaller than the absorption coefficient for electron scattering, one may conclude that electron scattering rather than photoionization is, in general, the essential absorption mechanism for the model here discussed. This result is strengthened by the circumstance that the red giants may well contain less heavy elements and, in particular, less metals than here assumed, which would still further reduce the photoionization. To

introduce this correction, new numerical integrations are needed. It appears improbable, however, that this change would alter the essential features of the model.

V. COMPARISON WITH SHELL-SOURCE MODEL

Recently a model has been studied which consists of an isothermal core with its nuclear fuel exhausted and a radiative envelope still containing unused fuel.[6] The energy source was assumed to be located in a narrow shell just outside the core. It was shown that for a fixed radius this model can give a higher central temperature than can the main-sequence models.

It remains to investigate whether the shell-source model could, under favorable circumstances, give stellar radii as large as that of even the biggest red giant while simultaneously providing internal temperatures high enough for the carbon cycle. Here again the U-V plane, as shown in Figure 1, is a convenient tool. A shell-source model is represented in this plane by a curve starting at the center point, following the isothermal core solution, jumping at an arbitrary point to a radiative envelope solution, and following this curve out to the surface.

The fitting conditions at the interface will again require continuity of pressure and temperature. Correspondingly, if it is assumed that hydrogen is exhausted in the core, the molecular weight and the density decrease by the same factor on passing from the core to the envelope. According to their definitions, U and V also have to decrease by the same factor at the interface. Therefore, if one neglects the shallow zone in which these transitions would actually occur in a continuous manner, the U-V-curve of the shell-source model is discontinuous at the interface and jumps from the fitting-point of the convective-core-curve to the fitting-point of the envelope-curve in a direction representing equal percentage reduction in U and V. Hence, the fitting-point of the envelope must lie in the part of the U-V plane below the lines marked "Convective Core" and "Limit for Shell Source" in Figure 1.

The essential temperature for the shell source is the temperature at the fitting-point of the envelope. For the radiative integrations the temperature is characterized by the nondimensional variable t. In Figure 1, points of equal t are connected by faint lines across the radiative solutions. The figure shows that in the part of the U-V plane in which the fitting-point of the envelope must lie the maximum value of t is approximately 3. According to the definition of t, this value gives the maximum temperature which under favorable circumstances can be reached in a shell-source model for any given star. For Capella A, for example, with $M = 4M_\odot$ and $R = 16R_\odot$, one finds with $\mu < 2$: $T < 35{,}000{,}000°$, which should be sufficient for the carbon cycle. On the other hand, for the K component of ζ Aurigae, with $M = 22M_\odot$ and $R = 200R_\odot$, one obtains: $T < 15{,}000{,}000°$, which is too low for the carbon cycle.

Thus the shell-source model appears to give sufficiently high temperatures for the carbon cycle if it is applied to giants of intermediate spectral type. Indeed, for Capella this has been proved by detailed computations.[7] But for late-type giants the shell-source model leads to the same difficulties as do the classical models. On the other hand, in models with noise zones this difficulty does not occur, since they give high central temperatures even for the biggest stars, as shown by the high values of t_c listed in Table 3.

VI. CONCLUSIONS

From the results discussed in Section IV, one may conclude that even the biggest red giants may have central temperatures high enough for the carbon cycle if these stars are built according to a model with an isothermal zone surrounding the convective core.

[6] M. Schönberg and S. Chandrasekhar, *Ap. J.*, **96**, 161, 1942; G. Gamow and G. Keller, *Rev. Mod. Phys.*, **17**, 125, 1945; M. H. Harrison, *Ap. J.*, **103**, 193, 1946; A. Reiz, *Ann. d'ap.*, **10**, 301, 1947.

[7] Reiz, *loc. cit.*

The introduction of the isothermal zone is at present based on the speculative assumption that the turbulence in the convective core emits a field of acoustical compression waves and that this noise is strong enough to carry alone the entire energy flux for some distance through the interior layers of a star. Only if this assumption is found to be justified by future investigations on the turbulent velocities in convective cores and on the noise emitted by this turbulence can one take the model here considered as a possible physical representation of the interior of red giants.

In the meantime, a check on the noise-zone model can be obtained by comparing the pulsation period of this model with the periods of cepheids. For this purpose the pulsation equation will have to be integrated for this model.

Appendix

Definitions and Equations

I. Definitions

Subscripts:

c denotes center of star,
1 denotes inner interface,
2 denotes outer interface.

Nondimensional variables p, t, q, and x:

$$P = p\,\frac{GM^2}{4\pi R^4},\quad T = t\,\frac{\mu H}{k}\,\frac{GM}{R},\quad M_r = qM,\quad r = xR\,.$$

Eigenvalue parameter, C:

$$C = \frac{3\kappa_0}{4ac}\left(\frac{k}{\mu HG}\right)^{7.5}\left(\frac{1}{4\pi}\right)^{2.75}\frac{LR^{1.25}}{M^{5.75}}\,.$$

Isothermal variables ψ and χ:

$$p = p_1\,e^{-\psi},\quad x = t_1 p_1^{-1/2}\,\frac{1}{\chi}\,.$$

Polytropic variables θ and ξ:

$$p = p_c\theta^{2.5},\quad x = t_c p_c^{-1/2}\,(2.5)^{1/2}\xi\,.$$

Homology invariant variables, U and V:

$$U = 4\pi\,\frac{r^3\rho}{M_r} = \frac{x^3 p}{tq} = e^{-\psi}\left(-\frac{d\psi}{d\chi}\right)^{-1}\chi^{-3} = \xi\,\theta^{1.5}\left(-\frac{d\theta}{d\xi}\right)^{-1},$$

$$V = \frac{\mu H}{k}\,\frac{GM_r}{rT} = \frac{q}{tx} = -\frac{d\psi}{d\chi}\,\chi = -2.5\,\frac{\xi}{\theta}\,\frac{d\theta}{d\xi}\,.$$

II. Differential Equations

In the radiative envelope:

$$\frac{dp}{dx} = -\frac{p}{t}\,\frac{q}{x^2},\quad \frac{dq}{dx} = \frac{p}{t}\,x^2,\quad \frac{dt}{dx} = -\frac{C}{x^2}\,\frac{p^{1.75}}{t^{3.25}}\,.$$

In the isothermal zone:

$$\frac{d^2\psi}{d\chi^2} = \frac{1}{\chi^4}\,e^{-\psi}\,.$$

In the convective core:

$$\frac{d^2\theta}{d\xi^2} + \frac{2}{\xi}\,\frac{d\theta}{d\xi} + \theta^{1.5} = 0\,.$$

III. AUXILIARY RELATIONS

Density in terms of nondimensional variables:

$$\rho = \frac{p}{t}\,\frac{M}{4\pi R^3} = \frac{p}{3t}\,\bar{\rho}\,.$$

Temperature and mass in isothermal zone:

$$t = t_1\,,\quad q = -t_1^2 p_1^{-1/2}\,\frac{d\psi}{d\chi}\,.$$

Temperature and mass in convective core:

$$t = t_c\theta\,,\quad q = -t_c^2 p_c^{-1/2}\,(2.5)^{1.5}\,\xi^2\frac{d\theta}{d\xi}\,.$$

IDEALIZED MODELS AND RECTIFIED LIGHT-CURVES FOR ECLIPSING VARIABLES*

HENRY NORRIS RUSSELL
Princeton University Observatory
Received August 15, 1948

ABSTRACT

The process of "rectifying" the observations of an eclipsing binary, so that a solution may be made from the rectified normals by the methods and tables used for spherical stars, has been completed by Merrill's method for rectifying the phase.

The properties of the "idealized" model, whose elements are thus obtained, are discussed. The outstanding perturbations, which cannot be removed by rectification, arise mainly from differences in the figures of the components and from gravity effect and reflection. For concentric eclipses the combined effect of the last two can be very closely represented by a change in the ordinary darkening coefficient.

The rectification formulae involve three parameters which can be simply obtained by harmonic analysis of the light outside eclipse, and two which depend on the wave length and on the temperatures of the components; the latter two parameters can at present be only rather roughly estimated theoretically. The accompanying uncertainty affects mainly the computed ellipticity.

To obtain the most favorable rectification, the number of uniformly distributed observations outside the eclipses should ordinarily be half the number within them—more if the uneclipsed intervals are short. To "bunch" the former near quadrature and just outside eclipse provides, theoretically, an equally accurate rectification with about half as many observations; but enough observations should be made at all phases to determine the variation with security. When asymmetry, representable by sine terms in the harmonic expansion, is present, a rough empirical rectification may be made. Practical suggestions for performing the rectification are also given.

I. MODELS OF ECLIPSING SYSTEMS

Variations in the light of eclipsing binaries provide an exceptionally attractive field of observation, partly because of recent increases in the accuracy of observation but mainly because the theoretical relationships of the phenomena are so complicated. Since the observable light of these variables is affected by many of their properties, which are otherwise almost entirely inaccessible to our study, the light of such stars provides unique opportunities for their investigation. For this very reason, theoretical discussion of the observations is intricate, and only the simplest cases are amenable to direct methods of solution.

A. THE SPHERICAL MODEL

For an assumed circular orbit, spherical stars, and limb darkening according to the "cosine law," the problem has been completely solved with the aid of tables of certain functions. Precise and relatively simple methods are available, permitting the calculation of the light-curve from the elements in all cases and of the elements from the light-curve, except in certain indeterminate cases, and likewise for the improvement of preliminary elements. The direct determination of the coefficient of limb darkening demands favorable geometrical conditions and precise observations. All the methods which have been proposed by various investigators—Russell and Shapley, Fetlaar, Sharbe, Kopal, Piotrowski, etc.—are based upon the same fundamental equations and basic functions and differ only in detail (including accuracy, rapidity, and convenience). J. E. Merrill's tables (now in press) give very completely the functions required in his extension of the first of these methods.

Eccentricity of orbit (in this, as in other cases) introduces considerable analytical complications but does not demand the introduction of radically new methods or additional tabular functions and is therefore not discussed here.

* *Contributions from the Lick Observatory*, Ser. II, No. 23.

B. THE STANDARD PHYSICAL MODEL

When the separation of the stars is less than eight or ten times their radii, the distortion of the components by centrifugal and tidal forces produces observable effects, as do also the variations of brightness over their surfaces, resulting from differences in the local value of gravity and from the heating of the surface of each by the radiation of the other.

This difficult problem has been solved by Kopal.[1] His method permits the calculation of the observed light received from a given system at any phase, given its fundamental physical properties.

The formulae involve series expansions and many new functions of the various arguments. To invert them and obtain a direct solution for the elements from the observations is hopeless.

C. THE IDEALIZED MODEL

A solution may be obtained in two steps, by devising an *idealized* model, intermediate in complexity, and combining the relative case of solution of the first with the capacity of the second to represent a wide variety of light-curves. These advantages are purchased by certain departures from the actual relations, so that, strictly speaking, it is a formal mathematical model and not a physical one. If a solution closely representing the observations can be made with this model, the transition to the physical model can be made by the *method of perturbations*. A light-curve is computed from the elements of model C by exact application of the idealized equations. From the corresponding physical elements a second light-curve is computed, with all the refinements of model B. By application of the differences of the two, with reversed sign, to the observed data, the latter are "cleared of perturbations"—exactly as for the effects of planetary attraction on a comet—and a solution of the "cleared" observations for model C gives improved elements, which should be definitive if the perturbations are small.[2]

If the idealized model is to have the practical advantages of the spherical one, it must involve the use of the same functions, which have been thoroughly tabulated. It has long been known that, by modifying the *light-intensities* computed from a suitable idealized model in accordance with simple transformation formulae, "rectified" values may be obtained to which most of the equations of the spherical model are applicable. Dr. Merrill has recently discovered that, by an even simpler rectification of the *observed phases*, a set of values is obtained for which all the equations of the spherical model are precisely applicable. If a set of observed data is thus rectified (with the appropriate constants), the resulting quantities will closely resemble those which would result from the eclipses of a pair of spherical stars, and all the methods and tables which have been developed for these are available for their discussion. From the resulting spherical elements, those of the idealized model follow simply.

Even if the hypothetical observations were perfectly accurate, discordances from the idealized solution would remain. If the properties of the actual system followed exactly the laws upon which model B is based, these discordances would represent the perturbations, diminished by the attempt to represent them by a curve of the "idealized" type.

D. THE EMPIRICAL MODEL

Many light-curves, however, show peculiarities, which are inexplicable by the standard physical model. Some of these, such as irregularities in period, suggest a dynamical source; others, such as asymmetry of the curve, appear to be of physical origin. Many

[1] *An Introduction to the Study of Eclipsing Variables* (Cambridge: Harvard University Press, 1946), chaps. vi–ix.

[2] It may be possible to adjust the transformation from the elements first found with model C to those next used with model B in such a way as to bring this about, but this need only be mentioned here.

of them are quite unexplained; others may be represented by special hypotheses. Their observed effects may be called *complications*. The models which may be invoked to explain these are of different degrees of empiricism. Examples are as follows:

a) The assumption that one component is intrinsically and irregularly variable, and the derivation of this variation from the observations, cleared (it is hoped) of other effects.

b) The representation of asymmetry in the light-curve, which repeats itself regularly, by harmonic terms for which no physical explanation is offered.

c) The explanation of occasional deviations of the light-curve from its normal form by assuming the existence of temporary bright or dark patches on the surface.

d) The explanation of a symmetrical light-curve, of a shape which is not explicable by the ordinary theory, on the assumption that the boundary of one component is diffuse. When the distribution of brightness (or opacity) has been determined from accurate observations by sound analytical methods (as for V 444 Cygni), this represents an extension of the physical model.

These "complications" and the even stranger ones which appear in spectrographic observations of eclipsing stars may, in the long run, lead to great advances in knowledge. It is possible, however, to make unreasonable hypotheses in trying to explain them. For example, the solutions representing the light-curve of the same system observed with different wave lengths should not give different orbital inclinations.

II. PROPERTIES OF THE IDEALIZED MODEL

In the spherical model, let L_1 be the (constant) light of one component and f_1 the fraction of this which is lost by eclipse at any instant. If $L = L_1 + L_2$, the light at any time will be

$$l = L - L_1 f_1 - L_2 f_2 . \tag{1}$$

Outside eclipse

$$f_1 = f_2 = 0 ; \qquad l = L .$$

During the eclipse of star 1, $f_2 = 0$ and

$$f_1 = \frac{L - l}{L_1}, \tag{2}$$

and during those of star 2, $f_1 = 0$ and

$$f_2 = \frac{L - l}{L_2}. \tag{3}$$

If any one of the ratios L_1/L, L_2/L, or L_1/L_2 is known, these equations determine f_1 and f_2. In terms of Merrill's tabulated functions,

$$f^{oc} = a^{oc} , \qquad f^{tr} = \tau a^{tr} . \tag{4}$$

These functions are completely defined as

$$a(x, k, p), \qquad \tau(x, k),$$

when x is the darkening coefficient, k the ratio of the radii of the circular disks, and p the ratio of the apparent distance of the center of the small disk from the rim of the large one to the radius of the small disk.

In the idealized model let I_1 be the (variable) light of star 1, as affected by its varying presentation at different phases but not by eclipse, and F_1 the fraction of this that is lost by eclipse at a given phase.

Its contribution to the observed light, then, is

$$\mathfrak{I}_1 = I_1(1 - F_1),$$

and the latter is

$$\mathfrak{J} = \mathfrak{J}_1 + \mathfrak{J}_2 = I_1(1 - F_1) + I_2(1 - F_2). \tag{5}$$

Then, during the two eclipses,

$$F_1 = \frac{I - \mathfrak{J}}{I_1}, \qquad F_2 = \frac{I - \mathfrak{J}}{I_2}, \tag{6}$$

where $I = I_1 + I_2$.

If the tables of τ and a, upon which f depends, are still to be used, the parameters, x, k, and p, which appear in these tables, must be capable of simple and unique definitions in terms of the geometrical and radiative properties of the idealized system. This condition suffices for an almost complete specification of these properties. In the spherical model, k is the ratio of the radii of the circular disks. In the idealized case the equivalent condition is that the apparent disks for any given system must at all phases be bounded by similar curves—a condition which demands that the surfaces of the components shall be similar in form. The ratio of dimensions is k in both cases.

To retain the same significance for p, it may be assumed that the boundaries of the disks are centrally symmetrical and similarly situated as well as similar—in which case the same will be true of the surfaces of the components in space.[3]

If two convex, centrally symmetric curves, similar and similarly situated, touch one another, the point of contact lies on the line joining their centers. Hence, if δ is the apparent distance of the centers at any phase, and r_g and r_s are defined as the radii of the disks along the line joining the centers, the equation

$$\delta = r_g + p\, r_s = r_g(1 + kp) \tag{7}$$

will make $p = -1$ at internal contact, $p = +1$ at external contact, and $p = 0$ when the center of the smaller disk lies on the periphery of the other.

The condition that f shall always have the "circular" value for two disks of uniform brightness demands that these disks shall be reducible to circles by transformations in which the area of every element of the plane is altered in the same ratio. The combination of this with central symmetry leads to elliptical disks and ellipsoidal components.

Finally, the conservation of the darkening coefficient x demands that the isophotes on each apparent disk shall be ellipses similar to and concentric with the limb and that the apparent brightness along an isophote of dimensions sin γ times that of the limb shall be $J_0(1 - x + x \cos \gamma)$. This is precisely the model adopted in 1912[4] and based on the same considerations, less formally expressed.

III. EXACTLY RECTIFIABLE MODELS

Still disregarding gravity effect and reflection, it has been proved[5] that if in an ellipsoid with semi-axes a, $b = a\sqrt{1 - e^2}$, and $c = a\sqrt{1 - f^2}$ the surface brightness varies as H^{-n} (where H is the perpendicular from the center to the tangent plane at the point considered) and the obliquity factor is $\cos^n \gamma$, so that the apparent surface brightness is given by $J = \text{Const.}\ (\cos \gamma/H)^n$, and if this ellipsoid rotates about its shortest axis c, then the light received from it at a distant point will be given by

$$I = I^{\max}(1 - z \cos^2 \theta)^{(n+1)/2}. \tag{8}$$

Here i is the inclination of the polar axis to the line of sight, θ the angle of rotation

[3] An investigation whether any other assumptions would lead to a similar definition of p is not attempted here. The present object is to find a satisfactory model, not to prove that no other exists.

[4] Russell and Shapley, *Ap. J.*, **36**, 400, 1912.

[5] Russell, *Ap. J.*, **102**, 11, 1942.

(measured from the epoch when the observer is in the plane containing the axes a and c), and

$$z = e^2 \sin^2 j \,, \tag{9}$$

where

$$\frac{\tan^2 j}{\tan^2 i} = \frac{1 - f^2}{1 - e^2} = \frac{c^2}{b^2} \,. \tag{10}$$

These equations are exact.

If $n = 0$ and $J = \text{Const.}$,

$$I = I^M (1 - z \cos^2 \theta)^{1/2} \,, \tag{11}$$

where I^M means $I^{\max}$. Applying this to the idealized model, we have, since the ellipsoids are similar,

$$\frac{I_1}{I_1^M} = \frac{I_2}{I_2^M} = (1 - z \cos^2 \theta)^{1/2} \,,$$

and

$$\Im = (1 - z \cos^2 \theta)^{1/2} (I^M - I_1^M f_1 - I_2^M f_2) \,. \tag{12}$$

Setting

$$\Im^R = \frac{\Im}{(1 - z \cos^2 \theta)^{1/2}} \,, \tag{13}$$

we have

$$\Im^R = I^M - I_1^M f_1 - I_2^M f_2 \,, \tag{14}$$

with the values of f corresponding to uniform circular disks ($x = 0$).

If $n = 1$,

$$J = \text{Const.} \frac{\cos \gamma}{H} \,, \qquad I = I^M (1 - z \cos^2 \theta) \,, \tag{15}$$

and

$$\Im^R = \frac{\Im}{(1 - z \cos^2 \theta)} = I^M - I_1^M f_1 - I_2^M f_2 \tag{16}$$

with the f's for circular disks with $x = 1$. In both cases, division of $\Im$ by a suitable factor reduces the expression for the light to the form which holds good for circular disks and rectifies it completely. As is well known, two models, for which the elements are the same except for the lengths of the polar axes (c_g, $c_s = kc_g$), will give strictly identical light-curves inside and outside eclipse, provided that the value of j given by equation (10) is the same. The idealized model may therefore be assumed to consist of similar prolate ellipsoids of revolution with orbital inclination j. If the ratio c/b can be estimated from other than photometric data, the corresponding inclination i follows from equation (10).

A similar rectification may be applied to the other co-ordinate, θ, of the light-curve.[6] The fundamental geometrical equation for a pair of similar prolate spheroids may be written[7]

$$\cos^2 j + \sin^2 j \sin^2 \theta = a_g^2 (1 + kp)^2 (1 - z \cos^2 \theta) \,. \tag{17}$$

Setting

$$\sin^2 \Theta = \frac{\sin^2 \theta}{1 - z \cos^2 \theta} \,, \tag{18}$$

we easily find

$$1 - z \cos^2 \theta = \frac{1 - z}{1 - z \sin^2 \Theta} \,,$$

[6] This elegant transformation is due to Dr. J. E. Merrill.

[7] Russell, *Ap. J.*, **36**, 15, 1912.

and equation (17) becomes

$$\frac{\cos^2 j}{1-z}+\frac{\sin^2 j-z}{1-z}\sin^2\Theta = a_g^2(1+kp)^2 .$$

Setting

$$\frac{\cos^2 j}{1-z}=\cos^2 i_r , \tag{19}$$

we have

$$\cos^2 i_r+\sin^2 i_r \sin^2\Theta = a_g^2(1+kp)^2 , \tag{20}$$

which is identical in form with the equation for spherical stars.

If, then, the observed intensity, $\mathfrak{J}$, is rectified by equation (13) for $x = 0$ or equation (16) for $x = 1$ and the observed orbital longitude θ by equation (18), the resulting light-curve will be identical with that produced by the eclipses of a pair of spherical stars, with radii a_g, ka_g, and inclination i_r, and the rectification will be perfect. By equations (19) and (9) we obtain

$$\tan^2 i_r = (1-z)\sec^2 j - 1 = (1-e^2)\tan^2 j ,$$

whence, by equation (10),

$$a\tan i_r = b\tan j = c\tan i . \tag{21}$$

An exact rectification can also be made if the apparent brightness

$$J = \text{Const.}\ (\cos\gamma/H)^n .$$

In this case

$$\mathfrak{J}^R = \frac{\mathfrak{J}}{(1-z\cos^2\theta)^{(n+1)/2}} ,$$

and Θ is still given by equation (18). This tempting formula for "partial darkening" is, however, of no practical value, since it disagrees with the facts. The corresponding expression for a sphere, $J = J^M\cos^n\gamma$, is seriously discordant with the observed brightness of the sun's disk[8] (for all wave lengths) and also with the results of modern astrophysical theory, while $J = J^M(1-x+x\cos\gamma)$ gives a good, though not a perfect, approximation to both.

IV. PARTIAL DARKENING; ALMOST EXACT RECTIFICATION

We may obtain a model in which the isophotes are ellipses similar to the boundary, and the brightness follows the cosine law, by assuming that the light of each ellipsoid is the sum of two parts, one of which shows uniform surface brightness without obliquity effect, while the other has inherent brightness varying as $1/H$ and obliquity factor $\cos\gamma$. This combination of two radiations differently affected in the same atmosphere is not physically real but is quite permissible in a formal model.

Let $I_1^M(1-X_1)$ and $I_1^M X_1$ be the amounts of light received from the two parts of the radiation of star 1 for $\theta = 90°$. The amount at any other phase will be

$$I_1 = I_1^M[(1-X_1)(1-z\cos^2\theta)^{1/2}+X_1(1-z\cos^2\theta)] . \tag{22}$$

Expanding in series, we have

$$\begin{aligned}\frac{I_1}{I_1^M} = 1 &-\tfrac{1}{4}z(1+X_1)-\tfrac{3}{64}z^2(1-X_1)\\ &-[\tfrac{1}{4}z(1+X_1)-\tfrac{1}{16}z^2(1-X_1)]\cos 2\theta\\ &-\tfrac{1}{64}z^2(1-X_1)\cos 4\theta .\end{aligned} \tag{23}$$

[8] Hertzsprung, *B.A.N.*, **8**, 140, 1937.

In practice z rarely exceeds 0.2, and for most stars $X \approx \frac{1}{2}$. The terms in z^2 are then of the order of 0.001 and may usually be neglected, giving

$$\frac{I_1}{I_1^M} = 1 - \tfrac{1}{4} z(1 + X_1) - \tfrac{1}{4} z(1 + X_1) \cos 2\theta \tag{24}$$

$$= 1 - \tfrac{1}{2} z(1 + X_1) \cos^2 \theta . \tag{25}$$

If $X_2 = X_1$, then $I_1/I_1^M = I_2/I_2^M = I/I^M$, and the light outside eclipse is exactly rectifiable by equation (23), and very approximately by equation (24) or equation (25).

If we set

$$I = A_0 + A_2 \cos 2\theta , \tag{26}$$

A_2 is negative, and

$$I^M = A_0 - A_2 , \tag{27}$$

$$z(1 + X) = -\frac{4A_2}{A_0 - A_2} . \tag{28}$$

The observed light may therefore be rectified by the equation

$$\mathfrak{J}^R = \frac{\mathfrak{J}}{1 - \tfrac{1}{2} z(1 + X) \cos^2 \theta} \tag{29}$$

or

$$\mathfrak{J}^R = \frac{\mathfrak{J}(A_0 - A_2)}{A_0 + A_2 \cos 2\theta} \tag{30}$$

with small outstanding errors of order z^2.

The distribution of brightness over the disks must now be considered. At any phase this is the sum of a part with $x = 0$ and total light equal to L_0, and one with $x = 1$ and light L_1. The isophotes for both are similar to the boundary, and the combined light will show cosine darkening with the coefficient $x = 3L_1/(2L_0 + 3L_1)$. Setting $L_1/L_0 = X(1 - z \cos^2 \theta)^{1/2}/(1 - X)$, we have

$$1 - x = \frac{2 - 2X}{2 - 2X + 3X(1 - z \cos^2 \theta)^{1/2}} .$$

The darkening coefficient on the apparent disk varies with the phase. The changes, which are approximately proportional to z, are very small. For the unusually large value $z = 0.20$ the values of x for various values of X and θ are given in Table 1. When X is fixed, the whole range in x is, at most, 0.028, while that from 0° to 45° (corresponding to a very wide eclipse) does not exceed 0.015. It is extremely difficult to determine x with this accuracy by observation, even in the most favorable cases, and in practice the variation may be disregarded. The idealized model, therefore, permits an adequate, though not an exact, rectification. The rectification of the light by equation (30) requires only a knowledge of the variation outside the eclipses. That of the phase by equation (18) also demands knowledge (or an estimate) of X (or of x, since $X = 2x/[3 - x]$). We here meet the difference between the geometric and photometric ellipticities discussed in Section VII.

This model, however, neglects three important properties of the system: the difference in shape of the components, the variations in surface brightness due to gravity, and to the reflection effect.

V. FIGURES OF THE COMPONENTS

To the first approximation, these are ellipsoids. Let m_1 be the mass of one; a_1, b_1, and c_1 its semi-axes; $\bar{r}_1$ their mean; and m_2, etc., those of the other.

The dynamical theory of equilibrium then gives

$$\frac{a_1 - b_1}{\bar{r}_1} = \frac{3m_2}{2m_1}\,\bar{r}_1^3(1 + 2K_1), \tag{31}$$

$$\frac{b_1 - c_1}{\bar{r}_1} = \frac{m_1 + m_2}{2m_1}\,\bar{r}_1^3(1 + 2K_1), \tag{32}$$

where K_1 depends on the central concentration of density and is less than 0.02 in all well-determined cases.

It is here assumed that the star rotates with uniform angular velocity equal to that in the orbit. If the rotational angular velocity is ω_1 times the orbital,

$$\frac{b_1 - c_1}{\bar{r}_1} = \frac{m_1 + m_2}{2m_1}\,\omega_1^2\bar{r}_1^3(1 + 2K_1). \tag{33}$$

If the equatorial sections of the two ellipsoids are similar, we must have (neglecting K)

$$m_2^2\bar{r}_1^3 = m_1^2\bar{r}_2^3\,; \qquad m_1\rho_1 = m_2\rho_2\,. \tag{34}$$

TABLE 1

θ	X				θ	X			
	0.2	0.4	0.6	0.8		0.2	0.4	0.6	0.8
0°	0.251	0.472	0.668	0.843	45°	0.262	0.487	0.681	0.851
15	.253	.475	.670	.844	90	0.273	0.500	0.692	0.857
30	0.256	0.480	0.674	0.847					

If the sections normal to the radius vector are similar,

$$m_2\omega_1^2\bar{r}_1^3 = m_1\omega_2^2\bar{r}_2^3\,; \qquad \omega_1^2\rho_2 = \omega_2^2\rho_1\,. \tag{35}$$

If both are similar, $r \propto m^{2/3}$ and $\omega \propto m^{-1/2}$. If the periods of rotation and revolution are the same, the components will be of the same shape only if they are equal in all respects. If both components are typical main-sequence stars, $r \propto m^{0.70}$,[9] and their equatorial ellipticities should be very nearly the same. For equal polar flattening, the less massive component must rotate faster, which seems improbable.

In a "typical Algol" system, the small, bright, massive component may be nearly spherical, while the other is greatly distorted. The effects of this distortion upon the variation during the deep primary eclipses are among the largest photometric perturbations. In a few cases which have been calculated numerically,[10] they can be closely represented by changing the darkening coefficient, along with the other elements; but it is not known whether this applies in general.

VI. GRAVITY EFFECT; THEORY

On a star distorted by tidal and centrifugal forces, the total energy flux emerging per unit area should be proportional to the local force of gravity. This conclusion depends on certain assumptions regarding internal convection currents, etc., but it will be adopted

[9] Russell and Moore, *The Masses of the Stars* (Chicago: University of Chicago Press, 1940), p. 112.

[10] Russell, *Ap. J.*, **90**, 670, 1939.

here. If g is the local value of gravity and g_m its mean, then $J = Jg/g_m$ for total radiation. For monochromatic radiation the variation may differ greatly. So long as the depth of the photospheric layers is small compared with the radius, the variations of surface brightness at any point on the surface of a distorted star, both with wave length and with obliquity of emission, should be the same as those on a spherical star having, over its whole surface, the same atmospheric composition and the same values of the total flux (or effective temperature) and of gravity as those for the point considered on the first star.

The theory of limb darkening, with its complicated dependence upon temperature, wave length, and composition, may be taken over bodily from the spherical case. The differences in monochromatic surface brightness J_λ should be the same as for spherical stars with effective temperatures corresponding to the local flux. To the first order, these may be represented by

$$J_\lambda = \bar{J}_\lambda\left(1 - y + \frac{y\,g}{g_m}\right), \tag{36}$$

where

$$y = \frac{\dfrac{\partial J_\lambda}{\partial T}}{\dfrac{\partial J}{\partial T}}. \tag{37}$$

Values of y may easily be computed from gray-body theory; but the actual values must be seriously influenced by departures from the assumed conditions. Formula (37) should give a better approximation at wave lengths for which the departure of the actual curve from Planck's theory is a maximum than for those at which it is rapidly changing.

Progress in the study of the opacity of stellar atmospheres should make it possible to predict the variations of y, as well as those of x, with reservations regarding the effects of differences in composition. The problem could also be solved if we had sufficient observational knowledge of the forms of the energy-curves of stars of different spectral types. Much information might be obtained by determination of the relative brightness of the components of eclipsing variables over a wide range of wave lengths. Finally, it should be possible to get fairly good values of y_λ from the ratio of the geometric and the photometric ellipticities (Sec. VII) for systems in which the mass ratio is known and the darkening has been directly determined.

At the present moment no determination by any one of these methods is available. Approximate values of y may be estimated from gray-body theory.[11] For stars of class B, in which most of the opacity comes from scattering by electrons and is independent of wave length, the value $y = 1$ may be adopted.[12]

VII. PHOTOMETRIC AND GEOMETRIC ELLIPTICITY

By Clairaut's theorem, the local gravity at any point on an ellipsoid in equilibrium under tidal and centrifugal forces is given, to the first order, by the equation

$$\frac{g}{g_m} - 1 = K'\left(\frac{r}{\bar{r}} - 1\right), \tag{38}$$

where r is the local and $\bar{r}$ the mean radius and $K' = (2K - 4)/(2K + 1)$.

It has been proved[13] that the light sent in any direction by an ellipsoid of axes $1 + a'$,

[11] The values derived by the writer (*Ap. J.*, **102**, 3, 1945), depending on a combination of gray-body theory and observed data for the sun, now have little weight.

[12] Z. Kopal, personal communication.

[13] Russell, *Ap. J.*, **90**, 658, 1939.

$1 + b', 1 + c'$ (when a', b', and c' are small) and having the apparent surface brightness

$$J = J_0(1 - x + x\cos\gamma)\left(1 - y + \frac{yg}{g_m}\right) \tag{39}$$

will be the same, to the first order in a', b', and c' as that from an ellipsoid of uniform apparent brightness $J_0(1 - \frac{1}{3}x)$ and parallel axes of lengths $1 + Na', 1 + Nb'$, and $1 + Nc'$, where

$$N = \frac{(15 + x)(1 - \frac{1}{4}K'y)}{15 - 5x}. \tag{40}$$

To the first order, the combined effects of limb and gravity darkening upon the light outside eclipses may be represented by increasing the ellipticities in the ratio N. The increased amount may be called the "photometric ellipticity," in contrast to the geometrical value.

The more reliable determinations of K range from 0.018 to 0.0018. The corresponding values of $\frac{1}{4}K'$ are -0.957 and -0.996. The Roche-model approximation

$$N = \frac{(15 + x)(1 + y)}{15 - 5x}, \tag{41}$$

suffices except in work so refined that many terms here neglected must be included.

VIII. RECTIFICATION OF THE LIGHT-CURVE

To the present approximation, the variation outside eclipse is N times that for a uniformly bright ellipsoid of the same shape. To get $N_1 = N_2$, we must assume $y_1 = y_2$. Then for the combined light outside eclipse

$$\frac{I}{I^M} = 1 - \tfrac{1}{4}Nz - \tfrac{1}{4}Nz\cos 2\theta = \frac{A_0 + A_2\cos 2\theta}{A_0 - A_2}. \tag{42}$$

Rectification of the light is made, as before, by

$$\mathfrak{Z}^R = \frac{\mathfrak{Z}(A_0 - A_2)}{A_0 + A_2\cos 2\theta}, \tag{30}$$

and involves only knowledge of the curve outside eclipses.[14] For rectifying the phase,

$$\sin^2\Theta = \frac{\sin^2\theta}{1 - z\cos^2\theta}, \tag{18}$$

where

$$Nz = \frac{-4A_2}{A_0 - A_2}. \tag{43}$$

This procedure demands knowledge of x and y. The two are probably closely correlated, so that $1/N$ may be estimated from x. For the present, we may tentatively adopt the values given in Table 2.[15] For the very large non-eclipse variation 0.3 mag., $z = 0.45/N$ and lies between 0.20 and 0.15. The values of $\sin\Theta/\sin\theta$ for these limits differ by 3 per cent if θ is small, otherwise less. Under ordinary circumstances the effect of the uncertainty of N upon the rectification will be small, and the value $1/N = 0.38$ may be adopted, in default of better information, without serious error.

[14] For the ellipsoid of Sec. IV, the first part of the light has $x = 0$, $y = 0$; the second $x = 1$, $y = \frac{1}{4}$ (eq. [47]). Application of eq. (41) leads to eq. (24). If y is the same for both parts of the light, eq. (42) is obtained after a little reckoning.

[15] Smaller values of x and y are omitted, since, for the hotter stars, electron scattering is dominant.

IX. APPARENT BRIGHTNESS ON THE DISKS

To the order of approximation here considered, the effect of gravity upon the escaping flux may be represented by the sum of two terms. One, due to rotation, increases the brightness at the poles, relative to the mean along the equator, by the fraction $K'(b - c)/b$. The other, due to tidal forces, diminishes that at the points in line with the companion, compared with the mean along the central section normal to this line, by the fraction $K'(a - b)/b$. Both effects vary as the square of the distance of a point on the surface from the related diametral plane.

In the absence of limb darkening, the isophotes for each effect separately are ellipses, similar in the first case to the projection of the equator and, in the other, to that of the normal section, but not, in general, concentric with them. When both effects are present and when limb darkening occurs, the isophotes are curves of higher degree.

Even an approximate rectification with the aid of the spherical model f-functions is possible only when the isophotes are concentric. This can happen only when the observer is on the line of centers—that is, for a concentric eclipse and for the tidal effect. At all other phases this effect has a component unsymmetrical about the center of the disk—increasing with the distance δ of the centers—and the asymmetry of the rotational effect is still greater.

TABLE 2

x	0.5	0.6	0.7	0.8
y	1.0	1.0	1.2	1.4
$1/N$	0.41	0.39	0.34	0.31

These effects are among the most important of Kopal's perturbations and may be fully handled by his method. The symmetrical effect for concentric eclipse gives rise to the largest of all the variations in surface brightness (except for rapidly rotating stars).

If the standard values of gravity and surface brightness on the ellipsoid refer to the extremity of the y-axis, we have, with suitably defined constants,

$$\frac{J}{J_b} = 1 - y + \frac{y\,g}{g_b} = 1 + K'y\left(\frac{r}{b} - 1\right). \tag{44}$$

Any point on the surface may be represented in terms of auxiliary angles β and λ, such that

$$x = a\cos\beta\,; \qquad y = b\sin\beta\cos\lambda\,; \qquad z = c\sin\beta\sin\lambda\,.$$

Then, to the first order in $a - b$, etc.,

$$r = b\,[1 + (a - b)\cos^2\beta + (c - b)\sin^2\beta\sin^2\lambda]\,. \tag{45}$$

The direction cosines of the normal to the surface are proportional to x/a^2, y/b^2, and z/c^2. It follows, after some reckoning, and neglecting terms of the second order, that

$$\frac{\cos\gamma}{\cos\beta} = \frac{r}{a}. \tag{46}$$

Set $1 - x + x\cos\gamma = \mathrm{A}(1 - x' + x'r/b\cos\beta)$, where

$$A = 1 - (a - b)\frac{x}{a}, \qquad A\,x' = \frac{b\,x}{a}.$$

Then

$$\frac{J}{J_0} = (1 - x + x\cos\gamma)\left[1 + K'y\left(\frac{r}{b} - 1\right)\right],$$

$$\frac{J}{AJ_0} = 1 - x' + x'\cos\beta + K'y(1 - x')\left(\frac{r}{b} - 1\right) + (1 + K'y)\left(\frac{r}{b} - 1\right)x'\cos\beta\,. \quad (47)$$

If $x = 1$ and $K'y = -1$, the terms in $(r/b - 1)$ vanish, and $x' = 1$. For the Roche model $K' = -4$, $y = \frac{1}{4}$. If $K'y = -x'$, these terms do not vanish, if $x < 1$, though their integral over the whole disk does.

To a fixed value of β corresponds an ellipse concentric with, and similar to, the limb. Along this ellipse the tidal effect, which is proportional to $a - b$, is constant. If $K' = -4$, $x = 0.6$, and $y = 1$ (total radiation), its amount is given by

$$J = -AJ_0(1.6\cos^2\beta + 1.8\cos^3\beta)\left(\frac{a}{b} - 1\right). \quad (48)$$

This effect is superposed upon that from the ordinary darkening, $J = (0.4 + 0.6\cos\beta)AJ_0$, and it brightens the limb.

TABLE 3

REPRESENTATION BY $a + b\cos\beta$

FUNCTION	a	b	RESIDUALS		MEAN SQUARE
			Greatest	Numerical	
$\cos^2\beta$	−0.3	+1.2	+0.3	−0.06	±0.058
$\cos^3\beta$	−0.4	+1.2	+0.4	−0.11	±0.100

The terms in $\cos^2\beta$ and $\cos^3\beta$ may be approximately represented by expressions of the form $a + b\cos\beta$. Least-squares solutions, with weights proportional to $\sin\beta\cos\beta$ (that is, to areas on the star disks) give the values in Table 3. The greatest positive and negative residuals and the mean-square residuals weighted according to area are added. As these effects are superposed upon a much greater brightness, the negative values give no trouble. For calculating eclipses, we need the difference of the obscuration F computed from the true, and F' computed from the approximate, formulae. For concentric eclipses, $F = I(\beta)/I(0)$, where

$$I = \int_\beta^{\pi/2} J\sin\beta\cos\beta\,d\beta\,.$$

If

$$J_n = \cos^n\beta\,, \qquad \text{then} \qquad I_n = \frac{1 - \cos^{n+2}\beta}{n+2},$$

and $F_n = 1 - \cos^{n+2}\beta$. Also, since $k = \sin\beta$, we find the values of F given in Table 4. The unit of F is the loss of light for total eclipse of the distribution concerned. With the constants of equation (48), $F = -(0.4F_2 + 0.36F_3)(a - b)AJ_0$, while the ordinary light of the disk, on the same scale, is $0.4\,AJ_0$. The change in the eclipse loss due to tidal distortion, then, is $-(F_2 + 0.9F_3)/(a/b - 1)$ times the whole light of the star. The greatest errors due to the use of the approximate formulae are $+0.84(a/b - 1)$ when $k = 0.53$, and $-0.059(a/b - 1)$ when $K = 0.93$. These are sensible in extreme cases; e.g., if $r_1 = 0.3$, $m_2 = 3m_1$, $a = 1.12b$, and the effect is 1 per cent of the light of the eclipsed star. In most cases it is negligible.

For central eclipses the tidal component of the gravity effect can be fairly closely represented by changing the limb darkening. This procedure may be regarded as another sort of rectification and will be automatically included if x is determined from the observations. The unsymmetrical tidal effect for noncentral eclipses and the gravity effect due to rotation must be handled as perturbations.

X. THE REFLECTION EFFECT

The reflection effect is the conventional but inaccurate name for the result of the heating of the side of each component which faces the other by the radiation of the latter. All the energy received is re-emitted, without altering the rate of escape from the deep interior. The whole radiation of the system into space is unaltered—the loss by eclipse in some directions being compensated for by increase of radiation in others. The theory of this effect, even for integrated radiation, is intricate, and no complete discussion has been published, even for spherical stars.

TABLE 4

VALUES OF F

k	F_2	F_2'	ΔF_2	F_3	F_3'	ΔF_3
0.0.....	0.000	0.000	0.000	0.000	0.000	0.000
0.1.....	0.020	0.018	+ .002	0.026	0.020	+ .006
0.2.....	0.078	0.071	+ .007	0.097	0.079	+ .018
0.3.....	0.172	0.157	+ .015	0.210	0.174	+ .036
0.4.....	0.294	0.272	+ .022	0.353	0.300	+ .053
0.5.....	0.438	0.411	+ .027	0.513	0.451	+ .062
0.6.....	0.591	0.565	+ .026	0.672	0.616	+ .056
0.7.....	0.740	0.723	+ .017	0.814	0.781	+ .033
0.8.....	0.870	0.870	.000	0.922	0.928	− .006
0.9.....	0.964	0.982	− .018	0.984	1.024	− .040
0.95.....	0.991	1.010	− .019	0.997	1.037	− .040
1.0.....	1.000	1.000	0.000	1.000	1.000	0.000

The approximate distribution of the energy re-emitted by a sphere exposed to a uniform beam of parallel radiation was found by Milne.[16] Allowance for the finite distance of the illuminating body leads to poorly convergent series,[17] and greater complications arise from the penumbral regions, where this body appears to be partly set. If L_1 is the total radiation which star S_1 emits in the direction of S_2, Milne finds that the amount ΔL_2 of this radiation "reflected" by S_2 toward the center of S_1 is $\frac{1}{2}\frac{7}{4}\, L_1 r_2^2$, while its apparent surface brightness is $\frac{1}{2}r_1^2(\cos\gamma + \frac{1}{2})^2$ times that of S_1. At other phase angles the intensity of the "reflected" light falls off, Milne finds, as $\Delta L_2 = L_1 r_2^2 f(\epsilon)$ where ϵ is the phase angle from full and f a complicated function having the harmonic expansion

$$f(\epsilon) = 0.278 + 0.347\cos\epsilon + 0.073\cos 2\epsilon + 0.005\cos 3\epsilon + 0.002\cos 4\epsilon\,.$$

Sahade and Cesco,[18] from a more exact numerical investigation, obtain

$$f(\epsilon) = 0.270 + 0.332\cos\epsilon + 0.072\cos 2\epsilon + 0.005\cos 3\epsilon + 0.002\cos 4\epsilon\,.$$

The value

$$f(\epsilon) = 0.28 + 0.35\cos\epsilon + 0.07\cos 2\epsilon \qquad (49)$$

may be adopted.

[16] *M.N.*, **87**, 43, 1926.

[17] Kopal, *op. cit.*, pp. 158–159.

[18] Quoted by Kopal, *ibid.*, pp. 153–154.

At the principal minimum, $\theta = 0$, the hotter star S_h is eclipsed, and the reflection effect on it is close to full phase. Hence $\cos \epsilon_h = \sin i \cos \theta$, and

$$f(\epsilon_h) = (0.28 - 0.07 \cos^2 i) + 0.35 \sin i \cos \theta + 0.07 \sin^2 i \cos 2\theta . \quad (50)$$

For the cooler star, $\cos \epsilon_c = -\sin i \cos \theta$. The full effect of reflection on the light of the system cleared of eclipse is

$$\begin{aligned} \Delta L &= L_c r_h^2 f(\epsilon_h) + L_h r_c^2 f(\epsilon_c) \\ &= (L_c r_h^2 + L_h r_c^2)(0.28 - 0.07 \cos^2 i + 0.07 \sin^2 i \cos 2\theta) \\ &\qquad + 0.35 (L_c r_h^2 - L_h r_c^2) \sin i \cos \theta . \end{aligned} \quad (51)$$

The term in $\cos 2\theta$ merges with that due to the ellipticity and diminishes it numerically. That in $\cos \theta$ led to the discovery of the effect. Its coefficient vanishes if the stars are of the same temperature and hence the minima of the same depth. Otherwise, the light is greater outside the shallower minimum.

XI. VARIATIONS WITH WAVE LENGTH

For measures in any limited region of wave length, let E be the luminous efficiency. If I_h represents the light of S_h in this system, its energy radiation will be proportional to I_h/E_h. If this is transformed back into light on S_c with efficiency E_c, it gives $I_h E_c/E_h$. If we substitute this for L_h in equation (51) and set[19]

$$G_c = \frac{I_h E_c r_c^2}{E_h}, \qquad G_h = \frac{I_c E_h r_h^2}{E_c}, \quad (52)$$

the effect on the uneclipsed light becomes

$$\Delta I = (G_c + G_h)(0.28 - 0.07 \cos^2 i + 0.07 \sin^2 i \cos 2\theta) - 0.35 (G_c - G_h) \sin i \cos \theta . \quad (53)$$

Since $I = Jr^2$,

$$\frac{G_c}{G_h} = \frac{\dfrac{J_h}{E_h^2}}{\dfrac{J_c}{E_c^2}}. \quad (54)$$

For Kuiper's temperatures and assumed wave lengths of λ 4250 and λ 5290 for photographic and visual observations, gray-body theory gives[20] the values of log J and log (J/E^2) for spectral types B–dM shown in Table 5. According to this table, the ratio G_c/G_h is positive for all observable stars. For a given difference in surface brightness, it is greater among the hotter stars and smaller among the cooler ones; hence the term in $\cos \theta$ should be small for the latter, especially for short wave lengths. Gray-body assumptions are, however, at their weakest here. In the cooler stars, absorption in the infrared may modify the energy-curves; and in the hotter ones the short-wave radiation may be greatly affected by absorption connected with the Lyman series. Moreover, such short-wave radiation as escapes and reaches a cooler star may be partly expended in stimulating line emission in its atmosphere beyond λ 3000.

From stars of class B, where electron scattering predominates, most of the incident

[19] In earlier papers this was called f. The change avoids confusion in notation.

[20] Russell, *Ap. J.*, **104**, 156, 1946 (abbreviated).

radiation should be really reflected, without change of wave length or luminous efficiency.[21]

From *A*0 to *G*0 the changes in E are small, especially for ordinary photoelectric work (λ 4500), and no great error will result from setting $G_c/G_h = J_h/J_c$. This correction is theoretically important only when the illuminating star is of class B, or the illuminated star of class G5 or later.

This is another case in which elementary theory must be improved by observation. Considerable material, of no high accuracy, is available. The latest investigation[22] showed that the correlation between the observed coefficient of cos θ and that computed from the elements of the system was decidedly improved by the introduction of gray-body values for the luminous efficiency, though in many cases there remained discordances too great to be attributed to observational error. Here, again, a notable improvement in our knowledge should come as a by-product of accurate observation of eclipsing systems in general.

TABLE 5

λ		*B*0	*A*0	*F*0	*G*0	*dK*0	*dM*0
5290.....	$\log J$	1.44	0.67	+0.17	−0.23	−0.67	−1.54
	$\log (J/E^2)$	3.12	.93	+ .18	− .19	−0.45	−0.66
4250.....	$\log J$	1.24	.38	− .22	− .71	−1.26	−2.35
	$\log (J/E^2)$	2.37	0.45	−0.18	−0.48	−0.62	−0.62

XII. RECTIFICATION FOR REFLECTION

The reversal in phase in the principal component of the reflection effect for the two stars has important consequences. The presence of terms in cos θ, with opposite signs, in the uneclipsed light I_1 and I_2 of the components makes it impossible to assume that the ratio of either one to their sum is constant. This excludes the process of rectification by division, which was so successful for ellipticity.

The process appropriate here was independently suggested by the discoverers of the reflection effect,[23] namely, the *addition* of enough luminosity to the outer face of each component to bring it up to equality with the illuminated side. In this early work the companion was supposed to exhibit hemispheres of uniform, but different, brightness, and the small effect on the brighter star was ignored. A complete rectification may be made by adding to the observed light the quantity

$$\Delta^{\text{ref}} = (G_c + G_h)(0.28 - 0.07 \cos^2 i + 0.07 \sin^2 i \cos 2\theta) + 0.35 (G_c - G_h) \sin i \cos \theta , \quad (55)$$

$$= C_0 + C_1 \cos \theta + C_2 \cos 2\theta .$$

If the observed light outside eclipse is

$$I = A_0 + A_1 \cos \theta + A_2 \cos 2\theta , \quad (56)$$

then

$$C_0 = -(0.8 - 0.2 \cos^2 i) \frac{G_c + G_h}{G_c - G_h} A_1 \operatorname{cosec} i$$

$$C_1 = -A_1 , \quad (57)$$

$$C_2 = -0.2 \frac{G_c + G_h}{G_c - G_h} A_1 \sin i .$$

[21] Suggestion by Dr. Kopal, in conversation.

[22] Paris Pişmiş, *Ap. J.*, **104**, 161, 1946.

[23] R. S. Dugan, *Pub. A.A.S.*, **1**, 311 and 320, 1910, and *Contr. Princeton U. Obs.* No. 1, 1911; J. Stebbins, *Ap. J.*, **32**, 185, 1910, and **33**, 395, 1911.

Unless $G_c - G_h$ is small, these equations suffice for the rectification. A_1 is negative and the C's are all positive.

The correction must be *added* to the observed luminosity of the system at all phases. It corresponds to adding light to the remoter sides of the components, and no sensible error is committed by continuing its application right through the eclipses. In certain cases—e.g., for a small star just disappearing behind a large one—a small portion of the remote half will be eclipsed; but this area will be near its boundary, where the added brightness is small, and, moreover, it will be foreshortened into a very narrow crescent, so that the effect of eclipsing it will be negligible.

The numerical effect of this rectification will appear small or moderate if shown by a table or plot of the light-intensity. In one showing stellar magnitudes, this effect may be very conspicuous, for the light added to the dark side of a faint companion may exceed what the latter originally had. The "reflected" radiation from S_c toward S_h is $0.70\ L_h r_c^2$. When $r_c = 0.3$, this is $0.063\ L_h$. For an eclipse of depth 3.5 mag., the dark side of the companion has at most 0.042 times the light of the primary, and the rectification raises this by a whole magnitude. Changes of three- or four-tenths of a magnitude are common, and allowance for luminous efficiency may increase them.

Rectification for ellipticity may be made by division of the intensity by a rectifying factor less than unity and equally well by subtraction of the corresponding amount from the magnitude. But the addition to the intensity required in rectification for reflection has no simple corresponding expression in magnitude.

If G_c and G_h differ little, A_1 is small, and equation (57) gives poor values for C_0 and C_2. In this case, values good enough for the first solution may be obtained from the formulae[24]

$$\begin{aligned} C_0 &= 0.064 \sin^2 \theta_e\ ; \qquad C_2 = 0.016 \sin^2 \theta_e \text{ (total eclipse)}\ ; \\ C_0 &= 0.08 \sin^2 \theta_e\ ; \qquad C_2 = 0.02 \sin^2 \theta_e \text{ (partial eclipse)}\ , \end{aligned} \tag{58}$$

where θ_e corresponds to external contact.

Much better values can be obtained from preliminary elements by equation (53) if the spectral types are roughly known. This may be done in the first solution if provisional elements are available from other sources.

XIII. DISTRIBUTION OF REFLECTED LIGHT ON THE DISK

Let $\bar{J}_2$ be the mean surface brightness of the side of S_2 opposite S_1, and ΔJ_2 that of the reflection at any point on the other side. Then, for total radiation and full phase,

$$\Delta J_2 = \tfrac{1}{2}\,(\bar{J}_1 + \overline{\Delta J}_1)\ r_1^2 (\cos\gamma + \tfrac{1}{2})^2\ ,$$

whence

$$\frac{\Delta J_2}{\bar{J}_2} = (\tfrac{1}{8} + \tfrac{1}{2}\cos\gamma + \tfrac{1}{2}\cos^2\gamma)\ r_2^2\, \frac{L_1 + \Delta L_1}{L_2}\ .$$

In the approximation to $\cos^2\gamma$ as in Section IX, the parenthesis is replaced by $(\frac{1}{8} + 1.1 \cos\gamma)$. The maximum error of light computed for a concentric eclipse is $0.007\ r_1^2(L_1 + \Delta L_1)/L_2$. For the extreme case $L_1 + \Delta L_1 = 40\ L_2$, $r_2 = 0.3$, this error amounts to $0.025\ L_2 = 0.007(L_2 + \Delta L_2) = 0.0006\ L_1$, and is negligible.

Reflection darkens the limb of S_2 by $J_2 L_1 r_2^2 / L_2$ (neglecting ΔL_1). The tidal portion of the gravity effect brightens it by $5.1\ J_2 m_1 r_2^3 / m_2$ (eqs. [48] and [31]). The effects are equal if $r_2 = 0.20\ L_1 m_2 / L_2 m_1$, and they approximately cancel each other for the majority of equal pairs. In unequal pairs reflection predominates on large faint companions.

The unsymmetrical part of the reflection for other phases belongs with the perturbations. Here also the gravity effect is opposite in sign, and the two roughly cancel each other. Their combined effect upon the form of the rectified light-curve during eclipses

[24] Russell, *Ap. J.*, **104**, 157–158, 1946; f and L are used there instead of G and I.

is likely to be less than that of the polar brightening due to rotation or of the difference in shape of the components if these are unequal. The last two effects must be neglected in preliminary and intermediate solutions; also the first two effects may be ignored.

Until the perturbations are to be taken into account, the rectified observations during the eclipses should be discussed with the tabular functions for spherical stars, and by the same methods. The darkening coefficient may be assumed in the first solution and, in favorable cases, may later be determined from the observations. The resulting values will be affected by gravity and reflection, as discussed above.

XIV. PERTURBATIONS OF LIGHT OUTSIDE ECLIPSE

The ellipsoidal expressions for the effects of figure of the components and gravity darkening are the leading terms of series involving powers of the radii r_1 and r_2 of the components. Kopal has given these in full[25] as far as r^5. The general expression for the terms in r^6 is very complicated, and the only ones so far calculated are those involving the square of the ellipticity. The influence of ellipticity upon the reflection effect is of the order of r^5 but has not yet been worked out. A large part of its effect upon the variation outside eclipse may be allowed for by substituting b^2 or bc for r^2 in the equations.

TABLE 6

I_1	0.1	0.2	0.3	0.4	0.5	0.6	0.7	0.8	0.9
$I_1 \frac{m_2}{m_1}$	0.24	0.35	0.42	0.47	0.50	0.51	0.50	0.46	0.37

Kopal's general expressions are much simplified for integrated light and for the Roche model ($x = \tau$ and $\Delta = 1$ in his notation). His equations (220.1) and (210) then give, in our notation, for the effect of tidal distortion,

$$\frac{I_1}{\bar{I}_1} = 1 + \frac{m_2}{m_1}\left\{ -\tfrac{13}{5} r_1^3 P_2(\cos\epsilon) - \tfrac{15}{16} r_1^4 P_3(\cos\epsilon) + \tfrac{1}{2} r_1^5 P_4(\cos\epsilon) \right\}.$$

Introducing $4P_2 = 3\cos 2\epsilon + 1$, $8P_3 = 5\cos 3\epsilon + 3\cos\epsilon$, $64P_4 = 35\cos 4\epsilon + 20\cos 2\epsilon + 9$, we find numerically

$$\frac{I_1}{\bar{I}_1} - 1 = \frac{m_2}{m_1}\left\{ \begin{array}{r} -0.65 r_1^3 + 0.07 r_1^5 - 0.35 r_1^4 \cos\epsilon - (1.95 r_1^3 - 0.16 r_1^5)\cos 2\epsilon \\ -0.59 r_1^4 \cos 3\epsilon + 0.27 r_1^5 \cos 4\epsilon \end{array} \right\} \quad (59)$$

$$= A_0 + A_1\cos\epsilon + A_2\cos 2\epsilon + A_3\cos 3\epsilon + A_4\cos 4\epsilon .$$

Here A_0 and A_1 slightly alter $\bar{I}_1$ and the reflection term. For the assumed conditions ($i = 90°$, $x = 0.6$, $y = 1$) our equations (9), (31), (40), and (41) give $A_2 = -1.95\, m_2 r_1^3/m_1$, agreeing with equation (59). The terms in 3ϵ for the two stars are of opposite sign and annul one another if the stars are identical; those in 4ϵ reinforce one another.[26]

The average mass-luminosity relation[27] gives $m \propto I^{0.26}$. Assuming this, we find the numerical dependence of $I_1 m_2/m_1$ on I_1, as shown in Table 6. The maximum value of A_3 for star 1 is therefore 0.30 r_1^4 times the light of the system—or 0.01 if $r_1 = 0.43$ and 0.001 if $r_1 = 0.24$. For A_4 we have 0.14 r_1^5, which is 0.001 if $r_1 = 0.38$. Except in refined work, these higher harmonics may be ignored. They belong, in any case, among the perturbations.

[25] *Op. cit.*, p. 139.

[26] *Ibid.*, p. 140.

[27] Russell and Moore, *op. cit.*, p. 112, eq. (115).

XV. EMPIRICAL VARIATIONS OUTSIDE ECLIPSE

According to the physical model B, the expression $A_0 + A_1 \cos\theta + A_2 \cos 2\theta$ should represent the light of the system outside eclipse within a few thousandths of a magnitude, and the addition of $A_3 \cos 3\theta$ should very rarely leave discordances exceeding 0.001 mag. The facts are very different. Asymmetry of the light-curve, both within and without the minima, is only too frequent and has often been confirmed by precise observation. In many cases where the variation repeats itself regularly, a tolerable representation of the uneclipsed light can be obtained only by the introduction of empirical sine terms.

No elementary explanation is available for these terms. The suggestion that the major axes of the ellipsoids are not parallel to the radius vector is inconsistent with Cowling's conclusion that the surfaces of the components have substantially their equilibrium form under the instantaneous rotational and tidal forces. Regular changes suggest forced oscillations dependent on the orbital motion, perhaps magnifying by resonance the effects of small orbital eccentricity. This is supported by a study by P. H. Taylor,[28] showing that, when the light-curve is asymmetrical, the radius of the larger component, in terms of that of the orbit, exceeds a certain limit, depending on the mass ratio. Nonradial oscillations may play a part. No specific theories are yet available.

These regular, but unexplained, variations present the computer with a difficult practical problem. Many of the light-curves, though asymmetric, are accurately defined by good observations, and it is "against human nature" to ask the observers to postpone the discussion of their work to await the possible results of future theoretical studies. Some method for rectification of the observations, even without a sound theoretical basis, seems unescapable for the present.

For the noneclipse variation, the obvious policy is to represent the observations by the general Fourier series.

$$I = A_0 + A_1 \cos\theta + A_2 \cos 2\theta \ldots + B_1 \sin\theta + B_2 \sin 2\theta \ldots . \qquad (60)$$

The extension of the curve across the minima by this equation affords the best basis for estimating the loss of light due to eclipse, and would presumably continue to do so even if a rational theory were available. The derivation of the light-loss at eclipse f, which may be used in determining approximate elements by the standard methods, is quite another matter. The process which produces the terms in $\sin m\theta$ may also produce terms in $\cos m\theta$; and the values of ellipticity and reflection derived from A_1 and A_2 may be affected, so that discrepancies between them and those calculated theoretically from the elements finally found for the system may be anticipated.

We do not know at the start whether the complications arise in one component or in both, or in what proportion. If they affect the brightness of both in the same proportion but produce no asymmetry of shape or of surface brightness, their effect can be completely removed by division by $A_0 + B_1 \sin\theta + B_2 \sin 2\theta$, leaving a symmetrical light-curve for discussion in the usual way. If they affect star 1 alone (with the same restrictions), the subtraction of $B_1 \sin\theta + B_2 \sin 2\theta$ from the observed light should give a symmetrical light-curve for the eclipse of star 2 and outside eclipse. Correction during the other eclipse demands the subtraction of $(1 - f_1)(B_1 \sin\theta + B_2 \sin 2\theta)$ from the observed light, or the addition of $f_1(B_1 \sin\theta + B_2 \sin 2\theta)$ to the light corrected as above. If I_1 and I_2 are approximately known (as when either eclipse is total, or from a preliminary solution), f_1 is given by equation (6) and the correction may be made. (Quantities of the second order in A_1, B_1, etc., are here disregarded.)

To separate the effects produced by the components is impracticable in the absence of theory—much less to take account of asymmetry in form or surface brightness. The computer, faced with this difficult problem, may make a trial to see whether the attribution of the complications to one component or the other, or to both in proportion to

[28] *Ap. J.*, **94**, 46, 1941.

their light, does most to remove the asymmetry of the eclipse curves—remembering that complications are more likely to occur in the component of lower density. He may then proceed to symmetrize the eclipses "by brute force," taking averages of the ascending and descending branches, and may solve the resulting symmetrical curve as usual.

So long as the variation repeats itself accurately and is free from the "humps" and other complications which sometimes appear, it is probable (considering the number of adjustable parameters) that he will finally obtain a light-curve which gives an apparently good representation of the observations. Enough violence will, however, have been done to these to make the precision of the results doubtful. They are likely in most, if not all, cases to give a good idea of the general properties of the system; but it would be illusory to calculate perturbations, solve by least squares, or, worst of all, give probable errors for the elements (though that found for an observation of unit weight will probably come out somewhat too great). When detailed physical theories of the complications become available, these very observations may afford the basis for important additions to knowledge.

XVI. DETERMINATION OF THE VARIATION OUTSIDE ECLIPSE

The coefficients A_0, A_1, and A_2 in equation (60) are of primary importance to the computer. They form the basis of all processes of rectification. In principle, they are defined by equations depending on the properties of the component stars; but in practice, until the coefficients depending on gravity effect and luminous efficiency have been well determined, their values must be found by observation. The inclusion of perturbations does not alter this fact, and, when complications are admitted, all the A's and B's become purely empirical.

The only difficulty is that the available range of θ is limited—from $\pm\theta_e$ to $\pm(180° - \theta_e)$. Excluding observations falling near but within these limits loses weight; including those during eclipse vitiates the results. A graphical method for fixing these limits and finding values of the A's and B's has been devised by Dr. Merrill. Draw a freehand light-curve to represent all the observations. Take readings from it for every 10° of θ (or other convenient interval) and let a, b, c, and d represent the readings for θ, $180° - \theta$, $180° + \theta$, and $360° - \theta$. It follows at once that

$$\begin{aligned}
\tfrac{1}{4}(a+b+c+d) &= A_0 + A_2\cos 2\theta + A_4\cos 4\theta \ldots, \\
\tfrac{1}{4}(a-b-c+d) &= A_1\cos\theta + A_3\cos 3\theta \ldots, \\
\tfrac{1}{4}(a+b-c-d) &= B_1\sin\theta + B_3\sin 3\theta \ldots, \\
\tfrac{1}{4}(a-b+c-d) &= A_2\sin 2\theta + B_4\sin 4\theta \ldots .
\end{aligned}$$

If these four quantities are plotted against cos 2θ, cos θ, sin θ, sin 2θ, they will give straight lines, provided that A_3, B_3, etc., are insensible. The slopes of the four lines will be A_2, A_1, B_1, and B_2. The last three must pass through the origin; and the first cuts the axis cos $2\theta = 0$ at the intercept A_0. If θ lies within eclipse, the plotted points on the first diagram will drop below the straight line—thus locating θ_e closely enough to define the safe limits of solution.

The uncertainty of the derived values of A and B may be estimated from the plots. If more accurate determinations are desired, it is relatively simple to pass at once to a least-squares solution. If it were not for the gaps caused by eclipse, the constants would be determined independently and strongly, but the necessary restriction leads to serious loss of weight.

Set, for convenience, $\eta = 90° - \theta$. Then equation (60) becomes

$$I = A_0 + B_1\cos\eta - A_2\cos 2\eta + A_1\sin\eta + B_2\sin 2\eta\,. \qquad (61)$$

The limits of observation are then from $-\eta_e$ to η_e, and from $180° - \eta_e$ to $180° + \eta_e$, where $\eta_e = 90° - \theta_e$. Suppose that there are N observations, equally and similarly distributed over these intervals, and symmetrically about their mid-points. The normal equations are greatly simplified by the symmetry and may be written:

$$\begin{aligned}
&N A_0 - N\,\overline{\cos 2\eta}\,A_2 = N\bar{I}\,,\\
&-N\overline{\cos 2\eta}\,A_0 + N\,\overline{\cos^2 2\eta}\,A_2 = N\,\overline{I\cos 2\eta}\,,\\
&N\,\overline{\sin^2\eta}\,A_1 = N\,\overline{I\sin\eta}\,,\\
&N\,\overline{\cos^2\eta}B_1 = N\,\overline{I\cos\eta}\,, \qquad N\,\overline{\sin^2 2\eta}B_2 = N\,\overline{I\sin 2\eta}\,,
\end{aligned}$$

where the bars denote mean values. The constants A_1, B_1, and B_2 are independently determined; A_0 and A_2 are correlated, but this may be avoided by setting

$$A_0' = A_0 - A_2\,\overline{\cos 2\eta}\,. \tag{62}$$

The new unknowns are free from correlation, and their weights are

$$\begin{aligned}
&p(A_0') = N\,, && p(B_1) = N\,\overline{\cos^2\eta}\,,\\
&p(A_1) = N\,\overline{\sin^2\eta}\,, && p(B_2) = N\,\overline{\sin^2 2\eta}\,.\\
&p(A_2) = N\,[\overline{\cos^2 2\eta} - (\overline{\cos 2\eta})^2]\,,
\end{aligned} \tag{63}$$

For numerous uniformly distributed observations the mean values may be replaced by integrals. Setting

$$\overline{\cos 2\eta} = \frac{\sin 2\eta_e}{2\eta_e} = g_2\,, \qquad \overline{\cos 4\eta} = g_4\,,$$

we easily find

$$\begin{aligned}
&p(A_1) = \tfrac{1}{2}N(1 - g_2)\,, && p(B_1) = \tfrac{1}{2}N(1 + g_2)\,,\\
&p(A_2) = \tfrac{1}{2}N(1 - 2g_2^2 + g_4)\,, && p(B_2) = \tfrac{1}{2}N(1 - g_4)\,.
\end{aligned}$$

The numerical values of these quantities are given in Table 7. Values of η_e less than 30° are omitted, as corresponding to components almost in contact. Table 7 also gives values of $N[\sigma(I)]^2/\sigma_0^2$ (where σ_0 is the mean error of unit weight) for the computed light at quadrature ($\eta = 0$), external contact ($\eta = \eta_e$), mid-eclipse ($\eta = 90°$), and for the average of phases distributed uniformly during the eclipse (90° to η_e). These are given for solutions including and excluding the asymmetric sine-terms. Their presence makes remarkably little difference in σ during the eclipses (since these terms are zero at mid-eclipse).

XVII. NUMBER OF OBSERVATIONS REQUIRED OUTSIDE ECLIPSE

The accuracy of the predicted value of the uneclipsed light near conjunction falls off rapidly with increasing duration of eclipse, owing to the greater extrapolation; and so does that of the computed rectification. Many more observations must therefore be made between the minima than would be required if the light were constant.

A full discussion of the influence of the accidental errors of the rectification upon those of the deduced elements would involve their effects upon the depths and shapes of the minima, and it would be very complicated. As a rough guide, we may take the weight of the difference of the calculated intensity, cleared of eclipse, at the epoch of conjunction, and the observed intensity at this phase.

Let the number of observations made during each eclipse be N_1, and in each non-eclipse interval N_2, and let the weight of the observed light at minimum be N_1/n_1, where n_1 is a factor depending mainly upon the shape of the eclipse curve. For a long total eclipse it may be 2, and for a narrow deep partial eclipse, 10 or more. The weight of the calculated light at this phase is $2\,N_2/n_2$, where n_2 is given in Table 7 for $\eta = 90°$.

If P is the weight of the difference between the observed and the calculated intensities, $1/P = n_1/N_1 + n_2/2N_2$. This is by no means an accurate index of the weight of the

TABLE 7

WEIGHTS OF HARMONIC CORRECTIONS

η_e	30°	45°	60°	75°	90°
g_2	0.8270	0.6366	+0.4135	+0.1910	0.0000
g_4	.4135	.0000	− .2067	− .1654	.0000
$\frac{1}{N}p(A_1)$	.0865	.1817	+ .2982	+ .4045	.5000
$\frac{1}{N}p(A_2)$	.0229	.0947	+ .2256	+ .3808	.5000
$\frac{1}{N}p(B)_1$	.9135	.8183	+ .7068	+ .5955	.5000
$\frac{1}{N}p(B_2)$	0.2982	0.5000	+0.6033	+0.5827	0.5000

VALUES OF $N[\sigma(I)]^2/\sigma_0$

η_e	30°	45°	60°	75°	90°
	Including Sine-Terms				
$\eta=0$	3.40	3.62	3.94	4.40	5.00
η_e	11.90	10.64	8.85	6.78	5.00
90°	159.	34.8	13.28	7.21	5.00
90° to η_e	88.6	24.9	11.66	7.06	5.00
	Omitting Sine-Terms				
$\eta=0$	2.31	2.40	2.52	2.72	3.00
η_e	8.56	8.03	7.26	6.23	5.00
90°	159.	34.8	13.28	7.21	5.00
90° to η_e	86.2	23.6	11.0	6.99	5.00

intensity at the rectified minimum, but it is usually a fairly good indication. If the whole number of observations is fixed, P will be a minimum if $N_2^2/N_1^2 = n_2/2n_1$. With $n_1 = 4$, as representing an average eclipse, and n_1 from Table 7, the maximum P is obtained when $N_2/N_1 = 2.1$, 1.3, and 0.9 for wide, average, and narrow eclipses ($\eta_e = 45°$, 30°, 15°), respectively.

To maximize P would usually require more observations outside eclipse than inside. But to change N_2/N_1 by a factor of 2 in either direction diminishes the weight of P by not more than one-ninth, so that the actual requirement is less severe. Moreover, the shape of at least one minimum must be accurately known to get a good solution. This can be found only from observations covering the whole range of the partial phases.

The differences of the rectification corrections during this interval are relatively small, unless the eclipses are long, so that the eclipse observations are predominant in determining the shape. Concentration of the observations within the eclipses is therefore the best policy; but if those outside eclipse are much less than half as many as those inside, this concentration may go too far.

When the eclipses are long, the proportion of observations in the shorter intervals outside should be greater. This is especially important for the W Ursae Majoris type, where the ellipticity is large and the eclipses partial and often shallow. Rectification may greatly reduce the depth of the secondary, and, until it has been made, it is hard to tell where the eclipses begin. Precise observations covering the whole period uniformly are here essential. The perturbations are large, and corrections to the constants of rectification should be included with those to the other elements in a definitive least-squares solution.

XVIII. OBSERVATIONS NEAR SELECTED PHASES

The weight of the computed light for mid-eclipse may be considerably increased by distributing the observations near strategic points rather than uniformly. The most obvious points are halfway between eclipses (giving the maximum effect of ellipticity) and just outside them. Observations have to be concentrated near the external contacts in any case; for an accurate determination of the "shoulders" of the curve (where f is small) is essential to a good solution. The only safe way to be sure of including the extremities of these shoulders is to observe well beyond the estimated external contact. Since, as will soon appear, observations outside eclipse here are of unusual value in determining the rectification, there is every reason why the region on both sides of the external contacts at each eclipse should be preferentially observed. Similar attention should be paid to the "toes" of the curve (near internal contact in a total eclipse or the middle of a partial one).

Let us now suppose that, of N observations outside eclipse, $\frac{1}{4}Nx$ are situated *just* outside, at mean phases $\pm\eta_1$, $180 \pm \eta_1$, and $\frac{1}{2}N(1-x)$ at 0°, 180°. Then in equation (63) we have

$$\overline{\cos^2\eta} = 1 - x\sin^2\eta_1\,, \qquad \overline{\cos^2 2\eta} = 1 - x\sin^2 2\eta_1\,,$$

$$\overline{\sin^2\eta} = x\sin^2\eta_1\,, \qquad \overline{\sin^2 2\eta} = x\sin^2 2\eta_1\,,$$

$$\overline{\cos 2\eta} = 1 - 2x\sin^2\eta_1\,, \qquad \overline{\cos^2 2\eta} - (\overline{\cos 2\eta})^2 = 4(x - x^2)\sin^4\eta_1\,.$$

When $\eta = \pm 90°$,

$$S = \frac{N[\sigma(I)]^2}{\sigma_0^2} = \frac{1 + \sin^2\eta_1 - (3\sin^2\eta_1 - \sin^4\eta_1)x}{(x - x^2)\sin^4\eta_1}\,.$$

This expression is a minimum if[29]

$$(3\sin^2\eta_1 - \sin^4\eta_1)x = 1 + \sin^2\eta_1 - \cos^2\eta_1\sqrt{1 + \sin^2\eta_1}\,.$$

The values of x and S are given in the upper lines of Table 8 and also the ratio $S(u)/S$, where $S(u)$ is the value for uniform distribution (Table 7). It appears that the substitution of "bunched" for uniformly distributed observations increases the weight of the computed intensity substantially threefold over the whole range of probable length of eclipse. The actual gain will be less, for the tabular $S(u)$ corresponds to η_e (the maximum value outside eclipse), while the mean value, η_1, for the actual observations must be less. If $\eta_1 = 0.9\eta_e$, the values $S(u)/S'$ result.

[29] The + sign of the radical gives $x > 1$.

The first two lines in the lower half of Table 8 give S for the fixed values $x = \frac{2}{3}$ and $x = \frac{4}{5}$. For all probable durations of eclipse the difference in weight is small.

According to this approximate criterion, as accurate a rectification of the observations during the eclipses can be obtained from a given number of observations concentrated just outside them and halfway between them as could be obtained from twice the number uniformly distributed.

It is clearly desirable—indeed, in the writer's opinion, essential for a definitive discussion—that there should be enough observations at all phases to define the course of the light-curve and to detect complications if any are present. The necessity of concentration

TABLE 8

MEAN ERRORS; FOR $\eta = 90°$; OBSERVATIONS BUNCHED

η_1	30°	45°	60°	75°	90°
	Most Favorable x				
x	0.60	0.71	0.84	0.95	1.00
S	55.9	11.9	4.40	2.43	2.00
$S(u)/S$	2.84	2.92	3.02	2.98	2.50
$S(u)/S'$	1.6	2.1	2.2	2.3	.....
	$x = \frac{2}{3}$				
S	57	12	5.00	3.35	3.0
	$x = 0.8$				
S	66	12.5	4.43	2.80	2.5
	Observations at η_1, 45° and 90°				
S	.....	12.5	6.33	4.27	.....

just outside the eclipses is an advantage. To realize it fully, as many additional observations should be made near each maximum, halfway between eclipses, as are made on each shoulder. Exact equality of the number is not important.

The last line of Table 8 gives the values of S which result from shifting half the observations on the shoulders to the "quarter-points," $\eta = \pm 45°$, with the same number once more at the maximum. For $\eta_1 = 45°$ this shift gives the same distribution as $x = 0.8$, and S is the same. For shorter eclipses, the change decidedly diminishes the weight and appears to be without theoretical advantage.

XIX. SUMMARY

a) Rectification is a process by which the observations of an eclipsing system showing ellipticity and reflection may be transformed into quantities from which a solution may be obtained by the methods available for spherical stars. The observed intensity and phase are both changed. For actual pairs the process is not exact, but it suffices to obtain

an idealized model (composed of similar ellipsoids), which gives a good general representation of the system and which serves as a basis for calculation of perturbations.

Parameters of two types are involved. Three of them may be very easily derived from the observations outside eclipse. Two others, which depend on the temperatures of the components and the wave length of observation, involve the theory of stellar atmospheres, and only rather rough estimates of their values can be made at present. (In the notation of this paper, the first three are called A_0, A_1, A_2; the others are N and $[G_c + G_h]/[G_c - G_h]$).

b) Rectification of the standard type is practicable where the light between eclipses can be represented by

$$I = A_0 + A_1 \cos\theta + A_2 \cos 2\theta \,. \tag{56}$$

(If θ is measured from the deeper minimum, A_1 and A_2 are negative.)

If $\mathfrak{I}$ is the observed light at any phase, rectification for reflection is made by *addition*, according to the equation[30]

$$\mathfrak{I}' = \mathfrak{I} + C_0 + C_1 \cos\theta + C_2 \cos 2\theta \,, \tag{55}$$

where[31]

$$C_1 = -A_1 \,; \qquad C_0 = -0.8\,\frac{G_c + G_h}{G_c - G_h}; \qquad C_2 = \tfrac{1}{4}C_0 \,, \tag{57}$$

and all three are positive.

Rectification for ellipticity is now made by *division* according to

$$\mathfrak{I}'' = \mathfrak{I}'\,\frac{A_0 + C_0 - A_2 - C_2}{A_0 + C_0 + (A_2 + C_2)\cos 2\theta}. \tag{64}$$

The intensity outside eclipse is now

$$I'' = A_0 + C_0 - A_2 - C_2 \,.$$

Rectification of the phase is made by *division*, the equation being

$$\sin^2\Theta = \frac{\sin^2\theta}{1 - z\cos^2\theta}, \tag{18}$$

where

$$Nz = \frac{-4\,(A_2 - C_2)}{A_0 - C_0 - A_2 + C_2}, \tag{65}$$

(The direct effect of reflection [eq. (53)] is to add $C_0 - C_1 \cos\theta + C_2 \cos 2\theta$ to the observed light. Subtracting this quantity, we have for ellipticity alone: $A_0 - C_0 + (A_2 - C_2)\cos 2\theta$, whence the above.) The ellipticity of the components is $\frac{1}{2}z \csc^2 j$ (eqs. [9], [10]).

The theoretical uncertainty of N affects only the rectification of the phase and the calculated ellipticity. There should be a close correlation between N and the darkening coefficient x. A value for the latter must be assumed before making any solution, and the relation between the two given in Section VII may be adopted.

The uncertainty in G is more serious, especially when C_0 and C_2 are derived from A_1. In most cases (Sec. XI) it should suffice in preliminary work to set G_c/G_h equal to J_h/J_c, that is, to the ratio of the depths of the minima, cleared of ellipticity and reflection.

[30] The previous notation has deliberately been modified here, since rectification is made in the inverse order.

[31] These equations are here simplified by setting $\sin i = 1$, which is unavoidable at this stage of approximation and usually introduces very small errors.

When the minima are of comparable depth, $G_c - G_h$ and A_1 are small, and C_0 and C_2 are ill determined. In this case approximate values may be found from equation (58), with the estimated duration of the minima.

Values of the depths and duration may be obtained by comparing the freehand curve representing the observations (which must be plotted at the start) with the computed non-eclipse curve (56) .From these values, $I - \mathfrak{J}$ may be read for the minima, $\theta = 0°$, 180°. The difference $I - \mathfrak{J}$ for a given phase is not altered by rectification for reflection, and the ratio of the values of this quantity at corresponding phases during the two eclipses is unchanged by rectification for ellipticity. Hence, the ratio of the unrectified value of $I - \mathfrak{J}$ at the primary minimum to that at the secondary gives an approximate value of J_h/J_c. The preliminary value of G_c/G_h may be set equal to this or may be derived as in Section XI. The value of θ_e for external contact may be estimated by inspection or preferably by the graphical process described in Section XVI. When preliminary elements have been found, better values for the reflection corrections may be obtained from equations (52) and (53) and used in the next step.

The present process is shorter than that suggested by the writer[32] in 1946, and it includes rectification of the phase.

The elements derived from the rectified data represent a system in which the light of the fainter sides of the components has been artificially raised to equality with that of the brighter. The calculated light I_h and I_c of the components represents the brighter sides. The light of their opposite undisturbed sides is $I_h - 0.70\ G_h$, $I_e - 0.70\ G_c$.

When empirical terms $B_1 \sin \theta + B_2 \sin 2\theta$ appear in the light outside eclipse, only a summary rectification is possible. In the absence of any adequate theory, this may be made either by subtraction or by division—as sketched in Section XV. The resulting elements are necessarily of a provisional character.

This paper presents, in somewhat amplified form, the content of lectures given at the Lick Observatory during the writer's stay as Morrison Research Associate in the autumn of 1947. He takes pleasure in using this opportunity to express his heartfelt thanks to all the members of the community for most stimulating professional associations and for hospitality which has made it one of the most pleasant experiences of a fairly long life. It is also a privilege to thank Dr. John E. Merrill for his great generosity in permitting the first publication of his important method for rectifying the phase (p. 392) and of his process for finding the Fomia coefficients (p. 406).

[32] *Ap. J.*, **104,** 159, 1946.

SIX-COLOR PHOTOMETRY OF STARS*
VI. THE COLORS OF EXTRAGALACTIC NEBULAE

JOEL STEBBINS AND A. E. WHITFORD
Mount Wilson and Washburn Observatories
Received August 3, 1948

ABSTRACT

Photoelectric measures in six colors have been made of eight bright extragalactic nebulae of types E to Sc. As was to be expected from their mixed stellar content, the nebulae show excess radiation in both the ultraviolet and the infrared over that of a star of matching color in the visual-photographic region. With a suitable combination of stars of early and late types, the color can be reproduced over the whole observed range, while the spectrum in the blue-violet would appear to be that of stars of an earlier type than the color class in the same region. There is no need to assume internal space absorption in the nebulae to account for the difference between spectral class and color class.

With the 1P21 photomultiplier tube and a two-filter system, magnitudes and colors of E-type nebulae in clusters have been measured with the 100-inch reflector down to $m_{pg} = 18.2$. The nebulae are found to be redder in proportion to their velocity of recession until for the Boötes cluster at 70,000,000 parsecs with $V = 38{,}900$ km/sec the color excess is 0.52 mag. on the International system, of which 0.22 mag. can be explained by the red shift, and 0.30 mag. is unaccounted for. Following are the tentative conclusions:

1. The reddening of the nebulae is proportional to the red shift. On the plausible assumption that the unexplained part of the excess is linear with distance, this result supports a linear velocity-distance relation.

2. The excess reddening can be explained as selective absorption by internebular material of mean density ten to one hundred times the smoothed density of the luminous nebulae in all space. The considerable inward corrections to the previously assumed distances would, however, be difficult to reconcile with the nebular counts.

3. The excess reddening can be interpreted as an intrinsic change in E-type nebulae in the 2×10^8 years since the observed light left the Boötes cluster. Fading of red supergiants as their energy sources are consumed could provide a mechanism.

4. Both the excess reddening and the ultraviolet excess found in the six-color results will affect the luminosity correction to be applied to a faint nebula with a large red shift. Previous conclusions about the interpretation of the nebular counts are therefore open to revision.

Because of their low surface brightness and small contrast with the sky background, the extragalactic nebulae present unusual difficulties in the spectrophotometry of their light. By the photographic method, even with a wide slit and very low dispersion, a long exposure is necessary. The difficulty of allowing for sky background, and especially that of connecting the results on luminous surfaces with those on point sources, prevent anything like the accuracy obtainable by the same methods when used on stars. It is in this field of photometry of faint surfaces that the ability of the photocell to integrate all the light reaching it is particularly advantageous. Diffuse objects requiring exposures of some hours to give measurable images on a photographic plate may be measured with a photocell in less than a minute, and, by "on-and-off" exposures of the cell to nebula and blank sky, useful results can be obtained when the sky background has an intensity ten or even fifteen times that of the nebula.

In 1940 we were able to place in operation a nebular photometer designed and constructed by Whitford at Madison for use with the 60- and 100-inch reflectors. One feature of the arrangement was the increase of the field to 19 mm, or an angular opening of 8′.6 at the focus of the 60-inch. A suitable positive lens in the main focal plane focused an image of the large mirror on the sensitive surface, the same-sized image whether from a star, a nebula, or an area of blank sky. For measures of color a system of filters was

* *Contributions from the Mount Wilson Observatory, Carnegie Institution of Washington*, No. 753.

provided, giving with the cesium oxide photocell a series of spectral regions from 3530 A to 10,300 A. We should have preferred to isolate these regions sharply, as can be done with a slit spectrometer, but such an arrangement would have reduced the intensities to impossibly small values. Thus we were constrained to the smearing effect of filters, but the advantages of multicolor photometry remained, which, to our knowledge, had not previously been applied to the nebulae.

After a start on the nebulae in the summers of 1940 and 1941, Whitford left for war service, and the next several summers were spent in part by Stebbins on calibration measures of stars. In fact, this side program on stars grew until it began to seem more important than the original plan for the nebulae. The results on stars from measures in six spectral regions instead of the customary two regions for color index opened up a new field for us, and several side investigations, such as space reddening of B stars, six-color photometry of stars of all types, and the changes of some well-known variable stars, were completed and published.[1] Nevertheless, we always expected to return to the nebulae, and the present report is on the work that we intended to carry through in the first place.

I. SIX COLORS OF BRIGHT NEBULAE

The description of the installation and the methods of observation for six colors were included in the first paper of the series. For convenience, the effective wave lengths of the combination of the photocell with different filters are repeated here in the headings of Table 1. As before, the sensitivity-curves and the resulting mean wave lengths refer to a source of uniform energy through the spectrum, without correction for the atmospheric extinction or for the two reflections from aluminum mirrors in the telescope. In a fundamental comparison of stars with black bodies, these effective wave lengths will, of course, have to be re-examined. For the present purpose they are presumably as reliable as the data ordinarily given in photographic or visual photometry. As before, the units in Table 1 and throughout this paper are: angstroms for λ, microns^{-1} for $1/\lambda$, and stellar magnitude for colors.

In the first paper the sensitivity-curves for the different filters were exhibited as functions of the wave length. These curves are now repeated on the scale of inverse wave lengths in Figure 1, together with the similar photographic and photovisual curves for the International system given by F. H. Seares.[2] Any criticism of the crude isolation of spectral regions by our filters applies with greater force to the standard photographic and photovisual systems. The photovisual curve includes a relatively narrow band of wave lengths, but the wide spectral range of the ordinary photographic plate, while making for great sensitivity, leads to many complications in the intercomparison of different color systems.

The procedure for measuring the colors of nebulae is the same as that for faint stars; differential readings between nebula and a sky-comparison area are taken by moving the photometer back and forth with the cross-slide screw. Even when only the bright central region of a nebula is concerned, the surface brightness of the sky, especially in the infrared,[3] may be several times that of the nebula; but useful measures apparently can be made with a ratio up to something like 10 or 15 to 1 for sky to nebula. For an extended object like M31, where the double-slide motion of the plate base will not reach outside the nebula, the whole telescope must be moved, and the measured sky deflections are subtracted from those of the nebula. But even here, with a focal diaphragm of a few minutes of arc, it may be sufficient simply to turn to a faint region of the nebula to get

[1] Stebbins and Whitford, *Mt. W. Contr.*, Nos. 680, 704, 712, 718; *Ap. J.*, **98**, 20, 1943; **101**, 47, 1945; **102**, 318, 1945; **103**, 108, 1946.

[2] *Mt. W. Contr.*, No. 685; *Ap. J.*, **98**, 302, 1943.

[3] Stebbins, Whitford, and Swings, *Mt. W. Contr.*, No. 703; *Ap. J.*, **101**, 39, 1945.

the sky background. To an observer measuring a nebula against the sky for the first time, the brightness of the sky may come as a shock. To take an extreme case, for M101 with an infrared filter and a diaphragm of 5′.7 on the 100-inch, the deflection from nebula plus sky was 165 mm; from sky alone 154 mm, or fourteen times the 11 mm net from nebula. In the other five colors the nebula and the sky gave not very different deflections, from

TABLE 1

SIX COLORS OF BRIGHT NEBULAE

NGC	Messier	Year	Diameter	Diaphragm	λ (A) / 1/λ (μ⁻¹) / Spec.	3530 2.83 U	4220 2.37 V	4880 2.05 B	5700 1.75 G	7190 1.39 R	10,300 0.97 I	Obs.
					Sb							
224.....	31	40	160′	3′.4	G5	+0.81	+0.53	+0.23	+0.02	−0.24	−0.84	3
224.....	31	44	160	5.7	G5	+0.87	+0.52	+0.28	+0.04	−0.31	−0.83	3
Mean..	31	....	160	.....	G5	+0.84	+0.52	+0.26	+0.03	−0.28	−0.83	6
					E *							
221.....	32	40	2.6	2.4	G3	+0.54	+0.45	+0.27	+0.03	−0.29	−0.91	2
					Sb's							
1068*....	77	42	2.5	0.7	G3	+0.21	+0.26	+0.18	+0.02	−0.19	−0.67	1
4736.....	94	41	5.0	3.4	F8	0.00	+0.13	+0.14	+0.06	−0.19	−0.58	2
4826.....	64	41	8.0	3.4	G3	+0.17	+0.21	+0.17	+0.03	−0.20	−0.60	2
Mean..	.....	....	.....	.....	G1	+0.13	+0.20	+0.16	+0.04	−0.19	−0.62	....
					Sc's							
598.....	33	40	60	3.4	A7	−0.36	0.00	−0.01	+0.04	−0.02	−0.20	2
5194.....	51	41	12	3.4	F8	−0.30	−0.05	+0.06	+0.06	−0.11	−0.58	2
5457.....	101	41	22	3.4	G0	−0.18	−0.06	+0.04	+0.10	−0.15	−0.21	1
Mean..	.....	....	.....	.....	F5	−0.28	−0.04	+0.03	+0.07	−0.09	−0.33	....

* This nebula has very strong emission lines (C. K. Seyfert, *Mt. W. Contr.*, No. 671; *Ap. J.*, **97**, 28, 1943), which may affect the color slightly. The intense [*O* II] line at λ 3727 would come in the band covered by the U filter.

6 to 9 mm each. The bright radiation of the night sky at 10,440 A, ascribed to molecular nitrogen,[3] always causes difficulty in measuring faint objects in that spectral region.

The results with six colors on the bright nebulae are in Table 1. The first three columns are self-explanatory. The diameters are from Shapley and Ames.[4] The diaphragms 3′.4 and 2′.4 are for the 100-inch telescope; 5′.7 and 0′.7 for the 60-inch. The spectra, usually noted as of dwarf type, have been kindly furnished from unpublished work by M. L. Humason. The colors, U to I, are, as always, referred to the mean of ten stars of average

[4] *Harvard Ann.*, Vol. **88**, No. 2, 1932.

type dG6. We note that the colors usually refer to small central regions of the nebulae; only for M32 does the diaphragm take in nearly all the diameter. The well-known difference between the inner and outer regions of the spirals can be ignored here.

The results in Table 1 are plotted in Figure 2. For comparison, the colors for giant and dwarf stars of several types are also shown. All the curves for the nebulae are concave upward, indicating relatively high intensities in the ultraviolet and infrared compared with normal stars. The curvature is in the same sense as that found for reddened B stars,[5] but much larger. Internal space reddening is therefore quite inadequate as an explanation, and we can safely assume that the curvature arises from the composite colors of mixtures of stars of different types.

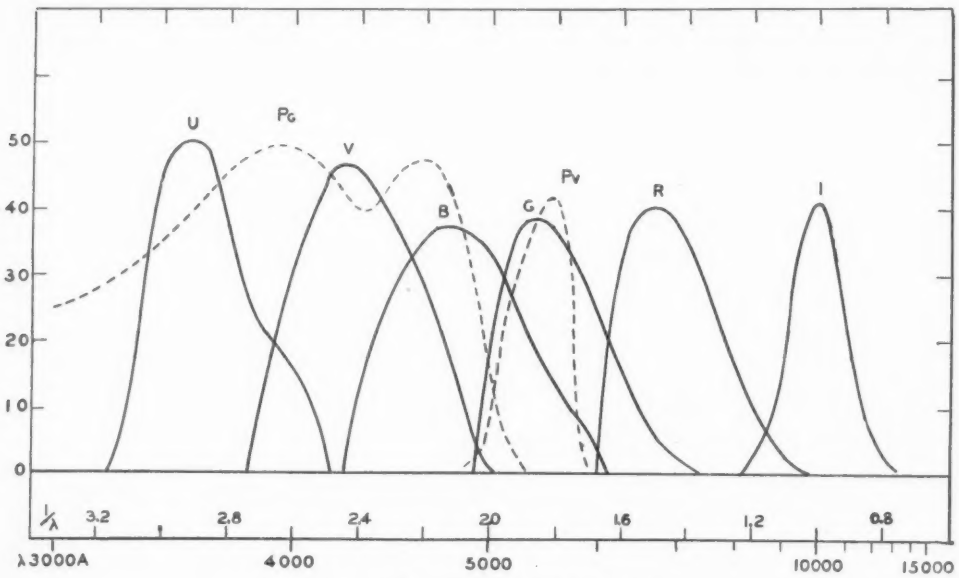

FIG. 1.—Color-curves of cell and filters

In each nebula the variation of the gradient with the wave length shows that a comparison of the spectral type with a color index may be misleading unless the spectrum and color refer to the same spectral region. Thus it is possible to build up a synthetic nebula with only a few types of stars, which will reproduce accurately the observed colors of a nebula and give the required spectrum in the blue. For example, we give in Table 2 an oversimplified combination, which nevertheless reproduces quite closely an average Sb object. The colors for dG0 are from the mean of five stars with average visual absolute magnitude $M_v = +4.3$; those for cM0 from a single star with $M_v = -2.3$. The Δm's are reduced to numbers, then combined in the ratio of two dG0 to one cM0 and again referred in magnitude to the mean of BGR. In the blue-violet the color excess found in our short-base-line C2 colors[6] is still there, but at 4880 A the relative intensity of the G stars is four times that of the M star, and this ratio increases for shorter wave lengths. Hence this system would show in the blue-violet region an early dG spectrum like the Sb nebulae; it would match their six colors; and it would conform with Baade's stellar population of type II in having no white supergiant stars and no red ones brighter than

[5] Stebbins and Whitford, *Mt. W. Contr.*, No. 680; *Ap. J.*, **98**, 20, 1943.

[6] Stebbins and Whitford, *Mt. W. Contr.*, No. 577; *Ap. J.*, **86**, 270, 1937.

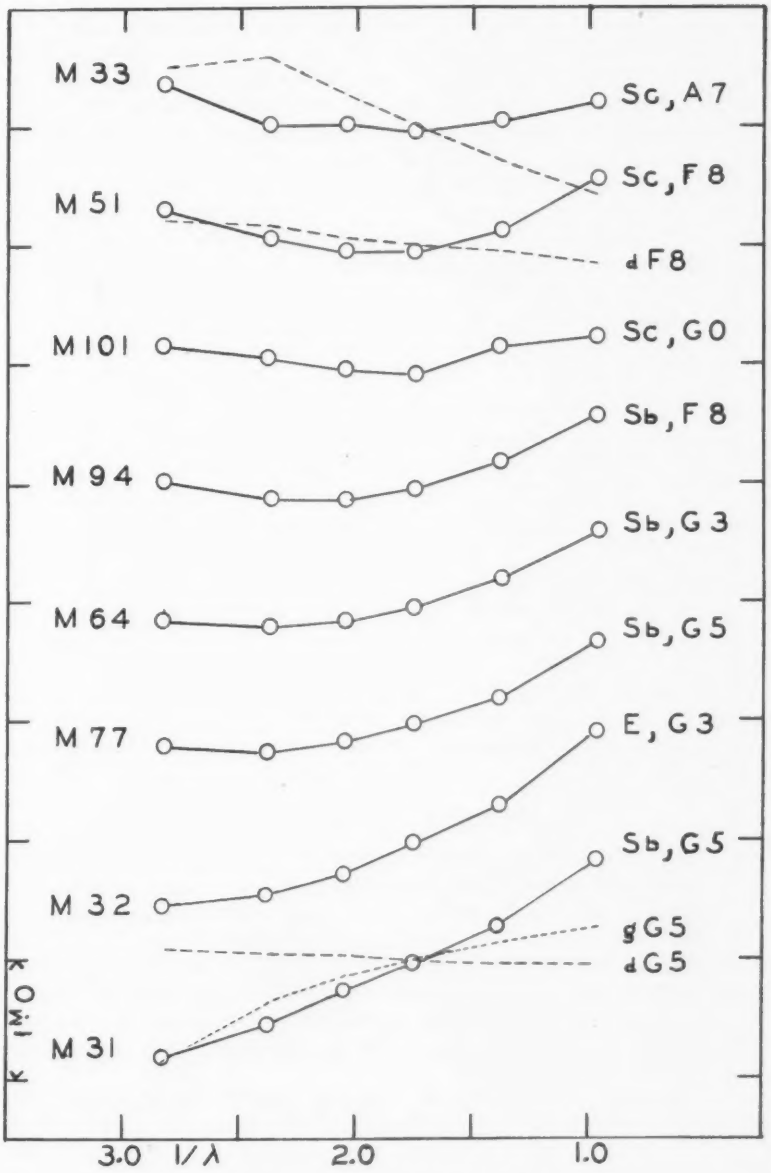

FIG. 2.—Six colors of bright nebulae

$M_v = -2.4$. There is nothing unique in choosing dG0 and cM0; we could do as well with gK5 and other combinations, but a large proportion of A or F stars would show a Balmer depression in the ultraviolet.

This result is in general accord with F. L. Whipple's[7] conclusion that the composite spectra of stellar mixtures would be of earlier type than the color class because the broader "line-classification" features of a small-scale spectrum come from stars hotter than the mean, and the narrower lines of the cool red stars are not resolved. In any event, now that the mixed stellar content shows up clearly in the six-color survey, previous inferences[6] about internal space reddening in nebulae will have to be abandoned.

The problem of reconstructing both the spectrum and the color of an external galaxy by summing up the effect of various synthetic mixtures of stellar types may be left to the future, when it is hoped that better spectra with measured equivalent widths may become available. Whipple's original attempt[7] used a frequency distribution of absolute magnitudes and spectral types derived from stars in the solar neighborhood, now known to be typical of population I. But, since both the present colors and the spectra deal with central regions of external galaxies, it is clear that the mixture in question is a product

TABLE 2

SYNTHETIC NEBULA OF TYPE Sb

Stars	U	V	B	G	R	I
dG0	−0.26	−0.15	−0.05	−0.01	+0.06	+0.15
cM0	+3.0	+1.33	+ .66	+ .02	− .69	−1.42
2dG0 +cM0	+0.19	+0.20	+ .18	+ .04	− .21	−0.61
Mean Sb	+0.13	+0.20	+0.16	+0.04	−0.19	−0.62

of the as yet unknown statistics of dwarf stars in population II. A unique reconstruction of the unresolvable portion of the population of extragalactic objects from color and spectrum studies may not be possible; an important factor will be the dispersion obtainable in the spectra.

II. TWO COLORS OF FAINT NEBULAE

With the advent of the R.C.A. multiplier photocell after the war, a powerful aid was given to the electrical photometry of stars. Although this multiplier does not have the wide spectral range of the cesium oxide cell used for six colors, the multiplier in combination with suitable filters will give magnitudes and two colors for stars 5 mag. fainter than can be reached in six colors. Our six-color cell is not a particularly sensitive one, and, moreover, to filter out one of the six spectral regions may mean a loss of 3 mag. from the total light, whereas for the multiplier the corresponding loss is about 1 mag. for each of the two colors. It is the same story as in stellar spectroscopy; with lower dispersion one can go to fainter stars.

The color-sensitivity curves of the 1P21 multiplier with the filters have been determined with a quartz monochromator at Madison, with the results shown in Table 3. The energy of the source at each wave length was measured with a thermocouple, and the response of the multiplier has been corrected to constant energy. In the table the column marked "Clear" gives the relative spectral response of the cell, including the optical system of the photometer, plus two reflections from the aluminum mirrors of the telescope, but without allowance for atmospheric extinction. The compound lens, used to focus an image of the main telescope mirror on the photocathode, had a flint-glass component,

[7] *Harvard Circ.*, No. 404, 1935.

which reduced the ultraviolet intensity and shifted the effective sensitivity-curve to the red of that of the bare multiplier. In the columns marked "Blue" and "Yellow" are the numbers under "Clear" multiplied, respectively, by the transmissions of the two filters. The blue filter was Schott BG12, 1 mm thick; the yellow was Schott GG7, 2 mm thick. Thus in the ideal case of a star or nebula of known spectral energy distribution, observed outside the atmosphere, we have the relative response of our receiver for all wave lengths. Such a case in the table is the nebula M32 to be discussed later in this paper. The values for constant E in Table 3 are shown graphically in Figure 3.

TABLE 3

COLOR SENSITIVITIES OF 1P21 MULTIPLIER WITH FILTERS

λ	CONSTANT E			M32		
	Clear	Blue	Yellow	E	Blue	Yellow
3400	0.529	0.275	.....	0.27	0.07	.....
3600	1.403	0.982	.....	0.35	0.34	.....
3800	1.752	1.367	.....	0.43	0.59	.....
4000	1.944	1.579	.....	0.52	0.82	.....
4200	1.982	1.605	.....	0.62	1.00	.....
4400	1.960	1.513	0.004	0.72	1.09	.....
4600	1.854	1.253	0.067	0.83	1.04	0.06
4800	1.708	0.734	0.533	0.93	0.68	0.50
5000	1.531	0.282	1.262	1.02	0.29	1.29
5200	1.338	0.078	1.180	1.07	0.08	1.26
5400	1.095	0.015	0.986	1.10	0.02	1.08
5600	0.745	0.009	0.681	1.10	0.01	0.75
5800	0.371	.....	0.337	1.09	.....	0.37
6000	0.198	.....	0.181	1.08	.....	0.20
6200	0.086	.....	0.079	1.06	.....	0.08
6400	0.023	.....	0.021	1.04	.....	0.02
Effective wave length	.....	.....	.....	.....	4320	5290

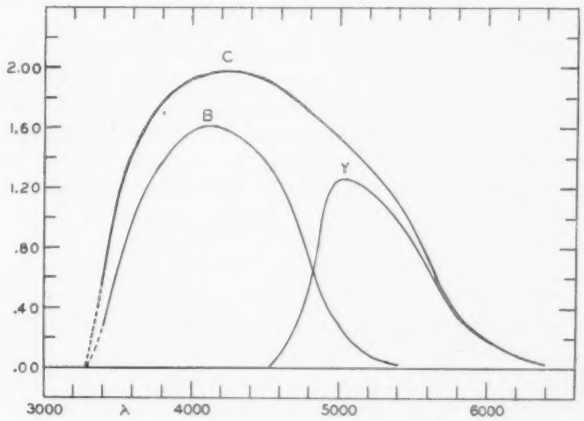

FIG. 3.—Color-curves of 1P21 multiplier and filters

Since our magnitudes and colors are to be reduced to the International system, we derive our effective wave lengths for comparison with F. H. Seares.[2] Using his equations (4) for effective wave length, λ_e, we have for either blue or yellow:

$$\lambda_e = \frac{\Sigma \lambda s y}{\Sigma s y}, \tag{1}$$

where s is the sensitivity factor under "Blue" or "Yellow" in our Table 3, and y is the relative energy of a black-body radiator, taken from Seares's Table 1. The resulting photoelectric effective wave lengths and the International ones from Seares's Table 3, both rounded off to 10 A, are given for three sample temperatures in our Table 4. We emphasize again that in this comparison for black bodies our effective wave lengths are for outside the atmosphere; those for the International system include the extinction at the Mount Wilson pole. Since the present paper is dealing mainly with colors, we leave

TABLE 4

PHOTOELECTRIC AND INTERNATIONAL EFFECTIVE WAVE LENGTHS FOR BLACK-BODY SOURCES

T	BLUE		YELLOW		Y−B		
	Pe	*Pg*	*Pe*	*Pv*	*Pe*	*Pg*	
11,000°	4120	4240	5230	5430	1110	1190	λ_e
5000	4260	4400	5280	5450	1020	1050	λ_e
(M32)	4320	.....	5290	.....	970	.....	λ_e
3000	4430	4560	5370	5480	940	920	λ_e
11,000	2.43	2.36	1.91	1.84	0.52	0.52	$1/\lambda_e$
5000	2.35	2.27	1.89	1.83	.46	.44	$1/\lambda_e$
(M32)	2.31	.....	1.89	.....	.42	.....	$1/\lambda_e$
3000	2.26	2.19	1.86	1.82	0.40	0.37	$1/\lambda_e$

the question of magnitudes for a later discussion of nebulae of different types. In Table 4 our blue and yellow effective wave lengths are on the short side of the International wave lengths, but the base lines for color index are almost the same. The values for M32 are from Table 3; we do not venture to derive photographic wave lengths for a nebula, since the necessary energy-curve beyond 3500 A is not available.

As the figures on black bodies are largely theoretical, we have made the usual comparison on the real stars of the North Polar Sequence. In Table 5 the headings are self-explanatory except for C_p, which is the value of the International color derived from the photoelectric observations. If we let C_{47} denote the observed color index with our filters, reduced to outside atmosphere, then for the 21 NPS stars we find the relation

$$C_{\text{int}} = 0.96 + 1.00 C_{47} \pm 0.01 \pm 0.02\,(\text{p.e.}), \tag{2}$$

where the coincidence in the scales given by the coefficient 1.00 of C_{47} is an unexpected but convenient accident. The C_p in the table is then simply the computed color from equation (2) to be compared with the observed C_{int} for each star. The stars are arranged in the order of increasing color and go down to magnitude 15.3 for No. 277. Most of those brighter than 7.0 were observed only once, but their colors are good enough for the pres-

ent purpose. The original measures give data for clear, blue, and yellow magnitudes; and, denoting the blue magnitudes by Pe_b, we find from ten stars, five white and five red,

$$Pe_b = Pg_{\text{int}} - 0.08 + 0.08C_p \pm 0.02 \pm 0.02\ (\text{p.e.})\,. \tag{3}$$

In other words, the effective wave lengths of the blue magnitudes are to the violet of Pg_{int} by 0.08 $(Pg - Pv)$. The corresponding figure from Table 4 is on the average about 0.17 $(Pg - Pv)$. The agreement is good enough between ideal black bodies and real stars.

We are now ready for the discussion of the colors of the faint nebulae. In the spring of 1947 we undertook a co-operative program with Messrs. Edwin Hubble and Walter Baade for measuring the magnitudes and colors of nebulae of different types and of some stars in Selected Areas. Whitford went to Mount Wilson for the months of March and April, and Stebbins followed for May and June. The outcome was the determination of

TABLE 5

COLORS OF THE NORTH POLAR SEQUENCE

NPS	Pg_{int}	C_{int}	C_p	$C_p - C_{\text{int}}$	NPS	Pg_{int}	C_{int}	C_p	$C_p - C_{\text{int}}$
2	5.21	−0.11	−0.11	0.00	19	12.68	+0.44	+0.40	−0.04
1	4.40	+ .03	− .07	− .10	25	14.12	+0.56	+0.57	+ .01
5	6.47	+ .03	+ .01	− .02	277	15.32	+0.74	+0.68	− .06
6	7.12	+ .06	+ .12	+ .06	8r	11.43	+0.96	+1.00	+ .04
10	9.14	+ .12	+ .16	+ .04	26	14.65	+1.00	+1.06	+ .06
4	5.94	+ .14	+ .13	− .01	4r	9.23	+1.02	+1.00	− .02
2s	6.46	+ .15	+ .24	+ .09	12r	13.78	+1.30	+1.28	− .02
3	5.76	+ .18	+ .16	− .02	3r	8.97	+1.41	+1.39	− .02
13	10.55	+ .22	+ .27	+ .05	1r	6.66	+1.53	+1.54	+ .01
3s	6.61	+ .23	+ .31	+ .08	2r	7.91	+1.57	+1.53	−0.04
16	11.57	+0.34	+0.31	−0.03					

magnitudes of about 175 nebulae, the colors of 100, and the magnitudes and colors of 50 stars in Selected Areas 57 and 61. The present discussion will deal only with the colors of a few faint E nebulae in clusters where the red shift has been well determined. From the whole material it appeared that the E nebulae form a homogeneous class with little color dispersion and that conclusions drawn from small samples may therefore be significant.

The results in Table 6 need little explanation. The identifications of the nebulae in Corona Borealis and Boötes are in Figures 4 and 5. The average velocities of the clusters of nebulae have been kindly furnished by M. L. Humason. The photographic magnitude Pg_p and the color C_p are on the International scale as derived from the photoelectric measures.

Inasmuch as the Boötes nebula was the faintest object we have ever attempted to measure, we reobserved it half-a-dozen times on three nights; Table 7 includes all the measures. The comparison star, SA 61, No. 99, was referred to the ninth-magnitude central star of that Area, which in turn was compared with stars of the North Polar Sequence. The small average deviations for the comparison star are illusory; about ±0.02 or ±0.03 mag. would be the average for magnitude 15.9. The magnitude 18.2 for the nebula represents about the practical limit for useful observations with the installation on the 100-inch telescope. Through the blue filter the magnitude to be measured was 19.3; the mean error of a single deflection was ±18 per cent; hence we place the limit of detection at about photographic magnitude 21. Moreover, the difficulty is enhanced by

the sky background. With the diaphragm of 11″ the ratio sky/nebula was: for blue, 4.2; for clear, 3.2; and for yellow, 2.2. This confirms what we have pointed out before—that for ordinary blue-sensitive photographic plates the action of the ultraviolet simply adds sky fog without contributing much to a nebular image. With such plates a filter cutting out all wave lengths shorter than 4500 A should give increased contrast between sky and nebula. For the bright E and Sb nebulae we get the greatest contrast in the six colors at 4880 A.

TABLE 6

COLORS OF FAINT E NEBULAE

Cluster	Nebula	Km/Sec	P_{gp}	C_p	Remarks
Virgo	.....	1240	9.5–15.6	0.86	18 nebulae
Coma	NGC 4872	6580	(15.1)	0.96	Central region
Coma	Anon	6580	17.4	0.96	
Coma	NGC 4889	6580	13.2	1.05	
Cor Bor	No. 1	22,000	16.8	1.13	
Cor Bor	No. 2	22,000	17.3	1.15	
Cor Bor	No. 3	22,000	17.1	1.13	
Cor Bor	No. 4	22,000	17.1	1.13	
Boötes	No. 1	38,900	18.2	1.36	

TABLE 7

FAINT NEBULA IN BOÖTES

1947	NEBULA NO. 1		SA 61, NO. 99	
	P_{gp}	C_p	P_{gp}	C_p
May 21	18.38	.....	.....	.....
May 21	18.13	1.40	15.92	0.69
May 21	18.18	1.22	.....	.....
May 22	18.22	1.23	15.92	.68
May 22	18.30	1.37	.....	.....
June 22	18.20	1.50	15.94	0.68
June 22	18.19	1.41	.....	.....
Means	18.23	1.36	15.93	0.68
Av. dev.	±0.06	±0.08	±0.01	±0.00

The data in Table 6 are shown graphically in Figure 6. The dispersion in C_p of the Virgo cluster is measured by a standard deviation of ±0.06 mag., which includes the errors of observation. There is no reason to expect smaller dispersion in the Coma and Corona clusters. For the linear relation shown in the figure we find, from the data in Table 6,

$$C_p = 0.84 + 0.0133 \times 10^{-3} V \,, \qquad (4)$$

where V is in km/sec.

Since this increase of color index with velocity or distance will obviously have a considerable effect upon the magnitudes and counts of faint nebulae, we have examined the results critically for any possibility of systematic errors. That the measured color of the nebula at magnitude 18.2 could be far wrong belies all our experience with any photoelectric cell. For stars, our colors agree with the North Polar Sequence over a range of 10 mag. down to 15.3 with the 60-inch, or an intensity of magnitude 16.4 with the 100-inch;

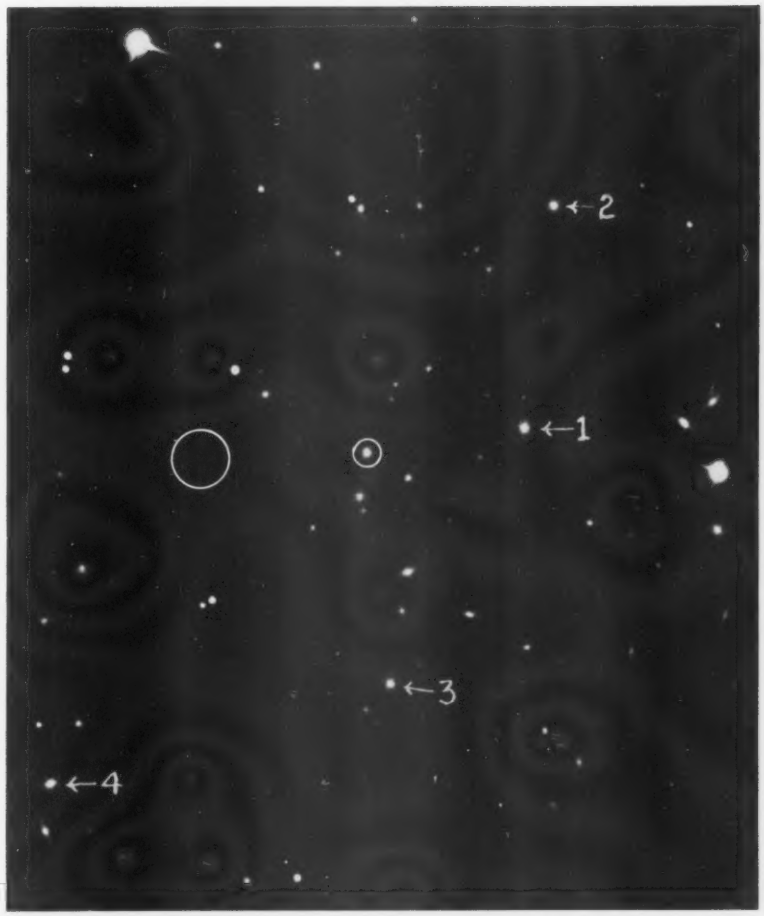

FIG. 4.—Nebulae in Corona Borealis. Diaphragms: larger circle, 24″ for magnitudes; smaller circle, 11″ for colors. In Nos. 3 and 4 the light of the nebula outside the small circle is three-fourths of that inside.

FIG. 5.—Nebula in Boötes. Diaphragm 11″ for both magnitude and colors

also the stars in the Selected Areas show no tendency toward progressive reddening in 8 mag. down to 17.5. For nebulae, the Virgo nebulae show no reddening in 6 mag. to 15.6; and, finally, in Coma the nebula at 17.4 has the color of the group determined from objects up to 4 mag. brighter.

Among other possibilities of systematic error, atmospheric extinction is also to be examined. The colors of stars and nebulae have been corrected by the formula

$$\text{Reduction to no atmosphere: } \Delta C = -(0^m.129 - 0.045C_{47})\sec z \pm 0.006 \pm 0.010 \text{ (p.e.)}. \quad (5)$$

This relation was determined from regular and special observations of stars at high and low altitudes, both east and west of the meridian, and its reliability is perhaps measured by the probable errors. For typical objects of different color we then have, for the reduction at the zenith,

$$C_p = 0.00 \quad +0.84 \quad +1.36$$
$$\Delta C = -0.17 \quad -0.13 \quad -0.11 .$$

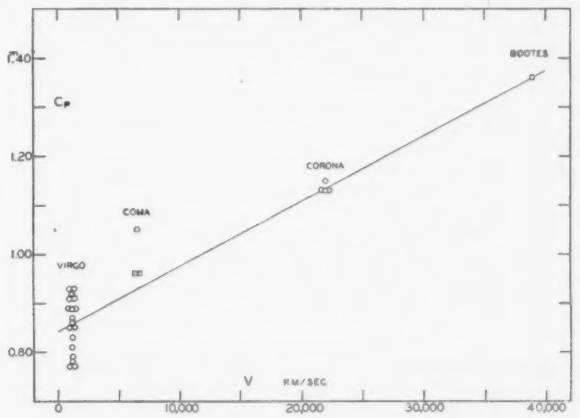

FIG. 6.—Colors and velocities of nebulae in clusters

With a difference of 0.02 mag. in the corrections for the extremes of the nebulae, all taken at high altitude, any residual error in the extinction can be ruled out.

Another possibility to be considered is that the larger proportion of the whole diameter that was included in the focal plane diaphragm in the case of small, faint nebulae could have a systematic effect on the color. The trouble with this assumption is that our measures included nearly the whole diameter of M32; but in any case we have no evidence of differential color between inner and outer regions of E nebulae. For Sb objects the possible effect would be the other way; the outer regions are bluer than the inner ones.

We are left, then, with a marked increase of color index of E nebulae with the distance, which we are convinced is real; and we have now to examine how much of this reddening can be accounted for by the red shift of the spectrum. The nebula in Boötes has a color excess of $1.36 - 0.84 = 0.52$ mag.; and the velocity of 38,900 km/sec corresponds to $1 + d\lambda/\lambda = 1.13$. Hence, if we have the complete energy-curve of a bright E nebula of the same intrinsic color, the calculation of the change of color for the red shift could be readily made. The critical point is, of course, what radiation from the ultraviolet is moved into the observed region. The best answer we have comes from the six-color results on the companion of the Andromeda nebula, M32, which, when compared with a star of known absolute energy-curve, gives us a standard. Although M32 is the only E-type

nebula measured on the six-color system, its use as a typical object seems justified, since both the older C_2 colors[7] and the present two-color system place it near the mean of other near-by samples of its class.

The best star for making the connection with an absolute-energy calibration turns out to be the sun. The solar energy-curves determined by E. Pettit[8] and by C. G. Abbot[9] are especially suited to our purpose, since they were taken with blackened receivers which integrated the absorption lines and continuum over a short range of the spectrum. The smoothed curve should then be on the same basis as the broad bands taken in by the six-color filters. On the other hand, the various absolute energy-curves of stars derived from photographs of the spectrum are so reduced as to evaluate the envelope-curve and ignore the presence of the resolved absorption lines.

The two solar energy-curves agree so closely as to be practically the same for our purpose; they inspire confidence because they are direct bolometric measurements, and they give the necessary ultraviolet portion needed for connection with our "ultra"-point. The remaining uncertainty is the place of the sun in our six-color system. We do have an at-

TABLE 8

ENERGY-CURVE OF M32

	Color	U	V	B	G	R	I	Remarks
	λ	3530	4220	4880	5700	7190	10,300	
(1).....	Sun=dG2, E	10.0	18.0	22.4	20.2	12.0	5.7	From Pettit's curve
(2).....	Sun, Δ mag.	+ 0.61	− 0.02	− 0.26	− 0.15	+ 0.41	+1.22	Referred to BGR
(3).....	dG2−dG6	− 0.08	− 0.07	− 0.02	− 0.02	+ 0.04	+0.07	6 colors; 6 dG2 stars
(4).....	M32−dG6	+ 0.54	+ 0.45	+ 0.27	+ 0.03	− 0.29	−0.91	6 colors, 2 nights
(5).....	M32−dG2	+ 0.62	+ 0.52	+ 0.29	+ 0.05	− 0.33	−0.98	(4)−(3)
(6).....	M32, Δ mag.	+ 1.23	+ 0.50	+ 0.03	− 0.10	+ 0.08	+0.24	(2)+(5)
(7).....	M32, E	0.32	0.63	0.97	1.10	0.93	0.80	Numbers from (6)

tempted direct measure of the sun in six colors without a telescope but with the intensity reduced by reflection from two small aluminum-coated convex mirrors. The result, placing the sun at about dG0, is considered by Stebbins to have some weight but is rejected by Whitford because of the probable stray light in his device. Since this is an observation which, if accordant, one keeps, but, if discordant, one rejects, we mention it here only to show that we are not oblivious to what ought to be done to place the calculated variation of color with red shift on a proper basis. In the present calculation, we assume, following W. W. Morgan and G. P. Kuiper,[10] that the sun is an average dG2 star. Whether the sun is taken as dG0 or dG2 makes little difference in the outcome.

In Table 8 are the steps of the procedure. We begin with the relative energy of the sun at the six-color wave lengths and end with the corresponding figures for M32. The unit for the energy is the mean of blue, green, and red. This energy distribution is shown by the curve in Figure 7. The next step is to displace that curve to the red by multiplying all wave lengths by the factor 1.13. Then we find the change in color C_p by taking the ratios of blue to yellow before and after displacement at the effective wave lengths for M32, namely, at 4320 and 5290 A, from Table 3. The result is the calculated change $\Delta C_p = 0.22$ mag. We note that the slight change in effective wave length caused by the shift of the curve is ignored. Also the over-all luminosity changes due to "number effect" and "energy effect," which must be included in consideration of the influence of the red shift on the nebular counts, have here been neglected because they are the same for all wave lengths and do not change the ratios which determine the colors.

[8] *Mt. W. Contr.*, No. 622; *Ap. J.*, **91**, 172, 1940.

[9] *Smithsonian Physical Tables* (8th ed., 1932), p. 608.

[10] G. P. Kuiper, *Ap. J.*, **88**, 429, 1938.

In his allowance for the effect of red shift upon photographic magnitudes, for lack of better information, E. Hubble[11] was forced to assume that the nebulae radiate somewhat like individual stars, and he assigned to the nebulae the same energy distribution as that of a black body at 6000°. That this assumption could be only a first approximation is shown by its neglect of the well-known depression of the ultraviolet intensity of the sun, and presumably of solar-type stars. Our six-color measures confirm the anticipated result that the nebulae radiate like mixtures of stars. Moreover, J. L. Greenstein[12] has shown that the color temperature of the Andromeda nebula, M31, is nearer 4200° than 6000° and that the corrections for this lower temperature produce serious difficulties in the interpretation of the nebular counts. In M31, Greenstein selected the nebula which we find has the gradient most nearly constant over all wave lengths, and, since his range in $1/\lambda$ was 2.55 to 1.54 as against our 2.83 to 0.97, he missed the extra intensity in the ultraviolet and the infrared. However, from our intermediate range of $1/\lambda$ from 2.37 to

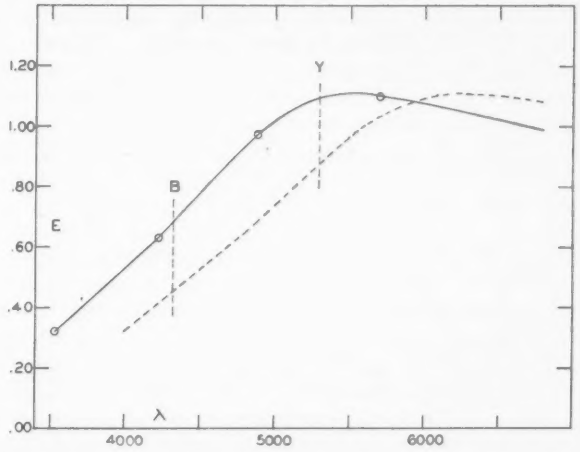

FIG. 7.—Energy-curve of an E-type nebula, M32. *Heavy line*, $V = 0$; *broken line*, $V = 38{,}900$ km/sec. Vertical lines indicate effective wave lengths for blue and yellow.

1.39 we have V − R = +0.80 for M31, and a color temperature of 4250° on our T_1 scale[13] as against Greenstein's 4200°. Without further scrutiny of the standards, this agreement would ordinarily be called a good one.

Carrying through the calculation for the displaced curve of a black body at 6000° in the same fashion as for M32, we find the color change $\Delta C_p = 0.17$ mag. Therefore, we have the following values for the effect of the red shift on the color of a nebula in the Boötes cluster with $V = 38{,}900$ km/sec.

	ΔC_p
Observed	+0.52
Computed, E nebula	+ .22
Computed, black body at 6000°	+0.17

As a further check on the energy-curve, the reference level of the six-color system was determined independently from the Göttingen[14] results on absolute energy distribution,

[11] *The Realm of the Nebulae* (New Haven: Yale University Press, 1936), p. 195.

[12] *McDonald Obs. Contr.*, No. 10; *Ap. J.*, **88**, 605, 1938.

[13] Stebbins and Whitford, *Mt. W. Contr.*, No. 712; *Ap. J.*, **102**, 318, 1945.

[14] Kienle, Strassl, and Wempe, *Zs. f. Ap.*, **16**, 201, 1938; Kienle, Wempe, and Beileke, *Zs. f. Ap.*, **20**, 91, 1940. Other published photographic determinations of absolute energy-curves do not give a sufficiently detailed tabulation of measured points for our purpose.

by using B and F stars common to both surveys. The comparison could not be extended to our "ultra"-point; but, over the range covered, the agreement with the results derived from the sun was satisfactory. As was expected, the evaluation via the Göttingen data gives slightly more violet energy in a dG6 star (and therefore in the nebulae) because of the neglect of the absorption lines in the comparison standards, the difference amounting to about 0.15 mag. This has the effect of reducing the "violet depression" in the M32 curve, which is a much more powerful factor in determining the color change produced by a velocity shift than is the exact temperature assumed. The calibration via the sun, then, gives about the maximum reddening from the velocity shift that can be derived by any method of reduction. We see no escape, therefore, from the conclusion that the nebula in Boötes has an unexplained color excess or reddening of $0.52 - 0.22 = 0.30$ mag.; and, because of the linear relation between color and velocity shown in equation (4) and Figure 6, there is every reason to believe that this reddening is a universal effect for E nebulae at all distances in every part of the sky. Moreover, the reddening is not a subtle effect; it was conspicuous in the first readings on the Boötes nebula. For brighter E's the deflections for blue and yellow were about equal, but for Boötes No. 1 the yellow was obviously about half again as bright as the blue, and, in 5 minutes after the start, one could see by mental arithmetic that the reddening was of the order of half a magnitude. No further observations or discussion could change this obvious fact. We attempted a dozen years ago to test the E nebulae for variation of color with increasing distance, but, as we stopped at magnitude 12.7, nothing was found.[7] The present observations, extending 5 mag. fainter with a base line two and a half times longer, had a better chance of revealing something.

Before considering possible explanations of the new effect, we may note that if the unexplained part of the reddening is proportional to the distance, which is a natural assumption, then the straight-line relation for Figure 6 requires that the red shift part also be proportional to distance. The new observations may therefore be taken as supporting a linear velocity-distance relation by a line of reasoning quite independent of magnitude scales. In fact, the addition of the color effect to this relation may simplify the problem of deriving distances. For instance, in the Coma cluster we get about the same colors over a range of 4 mag. But after the verification of the velocity-distance relation the trouble begins.

First, suppose that the reddening is simply selective absorption by internebular material of the same kind that gives the interstellar absorption in our galaxy. Also make the customary assumption that the total absorption is about four times the selective absorption on the International scale, and we get a photographic absorption $A_{pg} = 4 \times 0.30 = 1.2$ mag. for an uncorrected distance of 70,000,000 parsecs, corrected by a factor of 0.58 to 40,000,000 parsecs because of absorption. Then, within distances three or four times that of the Boötes cluster, we run into a virtual impenetrability of space at limits which heretofore have been considered attainable with present telescopes.

Also we can compare a selective absorption of 0.30 mag. at 40,000,000 parsecs with, say, 0.25 mag. at 1000 parsecs in the region near the sun. These figures give 3×10^{-5} for the ratio of densities, internebular to interstellar material. Taking the latter at 3×10^{-24} g/cm^3, we have something like 10^{-28} g/cm^3, or of the order of ten to one hundred times the smoothed density of luminous nebular material in all space according to Hubble.[15] Such a figure could perhaps be accepted; but to explain the reddening as a consequence of Rayleigh scattering by gas alone would require an impossibly high density and mass in internebular space, just as it would within the galaxy.

The great difficulty in accepting the hypothesis of reddening by internebular material is the absence of any evidence for it in the nebular counts. As is well known, counts of stars in the plane of the galaxy show an apparent outward decrease of density in all

[15] *Op. cit.*, p. 195.

directions; owing to interstellar absorption, there is a large effect at mean distances less than the 1000 parsecs that would give a reddening comparable to that of the Boötes nebula. Absorption corrections to the star counts restore an approximately uniform density. But Hubble[16] showed that the nebular counts down to magnitude 21 were consistent with a uniform distribution, assuming that space is transparent, that the nebulae radiate like black bodies at 6000°, and that the red shift is not a real recession. A real recession led to outward-increasing density. Internebular absorption would require inward correction factors to the photometric distances increasing rapidly with the fainter magnitudes from the ratio 1/0.58 mentioned for the Boötes nebula. A steep outward increase in density would be inescapable. The only explanation would lie in a relativistic universe of a very short radius of curvature, and a much higher mean density of matter than that previously assumed.

At first, the possibility of a time effect was considered—namely, that the nebulae were formerly redder than now and that what we observe is simply their progressive change in color in the interval of 2×10^8 years from the Boötes nebula inward. We rejected it because the time involved is only a small fraction of the accepted age of the sun and of our galaxy. The possibility of changes in the nebulae during the light-travel time has been in the background since it was mentioned by Hubble and Tolman[17] more than a dozen years ago. In the discussion at the meeting of the American Astronomical Society in Columbus in December, 1947, Dr. Martin Schwarzschild suggested that, since our measures were of E nebulae only, we are dealing with population II and that these objects may once have contained large numbers of high-luminosity red giants. These stars would have consumed their energy at a high rate[18] and have faded in the time since the light left the distant ones. In population II there is no interstellar material out of which a continuing supply of giants may be condensed.

The corrections to the photometric distances on the time-effect hypothesis would be much less than for the space-reddening hypothesis, and of the opposite sign. The intrinsic photographic brightness of a distant nebula would be greater than that of a near-by one, since the extra stars which have since faded must contribute to all wave lengths, though most strongly at the red end of the spectrum. An increase in the International color index of a nebula from 0.85 to 1.15 mag., which would give it the observed color excess of 0.30 mag. for the Boötes nebula, could be achieved by adding M supergiants of color index 1.7 mag. to give a photovisual increase of 0.64 mag. The photographic increase would be 0.34 mag., and the outward distance correction factor would be 1.17. Before such a factor were applied to nebulae in general, it would be necessary to know more about the colors of distant spirals, where the time effect would probably be quite different. But the correction is in a direction which lowers the space density of the more distant objects and thus helps to avoid outward increasing density. Corrections up to +0.63 mag. to the magnitudes of faint stars in M31 have been derived by W. Baade.[19] If applicable to all nebulae, these corrections are also in a direction which lowers the space density of the nebulae counted in the faintest magnitude intervals. Certainly, the magnitudes of the nebulae ought to be established beyond doubt; that is the reason the present program was undertaken.

We are well aware of the danger of drawing far-reaching conclusions from the observations of only a few objects; but, after all, the number of nebulae observed with the

[16] *Ibid.*, p. 187.

[17] *Mt. W. Contr.*, No. 527; *Ap. J.*, **82**, 302, 1935.

[18] A. Schatzman (*Ann. d'ap.*, **10**, 14, 1947) has discussed the effect of the short life of the red giants on the luminosity of nebulae and the consequences in interpreting the nebular counts. H. N. Russell (*Pub. A.S.P.*, **60**, 202, 1948) suggests the fading of the red giants as the reason for the present abrupt upper limit of luminosity in population II.

[19] *Mt. W. Contr.*, No. 696, p. 6; *Ap. J.*, **100**, 142, 1944.

greatest velocities is not very large either. To summarize, we seem to be justified in making the following tentative conclusions:

1. The energy-curves of the nebulae are those to be expected from mixtures of stars; they show excess energy in both the infrared and the ultraviolet over that of a black body. The ultraviolet excess must be taken into account in evaluating the effect of the red shift on the apparent photographic luminosity of a faint nebula.

2. The E nebulae show a reddening proportional to the red shift. This may be taken as corroborative evidence for a linear velocity-distance relation. About 60 per cent of the reddening is a color excess not explained as a consequence of the red shift.

3. If the excess reddening is a distance effect caused by selective absorption of internebular dark material, then the total mass of such material must be ten to one hundred times as great as the total mass of the luminous nebulae. The inward corrections to the photometric distances would, on such a hypothesis, be so great as to be very difficult to reconcile with the smooth run of the nebular counts.

4. If the excess reddening is a time effect, we are seeing a considerable change in the nature of E-type nebulae in only 2×10^8 years. The distance corrections would then be outward and smaller than for the space-reddening hypothesis.

5. Whatever the explanation of the color excess, the interpretation of the nebular counts will certainly be affected by new corrections involving the absolute energy-curves, by improved magnitudes, and by color and luminosity changes which are functions of the distance. Until these are better understood, previous conclusions about the outer regions of the observable universe may be considered open to revision.

We are indebted to Messrs. Edwin Hubble and Walter Baade for selecting the faint nebulae and arranging the observing program; also to them and to Edison Pettit for cooperation in the observations at the telescope.

This investigation was supported in its earlier stages by the Observatory Council of the California Institute of Technology and by the Research Committee of the Graduate School of the University of Wisconsin from funds supplied by the Wisconsin Alumni Research Foundation. The improvements in the method of using the 1P21 multiplier both at Madison and at Mount Wilson were made possible by a grant from the Gould Fund of the National Academy of Sciences.

RELATIVE TRANSITION PROBABILITIES OF THE SWAN BANDS OF CARBON*

ROBERT B. KING
Mount Wilson Observatory
Received July 30, 1948

ABSTRACT

The relative transition probabilities of the vibrational bands in the Swan system ($^3\Pi_g$–$^3\Pi_u$) of the carbon molecule C_2 have been derived from relative intensities of the band heads appearing in electric-furnace emission spectra under conditions of thermodynamic equilibrium. The method and possible sources of error are discussed. The results from furnace spectra are compared with those from theoretical and experimental work of other investigators.

The well-known Swan bands, belonging to the spectrum of the carbon molecule C_2, consist of several sequences of vibrational bands scattered throughout the visible spectrum. They arise from the electronic transition $^3\Pi_g$–$^3\Pi_u$, where $^3\Pi_u$ is probably the ground state. In the laboratory the Swan bands are observed in emission in several types of sources, including the graphite-tube electric furnace, in which some of the stronger bands may also be obtained in absorption. The Swan bands are among the outstanding features of R- and N-type stars and of the heads of comets.

Since the Swan bands exhibit a large range in intensities, studies of their intensities in celestial sources offer considerable promise; moreover, they arise from vibrational states of a sufficient range of energy to make determinations of excitation temperature practicable. In addition, some stars have bands due to the isotopic combinations $C^{12}C^{12}$, $C^{12}C^{13}$, and $C^{13}C^{13}$. The well-established theoretical formulae for the relative intensities of rotational lines in a band are of limited usefulness in interpreting stellar spectra, in the case of the Swan bands, because of blending due to low dispersion. More practicable applications might be found for data on the relative strengths of vibrational band heads. Because theoretical vibrational band intensities are subject to uncertainties and have not yet received extensive laboratory confirmation and because of the astrophysical importance of the Swan system in particular, measurements of the intensities of these bands produced in the graphite-tube electric furnace under conditions of thermodynamic equilibrium should be of value.

In the furnace the strongest Swan bands begin to appear in emission at about 2450° K, and the weaker are well developed at around 2850° K. In furnace absorption spectra, made with the aid of a tungsten-filament lamp operated at about 3200° K, the (0, 0) band λ 5165 can be seen from about 2800° to 3000°; above 3000° the bands begin to emit more energy in the line of sight than they absorb or scatter from the continuum. At the highest temperature, only λλ 5165 (0, 0), 5129 (1, 1), 4737 (1, 0), 4715 (2, 1), and 4697 (3, 2) appear in absorption. Therefore, while measurements of transition probabilities from absorption spectra would in some respects be simpler and subject to fewer uncertainties, it was necessary to use emission spectra for the major portion of the work.

The electric furnace[1] with tubes of Acheson graphite was used to excite the Swan bands. Prior to photographing the spectrum, the furnace was run for several minutes at a high temperature to drive off impurities. The pressure in the furnace was about 1 cm of *Hg*. Temperature measurements, on the inner surface of the furnace tube, were made with a

* *Contributions from the Mount Wilson Observatory, Carnegie Institution of Washington*, No. 752.

[1] A. S. King, *Mt. W. Contr.*, No. 247; *Ap. J.*, **56**, 318, 1922.

Leeds and Northrup optical pyrometer immediately before and after each exposure. If the temperature changed during an exposure, the mean of the two readings was used, although such changes were seldom over 5° or 10°.

Emission spectra were photographed in the first order of a 1-meter concave-grating spectrograph, with a dispersion of 16.8 A/mm. With this instrument the whole spectral region (λλ 4300–6200) covered by the bands could be photographed with one exposure. Eastman Panatomic-X film was used because it has a very uniform sensitivity throughout this region and has fairly fine grain with only moderate contrast. Films were developed in D-19 developer.

Because it was necessary to use a variety of exposure times, from 15 seconds to 4 minutes, in photographing the furnace band spectra, two calibration spectra, with ½- and 2-minute exposures, were photographed on each film by means of a tungsten-filament lamp and a platinum-on-quartz step-weakener. By using the appropriate calibration exposure, the maximum error due to change in gamma with exposure time was reduced to less than 2 per cent. Characteristic curves at wave lengths near the middle of each band sequence were used.

Film standardization, i.e., the determination of sensitivity as a function of wave length, was done with the aid of a graphite plug placed at the center of the furnace tube. Energy radiated by this plug should have very nearly a black-body distribution. A spectrum of the plug, at a temperature of about 2700° K, was photographed on each film through the same optical system used for the band-spectrum exposures, suitable exposures being obtained with the aid of a diaphragm in the optical path. At each band the ratio between the intensity of the observed black-body continuum and that of a theoretical black-body-curve at the same temperature was taken as the film-sensitivity factor for that wave length.

A furnace run consisted of fifteen or more furnace band spectra, with the accompanying calibration and standardization spectra. The furnace spectra started at about 2450° K, where only the (0, 0) band λ 5165 appears, and were photographed at 20° or 30° intervals up to a temperature of about 3000° K. Exposure times varied inversely with the temperature, from 4 minutes to 10 seconds, depending on the time required to bring the continuous background above the threshold of the emulsion. Measurements of densities of the band-head peaks and of the adjacent continuous background were converted to intensities by means of the proper calibration-curve, and the differences (peak intensity *minus* background intensity) were taken as apparent intensities of the bands. The apparent intensities, when corrected for film sensitivity as a function of wave length, became true relative intensities of the band-head peaks. In low-temperature spectra, only the strongest heads appeared; at the highest temperatures the weaker bands were measurable, but the strongest were too dense for accurate measurement.

Peak intensities are not exact indices of the true relative intensities of the vibrational bands in an electronic system. Differences exist in the quantum numbers and in the separations of rotational lines comprising the band heads, as well as in the energy distribution as a function of temperature. The structures of the Swan band heads, however, are similar. Each is composed of overlapping lines of the three *P*-branches. The distance from band origin to head, for the bands here treated, varies from about 5.7 to 7.1 A. Thus, with a spectrograph of constant dispersion, measurements of the band-head peak intensities should yield reasonably close approximations to the true relative band intensities. They certainly offer by far the most practicable method of attack in this case.

The relative intensities in emission of vibrational bands in a system are given by the formula

$$I = N'_v \cdot R^2 \cdot \nu^4 , \tag{1}$$

where N'_v is the number of molecules in the upper vibrational state v', R^2 the transition probability, and ν the frequency of the band. To compare intensities of bands photo-

graphed with different exposure times and arising from different vibrational states in the upper electronic term $^3\Pi_g$, we can set

$$N v' = N_0 \cdot e^{E_{v'}/kT} \cdot t \,, \tag{2}$$

where N_0 is a number proportional to the total number of C_2 molecules existing per second in the emitting vapor; the exponential is the Boltzmann factor, giving the relative numbers of molecules occupying the vibrational levels of energy $E_{v'}$ at the temperature T; and t is the exposure time.

A curve giving values of N_0 as a function of T was computed from the free-energy equations for C_2 given by K. K. Kelley.[2] These relative values of N_0 in the range of temperatures used are in accord with the results of recent investigations of the vapor pressure of C_2 by Brewer, Gilles, and Jenkins,[3] of the University of California, i.e., the slope of their vapor pressure versus temperature-curve is the same as Kelley's, although the absolute values are different.

If values of log I/ν^4 for a single band, derived from successive exposures at different temperatures, are plotted against values of log N_v' computed from equation (2), the points should lie along a straight 45° line, provided that self-absorption does not play a role. The positions of these lines for different bands measured along either axis should be proportional to the logarithms of the relative transition probabilities (R^2) of the bands. Since values of I were measured for each band head on as many spectra as possible in a single furnace run, usually eight or ten, the relative transition probabilities derived from the plots of log I/ν^4 versus log N_v' were based on the means of a number of measurements. The fact that the points did fall along 45° lines was taken to indicate (*a*) that the rate of growth of the emission-band peak intensities is directly proportional to the rate of increase of C_2 molecules, with temperature as calculated from the equations for vapor pressure as a function of temperature, and (*b*) that, in the intensity range used, self-absorption is not a factor.

This linear relationship between I and N_v' over the full temperature range covered by the experiments was further confirmed by the behavior of the (1, 0) band λ 4737 of the molecule $C^{12}C^{12}$ in relation to the (1, 0) band λ 4744 of the molecule $C^{12}C^{13}$. The statistical formula giving the relative numbers of the three possible molecular combinations, $C^{12}C^{12}:C^{12}C^{13}:C^{13}C^{13}$, is

$$r^2 : 2r : 1 \,,$$

where r is the abundance ratio $C^{12}:C^{13}$. In terrestrial carbon, this ratio[4] is very close to 90:1; the abundance ratio of the molecules $C^{12}C^{12}:C^{12}C^{13}$ should be about 45:1. The mean ratio, obtained from the furnace intensity measurements on λ 4737 and λ 4744 by plotting for each the values of log I/ν^4 versus log N_v' (assuming R^2 the same) and measuring the separation of the lines drawn through the points, is about 44:1. Since the measurements of I for λ 4737 were made at relatively low temperatures (2475°–2775° K) and those for λ 4744 at high temperatures (2725°–3025° K) and since the relative values of N_v' at these temperatures depend upon the slope of the vapor pressure versus the temperature-curve, the reasonable abundance ratio obtained indicates that, in the temperature range used in the experiments, the relationship between I and values of N_v' computed from vapor-pressure data must be very nearly linear.

It is possible that observed intensities of bands associated with the ground vibrational state (λλ 5165, 4737, and 4382) might be affected by self-reversal. Because band heads are made up of many closely packed narrow lines, self-reversal might be expected to produce only a general softening or reduction in intensity of the band head. If self-rever-

[2] *U.S. Bur. of Mines, Bull.*, No. 383, 1935.

[3] *J. Chem. Phys.*, **16**, 797, 1948.

[4] B. F. Murphy and A. O. Nier, *Phys. Rev.*, **59**, 771, 1941.

sal exists, relative transition probabilities for bands from different low vibrational states derived from absorption spectra should be different from those derived from emission spectra. To check this, absorption spectra of the λ 5165 and λ 4737 sequences were obtained in the second order of the 1-meter spectrograph and in the first order of the 15-foot spectrograph. From these spectra it was possible to measure the peak absorptions and to make determinations of the total absorption of the band heads λλ 5165 (0, 0), 5129 (1, 1), 4737 (1, 0), 4715 (2, 1), and 4697 (3, 2). The relative transition probabilities derived for these bands from these measurements showed no systematic differences related to v'' compared with those obtained from emission spectra; it was, therefore, concluded that self-reversal is negligible.

TABLE 1

RELATIVE TRANSITION PROBABILITIES OF C_2 SWAN BANDS

λ	v', v''	TRANSITION PROBABILITIES		
		Furnace	Theory	Johnson and Tawde
4382	2,0	0.044	0.034	0.035
4371	3,1	0.111	0.149	0.095
4365	4,2	0.252	0.215	0.180
4737	1,0	0.358	0.324	0.440
4715	2,1	0.525	0.422	0.545
4697	3,2	0.718	0.392	0.615
4684	4,3	0.952	0.334	0.657
4678	5,4	1.56	0.246	0.862
5165	0,0	1.000	1.000	1.000
5129	1,1	0.520	0.436	0.418
5097	2,2	0.256	0.144	0.116
5070	3,3	.....	0.022	0.044
5635	0,1	0.244	0.354	0.454
5585	1,2	0.470	0.511	0.419
5540	2,3	0.497	0.544	0.436
5501	3,4	0.802	0.498	0.440
5473	4,5	.....	0.435	0.324
6191	0,2	0.043	0.048	0.306
6122	1,3	0.123	0.121	0.475
6059	2,4	0.188	0.203	0.612

The measurements of relative transition probabilities for the Swan bands from furnace emission spectra as described above have, therefore, been based on certain premises, all except the first of which have been at least partially checked during the course of the investigation: (1) In the furnace the distribution of C_2 molecules in the vibrational levels of the upper electronic state is in accordance with the Boltzmann formula for thermodynamic equilibrium at the temperature of the wall of the graphite tube. (2) The relative numbers of C_2 molecules in the vapor in the furnace tube is proportional to the vapor pressure of C_2 at that temperature as determined by other investigators. (3) The total intensities of the bands are proportional to the peak intensities of the band heads as observed under low and constant dispersion. (4) Self-reversal in bands from the ground vibrational state ($v'' = 0$) is negligible.

The final results for the relative transition probabilities of the Swan bands are given in the third column of Table 1. These are mean values from four different furnace runs,

in each of which from three to thirteen individual intensity measurements on each band were made at different temperatures. The average differences between the results for a single band from different furnace runs was about 5 per cent.

Theoretical relative transition probabilities for the Swan bands have been calculated by K. Wurm[5] and by McKellar and Buscombe,[6] using the theory developed by E. Hutchisson[7] on the basis of quantum mechanics, for the relative intensities of electronic-vibrational bands in the spectra of symmetrical diatomic molecules. In the fourth column of Table 1 are listed the theoretical relative transition probabilities calculated by McKellar and Buscombe.[6] The scale is adjusted to that for the furnace values by setting R^2 for λ 5165 equal to 1.00. Many of the theoretical and furnace transition probabilities seem to agree within the theoretical and experimental uncertainties. The discrepancies which are probably real are (*a*) the tendency of the furnace values for the higher members of the λ 5635 and λ 4737 sequences to increase more rapidly than do the theoretical values and (*b*) the relatively large difference between the theoretical and the furnace values for λ 5635. The intensity measurements for the secondary heads of the λλ 5635, 5165, and 4737 sequences are the most uncertain because of blending by overlapping bands, and this uncertainty increases for the higher members. Nevertheless, the writer feels that these differences are, in part at least, real. On the other hand, the measurements of relative intensities of leading bands of each sequence are much more precise; therefore, the difference between the theoretical and the experimental values for λ 5635 seems larger than should be expected.

The theoretical transition probabilities, particularly those for higher members of sequences, are extremely sensitive to the value Δr, the difference in equilibrium separation of the atomic nuclei in the upper and lower electronic states; but Δr is not known with sufficient precision to remove all uncertainty from the calculations. McKellar and Buscombe adopted the value $\Delta r = 0.047$ A. A slightly different Δr might reduce the discrepancies between theoretical and furnace transition probabilities for higher members of the sequences but would, at the same time, upset the relatively good agreement between bands in the λ 6191 and λ 4382 sequences and the strengths of these as compared with λ 5165. It appears, therefore, that, while certain real differences exist between experimental and theoretical transition probabilities, they cannot be easily accounted for.

For comparison and completeness the last column of Table 1 lists the mean values of the transition probabilities derived by Johnson and Tawde[8] from measurements of band-head peak intensities in emission spectra of five different laboratory sources: Bunsen flame, oxy-coal gas flame, carbon arc in hydrogen, argon discharge tube, and spark under glycerine. Here again R^2 for λ 5165 is set at 1.00. Since the distributions of molecules in excited states in these sources do not necessarily correspond to conditions of thermodynamic equilibrium, Johnson and Tawde determined the distributions by assuming that the sum of the transition probabilities of all observed bands from each upper vibrational state (v') is a constant. The most significant difference between their results and those from furnace and theory is in the λ 6191 sequence, where the values of Johnson and Tawde are much larger than the furnace or the theoretical values.

It is a pleasure to acknowledge the kindness of Dr. Leo Brewer, of the Department of Chemistry of the University of California, in providing C_2 vapor-pressure data in advance of publication. Thanks are due also to Dr. Andrew McKellar, of the Dominion Astrophysical Observatory, Victoria, B.C., for furnishing his theoretical transition probabilities in advance of publication and for calling my attention to the work of Johnson and Tawde.

[5] *Zs. f. Ap.*, **5**, 260, 1932.

[6] *Pub. Dom. Ap. Obs., Victoria*, Vol. **7**, No. 23 (in press).

[7] *Phys. Rev.*, **36**, 410, 1930.

[8] *Proc. R. Soc., London, A*, **137**, 575, 1932.

AN EXTENSION OF THE SWAN SYSTEM OF THE C_2 MOLECULE

JOHN G. PHILLIPS
Yerkes Observatory
Received May 24, 1948

ABSTRACT

The analysis of the Swan system ($A^3\Pi_g - X^3\Pi_u$) has been extended to higher vibrational levels through the study of the Swan "tail" bands, at λλ 4770, 4836, 4911, 4997, 4395, and 4734. Detailed analyses have been carried out on the bands at λλ 4770, 4395, and 4734. The last two of these, at λλ 4395 and 4734, are headless bands that have not been previously mentioned in the literature. The vibrational numbers that were found for the six bands are included in Table 11. The (0–2), (1–3), (2–4), and (3–5) bands of the $\Delta v = -2$ sequence have also been analyzed, in order to complete the analysis of low vibrational levels. All the available material on the Swan bands was then used to obtain improved molecular constants for the two electronic states. These are given in Table 14.

A linear extrapolation of the vibrational quanta of the upper ($A^3\Pi_g$) state gives 5.30 e.v. as an upper limit for the dissociation energy of this electronic state. Depending upon whether it dissociates into ($^3P + {}^3P$) atoms or ($^3P + {}^1D$) atoms, the upper limit to the heat of dissociation of C_2 is 5.30 or 4.04 e.v.

A. INTRODUCTION

When the spectrum of the C_2 molecule is produced in the laboratory, several bands are found in addition to those belonging to recognized systems. Their heads have been measured by several investigators,[1] and it is commonly believed that they are produced by the C_2 molecule, since they are found only when the usual C_2 spectrum is excited. While the transitions responsible for most of these bands are completely unknown, four of them—at λλ 4770.13, 4836.13, 4910.99, and 4996.74—have long been suspected to be "tail" bands of the Swan system ($A^3\Pi_g - X^3\Pi_u$) for the following reasons: (1) They are found to the red of the $\Delta v = +1$ sequence of that system; (2) they are degraded in the opposite direction to the Swan bands (i.e., to the red); (3) the separations between successive bands increase with wave length; (4) their relative intensities decrease uniformly with increasing distance from the head of the $\Delta v = +1$ sequence; and (5) their general appearance is similar to the appearance of the "tail" bands of the violet *CN* system. A reproduction of the Swan system showing three of these bands is given in Figure 1, spectrum (*a*).

Up to the present time, no attempt has been made to test this identification. Such an investigation, however, would be of value, since it would provide a means for extending the analysis of the Swan system to higher vibrational levels, if the bands can actually be shown to be the tail bands.

A vibrational analysis of the Swan bands has been made by R. C. Johnson,[2] and an improvement of his constants for the lower state by J. G. Fox and G. Herzberg.[3] They find that for low vibrational levels the following equation holds:

$$\nu = 19373.87 + 1773.42\,v' - 19.35\,v'^2 - (1629.99\,v'' - 11.71\,v''^2).$$

On the basis of this equation, the $\Delta v = +1$ sequence would come to a "head of heads" at the 8–7 band, and the first tail band would be the 15–14 band. It is impossible to match these computed band origins with the observed heads; in fact, the extrapolation, if correct, would require a spacing between successive tail bands about half the observed

[1] See, e.g., R. W. B. Pearce and A. G. Gaydon, *The Identification of Molecular Spectra* (London: Chapman & Hall, Ltd., 1941).

[2] *Phil. Trans. R. Soc.*, **226**, 157, 1926/27.

[3] *Phys. Rev.*, **52**, 638, 1937.

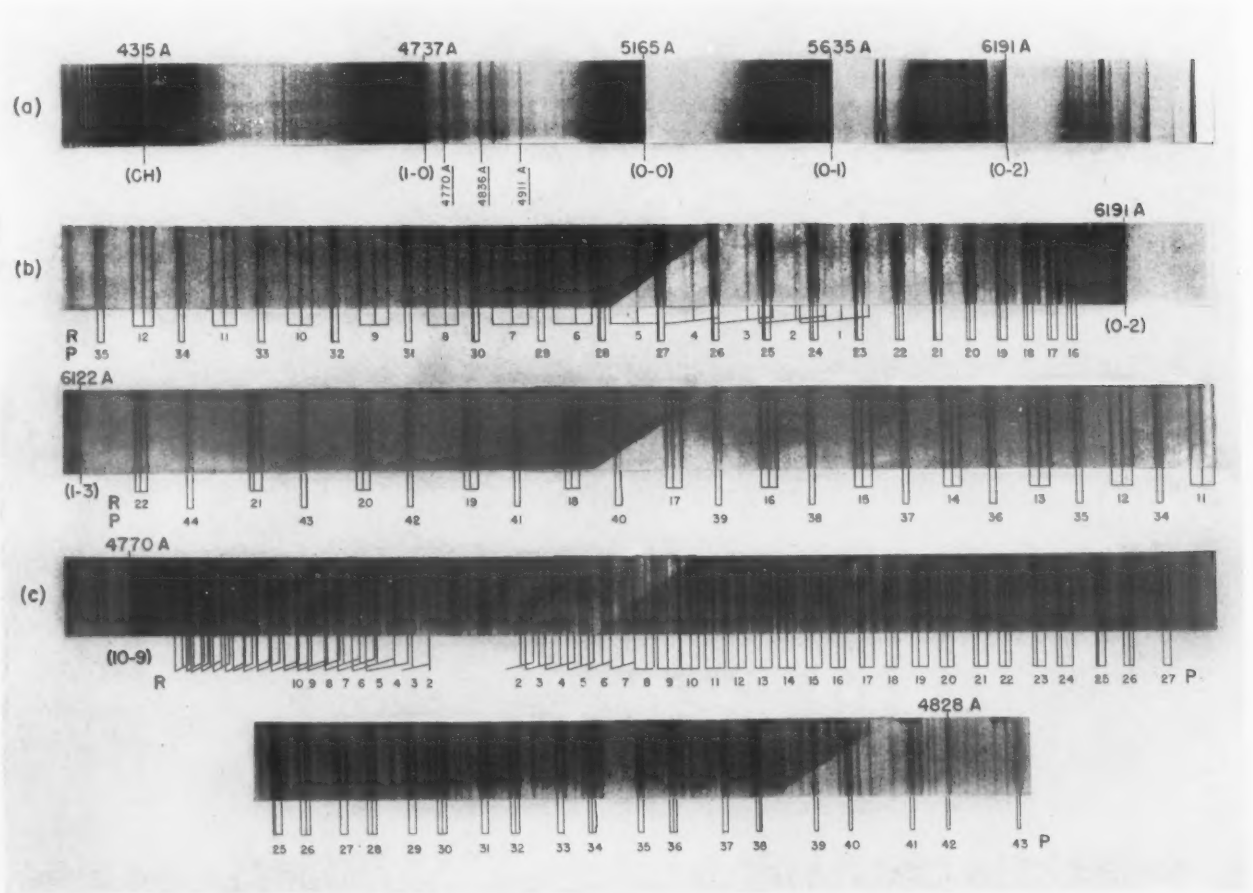

FIG. 1.—The Swan system of the C_2 molecule. (*a*) Low-dispersion spectrum showing the principal sequences of the Swan system and three "tail" bands, at λλ 4770, 4836, and 4911 A, to the red of the (1–0) sequence. (*b*) High-dispersion spectrum of the (0–2) band. (*c*) High-dispersion spectrum of the (10–9) band.

spacing. Thus, if the observed bands are actually the Swan tail bands, then Johnson's linear equation is not valid for higher vibrational levels.

For this reason, it was desirable that a study of the "normal" Swan bands be made, in order to extend the vibrational analysis to as high vibrational levels as possible, before attempting any extrapolation to the tail bands.

The investigation, therefore, was divided into two parts:

1. *The study of the normal Swan bands.*—Previous investigations had provided information about a number of the lower levels, but they were somewhat scattered, and undesirable gaps were left. Johnson's extensive investigation gave good measures of the band heads, but his analysis of the fine structures of bands from higher vibrational levels was not complete enough to yield accurate rotational constants for these levels. J. D. Shea[4] measured the (0–0), (0–1), (1–0), (1–1), and (1–2) bands. A. Budó[5] rediscussed Shea's measurements in the light of present-day theory and published rotational constants for the first two levels ($v = 0, 1$) of the upper and lower states. For the ground state, reliable constants were given for vibrational levels from $v'' = 3$ to $v'' = 6$ by Fox and Herzberg.[3] Finally, R. C. Johnson and R. K. Asundi[6] have published a list of band heads of the so-called "high-pressure carbon bands," and G. Herzberg[7] has shown that they are members of the Swan system, with a common upper level at $v' = 6$, and lower levels ranging from $v'' = 0$ to $v'' = 11$. However, while Johnson and Asundi did measure the fine structure of a number of these bands, they did not succeed in obtaining any rotational constants for the levels involved.

Thus constants were available for the first seven vibrational levels of the ground state, from $v'' = 0$ to $v'' = 6$, with the exception of the level with $v'' = 2$, while they were available only for the two levels with $v' = 0$ and $v' = 1$ of the upper state.

In view of this situation, it was considered worth while to remeasure a number of Swan bands, in order to extend the analysis of the upper state and to determine the constants for the lower level with $v'' = 2$. Accordingly, measurements and analyses were made on the bands of the $\Delta v = -2$ sequence, with heads at 6191.2 A (0–2), 6122.1 A (1–3), 6059.7 A (2–4), and 6004.9 A (3–5). This sequence was chosen for analysis because the bands were farther apart than in other sequences farther to the violet.

2. *The study of the tail bands.*—As many as possible of the tail bands were measured and analyzed. These included: (*a*) the band at 4770 A; (*b*) a partially blended band at 4734 A, which presumably immediately preceded the 4770 A band in the $\Delta v = +1$ sequence; (*c*) a headless band at 4395 A, just to the red of the (2–0) Swan band. Throughout the rest of this paper these bands will be referred to as "*a*," "*b*," and "*c*." A reproduction of band *a* is given in Figure 1, spectrum (*c*). Bands *b* and *c* have not been previously mentioned in the literature.

The analysis of these bands has shown that they are indeed members of the $^3\Pi_g - {}^3\Pi_u$ Swan system. The curves of ΔG versus v for the upper and lower states have been derived from the wave numbers of the origins of all the bands studied, and an estimate has been made of the dissociation energy of the upper state.

B. EXPERIMENTAL

The apparatus and techniques used to produce the C_2 spectrum have been described in a previous paper.[8] Briefly, the procedure was to stream a mixture of benzene vapor and purified argon through a discharge tube, which produced the C_2 spectrum with high intensity. The Swan and tail bands were photographed in the second and third orders of the 21-foot grating spectrograph, which gives a dispersion of 1.25 A/mm in the second order. The exposure times ranged from 3 to 30 minutes. 103*a*-O and I-F emulsions were used.

[4] *Phys. Rev.*, **30**, 825, 1927.

[5] *Zs. f. Phys.* **98**, 437, 1936.

[6] *Proc. R. Soc. London, A*, **124**, 668, 1929.

[7] *Phys. Rev.*, **70**, 762, 1946.

[8] J. G. Phillips, *Ap. J.*, **107**, 389, 1948.

C. THE $\Delta v = -2$ SEQUENCE

a) ROTATIONAL ANALYSIS

As an illustration of the structure of the Swan bands, a reproduction of the (0–2) band is given in Figure 1, spectrum (*b*). As can be seen, it consists of six branches, three of which form the head of the band. Since the bands degrade to the violet, the head-forming branches must be P branches, and the others R branches. For large rotational numbers the members of the P and R branches with the same K are close together, forming well-defined triplets. The task of assigning K values to the triplets was made relatively simple through the use of previously published combination differences, in the following way. Since the (0–2) and (1–3) bands have upper states in common with the (0–0) and (1–1) bands, respectively, the combination differences $\Delta_2F_i'(K) = R_i(K) - P_i(K)$ for the upper states of these latter two bands as given by Shea[4] were used to assign K values in the first two bands. Similarly, K values were assigned to the triplets of the (2–4) and (3–5) bands through the use of the combination differences $\Delta_2F_i''(K) = R_i(K-1) - P_i(K+1)$ derived by Fox and Herzberg[3] for the (0–4) and (0–5) Fox-Herzberg bands. Finally, the assignment found above in the case of the (1–3) band could be checked by comparing the resulting combination differences with those of the (0–3) Fox-Herzberg band. The comparison was satisfactory, providing a confirmation of the analyses of Shea and Fox and Herzberg.

Following the convention introduced by Budó, the subscripts i in the equations given above for the combination differences take the values 1, 2, or 3, depending on whether the quantum number $J = (K + 1)$, K, or $(K - 1)$, respectively, in the three sub-bands. Furthermore, since the $^3\Pi$ terms of the C_2 molecule are inverted, $J = (K + 1)$, K, or $(K - 1)$ for the sub-bands $^3\Pi_2 - {}^3\Pi_2$, $^3\Pi_1 - {}^3\Pi_1$, and $^3\Pi_0 - {}^3\Pi_0$, respectively. Fox and Herzberg had identified the sub-bands in their analysis mentioned above, so that from the comparison of the combination differences it was immediately possible to assign the red, central, and violet components of the triplets to the $^3\Pi_0 - {}^3\Pi_0$, $^3\Pi_1 - {}^3\Pi_1$, and $^3\Pi_2 - {}^3\Pi_2$ sub-bands, respectively.

As can be seen from Figure 1, the triplets of the (0–2) band are easy to identify, since this band is unblended with any other for small K values. Thus the procedure was to start with this band and to extend the branches as far to the violet as possible. Its analysis was carried through the succeeding bands to the head of the (3–5) band. With the branches of the (0–2) band identified, everything remaining between the (1–3) and the (2–4) band heads must necessarily be part of the (1–3) band. Thus the branches of this band could be identified unambiguously and could be extended, in turn, as far to the violet as possible, through the aid of the known combination differences. In this manner the branches in Tables 1–4 were picked out. Since it is desirable to have all the observational material grouped together, Tables 5, 6, and 7 present the wave numbers of the (8–6), (9–8) and (10–9) bands, respectively. The manner in which the analyses of these three bands were carried out will be described later in this paper.

With K values assigned to each triplet, the rotational constants B_v and D_v were evaluated according to the method of Budó[5] for $^3\Pi$ states. With his method, average combination differences $\Delta_2F_m(J) = \frac{1}{3}[\Delta_2F_1(J) + \Delta_2F_2(J) + \Delta_2F_3(J)]$ were found for each band; and then the $\Delta_2F_m(J)$ combination differences were treated as though they pertained to a singlet system. According to the usual methods,[9] the following equation was used to find the rotational constants:

$$\frac{\Delta_2F_m(J)}{J+\frac{1}{2}} = 4B_v - 8D_v(J+\tfrac{1}{2})^2.$$

[9] G. Herzberg, *Molecular Spectra and Molecular Structure*, Vol. I (New York: Prentice-Hall Book Co., Inc., 1939).

TABLE 1

WAVE NUMBERS OF THE LINES IN THE (0–2) BAND

($\nu_0 = 16165.79$ Cm^{-1})

J	$^3\Pi_0 - {}^3\Pi_0$		J	$^3\Pi_1 - {}^3\Pi_1$		J	$^3\Pi_2 - {}^3\Pi_2$	
	$R_3(J)$	$P_3(J)$		$R_2(J)$	$P_2(J)$		$R_1(J)$	$P_1(J)$
0	16170.08	.....	1	16172.50	.....	2	16176.28	.....
1	173.98	.....	2	176.63	.....	3	179.98	.....
2	178.68	.....	3	180.95	.....	4	184.01	.....
3	183.57	.....	4	185.82	.....	5	188.40	.....
4	189.00	.....	5	190.85	.....	6	193.21	.....
5	194.87	.....	6	196.32	.....	7	198.32	.....
6	200.63	.....	7	202.00	.....	8	203.77	.....
7	206.92	.....	8	208.04	.....	9	209.58	.....
8	213.17	.....	9	214.34	.....	10	215.71	.....
9	220.01	.....	10	220.97	.....	11	222.18	.....
10	226.83	.....	11	227.87	.....	12	228.95	.....
11	234.25	.....	12	235.11	.....	13	236.09	.....
12	241.69	.....	13	242.61	.....	14	243.47	.....
13	249.67	.....	14	250.46	.....	15	251.27	.....
14	257.70	.....	15	258.57	.....	16	259.27	.....
15	266.30	16151.61	16	267.02	16152.07	17	267.70	16152.43
16	274.96	153.35	17	275.73	153.90	18	276.32	154.18
17	284.13	155.52	18	284.80	155.97	19	285.39	156.30
18	293.37	157.86	19	294.11	158.41	20	294.60	158.67
19	303.18	160.67	20	303.81	161.12	21	304.32	161.42
20	313.00	163.64	21	313.72	164.17	22	314.13	164.39
21	323.42	167.06	22	324.03	167.50	23	324.48	167.78
22	333.80	170.65	23	334.50	171.16	24	334.86	171.37
23	344.86	174.70	24	345.44	175.14	25	345.87	175.39
24	355.83	178.90	25	356.54	179.42	26	356.81	179.58
25	367.50	183.57	26	368.03	184.01	27	368.41	184.23
26	379.11	188.40	27	379.72	189.00	28	380.13	189.00
27	391.36	193.70	28	391.81	194.13	29	392.21	194.35
28	403.55	199.12	29	403.91	199.68	30	404.40	199.68
29	416.39	205.06	30	416.94	205.48	31	417.38	205.68
30	429.21	211.08	31	429.76	211.64	32	429.98	211.64
31	442.68	217.66	32	443.16	218.07	33	443.44	218.26
32	456.02	224.31	33	456.57	224.84	34	456.87	224.84
33	470.12	231.51	34	470.61	231.92	35	470.85	232.08
34	484.06	238.76	35	484.59	239.27	36	484.77	239.27
35	.....	246.59	36	.....	247.01	37	.....	247.14
36	.....	254.45	37	.....	254.96	38	.....	254.96
37	528.67	262.92	38	529.08	263.39	39	529.32	263.39
38	543.72	271.38	39	544.12	271.86	40	544.12	271.86
39	559.63	280.50	40	560.08	280.95	41	560.29	280.95
40	575.37	289.57	41	575.89	290.03	42	575.89	290.03
41	591.85	299.28	42	592.29	299.74	43	592.54	299.74
42	608.08	308.97	43	608.63	309.41	44	608.63	309.41
43	625.20	319.30	44	625.62	319.76	45	625.78	319.76
44	642.05	.....	45	642.56	.....	46	642.56	.....
45	.....	340.48	46	.....	340.95	47	.....	340.95
46	677.27	351.35	47	677.63	351.92	48	677.99	351.92
47	695.71	.....	48	696.08	.....	49	696.08	.....
48	713.28	.....	49	714.00	.....	50	714.00	.....
49	732.45	387.01	50	732.97	387.28	51	732.97	387.28
50	750.87	398.82	51	715.25	399.21	52	751.25	399.21
51	.....	412.24	52	.....	412.68	53	.....	412.68

TABLE 2

WAVE NUMBERS OF THE LINES IN THE (1–3) BAND
($\nu_0 = 16348.10\ \mathrm{Cm}^{-1}$)

J	$^3\Pi_0 - {}^3\Pi_0$		J	$^3\Pi_1 - {}^3\Pi_1$		J	$^3\Pi_2 - {}^3\Pi_2$	
	$R_3(J)$	$P_3(J)$		$R_2(J)$	$P_2(J)$		$R_1(J)$	$P_1(J)$
0	16351.35	.....	1	16354.74	.....	2	16358.60	.....
1	356.28	.....	2	358.81	.....	3	362.23	.....
2	360.69	.....	3	363.05	.....	4	366.24	.....
3	365.90	.....	4	367.84	.....	5	370.56	.....
4	371.06	.....	5	372.80	.....	6	375.24	.....
5	376.78	.....	6	378.20	.....	7	380.25	.....
6	382.36	.....	7	383.78	.....	8	385.61	.....
7	388.56	.....	8	389.75	.....	9	391.36	.....
8	394.72	.....	9	395.91	.....	10	397.37	.....
9	401.44	.....	10	402.47	.....	11	403.74	.....
10	408.17	.....	11	409.24	.....	12	410.38	.....
11	415.40	.....	12	416.39	.....	13	417.38	.....
12	422.77	.....	13	423.72	.....	14	424.66	.....
13	430.61	.....	14	431.44	.....	15	432.29	.....
14	438.51	16332.06	15	439.40	16332.70	16	440.15	16333.10
15	446.93	333.59	16	447.70	334.11	17	448.42	334.50
16	455.43	335.24	17	456.24	335.82	18	456.87	336.18
17	464.44	337.36	18	465.16	337.82	19	465.75	338.18
18	473.51	339.60	19	474.28	340.16	20	474.82	340.48
19	483.10	342.26	20	483.77	342.77	21	484.32	343.10
20	492.76	345.16	21	493.50	345.74	22	493.97	346.00
21	502.91	348.45	22	503.60	348.93	23	504.11	349.22
22	513.13	351.92	23	513.91	352.46	24	514.33	352.73
23	524.00	355.83	24	524.59	356.28	25	525.01	356.54
24	534.83	359.91	25	535.47	360.44	26	535.87	360.69
25	546.16	364.38	26	546.71	364.84	27	547.08	365.10
26	557.56	369.11	27	558.20	369.62	28	558.55	369.55
27	569.31	374.16	28	569.95	374.60	29	570.25	374.87
28	581.57	379.48	29	582.16	380.01	30	582.52	380.25
29	592.54	385.08	30	593.00	385.61	31	593.30	385.61
30	606.37	391.36	31	607.05	391.81	32	607.50	391.81
31	620.00	395.91	32	620.68	396.35	33	620.68	396.35
32	633.04	403.91	33	633.44	404.40	34	633.72	404.58
33	646.89	411.02	34	647.28	411.64	35	647.28	411.93
34	660.39	418.05	35	660.66	418.37	36	661.12	418.56
35	675.57	425.69	36	675.57	426.07	37	675.57	426.36
36	689.23	433.21	37	689.65	433.40	38	689.65	433.77
37	.....	442.15	38	.....	442.15	39	.....	442.15
38	.....	449.62	39	.....	450.14	40	.....	450.14
39	.....	458.54	40	.....	459.01	41	.....	459.01
40	.....	467.24	41	.....	467.66	42	.....	468.51
41	.....	476.74	42	.....	477.18	43	.....	477.42
42	.....	486.05	43	.....	486.69	44	.....	486.69
43	.....	496.24	44	.....	496.67	45	.....	496.67
44	.....	.....	45	.....	.....	46	.....	.....
45	.....	.....	46	.....	.....	47	.....	.....
46	.....	527.26	47	.....	527.78	48	.....	527.78
47	.....	535.54	48	.....	538.99	49	.....	538.99
48	.....	549.64	49	.....	550.08	50	.....	550.08
49	.....	561.53	50	.....	561.96	51	.....	561.96
50	.....	573.26	51	.....	573.69	52	.....	573.69
51	.....	585.68	52	.....	586.16	53	.....	586.16
52	.....	597.93	53	.....	598.30	54	.....	598.30
53	.....	611.01	54	.....	611.50	55	.....	611.50
54	.....	623.84	55	.....	624.24	56	.....	624.24
55	.....	637.43	56	.....	638.08	57	.....	638.08

When $\Delta_2F_m(J)/(J+\frac{1}{2})$ was plotted against $(J+\frac{1}{2})^2$, a straight line was obtained. The intercept on the ordinate axis gave $4B_v$, and the slope of the line gave $8D_v$. The resulting rotational constants are given in Table 9. The agreement with previous determinations of most of these constants is satisfactory. These previous determinations are also included in Table 9.

TABLE 3

WAVE NUMBERS OF THE LINES IN THE (2–4) BAND
($\nu_0 = 16516.38$ Cm^{-1})

J	$^3\Pi_0-{}^3\Pi_0$		J	$^3\Pi_1-{}^3\Pi_1$		J	$^3\Pi_2-{}^3\Pi_2$	
	$R_3(J)$	$P_3(J)$		$R_3(J)$	$P_3(J)$		$R_1(J)$	$P_1(J)$
12	16589.66	.....	13	16590.75	.....	14	16592.29	.....
13	597.27	.....	14	598.30	.....	15	599.59	.....
14	605.08	.....	15	606.04	.....	16	607.05	.....
15	613.33	.....	16	614.22	.....	17	615.10	.....
16	621.66	16502.91	17	623.30	16503.60	18	623.30	16504.11
17	630.43	504.91	18	631.26	505.52	19	631.98	506.05
18	639.27	506.98	19	640.15	508.11	20	640.74	508.11
19	.....	509.59	20	.....	510.18	21	.....	510.60
20	658.05	512.31	21	658.89	512.98	22	659.43	513.28
21	668.00	515.44	22	668.69	516.04	23	669.26	516.39
22	677.99	518.74	23	678.75	519.39	24	679.20	519.69
23	688.46	522.40	24	689.23	523.04	25	689.65	523.36
24	699.06	526.37	25	699.77	526.96	26	700.20	527.26
25	710.27	530.60	26	710.85	531.22	27	711.27	531.57
26	721.22	535.16	27	721.91	535.87	28	722.30	535.87
27	732.97	540.15	28	733.57	540.58	29	734.03	540.88
28	744.57	545.10	29	745.14	545.64	30	745.56	545.89
29	756.79	550.62	30	757.43	551.11	31	757.78	551.39
30	769.02	556.22	31	769.90	556.68	32	769.90	556.99
31	781.81	562.25	32	782.45	562.79	33	782.74	563.05
32	794.55	568.50	33	795.21	569.31	34	795.45	569.31
33	808.09	575.15	34	808.47	575.65	35	808.77	575.89
34	821.16	581.93	35	822.08	582.52	36	822.08	582.52
35	835.02	589.19	36	835.76	589.66	37	836.09	589.88
36	849.00	596.55	37	849.59	597.27	38	849.83	597.27
37	863.47	604.35	38	863.99	604.80	39	864.29	605.08
38	.....	612.30	39	.....	612.92	40	.....	612.92
39	.....	620.68	40	.....	621.09	41	.....	621.35
40	.....	629.20	41	.....	629.79	42	.....	629.29
41	.....	638.08	42	.....	638.55	43	.....	638.76

When the rotational constants B_v are plotted against v, the diagram in Figure 2 is obtained. The constants computed for the Swan bands give the points on this diagram up to $v = 3$ for the upper state and $v = 6$ for the lower state. Apparently, up to these vibrational levels, the points on this diagram lie on straight lines.

b) THE DETERMINATION OF THE BAND ORIGINS

The band origins, ν_0, of the four Swan bands, were computed from the R branches, since they extended to much lower J values than did the P branches. The extrapolations to the origins would have been rather long if the usual method of combining the R and P branches had been followed. According to the theory of Budó, it is permissible to average the lines of equal J in the three sub-branches of the R branch. This is entirely analogous to the averaging carried out above in the case of the combination differences.

TABLE 4

WAVE NUMBERS OF THE LINES IN THE (3–5) BAND

($\nu_0 = 16667.50$ Cm^{-1})

J	$^3\Pi_0 - {}^3\Pi_0$		J	$^3\Pi_1 - {}^3\Pi_1$		J	$^3\Pi_2 - {}^3\Pi_2$	
	$R_3(J)$	$P_3(J)$		$R_2(J)$	$P_2(J)$		$R_1(J)$	$P_1(J)$
0	16670.87	.....	1	16673.90	.....	2	16677.99	.....
1	674.91	.....	2	677.63	.....	3	681.54	.....
2	679.20	.....	3	681.93	.....	4	685.33	.....
3	685.33	.....	4	686.57	.....	5	689.23	.....
4	689.23	.....	5	691.35	.....	6	693.95	.....
5	694.94	.....	6	696.51	.....	7	698.45	.....
6	700.20	.....	7	701.87	.....	8	703.69	.....
7	706.26	.....	8	707.58	.....	9	709.32	.....
8	712.11	.....	9	713.51	.....	10	715.15	.....
9	718.60	.....	10	719.73	.....	11	721.22	.....
10	724.95	.....	11	726.22	.....	12	727.58	.....
11	731.95	.....	12	732.97	.....	13	734.03	.....
12	738.94	.....	13	740.08	.....	14	741.09	.....
13	746.37	.....	14	747.32	.....	15	748.27	.....
14	753.92	.....	15	754.92	.....	16	755.83	.....
15	761.89	.....	16	763.02	.....	17	763.56	.....
16	769.90	.....	17	770.95	.....	18	771.67	.....
17	778.50	.....	18	779.28	.....	19	779.83	.....
18	787.02	.....	19	788.00	.....	20	788.64	.....
19	796.11	.....	20	796.87	.....	21	797.53	.....
20	805.36	16661.55	21	806.23	16662.27	22	806.19	16662.66
21	814.80	664.34	22	815.57	664.89	23	815.69	665.27
22	824.68	667.59	23	825.49	668.28	24	825.89	668.69
23	834.65	670.87	24	835.36	671.42	25	835.76	671.76
24	845.07	674.72	25	845.85	675.57	26	846.32	675.57
25	855.51	678.50	26	856.15	679.20	27	856.58	679.20
26	866.53	682.97	27	867.29	683.63	28	867.74	683.94
27	.....	687.23	28	.....	687.76	29	.....	688.05
28	.....	692.32	29	.....	692.97	30	.....	693.27
29	.....	697.07	30	.....	697.55	31	.....	697.79

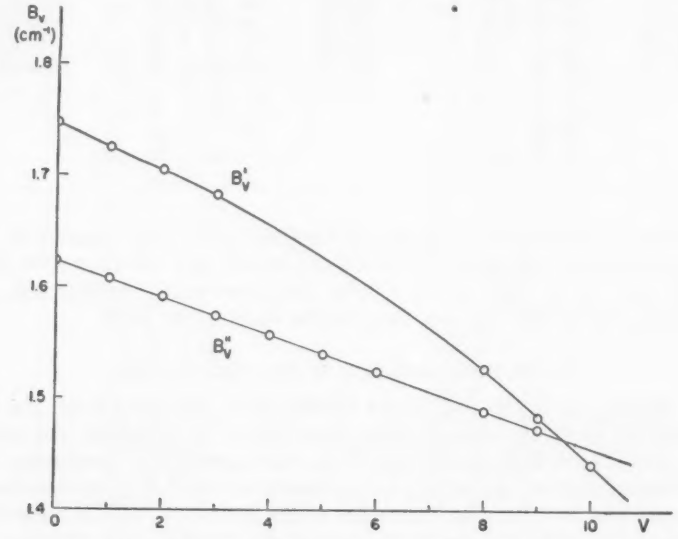

FIG. 2.—B_v-curves for the upper ($A\,^3\Pi_g$) and lower ($X\,^3\Pi_u$) states of the Swan system

We thus have the equation:

$$R_m(J) = \tfrac{1}{3}\,[R_1(J) + R_2(J) + R_3(J)]\,.$$

The quantities $R_m(J)$, B_v', B_v'', D_v', and D_v'' were then introduced into the equation

$$\nu_0 = R_m(J) - (B' + B'')(J+1) - (B' - B'' - D' + D'')(J+1)^2 + 2(D' + D'')(J+1)^3 + (D' - D'')(J+1)^4.$$

TABLE 5

WAVE NUMBERS OF THE LINES IN THE (8–6) BAND
($\nu_0 = 22744.68$ Cm^{-1})

J	$^3\Pi_0 - {}^3\Pi_0$		J	$^3\Pi_1 - {}^3\Pi_1$		J	$^3\Pi_2 - {}^3\Pi_2$	
	$R_3(J)$	$P_3(J)$		$R_2(J)$	$P_2(J)$		$R_1(J)$	$P_1(J)$
6	.....	22721.54	7	.....	22723.28	8	.....	22725.14
7	22770.30	718.94	8	22771.87	720.17	9	.....	721.81
8	773.51	715.88	9	775.04	717.19	10	22777.12	718.51
9	776.71	713.32	10	778.11	714.21	11	780.01	715.45
10	779.69	710.14	11	781.29	711.35	12	782.99	712.40
11	782.99	707.38	12	784.19	708.23	13	786.09	709.31
12	786.09	704.25	13	787.58	705.42	14	788.92	706.31
13	789.44	701.47	14	790.56	702.33	15	791.82	703.40
14	792.41	698.36	15	793.82	699.55	16	794.96	700.27
15	795.65	695.53	16	796.66	696.32	17	797.90	697.14
16	798.67	692.48	17	799.95	693.60	18	800.87	694.23
17	801.89	689.58	18	802.91	690.34	19	803.34	691.05
18	804.77	686.54	19	806.05	687.63	20	806.79	688.18
19	807.52	683.58	20	808.65	684.27	21	809.29	684.85
20	810.70	680.58	21	811.87	681.61	22	812.58	682.10
21	.....	677.50	22	.....	678.13	23	.....	678.68
22	.....	674.55	23	.....	675.55	24	.....	675.93
23	.....	671.34	24	.....	671.88	25	.....	672.34
24	.....	668.42	25	.....	669.38	26	.....	669.73
25	.....	664.92	26	.....	665.42	27	.....	665.78
26	.....	662.14	27	.....	663.00	28	.....	663.40
27	.....	658.22	28	.....	658.61	29	.....	658.81
28	.....	655.64	29	.....	656.50	30	.....	656.92
29	.....	650.27	30	.....	650.78	31	.....	650.78
30	.....	649.49	31	.....	650.27	32	.....	650.78
31	.....	646.69	32	.....	647.07	33	.....	647.50

For a given band, the computed values of ν_0 should show no systematic change with J. This provides a check on the internal consistency of the rotational constants. The resulting origins are included in Table 11. The method just described for computing the origins differed from that used by Shea in finding the origins of the (0–0), (0–1), (1–0), and (1–1) bands. He used the mean of the red and violet components of each triplet. Thus it was necessary to recompute the origins of these bands, using the method described above, in order to obtain a consistent set. The new origins for the (0–0), (0–1), and (1–0) bands are also included in Table 11. A similar discrepancy is found when the origins derived above for the $\Delta v = -2$ sequence are compared with those determined by Johnson for the same bands. This is on account of the fact that Johnson's origins were computed for the central components of the triplets only.

D. THE ANALYSIS OF THE TAIL BANDS

As was pointed out in the introduction, it is impossible to fit the four observed tail bands into Johnson's linear equation for the Swan bands. Therefore, if they are actually tail bands of the Swan system, one or both of the equations for $\Delta G'(v)$ and $\Delta G''(v)$ must depart from linearity as v increases. Initially, it was assumed that the equation for

TABLE 6

WAVE NUMBERS OF THE LINES IN THE (9–8) BAND
($\nu_0 = 21116.43$ Cm^{-1})

J	$^3\Pi_0 - {}^3\Pi_0$		J	$^3\Pi_1 - {}^3\Pi_1$		J	$^3\Pi_2 - {}^3\Pi_2$	
	$R_3(J)$	$P_3(J)$		$R_3(J)$	$P_3(J)$		$R_1(J)$	$P_1(J)$
14	(21160.24)*	.....	15	21161.58	.....	16	21162.67	.....
15	164.33	.....	16	(166.22)	.....	17	167.97	.....
16	165.52	21062.44	17	167.97	21063.62	18	169.52	21064.22
17	(169.17)	1060.57	18	(170.64)	1061.92	19	172.32	1063.62
18	(171.01)	1056.14	19	172.66	1058.10	20	173.53	1059.35
19	(174.40)	1053.70	20	(175.61)	1054.83	21	(176.92)	1056.14
20	(175.99)	1049.56	21	177.68	1050.96	22	178.65	1051.66
21	179.34	1046.92	22	(180.14)	1047.92	23	181.41	1049.05
22	181.41	1042.94	23	(182.34)	1044.21	24	183.30	1044.81
23	183.92	1040.09	24	185.08	1040.99	25	186.37	1041.98
24	186.37	1036.12	25	187.28	1037.36	26	(187.82)	1037.90
25	188.58	1032.87	26	189.73	1033.92	27	190.44	1034.81
26	190.79	1029.15	27	(191.86)	1030.30	28	(192.72)	1030.79
27	(193.27)	1025.90	28	194.14	1026.66	29	195.28	1027.45
28	195.28	1021.90	29	196.21	1022.94	30	196.80	1023.48
29	(197.83)	1018.46	30	(198.77)	1019.23	31	.....	1019.92
30	.....	1014.43	31	.....	1015.54	32	.....	1015.93
31	.....	1010.77	32	.....	1011.53	33	.....	1012.15
32	.....	1006.70	33	.....	1007.79	34	.....	1008.09
33	.....	21002.81	34	.....	21003.51	35	.....	21004.10
34	.....	20998.60	35	.....	20998.87	36	.....	20998.87
35	.....	994.54	36	.....	995.17	37	.....	995.73
36	.....	990.20	37	.....	991.37	38	.....	991.37
37	.....	995.77	38	.....	986.38	39	.....	986.87
38	.....	981.38	39	.....	982.47	40	.....	982.47
39	.....	976.73	40	.....	977.28	41	.....	977.77
40	.....	972.08	41	.....	973.18	42	.....	973.18
41	.....	967.13	42	.....	967.58	43	.....	968.01
42	.....	962.36	43	.....	963.00	44	.....	963.00

* Lines in parentheses in the R branches are blended with lines of the (1–0) band.

$\Delta G''(v)$ for the lower state was linear up to $v'' = 15$ at least and that the vibrational terms of the upper state could be represented by a third-order equation:

$$G_0'(v) = \omega_0' v' - \omega_0' x_0' v'^2 + \omega_0' y_0' v'^3 ,$$

where the energy levels are referred to the lowest level ($v = 0$) as zero.

The vibrational structure would then be given by the following equation, using the constants for the lower state as derived by Fox and Herzberg:

$$\nu = \nu_{00} + \omega_0' v' - \omega_0' x_0' v'^2 + \omega_0' y_0' v'^3 - (1629.99\, v'' - 11.71\, v''^2) .$$

This equation involves four unknowns; so four band origins of different v' are required for their determination.

A preliminary study of the series of triplets in band *b* showed that they were all members of the *P* branch of this band, which presumably immediately precedes the 4770 A band in the $\Delta v = +1$ sequence. From their intensity distribution and from the fact that they seemed to extend practically to the head of the (1–0) band, it was considered likely that the origin of band *b* was in the neighborhood of the (1–0) band head. Accordingly, as a rough approximation, the origin of this band was taken as being at 21,110 cm^{-1}, with the possibility of an error of ± 10 wave numbers.

Four different vibrational numberings for band *b* were then assumed, namely, (11–10), (10–9), (9–8), and (8–6). With each assumed numbering in turn, its origin was used, to-

TABLE 7

WAVE NUMBERS OF THE LINES IN THE (10–9) BAND

($\nu_0 = 20904.64$ Cm^{-1})

J	$^3\Pi_0 - {}^3\Pi_0$		J	$^3\Pi_1 - {}^3\Pi_1$		J	$^3\Pi_2 - {}^3\Pi_2$	
	$R_3(J)$	$P_3(J)$		$R_2(J)$	$P_2(J)$		$R_1(J)$	$P_1(J)$
1	.....	20896.51	2	20912.40	20893.35	3	.....	.....
2	20912.40	893.45	3	915.02	895.51	4	.....	20897.62
3	915.69	890.10	4	917.75	892.24	5	20922.14	894.66
4	917.75	887.33	5	920.49	889.20	6	924.20	891.17
5	920.76	884.50	6	922.98	885.83	7	926.42	887.94
6	922.98	880.97	7	925.55	882.70	8	928.47	884.50
7	926.08	878.05	8	928.01	879.13	9	930.72	880.97
8	928.01	874.15	9	930.39	875.85	10	932.61	877.36
9	930.96	871.07	10	932.61	872.23	11	934.80	873.89
10	932.61	867.15	11	934.80	868.79	12	936.73	870.02
11	935.38	863.92	12	937.05	864.99	13	938.80	866.50
12	937.05	859.86	13	938.80	861.41	14	940.62	862.42
13	939.46	856.48	14	940.89	857.45	15	942.50	858.79
14	940.89	852.28	15	942.50	853.71	16	943.73	854.56
15	943.12	848.70	16	944.30	849.60	17	945.57	850.83
16	944.30	844.31	17	946.07	845.72	18	947.45	846.33
17	946.43	840.62	18	947.45	841.46	19	948.97	842.39
18	947.01	836.00	19	948.70	837.44	20	949.65	838.39
19	949.30	832.16	20	950.36	833.05	21	951.48	834.18
20	949.92	826.92	21	951.48	828.39	22	952.04	829.06
21	951.48	823.39	22	953.63	824.21	23	954.34	825.19
22	952.86	818.15	23	953.63	819.45	24	954.09	819.93
23	954.09	813.99	24	954.72	815.71	25	955.75	816.34
24	954.09	809.04	25	955.32	810.04	26	955.75	810.37
25	955.75	804.72	26	956.39	805.35	27	957.06	806.15
26	.....	799.02	27	.....	800.05	28	.....	800.27
27	.....	794.60	28	.....	795.24	29	.....	795.96
28	.....	788.60	29	.....	789.70	30	.....	789.70
29	.....	784.06	30	.....	784.64	31	.....	785.33
30	.....	777.68	31	.....	778.71	32	.....	778.71
31	.....	772.99	32	.....	773.55	33	.....	774.20
32	.....	776.21	33	.....	767.14	34	.....	767.14
33	.....	761.37	34	.....	761.88	35	.....	762.43
34	.....	754.14	35	.....	754.95	36	.....	754.95
35	.....	749.17	36	.....	749.58	37	.....	750.12
36	.....	741.35	37	.....	742.07	38	.....	742.07
37	.....	736.24	38	.....	736.61	39	.....	737.08
38	.....	727.77	39	.....	728.32	40	.....	728.32
39	.....	722.57	40	.....	.....	41	.....	723.20
40	.....	713.31	41	.....	713.31	42	.....	713.79
41	.....	707.96	42	.....	707.96	43	.....	708.34
42	.....	697.31	43	.....	697.31	44	.....	697.79

gether with those of the (1–3), (2–4), and (3–5) bands, to find the constants in the above equation. On the basis of these constants, the origins of the four bands immediately following band *b* in the $\Delta v = +1$ sequence were computed and were compared with the observed heads at λλ 4770, 4836, 4911, and 4997. The correct numbering would give computed origins for the four bands that would be to somewhat longer wave lengths than the heads, since they degrade to the red, and, if anything, there should be a slight decrease in the separation between origins and heads with increasing vibrational number, since the difference between the rotational constants for the upper and lower states would be increasing. Computation showed that, if these bands are actually tail bands of the Swan system, then bands *a* and *b* are probably the (10–9) and (9–8) bands of the $\Delta v = -1$ sequence, and band *c* is the (8–6) band.

This tentative vibrational numbering was then verified by analyzing bands *a*, *b*, and *c*. Since the method of analysis was similar in the three cases, only band *a* will be discussed in detail.

As can be seen in Figure 1, spectrum (*c*), band *a*, with head at 4770 A, consists of an open *P* branch and a very congested *R* branch. It was comparatively easy to assign all the lines in the *P* branch to successive triplets. In order to analyze the *R* branch and to find the correct numbering of the triplets, the combination differences of the lower state of the Swan system were extrapolated. It was found that, for a given *K*, a plot of $\Delta_2 F_i''(K)$ versus *v* gave a straight line, as was to be expected, since the constants B_v'' varied linearly with v'', at least to $v'' = 6$. No serious error would be made if it were assumed that the straight lines on the diagram extended to $v'' = 9$. Now fairly extensive sets of combination differences were available for low values of *v*, but for $v'' = 6$ the only available data were those derived from the (0–6) Fox-Herzberg band,[3] and the published analysis covered only short parts of the *P* and *R* branches of this band at *K* values above $K = 18$. Therefore, it was considered worth while to remeasure this band on a more heavily exposed spectrogram than those which Fox and Herzberg had had available to them, so as to extend its analysis to smaller *K* values. This attempt was successful, the resulting combination differences, $\Delta_2 F_i''(K)$ for $v'' = 6$, being extended down to $K = 8$. These differences were plotted on the $\Delta_2 F_i''(K)$ versus *v* curves, together with those for the Swan bands, and the resulting straight lines were extrapolated to $v'' = 9$. The resulting combination differences are presented in Table 8.

These extrapolated combination differences were then used, together with the triplets of the *P* branch of band *a*, to predict the wave numbers that the members of the *R* branch would have, if this band were actually the (10–9) band. The procedure was to assume some numbering for the *P* branch and compute a corresponding *R* branch, which was then compared with the measured lines. If, for a given numbering, coincidences could be found with every member of the *R* branch, then it was assumed that the correct numbering had been obtained, and also that the *R* branch had been identified, since fortuitous coincidences with every predicted line would have been extremely unlikely. Two or three trials were sufficient to find a numbering which produced the coincidences given in Table 8, which presents a comparison between the extrapolated combination differences and the observed ones. It can be seen that, in general, the agreement is excellent. In the majority of cases where the difference between corresponding combination differences is in excess of 0.2 cm^{-1}, the error could be attributed to greater scatter of the points defining the extrapolated lines. In these cases the newly found combination differences were used to improve the slopes of these lines. The resulting *P* and *R* branches with their rotational numberings are given in Table 7 and in Figure 1. The intensities of the lines of the *R* branch are in agreement with what they should be on the basis of the analysis.

This successful analysis of band *a* proves that it is actually a tail band of the Swan system and that the vibrational numbering found from the rough analysis described earlier is the correct one, i.e., band *a* is the (10–9) band.

The analyses of bands *b* and *c* were carried out in a similar way. In the case of band *b* it was found that the *R* branch was blended with the (1–0) Swan band, so that only a few members of the *R* branch could be found. The rest were blended with the much more intense lines of the (1–0) band. It was possible by the comparison of combination differences to determine the rotational numberings of the branches of band *b* unambiguously; but, on account of the severe blending of the *R* branch, the rotational constants derived for this band have little weight. The resulting branches of bands *b* and *c* are given in Tables 6 and 5, respectively.

The same procedure was followed as in the case of the Swan bands to find the rotational constants for the upper and lower states and the band origins, ν_0, of the three tail bands. The resulting rotational constants are given in Table 9 and plotted in Figure 2.

TABLE 8

COMPARISON OF THE COMBINATION DIFFERENCES $\Delta_2F''(K)$ FOR THE 4770 A BAND (10–9), WITH THE EXTRAPOLATION FROM THOSE OF THE SWAN BANDS TO $v''=9$

K	4770 A Band			Extrapolated $\Delta_2F_v'(K)$		
	$\Delta_2F_1''(K)$	$\Delta_2F_2''(K)$	$\Delta_2F_3''(K)$	$\Delta_2F_1'(K)$	$\Delta_2F_2''(K)$	$\Delta_2F_3''(K)$
13	80.01	79.60	78.90	80.43	79.50	78.86
14	86.06	85.09	84.77	86.06	85.28	85.07
15	91.67	91.29	90.76	91.60	91.22	90.82
16	97.40	96.78	96.58	97.38	97.00	96.64
17	103.18	102.84	102.50	103.29	102.86	102.53
18	109.06	108.63	108.30	109.07	108.50	108.28
19	114.79	114.40	114.27	114.92	114.40	114.42
20	120.59	120.31	120.09	120.52	120.17	120.14
21	126.29	126.15	125.91	126.60	126.18	125.95
22	132.11	132.03	131.77	132.22	131.80	131.76
23	138.00	137.92	137.49	138.10	137.90	137.66
24	143.72	143.59	143.82	143.78	143.58	143.47
25	149.60	149.37	149.37	149.48	149.37	149.40
26	155.48	155.27	155.07	155.13	155.22	155.10
27	161.10	161.15	161.15	161.20	161.09	160.93

The constants B_v'' are seen to fall exactly on the straight line extrapolated from the lower states of the Swan bands. The constants B_v', on the other hand, are far below the straight-line extrapolation of the upper-state curve of the Swan bands, indicating a curvature in this upper curve and a crossing of the B_v'' versus v line. This crossing is to be expected, since the tail bands are degraded in the opposite direction to the Swan bands.

The band origins of the three tail bands that were analyzed are included in Table 11, together with their correct vibrational numberings. Since band *a*, with head at 4770 A, is the (10–9) band, it follows that those tail bands at λλ 4836, 4911, and 4997 that were not analyzed but which are undoubtedly further members of the $\Delta v = -1$ sequence are the (11–10), (12–11), and (13–12) bands, respectively. These bands are also included in Table 11. It is interesting that this numbering is exactly the one suggested by Fox and Herzberg.[3]

Perturbations are present in all the bands that were analyzed, i.e., the four members of the $\Delta v = -2$ sequence and the three tail bands. They provided useful checks on the rotational numberings that were adopted. An attempt was made to determine the type of the electronic state causing the perturbations, but without success.

E. THE ROTATIONAL CONSTANTS

As can be seen in Table 9, in general there is good agreement between the rotational constants obtained in this study and those obtained in previous investigations. To obtain the most probable constants, an average was taken of those pertaining to a given level, since there was, in general, no basis for preferring one evaluation over the other. The levels with $v'' = 5$ and $v'' = 6$ are exceptions to this rule. For them, the constants determined in the present study were preferred, since Fox and Herzberg observed only parts of the corresponding bands. The adopted constants are given in Table 10.

TABLE 9

ROTATIONAL CONSTANTS

State	v	Present Investigation		Previous Investigations		
		$B_v(\mathrm{Cm}^{-1})$	$D_v \cdot 10^8\ \mathrm{Cm}^{-1}$	$B_v(\mathrm{Cm}^{-1})$	$D_v \cdot 10^8\ \mathrm{Cm}^{-1}$	Source
Lower $^3\Pi_u$.....	0	.....	.....	1.6239	6.4	Budó
	1	.....	.....	1.6068	6.6	Budó
	2	1.5909	6.55	.....	.....	
	3	1.5738	6.26	1.5742	6.8	Fox-Herzberg
	4	1.5572	6.52	1.5572	6.6	Fox-Herzberg
	5	1.5398	6.38	1.5408	(6.6)	Fox-Herzberg
	6	1.5242	7.29	1.5233	(6.6)	Fox-Herzberg
	7	.....	.....			
	8	1.4894	5.43			
	9	1.4725	5.48			
Upper $^3\Pi_g$.....	0	1.7457	6.89	1.7452	6.8	Budó
	1	1.7252	6.90	1.7242	7.0	Budó
	2	1.7043	7.36			
	3	1.6811	7.55			
	.....	.....	.....			
	.....	.....	.....			
	.....	.....	.....			
	8	1.5267	11.42			
	9	1.4845	11.06			
	10	1.4413	12.72			

a) THE LOWER STATE ($X^3\Pi_u$)

The fourth column of Table 10 gives the differences between successive rotational constants. For the lower state these differences do not vary systematically with v, so that the linear equation,

$$B''_v = B''_e - a''_e\,(v'' + \tfrac{1}{2}),$$

can be used to describe the variation of B''_v with v''. In this equation, the first term,

$$B''_e = \frac{h}{8\pi^2 c \mu r''^2_e},$$

is the rotational constant corresponding to the equilibrium internuclear distance, r''_e. Since the nuclear vibrations are anharmonic, an increase in the amplitude of the vibrations produces an increase in the effective internuclear distance and a decrease in the value of B. Therefore, the second term in the equation above is added with a negative

sign to take into account this change in the effective internuclear distance. Graphical methods were used to determine the constants B_e'' and α_e''. The resulting equation is

$$B_v'' = 1.6326 - 0.01683\,(v + \tfrac{1}{2})\,\text{cm}^{-1}\,.$$

The computed B_v'' are given in the fifth column of Table 10 and the differences (O−C) in the sixth column.

TABLE 10

ADOPTED ROTATIONAL CONSTANTS

State	v	Adopted B_v(Cm^{-1})	ΔB (Cm^{-1})	Computed (Cm^{-1})	O−C (Cm^{-1})	Adopted $D_v \cdot 10^6$ (Cm^{-1})	Computed $D_v \cdot 10^6$ (Cm^{-1})	O−C (Cm^{-1})
Lower ($^3\Pi_u$)..	0	1.6239	.....	1.6242	−0.0002	6.4	6.9	−0.5
			0.0171					
	1	1.6068		1.6074	− .0006	6.6	6.8	−0.2
			.0159					
	2	1.5909		1.5905	+ .0004	6.6	6.6	0.0
			.0169					
	3	1.5740		1.5737	+ .0003	6.6	6.5	+0.1
			.0168					
	4	1.5572		1.5569	+ .0003	6.6	6.3	+0.3
			.0174					
	5	1.5398		1.5400	− .0002	6.4	6.2	+0.2
			.0156					
	6	1.5242		1.5232	+ .0010	7.3	6.0	+1.3
			.....					
	7	.....		1.5064	.....	.....	.....	.....
			.....					
	8	1.4894		1.4895	− .0001	5.4	5.7	−0.3
			.0169					
	9	1.4725		1.4727	− .0002	5.5	5.6	−0.1
Upper ($^3\Pi_g$)..	0	1.7454		1.7444	+ .0010	6.8	6.8	0.0
			.0207					
	1	1.7247		1.7257	− .0010	7.0	7.0	0.0
			.0204					
	2	1.7043		1.7046	− .0003	7.4	7.3	+0.1
			.0232					
	3	1.6811		1.6808	+ .0003	7.6	7.6	0.0
.....	.....	.....	.....	.....	.....	.....	.....	.....
.....	.....	.....	.....	.....	.....	.....	.....	.....
.....	.....	.....	.....	.....	.....	.....	.....	.....
	8	1.5267		1.5240	+ .0027	11.4	10.8	+0.6
			.0422					
	9	1.4845		1.4850	− .0005	11.1	11.7	−0.6
			0.0432					
	10	1.4413		1.4434	−0.0021	12.7	12.7	0.0

Similarly, the constants D_v'', which represent the influence of centrifugal force, can be represented by the linear equation

$$D_v'' = D_e'' + \beta_e''\,(v'' + \tfrac{1}{2})\,,$$

where D_e'' and β_e'' are analogous to B_e'' and α_e'' given above. A graphical solution gives the following values for the constants:

$$D_v'' = [7.02 - 0.15\,(v'' + \tfrac{1}{2})] \times 10^{-6}\text{cm}^{-1}\,.$$

The calculated values of D_v'' are given in the eighth column of Table 10 and the differences (O−C) in the ninth column.

b) THE UPPER STATE ($A^3\Pi_g$)

For the upper state, the differences between successive values of B'_v given in the fourth column of Table 10, are not constant but show an increase with v'. Thus the equations for B'_v and D'_v were extended by the addition of quadratic terms, as follows:

$$B'_v = B'_e - a'_e(v'+\tfrac{1}{2}) + \gamma'_e(v'+\tfrac{1}{2})^2 ,$$

$$D'_v = D'_e + \beta'_e(v'+\tfrac{1}{2}) + \delta'_e(v'+\tfrac{1}{2})^2 .$$

The coefficients were found by the method of averages. The resulting equations were

$$B'_v = 1.7527 - 0.01608(v'+\tfrac{1}{2}) - 0.001274(v'+\tfrac{1}{2})^2 \text{cm}^{-1} ,$$

$$D'_v = [6.74 + 0.103(v'+\tfrac{1}{2}) + 0.0442(v'+\tfrac{1}{2})^2] \times 10^{-6}\text{cm}^{-1} .$$

TABLE 11

BAND HEADS AND BAND ORIGINS

v', v''	λ_{head}	ν_{head}	ν_0
0– 0	5165.2 A	19354.9 cm^{-1}	19378.44 cm^{-1}*
0– 1	5635.5	17739.6	17760.36*
1– 0	4737.1	21104.2	21132.13*
0– 2	6191.2	16147.5	16165.79
1– 3	6122.1	16329.8	16348.10
2– 4	6059.7	16498.0	16516.38
3– 5	6004.9	16648.5	16667.50
(*c*) 8– 6 N†	.....	.....	22744.68
(*b*) 9– 8 RN‡	.....	.....	21116.43
(*a*) 10– 9 R§	4770.13	20958.0	20904.64
11–10 R	4836.13	20671.9	.....
12–11 R	4910.99	20356.8	.....
13–12 R	4996.74	20007.5	.....

* Recomputed from Shea's data.

† N = Headless band, called band *c* in this paper. Its origin is at 4395 A.

‡ RN = Band shaded to the red, but the head is not observed. This band is called band *b* in this paper. Its origin is at 4734 A.

§ R = Band shaded to the red.

The computed values of B'_v and D'_v are given in Table 10, together with the differences (O−C). It can be seen that, in general, the agreement between the observed and the computed constants is satisfactory.

The rotational constants derived above are summarized in Table 14.

F. VIBRATIONAL ANALYSIS

a) THE LOWER STATE ($X^3\Pi_u$)

The origins that are collected in Table 11, together with those of the four bands of the Fox-Herzberg system,[3] were used to obtain the vibrational terms, $G''_0(v)$, and vibrational quanta, $\Delta G''_{v+\frac{1}{2}}$ for the lower state, presented in Table 12. The quanta are plotted against vibrational number, v, in Figure 3. The fifth column of Table 12 shows that the vibrational quanta $\Delta G''_{v+\frac{1}{2}}$ for the lower state vary approximately linearly with v'' up to $v'' = 5$. The corresponding linear equation for the vibrational quanta is

$$\Delta G''_{v+1/2} = \omega''_0 - \omega''_0 x''_0 - 2\omega''_0 x''_0 v'' .$$

TABLE 12

VIBRATIONAL TERMS AND QUANTA FOR THE LOWER STATE ($X^3\Pi_u$)

v	$G_0''(v)$ (Cm^{-1})	$\Delta G''_{v+1/2}$ (Cm^{-1})	Source*	$\Delta_2 G''$ (Cm^{-1})	$G_0'(v)_{comp}$ (Cm^{-1})	O−C (Cm^{-1})
0.....	0.00				0.00	0.00
		1618.08		.....		
1.....	1618.08			−23.51	1618.01	+0.07
		1594.57				
2.....	3212.65			−23.19	3212.68	−0.03
		1571.38				
3.....	4784.03			−23.31	4784.01	+0.02
		1548.07	F-H			
4.....	6332.10			−23.59	6332.00	+0.10
		1524.48	F-H			
5.....	7856.58			−23.08	7856.65	−0.07
		1501.40	F-H			
6.....	9357.98			.....	9357.96	+0.02
		.....				
7.....	.....			.....	.....	
		(1452)	H-P			
8.....	.....			(−20)	.....	
		(1432)	H-P			
9.....	.....			(−26)	.....	
		(1406)	H-P			
10.....	.....			(−21)	.....	
		(1385)	H-P			
11.....	.....			.....	.....	

* F-H = Determined from the Fox-Herzberg system; H-P = Determined from the high-pressure bands.

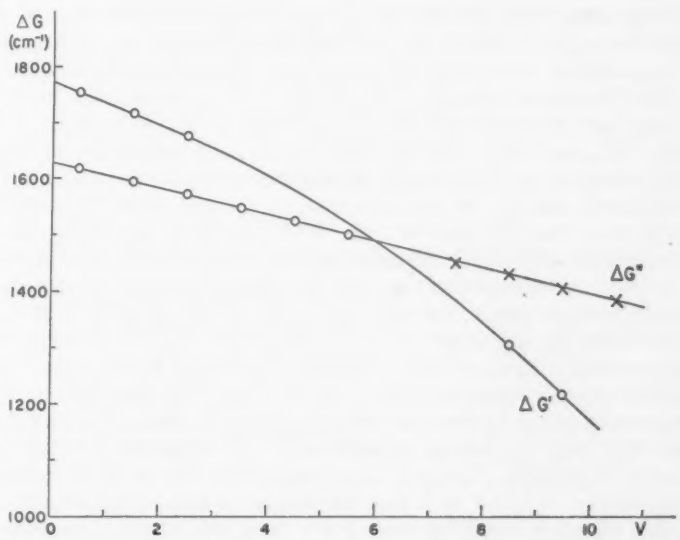

FIG. 3.—ΔG-curves for the upper ($A^3\Pi_g$) and lower ($X^3\Pi_u$) states of the Swan system. The points indicated by (×) are obtained from the "high-pressure" bands.

The constants, determined by graphical methods, are $\omega_0'' = 1629.68$ cm^{-1} and $\omega_0''x_0'' = 11.67$ cm^{-1}. The computed $G_0''(v)$ are given in Table 12, together with the differences (O−C). In general, the agreement is satisfactory. These constants are slightly different from those obtained by Fox and Herzberg ($\omega_0'' = 1629.99$ cm^{-1} and $\omega_0''x_0'' = 11.71$ cm^{-1}). Their constants were derived from the three vibrational quanta, $\Delta G_{3\frac{1}{2}}''$, $\Delta G_{4\frac{1}{2}}''$, and $\Delta G_{5\frac{1}{2}}''$, together with the computed origins derived by Johnson for the bands of low vibrational number. However, as pointed out in Section C, there is considerable difference between the band origins found by Johnson and those found in the present investigation, on account of differences in the methods used to find the origins. Thus the vibrational constants derived above are based upon more consistent data than Fox and Herzberg had available to them, and thus are probably more accurate.

In order to determine whether or not this linear equation was true for higher vibrational levels, use was made of the data on the so-called "high-pressure" bands of C_2. Herzberg[7] has shown that these high-pressure bands are members of the Swan system, with a common upper level at $v' = 6$, and with lower levels ranging from $v'' = 0$ to $v'' = 11$. The rotational constants that were found above were used in the usual manner[10] to determine the origins of these high-pressure bands from the measured band heads. Since all these bands have the same upper state, differences between the origins of the bands with neighboring lower states immediately gave the corresponding vibrational quanta. The vibrational quanta with $(v'' + \frac{1}{2})$ from $7\frac{1}{2}$ to $10\frac{1}{2}$ are given in Table 12. They are inclosed in parentheses to indicate that they are only approximate. However, the corresponding points, indicated by crosses on the ΔG versus v diagram of Figure 3, seem to lie on the straight line extrapolated from the lower levels. This is confirmed when these quanta are computed, using the linear equation derived above. The greatest difference, (O−C), is 3 cm^{-1}. Thus this linear equation seems to represent the levels to at least $v'' = 11$.

b) THE UPPER STATE ($A^3\Pi_g$)

The vibrational terms and quanta for the upper state from $v' = 0$ to $v' = 3$ were immediately found from the origins of the four members of the $\Delta v = -2$ sequence, knowing the quanta for the lower state. Furthermore, since it was shown above that the linear equation for the vibrational quanta of the lower state represents the levels to $v'' = 11$, this equation was used, together with the origins of the (8–6), (9–8), and (10–9) bands, to find the quanta $\Delta G_{8\frac{1}{2}}'$ and $\Delta G_{9\frac{1}{2}}'$. The resultant terms and quanta are given in Table 13. The second differences given in column 4 of this table are not constant but increase with increasing vibrational number, so that the equation for $\Delta G'$ would have to include terms of higher powers in v than the simple linear equation given above for the lower state. However, considerable difficulty is experienced when an attempt is made to find a single second-order or third-order equation that will reproduce the observed quanta. Even when least-squares solutions are made, the differences (O−C) range up to 4 cm^{-1}. Apparently, what causes the difficulty is the fact that for the lowest vibrational levels the change of $\Delta G'$ with v is practically linear, while for higher vibrational levels there is a marked departure from linearity. An equation that would represent the observations exactly would have to have as many terms as there are observed quanta. Since this would be unwieldy, it was decided that two third-order equations for the vibrational terms should be derived. The first of these (Eq. I below), would represent the terms of lowest vibrational level accurately from $v' = 0$ to $v' = 3$. For the purpose of computing origins of the normal Swan bands, this equation would be used. For $v' > 5$, say, it would be seriously in error. The second equation (Eq. II) would be based upon a least-squares solution, using all the observed vibrational terms and giving them equal weight. As mentioned above, this equation is only an approximate one. A fourth-order equation was found in a similar way, but so little was gained in the way of accuracy that it was decided to use the third-order equation.

[10] See, e.g., n. 9, p. 187.

The two equations are:

Equation I: $G_0'(v) = 1771.40\,v' - 17.200\,v'^2 - 0.5067\,v'^3$,

Equation II: $G_0'(v) = 1767.51\,v' - 13.900\,v'^2 = 1.0345\,v'^3$.

Table 13 gives the differences (O−C) for each of these equations. The constants in Equation I are included in Table 14.

TABLE 13

VIBRATIONAL TERMS AND QUANTA FOR THE UPPER STATE ($A^3\Pi_g$)

v	$G_0'(v)$ (CM^{-1})	$\Delta G'_{v+1/2}$ (CM^{-1})	$\Delta_2 G'$ (CM^{-1})	(O−C) (CM^{-1})	
				Equation I	Equation II
0	0.00			0.00	0.00
		1753.69			
1	1753.69		37.34	0.00	+1.12
		1716.35			
2	3470.04		40.75	+ 0.09	−1.10
		1675.60			
3	5145.64			− 0.08	−3.85
8	12724.22			− 86.75	+3.45
		1304.35			
9	14028.57		84.85	−151.45	+1.08
		1219.50			
10	15248.07			−239.25	−2.47

TABLE 14

CONSTANTS OF THE C_2 MOLECULE

	Lower State ($X^1\Sigma_u$)	Upper State ($A^3\Pi_g$)
B_e	1.6326 cm^{-1}	1.7527 cm^{-1}
B_0	1.6242 cm^{-1}	1.7443 cm^{-1}
α	0.01683 cm^{-1}	0.01608 cm^{-1}
γ		−0.001274 cm^{-1}
D	7.02×10^{-6} cm^{-1}	6.74×10^{-6} cm^{-1}
β	−0.15×10^{-6} cm^{-1}	0.103×10^{-6} cm^{-1}
δ		0.0442×10^{-6} cm^{-1}
r_e	1.3117 A	1.2660 A
ν_{00}		19378.44 cm^{-1}*
ν_e		19306.26 cm^{-1}
ω_0	1629.68 cm^{-1}	1771.40 cm^{-1}
ω_e	1641.35 cm^{-1}	1788.22 cm^{-1}
$\omega_0 x_0$	11.67 cm^{-1}	17.200 cm^{-1}
$\omega_e x_e$	11.67 cm^{-1}	16.440 cm^{-1}
$\omega_0 y_0 = \omega_e y_e$		−0.5067 cm^{-1}

* The vibrational constants for the upper state pertain to Equation I (see text).

G. THE DISSOCIATION LIMIT OF THE $^3\Pi_g$ STATE

If the $\Delta G_{v+\frac{1}{2}}$ versus v curve for the $^3\Pi_g$ state given in Figure 3 is extrapolated to the $\Delta G = 0$ line, then the area in the diagram inclosed by the curve and the ordinate and abscissa axes is equal to the dissociation energy of this state (in cm^{-1}). The uncertainty in the measurement is determined by the length of the extrapolation, since nothing is known of the true shape of this curve beyond the highest observed vibrational quantum. It is probable that the negative curvature that is observed continues to higher levels, although states for which the curve goes through an inflection point, with the "toe" of the curve showing positive curvature, have been observed in the case of some molecules. However, an upper limit of the dissociation energy can be found by extrapolating linearly from the two quanta at $v + \frac{1}{2} = 8\frac{1}{2}$ and $9\frac{1}{2}$. It is found that the abscissa axis is reached at $v' = 24$, and the corresponding dissociation limit is at 42,790 cm^{-1} (5.30 volts) above the level $v'' = 0$. The true value of this dissociation limit is probably somewhat lower than this.

If it were possible to determine the energy of the dissociation products of the $^3\Pi_g$ state, then the dissociation limit just obtained could be used to determine the heat of dissociation of the C_2 molecule, which is the dissociation limit of the ground ($^3\Pi_u$) state. But a $^3\Pi_g$ state may be formed by the combination of one carbon atom in the ground (^3P) state, with another in any one of the three lowest atomic states of carbon (^3P, ^1D, or ^1S), and it is impossible to say which one of the three possible combinations ($^3P + {}^3P$, $^3P + {}^1D$, or $^3P + {}^1S$) is the correct one. Taking each possibility in turn, the corresponding upper limits for the heat of dissociation are 5.30, 4.04, and 2.62 e.v.

It is of interest to compare these possible upper limits for the heats of dissociation with estimates made by others. L. Brewer, P. W. Gilles, and A. Jenkins[11] recently obtained a value of 4.7 e.v. from a study of the vapor pressure and heat of sublimation of graphite. This would seem to indicate that the first possibility (dissociation of the $^3\Pi_g$ state into two carbon atoms in the ^3P state) is the correct one. On the other hand, Herzberg[7] has suggested that the heat of dissociation must be close to 3.6 e.v., on the basis of his explanation of the selective emission of the high-pressure bands as being due to inverse predissociation. This value of 3.6 e.v. is close to the second of the two possibilities, i.e., dissociation of the $^3\Pi_g$ state into ($^3P + {}^1D$) atoms. The third possibility, 2.62 e.v., is undoubtedly too low, since vibrational levels of the lower state have been observed up to $v'' = 11$ at 17332 cm^{-1} (2.15 e.v.) with the corresponding quantum, $\Delta G''_{10\frac{1}{2}}$, equal to 1385 cm^{-1}. Furthermore, it has been shown that the vibrational quanta in the lower state up to $v'' = 11$ can be represented by a linear equation for $\Delta G''_{v+\frac{1}{2}}$, so that an unusually drastic departure from this linear equation would be required for higher vibrational levels in order for the dissociation limit to be at 2.62 e.v. Thus two possibilities remain for the heat of dissociation of the C_2 molecule, namely, 4.9 and 3.6 e.v.; and a definite decision as to which of these two possibilities is the correct one must be deferred until further information is available.

I wish to express my sincere thanks to Dr. G. Herzberg for many helpful suggestions and valuable advice given during the course of this investigation.

[11] *J. Chem. Phys.*, **16**, 797, 1948.

THE FAR VIOLET REGION IN THE SPECTRA OF THE COOL CARBON STARS*

ANDREW MCKELLAR
Dominion Astrophysical Observatory, Victoria, B.C.
Received July 13, 1948

ABSTRACT

A survey of the spectra of a number of the brighter N-type stars in the far violet has been made. Spectrographs of low dispersion were necessarily used because of the great decrease in intensity of light from the blue-green toward the violet. The spectrograms obtained are described. Perhaps the most interesting features found are a number of strong absorptions in the λλ 4100–3950 region of the spectrum of Y Canum Venaticorum. These are tentatively identified with the "λ 4050 group" of CH_2 bands. If correct, this identification provides direct observational evidence of polyatomic molecules in a stellar atmosphere and opens new possibilities of accounting for the very strong absorption of violet light in the atmospheres of the N-type stars.

INTRODUCTION

The extreme decrease in intensity from the blue-green to the violet region in the spectra of the cool carbon stars (spectral type N) has been recognized for many years. C. D. Shane[1] commented upon the phenomenon in his early comprehensive study of the carbon stars and was well aware that the effect was far more than would be expected on the basis of temperature alone. He evaluated the falling-off of intensity in arbitrary units and used it as one criterion in the spectral classification of the R- and N-type stars.

Recently, G. Shajn and O. Struve[2] have studied the phenomenon from a spectrophotometric point of view. They photographed the spectrum[3] of UU Aurigae (N3:$C5_3$) and compared it with that of an M-type star. A marked weakening of absorption lines in the N-type spectrum in the λλ 3900–4100 region, compared with the corresponding lines in the M-type spectrum, was found—an effect judged inappreciable at suitable comparison regions in the λλ 4400–4700 interval. It was therefore concluded, on the basis of the theory of blended lines, that the continuous absorption arose, in part at least, in the layers of the atmosphere where the absorption lines are formed.

From a visual comparison of the spectra of UU Aurigae and the M-type star in the far violet, with special attention being paid to the parts that appeared to be nearest to the continuous background, certain differences were noted. These led Shajn and Struve to suggest that the great weakening of the continuum in the violet more likely arose from as yet unidentified overlapping molecular absorption bands than from an increase in continuous absorption.

Spectrograms covering the far violet region have been obtained during the past year at Victoria for a number of cool carbon stars. The purpose of the present article is to describe the spectra. It is hoped that some of the features found may contribute to the solution of the interesting problem of the origin of the very strong absorption in the violet.

THE SPECTROGRAPHS

The observations were made with the two-prism ultraviolet-transmitting glass spectrograph, as adapted for use at the Cassegrain focus of the 72-inch reflector. With its

* *Contributions from the Dominion Astrophysical Observatory*, No. 15.

[1] *Lick Obs. Bull.*, **13**, 123, 1928.

[2] *Ap. J.*, **106**, 86, 1947.

[3] The R–N spectral types given are taken from R. F. Sanford's papers (*Ap. J.*, **82**, 202, 1935, and **99**, 145, 1944) and the C types from P. C. Keenan and W. W. Morgan (*Ap. J.*, **94**, 501, 1941).

camera lens of focal ratio 5 (focal length 20 cm and diameter 4.0 cm), the dispersion at λ 4000 is 104 A/mm. This arrangement will be referred to as the "ordinary UV spectrograph."

For the brightest early N-type stars, the ordinary UV spectrograph had sufficient speed; but for the later N-type stars, even with exposures of several hours, it was not fast enough to photograph the region below λ 4200. Therefore, a suitable lens of focal length shorter than 20 cm was sought, to use in an alternative camera for the UV spectrograph.

Professor A. M. Crooker of the University of British Columbia kindly loaned such a lens of focal ratio 1.5 (focal length 8.5 cm, diameter 5.7 cm). Opportunity is taken here to acknowledge gratefully his kind co-operation. Early in 1947 a camera for using the short-focus lens with the two-prism UV spectrograph was constructed by Mr. S. S. Girling at the Observatory. While the $f/1.5$ lens does not give either as good a definition or as flat a field as one specifically designed for a spectrograph, its performance is reasonably satisfactory for the type of survey work to be described. With this short-focus camera lens, the spectrograph, referred to as the "short-focus UV spectrograph," gives a dispersion of 290 A/mm at λ 4000 and is about seven times as fast as the ordinary UV arrangement.

THE OBSERVATIONS

All the spectrograms were obtained on Eastman 103*a*-O emulsion. There was no trouble in photographing the spectra of the early R-type stars well into the ultraviolet with the ordinary UV spectrograph. For example, a spectrogram of the star HD 76396 (R4:C1p_2), $m_v = 8.8$, with 3 hours' exposure was considerably overexposed at λ 3900 and extended down to λ 3450. For the N-type stars, however, the effect of the great decrease in violet light was at once apparent. It was found that satisfactory plates extending beyond λ 4100 could be secured only for the few brightest objects with exposure times up to 5 hours. These stars have visual magnitudes in the approximate range $m_v = 5$–7, and spectral types N0 and N1 (C4–C9). For comparison purposes, it may be noted that an early M-type star of the sixth magnitude would require an exposure time of about 8 minutes. The ratio found between the exposures necessary to record the spectra of the early N- and the M-type stars is thus compatible with the value of 30 estimated by Shajn and Struve.[2]

In the cases of the brightest of the later N-type stars, for example, Y CVn (N3:$C5_4$), $m_v = 4.8$–6.0, or RY Dra (N4p:$C4_4$), $m_v = 6.1$–7.1, the exposures necessary to record the λλ 4100–3900 region with the ordinary UV spectrograph were found to be prohibitively long. Recourse was had, therefore, to the short-focus UV spectrograph described in the previous section. With it, an exposure of 5 or 6 hours showed the spectrum of Y CVn quite well between λ 4000 and λ 4100. Its spectrum at λ 4800 can be obtained with good density with the short-focus UV spectrograph in less than 1 minute. The exposure ratio of 1 minute at λ 4800 to 6 hours at λ 4000 is astonishing, but no more striking than Shane had found in his work. He noted[1] that for Y CVn he could photograph the λ 4800 region with a small quartz slitless spectrograph in 1 second, whereas an exposure of 5 hours with the same instrument failed to show any light beyond λ 3900.

The violet region of the spectra of a number of carbon stars will be briefly described. Figures 1 and 2 have been prepared to illustrate the spectra and to aid in clarifying the description.

1. HD 76396, R4:C1p_2, $m_v = 8.8$; HD 156074, R0:$C1_2$, $m_v = 7.7$; and HD 182040, R2:$C1_2$, $m_v = 7.0$. These three are among the earliest of the carbon stars. As already noted, their spectra were easily photographed to λ 3450 in exposures up to a few hours, and the main reason for introducing the R-type stars into the discussion is to emphasize this point. The spectrum of HD 156074 is shown as *A* in Figure 1.

2. 19 Piscium (HD 223075), N0:$C6_2$, $m_v = 5.3$. This star is the best combination of brightness and early spectral type among those of class N. Its spectrum was photographed well into the violet with comparative ease with the ordinary UV spectrograph.

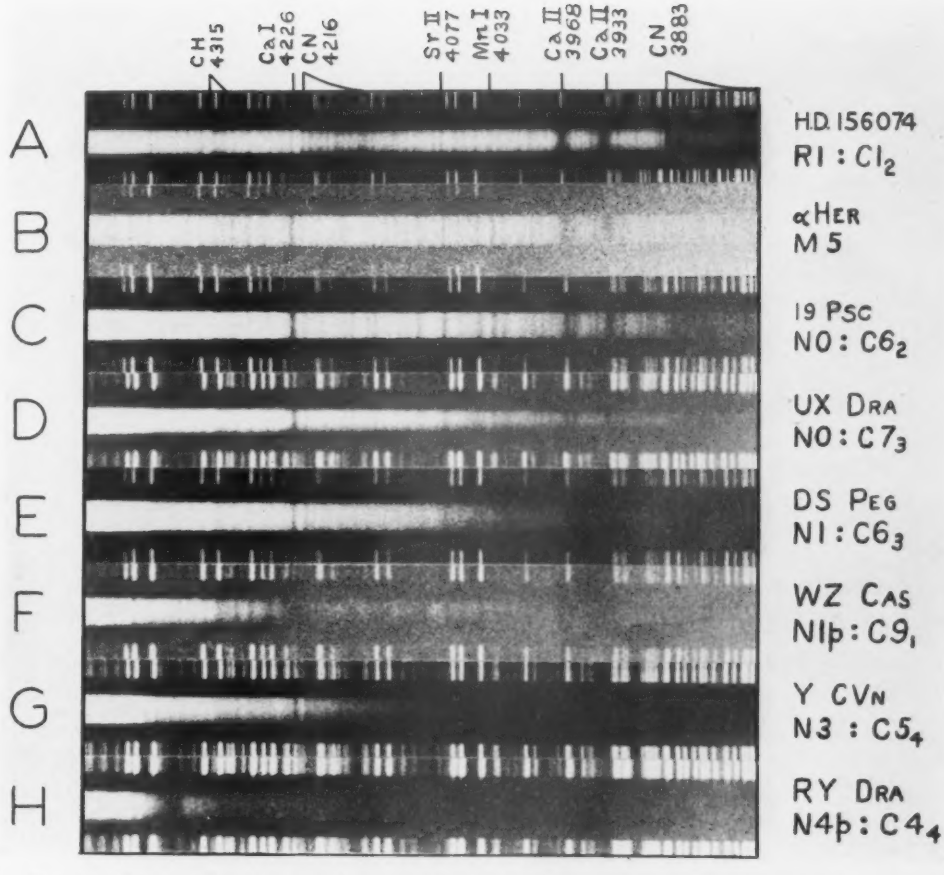

FIG. 1.—The reproductions are of spectra obtained with the ordinary UV spectrograph, dispersion 104 A/mm at λ 4000. The main features of the spectrograms are described in the text.

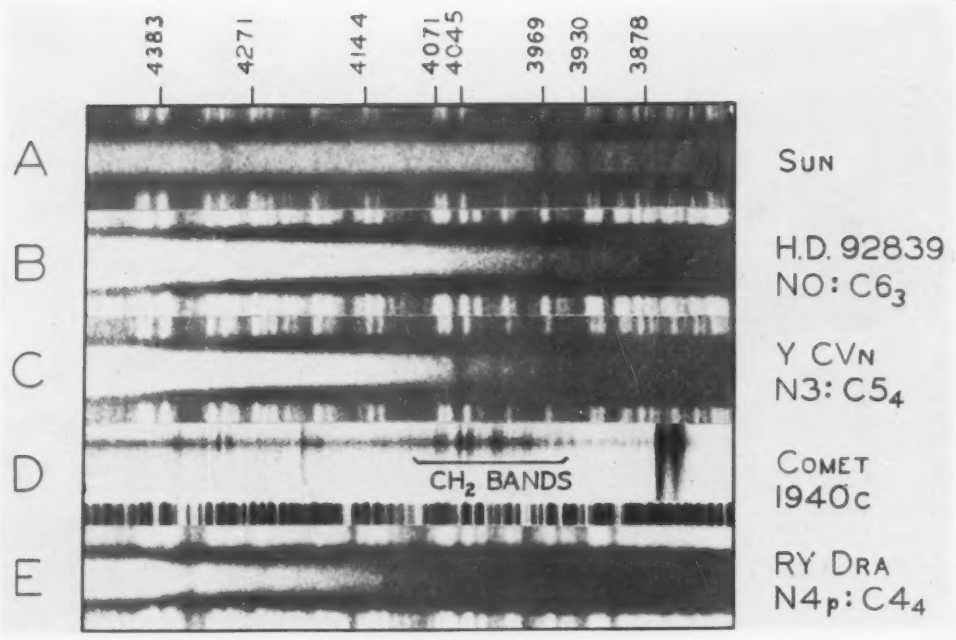

FIG. 2.—With the exception of the spectrogram of Comet 1940c, those of Figure 2 were secured with the short-focus UV spectrograph, dispersion 290 A/mm at λ 4000. The spectrogram of Comet 1940c was photographed at the McDonald Observatory. In the exposures an attempt was made to obtain optimum density in the λλ 4100–3900 region. The widening of the spectra toward the longer wave lengths is due to gross overexposure. For Y CVn the absorption bands attributed to CH_2 are readily seen, as is the sharp drop in intensity at λ 4135 for RY Dra.

The reproduction shown as *C* in Figure 1 is from a spectrogram obtained in an exposure time of 3 hours. For comparison, the spectrum of α Herculis, class M5, is shown directly above. It is seen that the H and K lines of *Ca* II are decidedly weaker for 19 Piscium than for α Herculis. However, the less intense atomic lines such as λ 4077 of *Sr* II and the $\lambda\lambda$ 4033–4036 group of *Mn* I are not weaker than their counterparts in the spectrum of α Herculis to the extent found by Shajn and Struve for UU Aurigae.

3. Figure 1, *D*, shows the spectrum of UX Draconis (HD 183556), N0:C7$_3$, m_v = 6.1–7.0, as photographed with the ordinary UV spectrograph in 5½ hours. Not only does the intensity fall off more rapidly in the violet than for 19 Piscium, but the spectral lines appear weaker in the region of wave lengths shorter than λ 4100.

4. The spectrum of DS Pegasi (HD 206570), N1:C6$_3$, m_v = 6.0–7.0, is shown in Figure 1, *E*. The exposure was 4 hours with the ordinary UV spectrograph. The spectrum is much like that of UX Draconis but perhaps shows to a slightly increasing degree the phenomenon of weakening of the lines investigated for UU Aurigae by Shajn and Struve.[2]

5. WZ Cassiopeiae (HD 224855), N1p:C9$_1$, m_v = 6.9–8.5, was photographed with the ordinary UV spectrograph, and a reproduction of a 4½-hour exposure is shown in Figure 1, *F*. It is the faintest among the group of N-type stars studied, yet its spectrum extends toward the far violet comparatively well. WZ Cas was judged the coolest of all the carbon stars listed by Keenan and Morgan,[3] which, if so, would indicate that extension of the spectrum into the violet may not be a function of temperature only. The distribution of intensity with wave length appears different for WZ Cas than for the other stars. The difference arises from the extremely strong λ 4226 resonance line of *Ca* I and from some unidentified absorption features in the $\lambda\lambda$ 4100–4200 region. These features appear wide and may very well be molecular bands. It is hoped to give them soon the more detailed study that they warrant. The λ 4045 line seems very strong. Probably a considerable contribution to it is made by the second doublet of the principal series of neutral potassium, λ 4044, λ 4047; for it is known that the resonance lines of the alkali metals are unusually intense in the spectrum of WZ Cas. The resonance lines of *Cr* I, $\lambda\lambda$ 4254, 4274, and 4289, are seen to appear with strength.

6. HD 92839, N0:C6$_3$, m_v = 6.3, has a spectrum which is probably much like those of UX Dra and DS Peg. It is shown in Figure 2, *B*, as photographed with the short-focus UV spectrograph in 4 hours. No details except the relatively weak H and K lines of *Ca* II are clearly seen in its spectrum. For comparison, the spectrum of the sky with the same instrument is reproduced directly above; the dispersion is so low that only such wide and strong features as the H and K lines and the G band are observable. Hence any absorption shown by the short-focus instrument must be intense.

7. Y Canum Venaticorum (HD 110914), N3:C5$_4$, m_v = 4.8–6.0, is the brightest N-type star that can be observed from Victoria. Even so, it was not easy to photograph in the far violet with the ordinary UV spectrograph, so use was made of the short-focus camera. Figure 1, *G*, shows a 2-hour exposure with the ordinary UV spectrograph and Figure 2, *C*, a 5½-hour exposure with the short-focus UV spectrograph. The main features on Figure 1, *G*, which has its optimum density about λ 4200, are the λ 4226 line of *Ca* I and the λ 4216 head of the 0, 1 sequence of violet *CN* bands. Both of these seem less intense than one would expect and have a "washed-out" appearance, suggesting that they were produced in an atmospheric region where continuous absorption was also taking place. Figure 2, *C*, shows the region from λ 4100 to λ 3950 quite well and reveals a number of absorption features which are perhaps the most interesting outcome of this investigation. To show up as they do, they must be very intense. The equivalent width of the absorption at λ 4053 measured from the apparent continuum on the spectrogram is 16 A.U. From the results of Shajn and Struve[2] on UU Aurigae, it may be inferred that this equivalent width should be increased at least several times to compensate for the

lowering of the continuum by extraneous absorption. This would lead to a very great intensity for λ 4053.

The centers of the main absorption features in the spectrum of Y CVn were measured on two plates. The mean wave lengths with roughly estimated intensities are listed in Table 1. One notes immediately that the strongest and sharpest feature, λ 4053, coincides closely in wave length with the strongest feature of the λ 4050 group of emission bands found in cometary spectra. This group has been shown by Herzberg[4] to arise from the CH_2 molecule.[5] Not only λ 4053 but also the absorptions at λλ 3994, 4018, and 4076 agree quite well in wave length with strong members of the λ 4050 group of CH_2 bands. The spectrum of Comet Cunningham (1940c), as photographed at the McDonald Observatory, showed the CH_2 bands very well and is included as Figure 2, *D*, so that a direct comparison may be made with the spectrum of Y CVn. In comparing the spectra of Y CVn and Comet 1940c, it should be noted that (*a*) the dispersion and resolving power of the spectrogram of Y CVn is extremely low; (*b*) the physical conditions under which the stellar and cometary bands are produced are very different; (*c*) the stellar bands are in absorption and the cometary bands in emission, so the usual differences between the

TABLE 1

ABSORPTION FEATURES IN THE SPECTRUM OF Y CVn

Intensity	λ	Identification
1	4104	.....
2−	4076	CH_2 (?)
6	4053	CH_2 (?)
1	4032	.....
4+	4018	CH_2 (?)
3	3994	CH_2 (?)
4	3970	CH_2(?) and *Ca* II
2	3942	.....

same band systems in absorption and emission may be expected to be present; and (*d*) the stellar bands might be expected to show some isotope effect involving C^{13}, which manifests itself strongly in the C_2 Swan system for Y CVn, whereas the cometary bands show no evidence of C^{13}. Under the circumstances, the coincidences in wave length and in general appearance seem sufficiently good to permit, at least tentatively, the identification of the absorption bands with those of CH_2. Unfortunately, points *a*–*d* above cannot be investigated quantitatively at present because the laboratory analysis of the λ 4050 CH_2 bands has not yet been completed. Dr. G. Herzberg hopes to be able to take up the CH_2 problem again in the laboratory in the near future.

From a general point of view, the molecule CH_2 is a satisfactory identification, being a combination of two atoms of hydrogen, by far the most abundant element cosmically, with one atom of carbon, an element which, according to current ideas, has an unusually high abundance in the R- and N-type stars. The very interesting questions invoked by the proposed identification, including the possible role of polyatomic molecules in contributing to the general absorption in the violet region of the N-type stars, are reserved for discussion in the joint paper with P. Swings which follows this one.

[4] *Ap. J.*, **96**, 314, 1942.

[5] Dr. Herzberg has pointed out that there should be kept in mind the slight possibility that the λ 4050 group is not due to CH_2 but to another polyatomic molecule consisting of carbon and hydrogen, for example, C_2H. However, the evidence in favor of the CH_2 identification is so strong that in this paper and the following one the bands are referred to as "CH_2 bands."

8. RY Draconis (HD 112559), N4p:$C4_4$, m_v = 6.1–7.1, is, among the stars studied, that most difficult to photograph in the far violet. Figure 1, *H*, shows an exposure of 16½ hours with the ordinary UV spectrograph; Figure 2, *E*, an exposure of 5½ hours with the short-focus UV spectrograph. In the former the heads of the red-degraded unidentified blue-green bands at λ 4352 and λ 4261 are prominent features. The spectrogram with the short-focus camera is seen to cut off abruptly at λ 4135. This sharp drop may be caused by bands in the unidentified system farther to the violet than heretofore found. However, the unidentified bands are degraded to the red from sharp heads at their short-wave-length edges. No certain identification is apparent at present for the sharp cutoff.

On the original plate a slight amount of plate-blackening extends beyond the edge at λ 4135. At λ 4053 there is some evidence of an absorption feature, which would correspond to that found in the spectrum of Y CVn. A stronger spectrogram of RY Dra would be necessary to be certain of this point. If verified, it would enhance the possibility that the unidentified blue-green bands might arise from polyatomic rather than diatomic molecular absorption.

SUMMARY

As noted earlier, the paper following this one contains discussions of various points in connection with the possible presence of polyatomic molecules in the atmospheres of the cooler carbon stars. No attempt will be made here to introduce or discuss the questions.

The most interesting observational results may be summarized as follows:

1. For the earlier N-type stars, the general effects observed by Shajn and Struve have been verified qualitatively.

2. The spectrum of WZ Cas appears sufficiently different from those of other N-type stars to warrant further study.

3. A number of very strong absorption features, the most prominent at λ 4053, were found in the spectrum of Y CVn in the λλ 4100–3950 region. These are tentatively identified with the λ 4050 group of bands of CH_2. If this identification is found by subsequent work to be correct, it will be the first direct observational evidence of the existence of polyatomic molecules in stellar atmospheres.

4. In the spectrum of RY Dra, a sharp cutoff occurs at λ 4135 which is not present for the other stars studied. On the very weakly exposed region beyond λ 4135, there was some evidence of the same absorption feature at λ 4053 noted for Y CVn.

POLYATOMIC MOLECULES IN LATE-TYPE STARS*

P. SWINGS AND A. MCKELLAR
University of Liége, Liége, Belgium, and
Dominion Astrophysical Observatory, Victoria, B.C.
Received July 13, 1948

ABSTRACT

Some general problems connected with the presence of polyatomic molecules in stellar atmospheres are noted, and, in particular, reasons are advanced in favor of attributing at least part of the intensity drop and fluctuations in the spectra of the N-type stars violetward of λ 4100 to the triatomic molecule CH_2.

INTRODUCTION

Absorption by polyatomic molecules is detected in the atmosphere of the earth (O_3, H_2O, CO_2, CH_4, N_2O) and of planets (CO_2, CH_4, NH_3), while emission bands of the triatomic molecules CH_2 and NH_2 are found in cometary spectra. No polyatomic molecule has heretofore been identified in a stellar atmosphere. Yet triatomic molecules may be abundant in the coolest stars, even under the assumption of thermodynamical equilibrium. H. N. Russell[1] has estimated the abundances of H_2O and CO_2 in giant and dwarf stars of the K–M branch of the spectral sequence and has concluded that in those of latest type the abundance of H_2O is of the same order as that of oxygen or nitrogen atoms. On the other hand, the abundance of CO_2 in a stellar atmosphere is always very small compared with that of oxygen atoms. The greater calculated abundance of H_2O compared with CO_2 is due to the high abundance of hydrogen compared with oxygen and carbon. In actual stellar atmospheres of very late type we may expect H_2O molecules to be even more abundant than would be indicated by Russell's theoretical estimates, since the photodissociating radiation may be absorbed in the lower layers before reaching the coolest outer layers, where the presence of polyatomic molecules would be favored.[2] The possible presence of another triatomic molecule, HCN, has been suggested by B. Lindblad and E. Stenquist[3] in order to explain certain absolute-magnitude effects on the CN bands.

Probably high-dispersion spectrograms would be required in any attempt to detect H_2O in a stellar atmosphere of very late type. The problem is not perfectly straightforward, since, of course, telluric H_2O lines would be present. The effect of radial velocity could be used in separating telluric and stellar lines. Also, on account of the higher stellar temperature, the bands would have an entirely different intensity distribution, and some bands not present in the spectrum of the earth's atmosphere would appear, for which radial-velocity effects need not be invoked. However, on the other hand, the absolute intensities of the additional bands are very small, and it does not seem likely that they would suffice for the detection of H_2O in stellar atmospheres. Two other triatomic molecules containing two hydrogen atoms are CH_2 and NH_2. Their stellar bands would not be blended by telluric lines, since the amounts of CH_2 and NH_2 in the earth's atmosphere must be very low. Because of the absence of data on the essential physical constants of CH_2 and NH_2, a calculation of the abundances of these two compounds in the atmospheres of late-type stars is at present impossible. Moreover, as mentioned above,

* *Contributions from the Dominion Astrophysical Observatory*, No. 16.

[1] *Ap. J.*, **79**, 317, 1934.

[2] P. Swings, *Pub. A.S.P.*, **54**, 232, 1942.

[3] *Astr. iakt. och und. Stockholm Obs.*, Vol. **11**, No. 12, 1934.

conditions of thermodynamical equilibrium assumed in calculations do not necessarily prevail in the stellar regions of highest molecular abundance.

While any detailed calculation of the abundances of CH_2 cannot be made at present, we may expect it in late carbon stars to reach abundances of the same order as those of H_2O in late-type oxygen stars. Moreover, from the high intensity of the CH_2 emission in comets at large heliocentric distances, one could justifiably assume that the oscillator strength of the band near λ 4050 is not small. Hence the existence of CH_2 in late carbon stars appears to be fairly probable.

THE OBSERVATIONAL DATA AND THEIR DISCUSSION

A recent paper by G. Shajn and O. Struve[4] brings new observational information on the violet region of the late carbon stars, in addition to that contained in C. D. Shane's pioneering work.[5] From Shajn and Struve's paper it appears reasonably certain that the sudden intensity drop of the continuous background of the late N-type stars violetward of λ 4100 is due to the effect of molecular bands rather than (or in addition) to a purely continuous absorption. The presence of an absorption band with structure could explain more reasonably why the spaces between absorption lines near λ 4036 and λ 4009 could look like emission lines in the spectrum of the N-type star, UU Aurigae, while the background near λ 4052, which is also free from absorption in M-type stars, does not appear in the N types. It could also explain why the intensity of λ 4072, *Fe* I, is reduced to a lesser extent than is the neighboring line λ 4063, *Fe* I. Atomic negative ions or quasi-molecules giving rise to continuous absorption would not be likely to produce the observed structure.

In trying to identify the molecule responsible for the intensity drop and fluctuations in the spectrum of UU Aurigae as described by Shajn and Struve, the following considerations present themselves:

1. The permitted spectra of neutral diatomic molecules, composed of the cosmically abundant atoms, hydrogen, carbon, nitrogen, and oxygen, have been studied extensively in the laboratory, and no known band explains the observed phenomenon. The spectra of the oxides of all abundant elements are well known, and none explains the observed absorption. Moreover, oxides are not likely to be abundant in a late carbon star. Compounds of hydrogen, carbon, or nitrogen with an abundant element may possibly provide the explanation, but no such compound is known to have its strongest absorption system around λ 4050.

2. Forbidden bands (such as the Vegard-Kaplan system) or bands of positive molecular ions (such as N_2^+ or CO^+), which appear in this region, should not be expected to reach any appreciable intensity in a stellar atmosphere.

3. The molecular band responsible for the absorption has no sharply defined head, which otherwise would appear on the stellar spectrograms.

4. The identification problem presents some similarity with that encountered in cometary spectra, where many fruitless attempts were made to attribute the so-called "λ 4050 group" to a hypothetical diatomic molecule.

It seems probable that the absorption in the N stars in the λ 4050 region is due to a polyatomic molecule, just as the "λ 4050 group" of cometary spectra was finally identified with CH_2. In fact, this same molecule may be at least partly responsible for the depression in the N stars. The absence of a segment of continuous background of the N spectra near λ 4052 could be due to absorption by the strongest CH_2 feature at this wave length. The absence of CH_2 in M stars is, of course, readily understood.

McKellar's investigation of the spectrum of Y Canum Venaticorum in the λλ 4100–3950 region[6] has brought additional and more specific observational information on this

[4] *Ap. J.*, **106**, 86, 1947.

[5] *Lick Obs. Bull.*, **13**, 123, 1928.

[6] *Ap. J.*, **108**, 453, 1948.

matter. The absorption features which he has observed in Y Canum Venaticorum, the strongest of which is located at λ 4053, appear to coincide in wave length with the CH_2 maxima observed in cometary spectra. The correspondence between the relative intensities of the stellar absorption features and those of the CH_2 emissions in comets is also about as good as may be expected. There are, indeed, numerous reasons why the intensity distribution within the CH_2 absorption bands of an N star could differ from that of the CH_2 emission bands in a comet, e.g., the different rotational temperatures, the different excitation mechanisms (especially the effect of the solar absorption lines on the profile of the CH_2 emission in comets, assuming that the emission bands are produced by the resonance phenomenon), and the differences in relative abundances of C^{12} and C^{13}. A detailed argument must await a more or less complete laboratory analysis of the CH_2 spectrum.

While the identification of CH_2 in late N-type stellar atmospheres, if correct, provides satisfactory solutions to most of the questions raised by the observations in the violet spectral region, there remain one or two apparent difficulties which may be resolved by further observations and by laboratory work on CH_2. For example, whereas the maximum intensity of the CH_2 bands is in the λλ 4070–4000 interval, Shajn and Struve found that for UU Aurigae the H and K lines of *Ca* II, λ 3968 and λ 3934, exhibited the effects of stronger superposed absorption than did the *Fe* I and other lines from λ 4078 to λ 4032. Examination of the spectrum of CH_2 as produced in the laboratory by Herzberg[7] reveals that a fairly diffuse feature of moderate intensity appears about λ 3970, very near the position of the H line of *Ca* II; but nothing is shown near the K line. In cometary spectra CH_2 emission cannot give information on this point, since, being a resonance phenomenon, it would not be expected to show anything very near λ 3968 or λ 3933 because of the wide and strong *Ca* II absorption lines in the spectrum of the exciting solar radiation. Hence the greater weakening of the H and K lines compared to the lines from λ 4070 to λ 4000, if firmly established by further observations, does not seem explicable on the basis of CH_2 absorption alone. It would appear necessary to invoke an additional source of opacity.

The presence of a CH_2 feature in the laboratory spectrum at λ 3970 and not at λ 3933 brings forward a further item of interest. If CH_2 absorption is important and if it occurs in the same levels of the atmosphere as the *Ca* II lines, there should be found a greater weakening of the H line than of the K line. A very slight effect in this direction (reduction of the intensity of H compared to the comparison M-type spectrum by a factor of 6.8 and of K by a factor of 6.5) is shown in the measurements of Shajn and Struve for UU Aurigae. However, the difference probably does not exceed their errors of measurement. More precise and extensive data will be required to provide a positive answer.

It might be noted that the amount by which Shajn and Struve found the intensities of the spectral lines of UU Aurigae decreased in the violet indicated that the weakening of the continuous background of the N-type star compared to its M-type counterpart should have been about 1.6 mag. However, the observed difference in the λλ 4100–3900 region was about 4 mag. The question as to whether this large discrepancy arose either from inadequacies in the simple theory of blended lines or in the assumption that it could be applied to the observations in this case was left unanswered. Effects of possible stratification in the atmospheres, especially of the N-type star, and of the choice of the comparison star enter into the problem. Again, more complete and, if possible, more accurate observational material is required before all aspects of the role of CH_2 can be discussed.

As noted earlier, it would be interesting to search for the presence of absorptions arising from NH_2. The spectrum attributed to this molecule is of the "many-line" type and extends through the yellow and red regions. It has been photographed in the laboratory in emission by various investigators[8] but, unfortunately, has not been analyzed. There-

[7] *Ap. J.*, **96**, 314, 1942.

[8] See, e.g., W. B. Rimmer, *Proc. R. Soc., London, A*, **103**, 696, 1923.

fore, the lines which should appear strongest in absorption cannot be designated with certainty. The strongest group of emission lines appears at λλ 5705–5708, 5972–5977, 6295–6302, and 6332. Grating spectrograms (dispersion, 15 A/mm) covering the red region were available at Victoria for twenty-five N-type stars, including those discussed in the preceding paper. Examination of the plates at λ 6300 and λ 6332 did not show any notable differences between early and late N-type spectra. While, among the multitude of lines present, there are some corresponding closely in wave length to strong NH_2 lines, they cannot be safely identified as NH_2. We conclude that, to settle the question of the presence or absence of NH_2 band lines, a full and separate investigation, covering various regions of strong NH_2 emission, would be necessary. It would be desirable to include late M-type as well as N-type stars.

From the blue-green down into the violet region of the spectra of some late N-type stars, a number of unidentified molecular absorption bands are found. In some stars (e.g., RY Draconis) they are very strong. McKellar[9] in a recent study of the bands suggested, among possible carriers of the bands, the molecules *TiH* or *FeH*, but attempts to produce *TiH* bands in the laboratory have not yet been successful. The suggested identification of CH_2 bands for Y Canum Venaticorum brings forward the possibility that the blue-green systems may arise from a polyatomic molecule. It would be interesting to extend present observational material to investigate whether there are any similarities in the behaviors of the blue-green bands and λ 4053 absorption, from star to star. It may be significant that in the spectrum of Y Canum Venaticorum the blue-green bands are present but weak, while the λ 4050 group is of considerable strength, and for RY Draconis the blue-green bands are very strong and the whole region to the violet of λ 4135 is almost completely absorbed.[10]

[9] *J.R.A.S. Canada*, **41**, 147, 1947; *Contr. Dom. Ap. Obs.*, No. 7, 1947.

[10] *Ap. J.*, **108**, 453, 1948.

THE ABSORPTION-LINE SPECTRA OF THE CENTRAL STARS OF THE PLANETARY NEBULAE

LAWRENCE H. ALLER*
Kirkwood Observatory, Indiana University
Received May 13, 1948

ABSTRACT

Under the terms of a co-operative arrangement with the University of Chicago and the University of Texas, a systematic spectroscopic study of the brighter central stars of the planetary nebulae has been undertaken at the McDonald Observatory. The intensities of all available absorption lines have been measured. From the Balmer lines it is possible to estimate the number of hydrogen atoms above the photosphere and the electron pressure, which is equal to half the gas pressure if hydrogen is the most abundant element. If the atmosphere is in hydrostatic equilibrium, the gas plus radiation pressure must just balance the weight of the overlying layers. Hence we may estimate the effective surface gravity of the star; and, if we can allow for the radiation pressure and find the stellar radius, we may obtain a lower limit to the mass of the star.

To within the limits imposed by observational uncertainties the spectra of these stars appear consistent with the suggestion that they are submain-sequence dwarfs with masses appropriate to their luminosities in accordance with the mass-luminosity law. There is no evidence from their spectra that they are white dwarfs or dense, extremely massive stars. The hotter planetary nuclei may resemble the old novae, although the absorption-line objects seem cooler and larger.

Attention is called to the high-excitation character of the nucleus of NGC 246.

I. INTRODUCTION

Further progress in the interpretation of the planetary nebulae would appear to depend, to some extent, on better information concerning their central stars. Thanks to the work of W. H. Wright,[1] Plaskett and his co-workers,[2] Struve and Swings,[3] and others, we have good qualitative information on the spectra of these objects. The planetary nuclei show spectra of four general kinds: (1) Wolf-Rayet type, e.g., NGC 40, BD +30°3639; (2) combined absorption and emission features, e.g., NGC 6543 and IC 418; (3) spectra predominantly of the absorption type with but few emission lines, e.g., NGC 2392, NGC 6891; and (4) continuous spectra with no trace of emission lines with the dispersion available, e.g., NGC 7662 or NGC 7009.

Under the terms of a co-operative arrangement between the University of Chicago, the University of Texas, and Indiana University, I have undertaken a spectroscopic and spectrophotometric study of the brighter nuclei of the planetary nebulae, with the aim of applying techniques worked out for other hot stars to an interpretation of these objects. The McDonald plates have been supplemented by observations taken with the quartz slitless spectrograph at the Crossley reflector of the Lick Observatory. The latter spectra are to be used primarily for measuring the energy distribution in the emission lines and in the continuous spectrum. In this paper I shall confine my attention to the absorption lines; the emission features will provide material for later articles.

II. THE OBSERVATIONS

The McDonald survey covers planetary nuclei brighter than apparent magnitude 12.0 and a few fainter objects as well. For the brighter nuclei, I have employed the

* Research Associate of the McDonald Observatory of the University of Texas.

[1] *Pub. Lick Obs.*, **13**, 193, 1918.

[2] *Pub. Dom. Ap. Obs., Victoria*, **1**, 366, 1922.

[3] *Proc. Nat. Acad. Sci.*, **26**, 548, 454, 1940; **27**, 225, 1941; *Ap. J.*, **92**, 289, 1940.

Cassegrain spectrograph with quartz prisms and 500-mm camera. For fainter objects it has been necessary to use the $f/2$ Schmidt camera. To make a photometric study of the absorption lines it is necessary to use as high a dispersion as possible; hence only plates made with the 500-mm camera have been employed for this purpose. The $f/2$ films are of great assistance for a qualitative study of the spectra of the fainter stars.

The usual observational procedure has been to lengthen the slit to the diameter of the nebular image and to let the latter drift slightly, so as to obtain a widened spectrum of the central star. The distinction between nebular and nuclear emission lines then may be easily made.

Table 1 lists the McDonald observations of interest in the present connection. Successive columns give the NGC number of the object, the α and δ for 1900, the magnitude

TABLE 1

LIST OF PLANETARY NUCLEI STUDIED FOR ABSORPTION-LINE INTENSITIES

Object	α	δ	Mag.	Spectral Class	Plate	Camera	Quality
NGC 246.....	$0^h42^m.0$	$-12°25'$	11.2	O7	CQ4610	500-mm	p
					4618	500-mm	g
					4624	500-mm	g
					6277	Q $f/2$	g
NGC 1535.....	4 9.6	−13 0	11.8	Cont.	6362	Q $f/2$	g
					6363	Q $f/2$	f
IC 418.....	5 22.8	−12 45	10.8	WC7+O5	4653	500-mm	g
					6364	Q $f/2$	p
NGC 2392.....	7 23.3	+21 7	10.5	O8e	4652	500-mm	f
					5222	500-mm	g
NGC 3242.....	10 19.9	−18 8	11.9	Cont.	7944	Q $f/2$	g
IC 3568.....	12 30.4	+83 7	12.0	Cont.	8045	Q $f/2$	g
					8074	Q $f/2$	f
IC 4593.....	16 7.0	+12 20	10.2	Cont.	4593	500-mm	g
					4603	500-mm	f
					5959	500-mm	g
NGC 6210.....	16 40.3	+23 59	11.7	O6+WC7	4599	500-mm	g
					4628	500-mm	g
NGC 6543.....	17 58.6	+66 38	11.2	WN6	4600	500-mm	g
					4637	500-mm	g
NGC 6826.....	19 42.1	+50 17	10.7	WN6, O5	4590	500-mm	f
					4596	500-mm	f
					5960	500-mm	g
NGC 6891.....	20 10.4	+12 24	11.6	Cont.	4613	500-mm	f
					4622	500-mm	g
NGC 7009.....	20 58.7	−11 46	11.9	Cont.	4609	500-mm	p
					4617	500-mm	p
					4623	500-mm	f
					6360	Q $f/2$	f
NGC 7662.....	23 21.1	+41 59	12.7	Cont.	6281	Q $f/2$	g

of the central star as given by Berman,[4] the spectral classes assigned by Verontsov-Velyaminov,[5] the plate number, the camera used, and the quality.

Satisfactory plates with the 500-mm camera, which gives a dispersion of 75 A/mm at $H\gamma$, have been obtained for the central stars of NGC 246, 2392, 6210, 6543, 6891, and IC 418 and 4593. In addition, I have paid special attention to the central stars of NGC 1535, NGC 3242, IC 3568, NGC 7009, and NGC 7662, whose spectra have been described as continuous. Unfortunately, the 500-mm camera (CQ) plates of NGC 7009 and NGC 7662 were somewhat underexposed. The strong nebular recombination lines of *He* II, *H*, etc., would tend to obliterate the corresponding presumably weak absorption lines in the central star. Plates taken with the $f/2$ camera give insufficient dispersion to detect more than the strongest absorption lines. Thus strong λ 4452 *He* II absorption appears in the spectra of the nuclei of NGC 1535 and IC 3568, but other lines have not been found because of the low dispersion and the intense superposed nebular lines. Until satisfactory higher-dispersion plates of these objects have been obtained, we shall not be able to assign them spectral classes.

III. PHOTOMETRIC PROCEDURE

Mention may be made here of two devices employed for the photometric calibration of the plates—a spot sensitometer and a wedge slit. The second method involves replacing the slit of the Cassegrain spectrograph by a wedge slit and illuminating it by artificial light reflected from a white diffusing screen. Calibration-curves derived by the two procedures are in good agreement. I traced the plates with the Beals-type microphotometer of the Yerkes Observatory.

The measurement of the intensity of a stellar absorption line upon which a strong nebular emission is superposed presents a formidable problem. Invariably, $H\beta$ was unmeasurable, $H\gamma$ and $H\delta$ were partly masked, and sometimes only rough intensity estimates were possible. In NGC 6891, $H\gamma$ and $H\delta$ could be measured with seeming confidence. In other objects in which these absorption lines could be recognized, I had the feeling that the measured intensities tended to be too low; but there appears little possibility of securing improved values without going to higher dispersion. The object IC 418 has such strong hydrogen lines that none of the nuclear absorption lines are observable, and only the strongest *He* II lines can be seen. In a number of nuclei the higher members of the Balmer series are readily measurable.

The Eberhard effect complicates the measurement of absorption lines underlying strong nebular emission; but, if it is present, the strong forbidden nebular lines will also show spurious underlying absorptions, and upon such a plate only those absorption lines that are not associated with nebular emissions will be measurable. Fortunately, the Eberhard effect was encountered on only one plate.

Table 2 lists the intensities of the absorption lines measured in the central stars of NGC 2392, IC 418, NGC 6543, NGC 6891, IC 4593, NGC 6826, and NGC 6210. The emission lines measured in the spectra of these stars will be discussed later. In a star such as the NGC 2392 nucleus, which shows good absorption lines, the accidental error in the measured line intensities is of the order of 15 per cent for the stronger lines. The weaker lines and lines like $H\delta$ or $H\gamma$, which are confused with nebular emissions, may be seriously in error.

IV. THE HYDROGEN LINES

Aside from the observational difficulty arising from the superposition of the nebular emission, the interpretation of the Balmer line intensities is complicated by their confusion with the Pickering *He* II lines. From a comparison of alternate members of the Pickering series with the Balmer lines, which represent *H* I+*He* II absorption, we may estimate the amount by which the Balmer lines are to be corrected for the contribution

[4] *Lick Obs. Bull.*, **18**, 57, 1937.

[5] *Russ. A.J.*, **24**, 88, 1947.

of *He* II. This crude procedure is seemingly justified for the higher members of the Balmer series—certainly, within the limits of the present observational accuracy. Its application to $H\gamma$ and $H\delta$ can give us only a lower limit to the intensities that these lines would have in a pure hydrogen atmosphere at the same temperature and electron pressure.

If we can suppose that the hydrogen lines are formed in a thin layer, then the equivalent width, W_λ, of the line corresponding to the (2–n) transition will be related to the number of atoms in the second level above the photosphere by

$$W_\lambda = \frac{\pi e^2}{m c^2} \lambda^2 N_{02} H f_{2n}, \qquad (1)$$

TABLE 2

ABSORPTION LINES IN CENTRAL STARS OF PLANETARY NEBULAE
(Intensities in Equivalent Angstroms)

Wave Length	Identity	NGC 2392	IC 418	NGC 6543	NGC 6891	NGC 4593	NGC 6826	NGC 6210
4541.58	*He* II	0.85	0.55	0.47	0.67	0.76	0.80	0.85
4471.6	*He* I	0.54	.....	.....	.....	.....	.....	.....
4340	*H* I, *He* II	1.20	.....	.....	1.8	1.53	1.55	1.47
4200	*He* II	0.67	1.36	.....	0.73	0.45	0.51	0.28
4100	*N* III, *He* II, *H* I	1.82	.....	.....	1.94	1.10	1.28	.....
4025.6	*He* II	0.70	.....	.....	.....	.....	.....	.....
3969	*H* I, *He* II	0.72	.....	.....	.....	1.23	1.05	1.36
3965	*He* I	0.19	.....	.....	.....	.....	.....	.....
3933	*Ca* II (ints)	0.41	.....	0.36	0.33	0.28	0.30	0.38
3923.5	*He* II	0.47	0.58	.....	0.28	0.43	0.30	0.19
3889.0	*H* I, *He* II	0.66	.....	1.30	1.46	1.30	1.15	1.10
3858.0	*He* II	0.31	0.65	.....	1.1:	0.20	0.30	0.24
3835.2	*H* I, *He* II	0.65	0.81	0.56	0.95	1.00	0.92	1.00
3813.5	*He* II	.....	0.4	.....	.....	.....	.....	.....
3797.3	*H* I, *He* II	0.74	1.4	0.70	1.06	1.20	0.67	0.67
3781.3	*He* II	.....	0.36	.....	.....	.....	.....	.....
3770.6	*H* I, *He* II	0.45	.....	.....	0.50	0.78	0.55	.....
3750.1	*H* I	0.36	.....	.....	0.41	0.52	0.40	.....
3734.4	*H* I, *He* II	0.27	.....	.....	0.58	0.40	0.35	.....
3721.9	*H* I	.....	.....	.....	0.28	.....	.....	.....
3712.0	*H* I	.....	.....	.....	0.24	.....	.....	.....
3705.1	*He* I	0.23	.....	.....	.....	.....	.....	.....
3634.3	*He* I	0.11	.....	.....	.....	.....	.....	.....
3554.5	*He* I	0.46	.....	.....	.....	.....	.....	.....
3483.0	*N* IV	0.45	.....	.....	.....	.....	.....	.....
3478.7	*N* IV	0.26	.....	.....	.....	.....	.....	.....

a formula used extensively by Unsöld;[6] the same principle was applied to emission lines of the solar chromosphere by Menzel.[7] Here f_{2n} is the oscillator strength for the Balmer line in question, and the other symbols have their usual meaning. If we measure the wave length, λ, in centimeters and W_λ in angstrom units, we may write equation (1) as

$$\log N_{02} H = 4.05 - \lambda^2 f_{2n} + \log W_\lambda = C_n + \log W_\lambda . \qquad (2)$$

We plot $\log N_{02} H$ against n and find that, for the earlier members of the series, the lines give successively greater values of $\log N_{02} H$, since these lines are not formed in a thin layer and W is not proportional to the number of atoms. Then the curve flattens, the lines begin to coalesce, we tend to draw the continuum too low and measure W too small, and the curve begins to fall. An extrapolation of the curve, in the manner suggested by

[6] *Zs. f. Ap.*, **21**, 38, 1941.

[7] *Pub. Lick Obs.*, Vol. **17**, 1931: "A Study of the Solar Chromosphere."

Unsöld, gives an estimate of log $N_{02}H$, the number of hydrogen atoms above the photosphere and in the second level. Table 3 gives, for each central star, the equivalent width corrected for blending with *He* II, log $N_{02}H$, computed from each spectral line, and the finally extrapolated value of this quantity for the star.

For comparison we may mention results obtained by Unsöld[8] for several hot stars, including 10 Lac, discussed also by the writer.[9] For the supergiants, λ Ori (07.5) and 9 Cam (09), log $N_{02}H$ was 15.8 and 15.7, respectively, while for the main-sequence star, 10 Lac, log $N_{02}H$ = 15.8. For the central stars of the planetary nebulae, the mean value of log $N_{02}H$ = 15.16, which means that there seems to be about a fourth as much material above the photosphere of the central star of a planetary as above main-sequence or supergiant stars of the same spectral types. The different stars appear to give fairly concordant results; it seems possible that our average for this group of five stars is correct to within a factor of 2.

TABLE 3

CORRECTED INTENSITIES OF THE BALMER LINES

n	λ	log C_a	NGC 6891		NGC 6826		NGC 2392		IC 4593		NGC 6210	
			W	log $N_{02}H$	W	log $N_{02}H$	W	log $N_{02}H$	W	log $N_{02}H$	W	log $N_{02}H$
5	4340	14.13	1.10	14.17	0.90	14.09	0.45	13.78	0.75	14.01	0.91	14.09
6	4101	14.48	1.24	14.57	.63	14.28	.30	13.96	0.52	14.20	.....	.....
7	3970	14.75	.....	.....	.65	14.56	.43	14.39	0.72	14.61	1.02	14.76
8	3889	14.96	0.88	14.90	.85	14.89	.40	14.56	1.00	14.96	0.82	14.88
9	3835	15.14	0.57	14.90	.62	14.93	.39	14.73	0.80	15.04	0.75	15.02
10	3797	15.31	0.63	15.11	.47	14.98	.44	14.96	0.90	15.27	0.50	15.01
11	3770	15.45	0.30	14.93	.38	15.03	.27	14.88	0.58	15.22	.....	.....
12	3750	15.57	0.25	14.96	.28	15.02	.22	14.90	0.39	15.16	.....	.....
13	3734	15.60	0.35	15.24	0.24	15.07	0.16	14.90	0.30	15.07	.....	.....
14	3722	15.79	0.17	15.02	.....	.....	.....	.....	.....	.....	.....	.....
15	3712	15.87	0.14	15.03	.....	.....	.....	.....	.....	.....	.....	.....
Final log $N_{02}H$	.....	.....	.....	15.16	.....	15.12	.....	14.96	.....	15.35	.....	15.10

A second item of interest is the electron density in the atmosphere—this is the quantity which helps distinguish supergiants, main-sequence stars, and subdwarfs. For a normal early-type star two methods are available for estimating the electron density. One method is based on the fact that the equivalent widths of the earlier members of the Balmer series, e.g., *Hα*, *Hβ*, *Hγ*, and *Hδ* depend not only on the number of atoms in the second level but also on the electron pressure which determines the broadening coefficient of the line.[6] The greater the electron pressure, the greater the equivalent width. Unsöld has employed this method to estimate the mean electron densities in the atmospheres of early-type stars. From the theoretical standpoint we can see that it gives only a rough log N_e, since the assumption is made that the line is formed in an isothermal atmosphere of constant density. A more serious objection to its application in the present problem is the circumstance of the blending of *Hγ* and *Hδ* with the Pickering lines and the influence of overlying nebular lines upon the measured intensities. The measured equivalent widths are almost certainly too small; hence the derived values of the electron density will be a lower limit. The most accurate values of W_λ are those determined for NGC 6891, while NGC 2392 appears to give poor W_λ's.

The number of resolvable lines of the Balmer series will give us an additional estimate of the electron density. If n_m is the principal quantum number of the last still-resolved

[8] *Zs. f. Ap.*, **23**, 100, 1944.

[9] *Ap. J.*, **104**, 347, 1946.

Balmer line, the concentration of free electrons (or ions) per cubic centimeter is given by the Inglis-Teller formula:[10]

$$\log N = 23.26 - 7.5 \log n_m .$$

Unfortunately, the confluence of the stellar lines often underlies that of much stronger nebular emission, and it is not possible to establish n_m with certainty. In IC 4593 and NGC 6826 the last Balmer line appears to be recognizable, while in NGC 2392, where the nebular spectrum is much weaker, it seems quite definite that $n_m = 14$, λ 3722, is the last line of the Balmer series.

Table 4 summarizes the estimates of log N_e based on $H\gamma$ and $H\delta$ and n_m, together with the values adopted for further computations. The agreement between the electron densities computed by the two methods is good for NGC 6826, fair for IC 4593, and poor for NGC 2392. Since the determination of n_m seems most accurate for NGC 2392, we may conclude that the log N_e estimated from n_m is the more reliable. Inspection of the plates and tracings suggests that $H\gamma$ and $H\delta$ are measured systematically too weak; if W_λ for $H\gamma$ is in error by a factor of 2, log N_e would be 14.0—in fair agreement for the values of the others. In this star, $H\delta$ appears to be badly blended with λ 4089 *Si* IV, as

TABLE 4

ELECTRON DENSITIES DERIVED FROM BALMER LINES

OBJECT	LOG N_e		n_m	LOG N_e FROM n_m	LOG N_e (ADOPTED)
	$H\gamma$	$H\delta$			
NGC 6891	14.04	14.26	.....	.....	14.15
NGC 6826	13.87	13.56	15	13.76	13.75
NGC 2392	13.28	12.92	14	14.66	14.5
IC 4593	13.67	13.45	15:	13.8	13.65
NGC 6210	13.90	.....	.....	.....	13.9

well as *N* III λ 4097 and λ 4103. The adopted values of log N_e would appear to represent lower limits in most stars. In the supergiants λ Ori and 9 Cam, Unsöld finds log N_e = 14.17 and 13.75, respectively. In 10 Lac the electron density is higher; Unsöld found log N_e = 14.37, while the writer obtained 14.10. The electron densities appear to be comparable with those in other stars of the same spectral class.

As an alternative mode of treating the higher members of the Balmer series, I have computed theoretical equivalent widths on the basis of Pannekoek's[11] assumption that the Stark pattern produced by the interatomic fields gives a uniform spreading-out for a given field and that the ratio of line to continuous absorption is constant with depth. As parameters I have employed the number of atoms per gram in the second energy level n_{02}, divided by the continuous absorption coefficient, k, and the electron pressure. It turns out that, for the higher members of the series, the equivalent width is insensitive to the electron pressure, but we may obtain log n_{02}/k. The accompanying tabulation

Object	log n_{02}/k	log $N_{02}H$	Optical Depth	Object	log n_{02}/k	log $N_{02}H$	Optical Depth
NGC 2392	15.48	14.96	0.30	NGC 6826	15.62	15.12	0.31
NGC 6891	15.68	15.16	0.30	NGC 6210	15.72	15.10	0.24

gives the results of such calculations. A comparison of log n_{02}/k and log $N_{02}H$ will give the optical depth effective for the formation of the hydrogen lines. Notice that the ef-

[10] *Ap. J.*, **90**, 439, 1939.

[11] *M.N.*, **98**, 701, 1938.

fective value of the optical depth is near 0.3, in harmony with the result found by Strömgren for an atom in the sun that becomes easily ionized with depth, e.g., sodium.[12]

V. TEMPERATURES AND SPECTRAL CLASSES OF THE PLANETARY NUCLEI

The temperatures of the central stars of the planetary nebulae may be estimated either from their spectral classes (when known) or from a comparison of the luminosity and spectrum of the surrounding nebula with that of the central star.

I have employed the criteria suggested by R. M. Petrie[13] to estimate the spectral classes from the absorption lines. Except for NGC 2392, it is possible to apply only the *H/He* II ratio. Since the Balmer lines tend to be confused with the nebular emissions and are sometimes, therefore, measured too weak, the derived spectral classes may tend to be systematically too early. For the objects studied, the spectral classes seem to fall between O5 and O7, and the corresponding temperatures range from 33,000° to 35,000° K.

Second, one may utilize the magnitude difference between the central star and the nebula in conjunction with the theory of nebular luminosity,[4] in the manner suggested by Zanstra. Thus one may put

$$m_s - m_n = \delta(T),$$

TABLE 5

TEMPERATURES AND SPECTRAL CLASSES OF PLANETARY NUCLEI

Nebula	Spect.	Temperature			
		Spect. Cl.	Berman	Stoy	Adopted
NGC 6891.....	O7	32,900	30,000	40,000	32,000
NGC 6826.....	O6	34,600	30,000	48,000	32,000
NGC 2392.....	O5.5	35,000	35,000	70,000	35,000
IC 4593.....	O6.5	34,000	25,000	40,000	25,000–34,000
NGC 6210.....	O7	32,900	30,000	57,000	32,000

where $\delta(T)$ can be calculated as a function of the temperature. Part of the nebular emission comes from the recombination of protons and free electrons, liberated by photoionization from radiation emitted beyond the Lyman limit in the central star, and part comes from forbidden lines excited by inelastic impacts by the free electrons. The higher the color temperature of the star beyond the Lyman limit, the greater will be the magnitude difference between the nebula and the star. Berman employed this method to estimate the temperatures of the planetary nuclei.

Third, one may employ a method due to Stoy,[14] wherein one compares the sum of the intensities of the Balmer lines with the sum of the intensities of the forbidden lines. In accordance with the arguments of Zanstra and Menzel, the former is determined by the number of quanta radiated by the central star beyond the limit of the Balmer series, while the latter is determined by the amount of energy radiated beyond the Balmer limit. Hence a comparison of the two should give the color temperature in the far ultraviolet, on the assumption that the stars radiate there like black bodies.

Table 5 gives the temperatures estimated by the three methods. The temperatures in the third column correspond to the spectral types and Petrie's temperature scale, those in the fourth column are taken from Berman's work, while those in the fifth column are derived from nebular line intensities measured upon plates taken at the

[12] *Festschrift für Elis Strömgren* (Copenhagen: E. Munksgaard, 1940), p. 218.

[13] *Pub. Dom. Ap. Obs., Victoria*, **7**, 321, 1947.

[14] *M.N.*, **93**, 588, 1933.

Lick Observatory; the intensity of $H\alpha$ was extrapolated from the observed Balmer decrement. In the application of the Stoy method, I have assumed that the electron temperature of the gaseous nebula is near 10,000° K. The temperatures derived from the spectral classes tend to be larger than those obtained by Berman, while the Stoy method seems to give temperatures that are much too high. The discordances suggest that in the far ultraviolet the planetary nuclei do not radiate like black bodies but may have extended chromospheres with strong bright lines, whose principal probable members have been suggested by Swings.[3] The nebula NGC 2392 shows a high excitation spectrum with [*Ne* v] lines. Other planetary nebulae of comparable excitation tend to have nuclei showing only a continuous spectrum (e.g., NGC 3242), while in some instances the spectrum of the central star is not observed at all (e.g., NGC 7027). Hence there appears to be a good chance that this star will show strong deviations from a black body in the ultraviolet, and similar departures probably exist for the other stars as well. The appearance of emission lines in the stellar spectra hint that bright-line radiation may be important in the far ultraviolet.

The adopted temperatures are based primarily on the Petrie temperature scale, with the Berman temperatures used as a check. For IC 4593, I have carried out calculations for two values of the temperature, to illustrate the uncertainty of this quantity upon estimates of bolometric luminosity, radius, and mass.

VI. ESTIMATION OF EFFECTIVE SURFACE GRAVITIES

Our interest in the intensities of the Balmer lines in the central stars of the planetary nebulae arises partly from the possibility that from the mass of material above the photosphere and from the electron pressure, which we have attempted to estimate from the temperature and electron density, we may be able to estimate the effective surface gravities of these stars. If the stellar radii are known, the effective surface gravities may then give us a lower limit to the stellar masses.

At the base of the layers producing the stellar absorption lines, the gas pressure, P_g, must balance the weight of the overlying layers,

$$P_g = m_H g_{\text{eff}} \Sigma \mu N H \,, \tag{3}$$

where NH is the total number of atoms above the photosphere, μ is the molecular weight, and g_{eff} is the effective surface gravity. The gas pressure at the base must be twice the mean gas pressure $\bar{P}_g$ and $\bar{P}_g = 2P_e$, since the material, predominantly hydrogen, is singly ionized. From equation (3) we obtain, by multiplication by P_e,

$$4P_e^2 = m_H g_{\text{eff}} \Sigma N H P_e \mu \,. \tag{4}$$

For the hydrogen atoms we derived NHP_e from the number of second-level atoms above the photosphere by means of the combined Boltzmann and Saha equation, viz.,

$$\log \frac{NHP_e}{N_{02}H} = -\frac{5040}{T}(I - \chi_2) + \frac{5}{2}\log T + \log \frac{2\varpi_{1,0}}{\varpi_{0,2}} - 0.48 \,, \tag{5}$$

where I is the ionization potential, χ_2 is the excitation potential of the second level, T is the adopted temperature, $\varpi_{1,0}$ is the statistical weight of the ionized atom, and $\varpi_{0,2}$ is the statistical weight of the second level. Except for helium, the other elements contribute very little by mass or volume to the stellar atmosphere.

The numerical value of the term on the right-hand side of equation (4) will depend on the assumption made concerning the composition of the atmosphere. I have carried out calculations of the surface gravity on the assumption that the number of helium atoms is one-tenth the number of hydrogen atoms. Then μ is 1.29 and $m_H \Sigma N H \mu = 1.42\, N H m_H$. If we suppose that there are five times as many hydrogen as helium atoms, μ is 1.5,

and the coefficient is 1.80 instead of 1.42. Our computed effective surface gravities then must be diminished by 20 per cent.

If we can suppose that the atmosphere is in static equilibrium, the acceleration experienced by a mass at the surface of a star is the resultant of the usual surface gravity, g, due to the mass of the star and the radiation pressure which we may denote as g'. That is

$$g_{\text{eff}} = g - g' \tag{6}$$

where

$$g = g_0 \frac{\mathfrak{M}}{R^2} . \tag{7}$$

Here $\mathfrak{M}$ and R are, respectively, the mass and radius of the star in terms of the sun, and g_0 is the acceleration of gravity at the solar surface. If we can suppose that the contribution of line absorption to the radiation pressure can be neglected, then

$$g' = \frac{\bar{k}F}{c} = \bar{k}\sigma \frac{T_e^4}{c} , \tag{8}$$

TABLE 6

ESTIMATED SURFACE GRAVITIES OF PLANETARY NUCLEI

Object	T_e	log NHP_e	log P_e	log g_{eff}	log $\bar{k}$	log g'	log (g_e+g')
NGC 6891.....	32,000	24.83	2.80	4.99	+0.30	3.66	5.01
NGC 6826.....	32,000	24.79	2.40	4.23	+ .06	3.42	4.29
NGC 2392.....	35,000	24.77	3.20	5.75	+ .50	3.98	5.76
IC 4593.....	34,000	25.09	2.32	3.77	− .12	3.28	3.89
	25,000	24.59	2.19	4.01	+ .30	3.08	4.06
NGC 6210.....	32,000	24.77	2.55	4.55	+0.10	3.46	4.58

where $\bar{k}$ is the straight mean value of the absorption coefficient,

$$\bar{k} = \frac{1}{F} \int_0^\infty k_\nu F_\nu d\nu , \tag{9}$$

and T_e is the effective temperature of the star. Table 6 gives $N(H)HP_e$, i.e., the number of hydrogen atoms above the photosphere; log P_e; the resultant g_{eff}; $\bar{k}$ as computed from the effective temperature and the electron pressure of each star; log g'; and, finally, log g = log $(g_{\text{eff}} + g')$.

VII. THE APPARENT MASSES OF THE PLANETARY NUCLEI

We may call the mass estimated from equation (7) the "apparent" mass of the star. To obtain an estimate of this quantity, we must know the temperature and the absolute magnitude, whence we may derive the radius by means of the well-known expression:

$$M_p = -0.83 - 5 \log R + \frac{36{,}600}{T} + 2.5 \log (1 - 10^{-14{,}600/T}) . \tag{10}$$

This formula is based on the assumption that the star radiates like a black body throughout most of its spectrum. Hence there is some question as to precisely what temperature ought to be employed. A consistent procedure would appear to be to employ the temperature from Table 5. We shall further suppose that deviations from a black body are small, except perhaps in the far ultraviolet.

The major difficulty in the application of equation (10) lies not in the uncertainty in the temperature but in the uncertainty in M_p, which depends on relatively rough values of the photographic magnitude, crude distance estimates, and cruder corrections for space absorption. I have taken the photographic magnitude of the central star, m_p, from the work of Berman and Parenago. These values may sometimes be in error by as much as half a magnitude, but, unfortunately, better values are not available.

The distance in parsecs is derived from the work of Berman and Parenago[15] and from the intensity of the interstellar K line interpreted with the aid of Sanford's[16] distance-equivalent width correlation. Berman's values are derived from the radial velocities of the planetary nebulae, together with the theory of galactic rotation, while Parenago's estimates are obtained from statistical parallaxes. Both distance estimates are highly uncertain. Parenago finds the known planetary nebulae to be confined to regions close to the sun, while Berman found them distributed over the whole galaxy. Minkowski's recent investigations suggest that the planetary nebulae are found at great distances—at least in the direction of the galactic center. The distances given by Berman may be of the correct order of magnitude, even though the individual values may be appreciably in error. With new proper-motion data, a re-analysis of the whole problem could be undertaken and the distances of these objects placed upon a more secure basis.

Distances estimated from the intensities of the interstellar lines and a mean calibration-curve can have, at best, but a rough statistical significance. It would be better to establish the interstellar line-intensity–distance relation for the vicinity of each nebula by observations of the K line in distant B stars.

Second, one must consider the effects of space absorption. I have taken Stebbins and Huffer's measures of the colors of B stars[17] near the objects in question and have tried to infer from them the color excess per kiloparsec and, finally, the total absorption from the A/E ratio of 8.1 suggested by Greenstein and Henyey.[18] The interstellar material is so extremely patchy that stars but a few degrees apart show a considerable difference in reddening. Nevertheless, even though the uncertainties are large, it seems preferable to estimate the space absorption per kiloparsec from the stars near each object rather than to adopt some kind of a mean absorption coefficient.

Because of our ignorance of the distances of the planetaries, I have carried out the calculations of the radii and masses of their nuclei with both the Parenago and Berman distances. Table 7 lists the apparent photographic magnitude, m_p; the distance in parsecs as given by Parenago, by Berman, and as estimated from the intensity of the interstellar K line; the absorption in magnitudes per kiloparsec as deduced from the Stebbins-Huffer measures; then M_p, log R (from eq. [10]), and log $\mathfrak{M}$ from equation (7) for the Parenago and Berman distances. For IC 4593, two values are given because there are two estimates of the surface temperature. For comparison, Table 8 gives the bolometric absolute magnitudes[19] of these stars and corresponding masses deduced from the mass-luminosity law.

From a comparison of Tables 7 and 8 we note that NGC 6891 and NGC 2392 have the highest apparent masses—giving the values closest in agreement with the predictions of the mass-luminosity law. For these objects it would appear that the determination of the log P_e and log g were the most reliable. For the other objects the earlier Balmer lines were probably measured systematically too weak; hence the corresponding g-values and apparent masses seem certain to be lower limits. The influence of a small error in W_λ upon log g_{eff} is very large. Thus, if we take log P_e from $H\delta$ instead of from λ 4340 in NGC 6891, i.e., 2.91 instead of 2.80, log $\mathfrak{M}$ would come out 0.95. An error of a factor of 2 in log W_λ in $H\gamma$ and $H\delta$ in NGC 6826 would result in log P_e being increased by 0.65

[15] *Russ. A.J.*, **23**, 78, 1946

[16] *Ap. J.*, **86**, 136, 1937.

[17] *Pub. Washburn Obs.*, **15**, 217, 1934.

[18] *Ap. J.*, **93**, 327, 1941.

[19] The bolometric corrections are obtained from Kuiper's table, *Ap. J.*, **88**, 453, 1938.

and log $\mathfrak{M}$ by 1.30; and the mass of the star would then agree with the predictions of the mass-luminosity law. Because the derived masses are so very sensitive to the computed electron pressure, there appears to be no hope of getting improved estimates until much higher-dispersion material is available.

If we can suppose that the atmospheres of these stars are similar to those of main-sequence objects of the same spectral class, the derived masses may not be without meaning. Unsöld applied this method to main-sequence early B stars and showed that the masses derived from the surface gravities were in good agreement with the predictions of the mass-luminosity law.

TABLE 7

ESTIMATED RADII AND MASSES

Object	m_p	Distance			A/Kpc	M_p		log R		log $\mathfrak{M}$	
		P	B	Int.		P	B	P	B	P	B
NGC 6891	11.6	1400	2750	800	0.00	+0.85	−0.60	−0.20	+0.09	+0.17	+0.75
NGC 6826	10.7	660	1050	600	.24	+1.44	+0.35	− .32	− .10	− .79	−0.35
NGC 2392	10.5	580	860	1000	.80	+1.24	+0.11	− .31	− .08	+ .70	+1.08
IC 4593	10.2	1200	2000	800	.00	−0.20	−1.30	+ .10	+ .32	− .18	+0.26
								− .01	+ .21	− .57	−0.13
NGC 6210	11.7	1050	1750	1000	0.16	+1.43	+0.22	−0.31	−0.08	−0.48	−0.02

TABLE 8

BOLOMETRIC MAGNITUDES AND CORRESPONDING MASSES

Object	Bolometric Magnitude		Predicted log Mass	
	P	B	P	B
NGC 6891	−2.0	−3.4	+0.76	+0.91
NGC 6826	−1.4	−3.2	+ .70	+ .89
NGC 2392	−1.9	−3.0	+ .75	+ .87
IC 4593	−2.6	−3.7	+ .82	+ .94
	−3.2	−4.4	+ .89	+ .90
NGC 6210	−1.4	−2.6	+0.70	+0.80

To within the limits of the observational uncertainties, we may say that the spectra of the central stars of the planetary nebulae appear consistent with the suggestion that these objects are submain-sequence dwarfs with masses appropriate to their luminosities in accordance with the mass-luminosity law.

It is more difficult to assess the significance of the apparent masses. We have neglected the possible role of radiation pressure in the resonance lines as a factor in the mechanical support of the atmosphere. Furthermore, the atmosphere may not be in equilibrium at all but in some kind of a kinematical steady state, with ascending and descending currents of gas. Hence the derived masses can be strictly regarded only as lower limits.

Dr. Olin Wilson has generously communicated to me the results of his study of the nucleus of NGC 2392 in advance of publication. He finds the different absorption lines to give different Doppler displacements, in the sense that the smaller the excitation of

the line, the greater the outward velocity as though the material was accelerated as it moved outward in the atmosphere and the excitation diminished. Conclusions based on the assumption of a static atmosphere, therefore, are to be regarded with reserve.

The earlier discussions by Menzel,[20] Gerasimovič,[21] and Milne[22] suggested that the central stars of the planetaries had bolometric magnitudes near +1 and therefore must be white dwarfs if they followed the mass-luminosity law. Present indications are that they are much brighter than +1. The objects discussed in this paper appear to have surface gravities five to ten times those of main-sequence stars, and radii comparable with that of the sun rather than with a white dwarf—a result in agreement with that of Beals.[23] The densities may therefore be expected to be about ten times that of the sun; and, if the NGC 2392 nucleus were built on the same model as the sun, the central density would be about 1000—still probably below the density where degeneracy sets in. Since radiation pressure must be important in their interiors, these stars are not likely to be built on the same model as the sun, and the central density is less than in the homologous model.

The line-intensity data give no support to the suggestion that these stars are massive objects, i.e., about one hundred times as massive as the sun. From a study of the relative shifts of absorption and emission lines, Cillié[24] suggested that the nucleus of NGC 6826 was a massive star; but there is nothing in the line profiles to suggest a white-dwarf character.

McLaughlin[25] has called attention to the similarity in dimensions, luminosity, and surface temperature between the ex-novae and the planetary nuclei. Both are dense blue stars with radii less than that of the sun. The absorption-line objects discussed in the present paper, however, appear to be cooler, larger, and presumably less dense than the old novae. As a class the planetary nuclei appear to cover an appreciable range in size, surface temperature, and perhaps luminosity and density.

The planetary nuclei appear to represent the high-temperature end of the Type II class of stars. Their photographic magnitudes appear to be comparable with those of cluster-type variables, suggesting that the high-temperature end of the Type II sequence runs horizontally on the Russell diagram.

VIII. HELIUM LINES IN THE PLANETARY NUCLEI

With the present data it is not possible to make a comparison of the abundances of the light-elements in a planetary nucleus and a main-sequence Type I object of the same spectral class. About all that is possible is a comparison of the Pickering *He* II lines with the Balmer lines to obtain an estimate of the relative numbers of doubly ionized helium and ionized hydrogen atoms above the photosphere. If we know what fraction of helium is doubly ionized, we can compare the relative proportions of hydrogen and helium.

For each line of the Pickering series one may compute the number of *He* II atoms in the $n = 4$ level above the photosphere, $N_{1,\,4}H$, and extrapolate for large n as we did for hydrogen:[26]

$$\log N_{1,\,4}H = 4.05 - \log \lambda^2 f_{4n} + \log W_\lambda = \log C_a + \log W_\lambda \,, \tag{11}$$

[20] *Pub. A.S.P.*, **38**, 295, 1926.

[21] *Observatory*, **54**, 108, 1931; see also *Harvard Bull.*, No. 864, p. 13, 1929.

[22] *Observatory*, **54**, 140, 1931.

[23] *J.R.A.S. Canada*, **169**, 1940.

[24] *M.N.*, **94**, 48, 1933.

[25] *Pop. Astr.*, **49**, 292, 1941.

[26] The subscript "1, 4" means we deal with the fourth level of singly ionized atom.

where the value of f may be computed from the hydrogenic formula,[27]

$$f_{n'n} = \frac{2^6}{3\sqrt{3}\pi}\frac{1}{\varpi_n}\frac{1}{\left(\frac{1}{n'^2}-\frac{1}{n^2}\right)^3}\left|\frac{1}{n^3}\frac{1}{n'^3}\right| g_{nn'} .$$

Table 9 gives the wave length, n, f-value, and log C_a for the relevant Pickering lines, while Table 10 gives the details of the calculation of log $N_{1,4}H$ from the Pickering lines; log $N(He^{++})P_eH$; log $N(He)/N(He^{++})$, where $N(He)$ denotes the total number of helium atoms; and, finally, the ratio of hydrogen to helium for the assumed temperature and

TABLE 9

OSCILLATOR STRENGTHS FOR THE *He* II LINES

n	Wave Length	f_{4-n}	log C_a	n	Wave Length	f_{4-n}	log C_a
9.....	4541	0.01872	14.46	17.....	3858	0.00172	15.64
11.....	4199	.008185	14.84	19.....	3813	.001195	15.81
13.....	4026	.00436	15.20	21.....	3781	0.000865	15.96
15.....	3924	0.00266	15.44				

TABLE 10

THE PICKERING SERIES

n	λ	NGC 2392		IC 418		NGC 6891		IC 4593		NGC 6826		NGC 6210	
		log $W\lambda$	log $N_{1,4}H$	log $W\lambda$	log $N_{1,4}H$	log $W\lambda$	log $N_{1,4}H$	log $W\lambda$	log $N_{1,4}H$	log $W\lambda$	log $N_{1,4}H$	log $W\lambda$	log $N_{1,4}H$
9.....	4541	−0.07	14.39	−0.26	14.20	−0.17	14.29	−0.12	14.34	−0.10	14.36	−0.03	14.4
11.....	4200	− .17	14.67	+ .1	15.0	− .13	14.71	− .35	14.49	− .29	14.55	− .52	14.3
13.....	4026	− .16	15.05	.....	.....	.....	.....	.....	.....	.....	.....	.....	.....
15.....	3924	− .34	15.10	.....	.....	−0.55	14.89	− .36	15.08	− .52	14.92	.....	.....
17.....	3858	−0.51	15.13	− .19	15.45	.....	.....	−0.70	14.94	−0.52	15.12	−0.65	15.0
19.....	3813	.....	.....	− .42	15.39	.....	.....	.....	.....	.....	.....	.....	.....
21.....	3781	.....	.....	−0.44	15.52	.....	.....	.....	.....	.....	.....	.....	.....
Final log $N_{1,4}H$.....		.....	15.20	.....	15.56	.....	14.90:	.....	15.10	.....	15.20	.....	15.0:
log $N(He^{++})HP_e$.....		.....	24.41	.....	.....	.....	24.0	.....	24.24	.....	24.27	.....	24.0
log $N(He)/N(He^{++})$.....		.....	0.35	.....	.....	.....	0.6	.....	0.60	.....	0.35	.....	0.4
H/He.....		.....	1.0	.....	.....	.....	2	.....	1.8	.....	1.5	.....	2

electron pressure. The results suggest that helium is comparable in abundance with hydrogen. The determination is rough, however, not only because of the uncertainties in the line intensities and in the electron pressure but also because the excitation of *He* II increases rapidly with the depth. That is, the effective depth at which the helium lines are formed is much greater than the effective optical depth where the Balmer lines are formed. Hence we cannot use the same temperature and electron pressure for calculating the equilibrium of hydrogen and ionized helium. The proper treatment of this problem would require a detailed integration through the atmosphere, taking into account the change of ionization and excitation with depth. With the aid of a model atmosphere computed for 10 Lac, I have estimated the effect of this stratification upon the estimated H/He ratio, and it would appear that the values listed in Table 10 are too small by a factor of about 2. The present data do not justify the more precise calculations necessary to establish this relation better.

[27] See Menzel and Pekeris, *M.N.*, **96**, 77, 1935.

IX. THE CENTRAL STAR OF NGC 246

Among the more interesting of the planetary nuclei with absorption lines is the central star of NGC 246. The nebular emission is so weak that we can observe the practically unobstructed spectrum of the nucleus. Berman gives the distance of this object as 1400 parsecs, while Parenago assigns 950 parsecs. With an adopted distance of 1400 parsecs, the absolute magnitude is +0.5; and, with a temperature of 35,000° K, from the Zanstra theory, the radius turns out to be 0.7 that of the sun; and the bolometric magnitude is about −3.0. The measured line intensities are as shown in the accompanying tabulation. *Hβ* may be affected with emission. In the stellar spectrum appear the

λ	Ion	$W\lambda$	λ	Ion	$W\lambda$
4861	*H* I, *He* II	0.85	4340	*H* I, *He* II	0.40
4686	*He* II	0.83	4200	*He* II, *N* III	.62
4650	*C* III	1.6	4026	*He* II	.23
4541	*He* II	0.84	3931	*C* IV	0.70
4441	*C* IV	1.35			

λ 3811, λ 3838, emission lines of *O* VI with intensities of 0.63 and 0.57 equivalent angstroms of the underlying continuum. The spectrum seems to be of higher excitation than any other absorption object studied. The assigned temperature of 35,000° K may be too low.

I wish to express my gratitude to Dr. W. A. Hiltner and Dr. D. M. Popper, who obtained spectrograms of the nuclei of NGC 2392, IC 418, NGC 3242, and IC 3568 for me, and to Dr. F. K. Edmondson, who helped me obtain most of the other spectrograms. Drs. R. M. Petrie, D. H. Menzel, O. C. Wilson, and C. S. Beals read the manuscript and offered helpful suggestions.

THE SPECTRUM OF GAMMA PEGASI. II

ANNE B. UNDERHILL*
Yerkes Observatory
Received June 4, 1948

ABSTRACT

Two 10.38 A/mm coudé plates of γ Pegasi have been measured for wave length between $H\beta$ and λ 5323. The elements found are *H*, *He* I, *C* II, *N* II, III, *O* II, *Ne* I, *Al* II, III, *Si* II, *P* II, *S* II, *Cl* II, *A* II, and *Fe* III. There is little doubt that there is a weak feature at λ 4910.76 which may be identified as the forbidden *He* I line 2^1P-4^1P λ 4910.75.

A previous study[1] of the spectrum of γ Pegasi had suggested the presence of the forbidden *He* I line $2^1P - 4^1P$ λ 4910.75, but the evidence for the presence of this line was not conclusive. Further plates exposed especially for this region were necessary for a decision to be made. Through the kindness of Dr. P. W. Merrill, of the Mount Wilson Observatory, I was able to secure two 10.38-A/mm, fine-grained, contrasty (III-J) coudé plates of γ Pegasi, centered at the λ 4900 region. Since these plates showed many lines beyond the limit of previous investigations of the spectrum of γ Pegasi, it seemed worth while to measure them for wave length and to compile a list of absorption lines in the region beyond $H\beta$ as well as to search for the forbidden *He* I line λ 4910.75.

Both plates (Ce 5050 and Ce 5051) were measured in the direct and reverse directions, and mean wave lengths were derived from each plate. After the correction for radial velocity—determined from well-known *Si* II, *Si* III, *Mg* II, and *O* II lines in the usual photographic region of the spectrum—had been applied, the wave lengths from the two plates were combined to give the list of wave lengths in Table 1. In the region from $H\beta$ to λ 4922 the measures of Paper I are combined with the new measures. All series of measures are given equal weight. Most of the entries in Table 1 are mean values from at least two plates. The values in parentheses are from one plate only. Since the plates Ce 5050 and Ce 5051 are quite unequal in density, more lines may be seen on the one than on the other, depending upon which has the more favorable density at the point of measurement. The latter part of the table, from λ 5281.60 to λ 5323.39, is from Ce 5050 only, since Ce 5051 is too weak in this region for accurate measurement. The estimated intensities are on the same scale as is used in Paper I. The entry 00 means that the line is on the verge of visibility. However, since each feature was measured in the direct and reverse direction and since the plates are fine grained, it is not likely that many of these very faint lines are spurious. Features noted as doubtful during the measurement have been excluded from the list. Except in the last part of the table, $\lambda > 5281.60$, all unidentified lines listed are measured on both plates. The lines were identified chiefly from the Revised Multiplet Table[2] in the manner described in Paper I. Additional lines of *Ne* I were identified from the work of Meggers and Humphreys[3] and of Paschen.[4] Many lines of *Fe* III were identified from an unpublished list of *Fe* III lines prepared by Mrs. Sitterly. I am very grateful to Mrs. Sitterly for again lending me this very useful list of lines. The limit for coincidence of laboratory and stellar wave length was set at ± 0.20 A.

* This work was done during tenure of a scholarship from the Canadian Federation of University Women.

[1] *Ap. J.*, **107**, 337, 1948. This paper will be referred to as "Paper I."

[2] C. Moore, *Contr. Princeton U. Obs.* No. 20, Parts I and II, 1945.

[3] *J. Research Nat. Bur. Standards*, **13**, 293, 1934.

[4] *Ann. d. Phys.*, **60**, 405, 1919.

TABLE 1

THE SPECTRUM OF γ PEGASI FROM Hβ TO λ5323

λ	Int.	Identification	λ	Int.	Identification	λ	Int.	Identification
4861.30	40	H .33(Hβ)	4924.37	0	ClII .28(18)	(4995.01)	00	Ne I .93(7)
		N III .33(4)	25.26	1	ClII .17(15)	(95.57)	1	ClII .52(60)
62.44	0	....			S II .32(10)	96.28	1	....
62.75	0	FeIII .66(tr)			FeIII .40(2)	(96.70)	0	FeIII .81(1)
63.60	00	FeIII .73(tr)	26.04	0	....	97.76	00	FeIII .66(1)
64.33	00	P II .38(4)	(26.38)	00	FeIII .34(1)	4999.00	1*	FeIII .82(1)
		Ne I .35(3)	27.06	00	P II .17(4)	5000.68	1	AlII .97(3)
64.72	0	....	27.78	0	?FeIII .56(2)	01.20	5	N II .13(7)
65.46	0	Ne I .50(6)	28.79	00	FeIII .92(1)			.47(8)
		FeIII .29(tr)	30.13	00	....	02.68	1	N II .69(2)
67.04	00	Ne I .01(5)	(31.17)	00	FeIII .19(1)	04.00	0	FeIII .92(3)
		N III .18(5,5)	33.19	00	A II .24(6)	04.67	0	FeIII .57(3)
(68.19)	00	FeIII .02(1)			FeIII .13(1)	05.11	3	N II .14(10,10)
		Ne I .27(5)	(33.95)	0	FeIII .86(1)			Ne I .16(10)
68.92	0	....	35.36	0	....	05.84	0	....
69.58	00	....	(36.44)	00	FeIII .59(1)	06.41	00	FeIII .36(1)
70.46	00	....	36.96	0	ClII .99(25)	(06.80)	0	S II .71(2)
71.70	0	O II .53(3)	39.68	00	....	07.24	1	N II .32(7)
		FeIII .86(2)	39.75	0	....	07.89	0	....
72.34	00	FeIII .51(1)	(40.54)	0	FeIII .46(4)	09.36	0	A II .35(8)
(73.80)	00	FeIII .74(1)	41.19	0	O II .12(5)			S II .54(1)
		N III .58(2)	42.02	00	....	(10.14)	00	FeIII .04(1)
74.24	0	....	42.96	1	A II .96(4)	10.62	1	N II .62(6)
74.72	0	FeIII .54(1)			O II .06(7)	(11.59)	0	FeIII .70(1)
79.96	0	A II .90(12)	(45.02)	00	Ne I .99(6)	12.20	0	N II .03(2)
81.06	00	....	46.10	0	....	13.08	1	....
81.84	00	N III .81(0)	47.04	00	....	14.06	2	S II .03(1)
82.19	00	A II .25(-)	48.04	0	FeIII .96(4)	(14.84)	00	FeIII .66(1)
83.38	0	....	50.65	0	....	15.64	10	He I .68(6)
(83.75)	0	S II .73(1)	51.25	00	....			FeIII .75(1)
(84.02)	00	N III .14(1)	(52.71)	00	FeIII .78(1)	(16.69)	0	FeIII .61(1)
85.66	00	S II .63(2)	53.66	0	....	(17.52)	00	A II .63(2)
88.24	0	A II .29(0)	(54.38)	0	P II .33(5)	18.25	00	....
89.50	00	....			FeIII .20(1)	(20.09)	00	FeIII .99(2)
90.99	0	O II .93(4)	(55.19)	00	FeIII .24(1)	22.28	0	?FeIII .03(3)
(92.23)	00	Ne I .09(9)	(55.69)	0	O II .78(3)	(23.44)	00	FeIII .31(1)
93.00	0	....	(56.40)	0	....	24.42	0	FeIII .37(1)
94.26	0	....	(56.86)	00	Ne I .03(10)	25.04	0	FeIII .05(1)
98.32	0	?AlII .52(2)	59.56	0	C II .52(0d)	25.69	0	N II .66(6)
4898.97	0	?AlII .76(5)	(60.42)	0	?FeIII .63(1)			FeIII .77(1)
4900.58	0	S II .47(2)	61.29	0	FeIII .42(1)	26.46	0	FeIII .41(1)
02.41	0	....	62.41	00	FeIII .21(1)	27.04	0	S II .19(2)
03.36	00	?FeIII .12(1)	67.74	0	FeIII .07(2)			FeIII .98(2)
04.51	0	?A II .75(6)			.51(1)	28.52	0	....
		?ClII .76(135)	(68.81)	0	FeIII .83(1)	29.53	00	....
05.78	0	....	(70.05)	00	ClII .12(50)	30.30	00	....
06.89	1	O II .88(5)	72.63	0	....	31.20	00	Ne I .35(9)
		SiII .88(-)	73.46	0	Ne I .54(6)	31.86	0	....
07.81	00	....			?FeIII .25(1)	32.39	2	S II .41(2)
08.47	00	....	74.28	0	FeIII .32(1)			FeIII .40(3)
09.15	00	....	76.52	00	....	33.36	0	FeIII .22(3)
10.76	0	[He I] .75(-)	77.72	00	FeIII .80(1)			C II .2(1d)
11.42	00	....	78.63	0	....	33.96	0	....
12.00	00	....	79.48	0	....	34.95	0	....
12.89	00	....	81.00	1*	FeIII .80(1)	(35.68)	0	FeIII .58(5)
13.42	0	FeIII .57(3)	82.60	00	....	36.06	0	Ne I .99(5)
14.23	00	FeIII .36(1)	(83.09)	0	FeIII .98(1)			FeIII .17(5)
		A II .32(2)	(83.93)	00	FeIII .85(2)	37.20	00	C II .0(0d)
		ClII .32(12)	84.52	0	FeIII .52(3)	(38.97)	00	FeIII .79(1)
14.78	00	FeIII .95(1)	85.64	0	....	40.28	0	....
15.36	00	....	(86.13)	0	FeIII .15(1)	41.02	1	SiII .06(8)
16.35	00	....	87.24	0	N II .38(4)			FeIII .13(1)
17.06	0	S II .15(7)			FeIII .14(1)	41.73	0	....
17.93	00	?FeIII .16(1)	(88.99)	1*	FeIII .93(1)	42.35	00	....
		?ClII .72(125)	89.55	0	....	43.00	0	Ne I .85(3)
18.76	00	?AlII .93(3)	90.36	0	....			FeIII .09(1)
19.36	0	....	91.00	0	N II .22(2)	44.14	0	FeIII .09(1)
19.96	00	....			?FeIII .79(4)	45.04	3	N II .10(8)
20.47	1n	[He I] .35(-)	91.69	0	FeIII .65(1)			FeIII .16(2)
21.99	10	He I .93(4)			S II .94(1)	46.10	0	....
(22.59)	00	FeIII .61(1)	93.18	1	....	46.94	00	....
4923.41	0	....	4994.30	1	N II .36(6,6)	5047.72	8	He I .74(2)

TABLE 1 -- Continued

λ	Int.	Identification	λ	Int.	Identification	λ	Int.	Identification
		FeIII .43(2)	(5109.10)	00	FeIII .19(1)	5156.09	1	FeIII .97(4)
		.12(2)	10.26	0	FeIII .20(1)	56.62	00	Ne I .66(6)
5048.79	00	....	12.16	0	....	57.27	1*	FeIII .13(1)
(49.19)	00	FeIII .17(1)	12.90	0	?FeIII .69(1)	57.92	0	FeIII .85(4)
(49.68)	00	?FeIII .39(1)	(13.26)	0	CIII .36(40)	58.41	00	?FeIII .62(2)
51.30	1	....			FeIII .21(1)	59.00	00	Ne I .89(6)
52.15	0	....	(13.98)	00	C II .07(2)	(59.32)	00	FeIII .51(1)
53.32	1	....			FeIII .10(1)	59.91	1	O II .02(4)
53.82	00	....	14.62	00	....	60.34	0	?FeIII .62(1)
54.56	0	FeIII .53(2)	15.50	00	FeIII .41(2)	(61.34)	00	FeIII .66(0)
56.08	1	SiII .02(10)	(16.14)	00	FeIII .12(2)	(62.98)	00	FeIII .30(1)
		.35(2)	16.68	0	Ne I .50(3)			A II .30(1)
(56.87)	0	FeIII .72(1)	(17.15)	00	Ne I .01(5)	63.76	0	FeIII .74(1)
(57.36)	00	FeIII .41(1)			FeIII .23(2)			AlIII .20(7)
57.78	0	....	17.64	0	....	64.40	0	?FeIII .63(0)
58.36	00	?FeIII .15(0)	18.29	0	....	65.96	00	A II .82(5)
(58.71)	00	FeIII .39(1)	18.78	0	....	(66.43)	00	FeIII .33(1)
59.93	00	?FeIII .71(1)	19.54	0	C II .55(2)	66.95	0	....
60.36	0	....	20.42	0	Ne I .51(4)	67.54	00	....
(61.55)	00	FeIII .63(3)	21.76	0	C II .69(1)	(68.06)	0	N II .24(1)
62.33	00	?A II .07(3)	(22.52)	0	?Ne I .34(3)	68.92	0	....
(62.72)	00	FeIII .63(1)			.25(3)	70.02	0	N II .08(1)
63.13	0	FeIII .30(2)	22.92	00	....	70.70	0	FeIII .34(3)
63.32	0	....	(23.23)	00	FeIII .20(2)	71.32	0	N II .46(1)
64.56	0	....	23.96	0*	FeIII .32(tr)	(71.39)	00	?FeIII .64(3)
65.33	0	....	25.46	0	FeIII .34(2)	(72.55)	00	AlIII .6(1)
65.94	0	FeIII .93(2)	26.12	0	S II .13(2)	73.12	00	CIII .15(25)
66.62	00	....			A II .84(0)			FeIII .08(2)
67.53	00	....	27.40	2	FeIII .32(6)	73.71	0	FeIII .74(1)
68.22	0	CIII .10(10)	(28.71)	00	FeIII .57(1)	75.74	00	N II .39(3)
		FeIII .03(1)	29.40	0	FeIII .29(1)			CIII .35(20,20)
(69.07)	0	FeIII .13(1)	30.30	0	?FeIII .03(1)			FeIII .61(0)
69.33	00	....	31.05	0	....	77.53	00*	FeIII .73(5)
71.62	00	FeIII .44(3)	(31.54)	00	FeIII .50(1)	78.19	0	....
72.24	0	....	32.08	1*	FeIII .23(1)	(78.62)	0	FeIII .57(2)
73.63	1	N II .60(3)	(32.30)	0	C II .96(3)	79.52	00*	N II .50(5,5)
(73.83)	0	FeIII .78(3)	33.26	1*	C II .29(2)			FeIII .52(2)
(74.36)	00	Ne I .20(5)	33.78	0	FeIII .67(1)	(80.56)	00	FeIII .47(2)
(75.67)	0	FeIII .62(3)	34.46	00	FeIII .62(1)	82.81	0	....
76.43	0	Ne I .58(5)	35.06	0	....	(83.53)	00	FeIII .72(0)
		FeIII .39(1)	35.68	0	FeIII .72(2)	84.21	00	....
(77.33)	00	FeIII .30(1)	36.43	0	FeIII .52(2)	(84.62)	00	FeIII .44(0)
78.59	0	Ne I .76(3)	37.20	00	C II .26(0)	85.32	00	FeIII .33(1)
81.53	00	?Ne I .36(3)			FeIII .27(1)	86.56	00	....
(82.03)	0	FeIII .14(3)	37.78	00	....	87.13	0	....
(82.65)	0	FeIII .32(3)	(38.54)	00	FeIII .50(1)	87.33	0	....
84.99	00	AlII .02(4)	39.26	0	FeIII .37(2)	(88.46)	00	Ne I .61(3)
(86.64)	0	FeIII .69(3)			C II .21(1)	89.03	00	....
88.02	00	....	40.00	0	FeIII .07(1)	89.50	0	CIII .70(25)
88.85	0	....	40.32	0	FeIII .95(1)	(89.90)	00	FeIII .39(2)
89.74	00	....	41.54	00	....	90.56	0*	O II .56(3)
(90.45)	0	A II .55(2)	(41.94)	00	?FeIII .20(1)			N II .42(2)
		Ne I .32(2)	42.41	1	S II .33(1)			FeIII .54(2)
91.20	0	....	43.46	1	C II .49(2)	91.12	00	FeIII .05(2)
92.16	0*	FeIII .15(tr)	44.50	0	....	(92.04)	0	FeIII .06(2)
93.96	0	FeIII .05(1)	45.12	3	FeIII .04(1)	(92.69)	0	SiII .75(-)
95.37	00	FeIII .30(1)			C II .16(5)	(93.07)	00*	CIII .03(10)
96.54	0	FeIII .74(2)			?A II .36(3)			Ne I .13(3)
97.26	0	FeIII .45(2)			Ne I .94(10)			.22(3)
(98.23)	0	CIII .34(20)			.01(10)	93.99	0	FeIII .39(4)
		FeIII .33(tr)			.12(5)	94.92	0	....
(5099.35)	00	CIII .30(100)	47.74	00	....	(95.34)	00	FeIII .24(2)
(5100.50)	00	AlII .34(1)	48.23	0	FeIII .20(1)	95.79	00	....
		FeIII .71(10)	49.30	00*	FeIII .33(7)	96.32	0	FeIII .99(1)
01.31	0	....	49.96	0	Ne I .03(5)	97.76	0	....
02.06	0	....	51.06	2	C II .03(3d)	98.54	0	....
(03.00)	00	CIII .04(125)			FeIII .13(1)	(99.01)	0	FeIII .95(4)
04.60	00	N II .45(2)	51.62	0	....			S II .39(1)
		Ne I .70(5)	52.18	0	P II .20(4)	5199.62	0*	N II .50(00)
05.23	00	?FeIII .63(2)	52.86	0	....	5200.16	00	....
		.02(2)	53.76	0	....	01.06	1	S II .00(3)
(06.52)	00	FeIII .34(tr)	54.29	00	....	(01.59)	0	?S II .32(2)
(07.33)	0	FeIII .32(1)	55.07	0	....			FeIII .60(2)
(5103.26)	0	FeIII .36(1)	(5155.43)	0	Ne I .42(6)	5202.14	0	....

TABLE 1 — Concluded

λ	Int.	Identification	λ	Int.	Identification	λ	Int.	Identification
5203.03	00	FeIII .97(2)	5248.44	00*	FeIII .28(4)	5288.11	0	....
(03.61)	00	?FeIII .82(2)	50.40	0	....	89.00	1	FeIII .84(2)
04.29	00	A II .46(0)	51.13	00*	FeIII .23(4)	89.74	00	....
05.30	00	?FeIII .58(2)	(54.38)	00	FeIII .45(1)	90.28	00	FeIII .44(2n)
05.95	00	....	55.68	00	....	91.89	00	FeIII .78(5)
06.76	0	O II .73(5)	(56.79)	0	FeIII .79(2)	93.40	00	....
07.42	00	FeIII .52(1)	(57.26)	00	FeIII .29(2)	94.87	00	SiII .97(-)
(08.44)	00	FeIII .44(1)			C II .36(2)	95.81	00	?P II .09(8W)
(08.82)	0	Ne I .86(7)	58.36	00	....	96.86	0	....
11.10	00	....	59.81	0	C II .62(3)	98.17	00	Ne I .19(8)
11.36	0	FeIII .74(1)	60.62	0	....			?FeIII .95(5)
(12.65)	0	S II .61(3)	61.60	0	FeIII .79(1)	99.17	00	....
13.58	00	FeIII .67(2)	62.93	0	....	5299.97	00	FeIII .95(5)
14.46	0	Ne I .34(5)	(65.05)	00	FeIII .01(1)	5300.76	00	FeIII .89(1)
(14.99)	00	?FeIII .74(3)	66.54	00	FeIII .52(3)	02.56	0	FeIII .48(6)
15.54	0	FeIII .65(3)	67.03	1	....	03.76	00	FeIII .77(1)
(16.89)	00*	FeIII .99(3)	67.98	0	....	04.25	00	....
		A II .84(3)	(69.00)	0	FeIII .15(4)	04.81	00	FeIII .73(1)
17.76	00*	ClII .93(150, 150)	69.82	0	....			Ne I .76(7)
			72.20	0	FeIII .03(3)	05.85	00	A II .77(3)
19.20	00	FeIII .23(1)	(72.73)	00	FeIII .86(6)	06.66	0	FeIII .57(4)
19.90	00	....			N III .60(1)	07.40	0	....
(20.50)	00	FeIII .51(tr)	73.12	1	....	08.21	0	FeIII .22(1)
(21.21)	00	ClII .34(75)	(73.84)	0	Ne I .04(5.5)	09.02	1	....
21.93	00	FeIII .09(1)	74.50	0	....	09.57	00	FeIII .54(3)
23.33	0	....	75.42	0	....	10.00	0	....
24.38	00	....	76.26	1	FeIII .20(7)	10.95	0	AlII .76(2)
(25.52)	0	FeIII .38(2)	(76.67)	0	AlII .42(2)			?FeIII .19(4)
(26.28)	00	FeIII .08(3)			.81(2)	11.82	0	....
(28.74)	00	FeIII .65(3)	77.34	0	....	12.71	00	....
29.44	00	FeIII .57(2)	78.08	0	FeIII .96(1)	13.50	1*	N II .43(0)
(30.41)	00	FeIII .31(2)	78.72	00	?FeIII .98(2)	14.47	00	N III .45(2)
30.76	00	FeIII .86(2)			AlII .62(3)	15.06	0	?Ne I .78(45)
31.28	0	....	79.52	0	....	15.63	00	....
(31.84)	0	FeIII .89(1)	80.17	00	AlII .21(6)	16.27	0	AlII .07(7)
(33.48)	0	FeIII .55(1)			Ne I .07(6)			P II .07(7W)
34.26	00	?Ne I .03(6)	80.62	0	....	17.30	00	....
35.10	00	....				17.80	00	....
35.44	0	FeIII .30(5)	81.60	0	....	18.46	0	FeIII .54(2)
36.74	00	....	82.44	0	?FeIII .15(7)	18.94	0	....
38.40	00	....	83.31	0	....	19.38	0	....
39.02	0	....	84.33	00	....	20.36	00	FeIII .20(2)
41.57	0	....	84.82	0	FeIII .85(5)	20.92	00	?S II .70(3)
43.24	1	FeIII .26(10)	85.64	0	ClII .48(30)			N II .96(3,3)
44.31	0	....			?AlII .85(6)	21.59	00	....
45.00	00	FeIII .33(2)	86.43	0	....	22.76	00	....
5245.38	0	?FeIII .68(2)	5287.30	00	....	5323.39	0	....

*Observed intensity of this line is not consistent with the identification given.

There are a few entries in Table 1 for which $\lambda_{star} - \lambda_{lab} > \pm 0.20$ A; they are indicated by a question mark. These identifications are put in the table as suggestions only; for, although there is some expectation that these lines will appear, since many other lines of equal or less intensity in the spectrum in question are found, the wave-length discrepancy is larger than it should be. The laboratory wave lengths are given to the nearest hundredth of an angstrom. The laboratory intensity is entered in parentheses following the wave length. Of the 497 lines in Table 1, 332 were measured on at least two different plates. Only 66.5 per cent of the lines are identified. The mean density of lines per angstrom is 1.1, in good agreement with the mean density of lines found in Paper I. For all lines the average residual $\lambda_{star} - \lambda_{lab}$ without regard to sign is ± 0.10 A; the average residual with regard to sign is 0.00 A. The latter result indicates that there is no systematic error in the wave lengths of Table 1. The mean residual ± 0.10 A is consistent with the accuracy of measurement possible on 10.38-A/mm plates for the very faint lines which constitute the bulk of Table 1. For all lines of intensity $\geqslant 1$, except lines of *H* and *He*, the average residual without regard to sign is ± 0.03 A.

Most of the atoms and ions identified in Paper I are represented in the spectrum of γ Pegasi between $H\beta$ and λ 5323, with line intensities closely paralleling the laboratory intensities. The elements found are *H*, *He* I, *C* II, *N* II, III, *O* II, *Ne* I, *Al* II, III, *Si* II, *P* II, *S* II, *Cl* II, *A* II, *Fe* III. There is little doubt that there is a weak feature at λ 4910.76 which may be identified as the $2^1P - 4^1P$ forbidden line of *He* I. It should be emphasized, however, that this line is very weak. Since the coudé plates studied here were obtained with a grating instrument, there is a possibility that some of the lines found might come from the superposed third-order spectrum of the λ 3400 region, for the comparison spectrum of the iron arc does show third-order lines. A search was made for the lines measured by Struve[5] in the far ultraviolet spectrum of γ Pegasi, but no conclusive evidence of their presence could be found. Also there is no clear indication of a strong third-order continuum extending beyond the limit of the sensitivity of the plate for the second-order spectrum. It is thus unlikely that any of the lines measured are spurious in the sense that they are superposed lines from the third-order spectrum of the far ultraviolet.

In conclusion I should like to express my thanks to Dr. P. W. Merrill of the Mount Wilson Observatory, whose kind offer to take some high-dispersion plates of γ Pegasi in this hitherto unexplored region made this investigation possible.

[5] *Ap. J.*, **90**, 699, 1939.

THE BALMER SERIES IN THE SPECTRUM OF HD 45910*

PAUL W. MERRILL
Mount Wilson Observatory
Received July 29, 1948

ABSTRACT

The hydrogen lines in this very peculiar Be star have been studied in more detail than was possible in previous observations. The changes in structure and displacement from plate to plate are very striking. On most plates the lines are clearly double, with interesting changes in the displacements and relative intensities of the components from line to line along the series. It is possible that the lines toward the limit of the series represent a higher atmospheric level than do the lines of longer wave length. On this hypothesis there is an acceleration of the atoms toward the center of the star, although the motion is outward.

The lines of *Ca* II behave much like those of hydrogen. If the hydrogen components exhibit a progression in displacement from line to line along the series, the *Ca* II velocities agree with those from hydrogen lines of the higher quantum numbers. Lines of ionized metals are subject to radical variations in intensity and displacement. On most plates the displacements agree with those for hydrogen and *Ca* II, but one plate offers a striking exception. On one spectrogram in the red, faint lines of *Fe* I and *Ca* I, resembling those of type M2, appear, but the sodium lines are lacking.

The spectrum of the peculiar Be star, HD 45910,[1] is known for rapid and pronounced variations, which indicate that the stellar atmosphere is phenomenally active. Several series of observations[2,3,4,5] have shown that the hydrogen lines undergo striking variations in intensity and structure and that numerous lines of ionized metals, usually weak or absent, are sometimes strong. Spectrograms obtained at Mount Wilson between 1938 and 1947 show many variations similar to those previously observed. The general behavior of the spectrum seems not to have changed markedly in the interval from 1920 to 1947.

ONE-PRISM SPECTROGRAMS

On the Mount Wilson low-dispersion spectrograms (Table 1) the dark hydrogen lines have their usual large and variable negative displacements. On several plates the displacements are not the same for all the hydrogen lines but increase algebraically in passing from $H\beta$ toward the limit of the series; see Figure 1, in which the measured displacements are plotted against the quantum numbers of the upper level ($H\beta = 4$, $H\gamma = 5$, etc.). The marked discrepancies shown on some plates by $H\gamma$ and especially by $H\beta$ are probably due to the relatively strong emission at these lines; plate C 7227 (Fig. 1) offers an extreme example. Beyond $H\gamma$ or $H\delta$ the emission is weak. On two plates, C 7670 and γ 23891, the dark hydrogen lines are clearly double, with widely spaced components (Table 1).

A stellar K line of *Ca* II whose displacement is approximately that of the ultraviolet hydrogen lines (or of one component) is present on most plates. A sharp interstellar component was measured on all plates except C 7670, where it is covered by a strong stellar line; the mean radial velocity is $+18.5 \pm 0.8$ km/sec. This velocity is slightly smaller

* *Contributions from the Mount Wilson Observatory, Carnegie Institution of Washington*, No. 751.

[1] 1900 R.A. 6^h25^m2; Dec. $+5°57'$; Mag. 6.7.

[2] 1920–1923: P. W. Merrill, *Pub. A.S.P.*, **35**, 303, 1923.

[3] 1922–1923: J. S. Plaskett, *Pub. A.S.P.*, **35**, 145, 1923.

[4] 1922–1926: J. S. Plaskett, *Pub. Dom. Ap. Obs., Victoria* **4**, 1, 1927.

[5] 1940–1942: O. Struve, *Ap. J.*, **98**, 212, 1943.

than the more accurate value $+22.7 \pm 0.23$ km/sec derived from the coudé spectrograms (see Table 2). The difference may possibly be due to a weak unresolved component on the shortward side of the interstellar line. On plate C 7670 the radial velocity derived from several narrow absorption lines of *Fe* II is +15 km/sec, a value which does not agree with the velocity from either component in the Balmer series.

TABLE 1

SPECTROGRAMS OF HD 45910, DISPERSION 38 A/MM
(Displacements of Dark Lines in Km/Sec)

PLATE	DATE	HYDROGEN		*Ca* II	
		5	10	Stellar	Interstellar
C 7227	1938 Nov. 6	−196	−136	−115	+17
γ 21566	Nov. 30	(−170)	.....	.....	(+15)
C 7443	1940 Jan. 21	−192	−182	−168	+22
C 7670	1941 Feb. 6	−190, (−13)	.....	Blend	
E 70*	Mar. 7	−97	− 72	(−102)	+16
γ 23891	Nov. 26	−186, −40	bl.	−151	+18
γ 24666	1942 Nov. 2	−170	.....	.....	+18

* Dispersion, 67 A/mm.

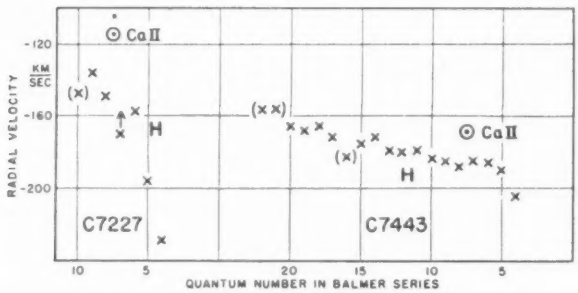

FIG. 1.—Radial velocities measured with low dispersion

COUDÉ SPECTROGRAMS

The coudé spectrograms (Table 2), because of their higher dispersion—10.3 A/mm—and their relatively long range of fairly uniform density, offer a favorable opportunity for detailed study of the complex structure of various lines. Most of the plates record the whole series of Balmer lines except *Hα*; one plate, Ce 4036, shows *Hα*. The general appearance of the spectrograms is illustrated in Figure 2, and the structure of many lines is brought out by the microphotometer tracings in Figures 4 and 5.

The lines of hydrogen with their radical changes in structure from plate to plate present clear evidence of extraordinary motions in the star's atmosphere. Moreover, many plates show progressive changes from line to line along the Balmer series which are probably related to differences in pressure; these changes may yield valuable information concerning velocities and accelerations of the gases at various levels above the star's photosphere. For these reasons the measured displacements of numerous hydrogen lines have been studied in some detail.

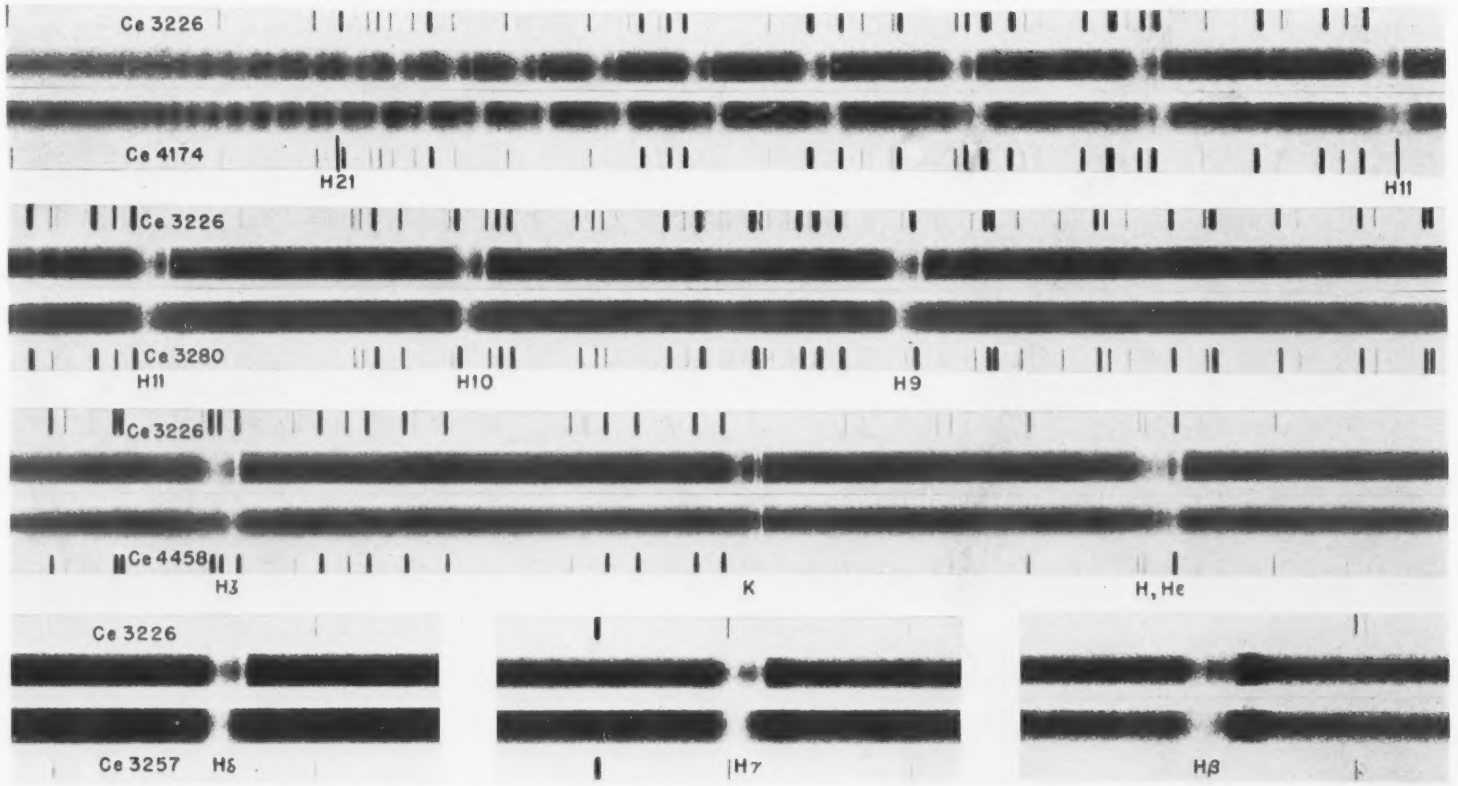

FIG. 2.—Spectrograms of HD 45910

TABLE 2

SPECTROGRAMS OF HD 45910, DISPERSION 10 A/MM
(Displacements of Dark Lines in Km/Sec)

PLATE COUDÉ	DATE	HYDROGEN												Ca II	
		5		10		15		20		25		30		Stellar	Interstellar
2738	1942 Mar. 3	−195	−28	−180	−28	(−162)	−24	.....	.....	.....	.....	.....	...	....	+20.8
2936	Dec. 26	−142	−14	.....	.....	.....	.....	.....	.....	.....	.....	.....	...	..... −11	+20.8
3226	1943 Oct. 7	−176	−14	−148	−12	−132	−12	−130	−12	(−130)	....	(−130)	...	−133 −16	+23.5
3257	Oct. 20	−172	....	−170	....	−168	....	−166	....	−160	....	.....	...	−169 (0)*	+21.5
3280	Nov. 12	−212	....	−180	....	−176	....	−168	....	−168	....	(−170)	...	−168 (+ 3)*	+22.5
3368	1944 Jan. 18	−238	−62	−238	−68	.....	−68	.....	−68	.....	−64	.....	...	..... −69	+21.4
3384	Feb. 8	−208	−80	.....	−58	.....	.....	.....	.....	.....	.....	.....	...	....	+23.9
3629	Oct. 30	.....	(− 8)	.....	0	.....	0	.....	0	.....	+ 2	.....	+2	..... (− 5)	+24.3
4036†	1945 Oct. 24	(−236)	−91†	.....	.....	.....	.....	.....	.....	.....	.....	.....	...	....	+22.4†
4045	Oct. 26	−200	−84	−188	....	−176	....	.....	.....	.....	.....	.....	...	−167 (−88)	+23.0
4107	Dec. 23	−234	....	−228	....	.....	.....	.....	.....	.....	.....	.....	...	..... (+ 4)*	+21.6
4132	1946 Jan. 16	(−234)	....	(−244)	....	.....	.....	.....	.....	.....	.....	.....	...	..... (+ 5)*	+23.4
4140	Jan. 18	−216	(−16)	−208	(−16)	.....	.....	.....	.....	.....	.....	.....	...	..... (0)*	+22.8
4174	Feb. 16	−152	−26	−132	−24	−132	−18	−130	−10	.....	− 8	.....	−6	..... −10	+24.9
4182	Feb. 17	−152	−34	−130	−24	−126	−20	−128	−16	.....	−10	.....	−4	−118 − 8	+23.3
4458	Oct. 11	.....	−42	.....	−44	.....	−40	.....	−28	.....	−27	.....	...	..... (−41)	+23.6
4929	1947 Oct. 24	−200	....	−172	+ 4	−160	+ 4	.....	.....	.....	.....	.....	...	−149 (− 1)*	+22.0

* Extremely weak line close to the interstellar line.

† Visual region, dispersion 20 A/mm. The displacements in the third column are derived from $H\alpha$; that in the last column is derived from the interstellar D lines.

On most plates two absorption components are visible at all or some of the hydrogen lines. Usually both components are somewhat widened; on a few plates one component is diffuse and vague; and on three plates (Ce 3226, 4045, 3368) one component is sharp, the other wide. Plots of measured displacement against quantum number, similar to those in Figure 1, were prepared for all the coudé plates. A number are reproduced in Figure 3. The accuracy of measurement, which depends on the sharpness and intensity

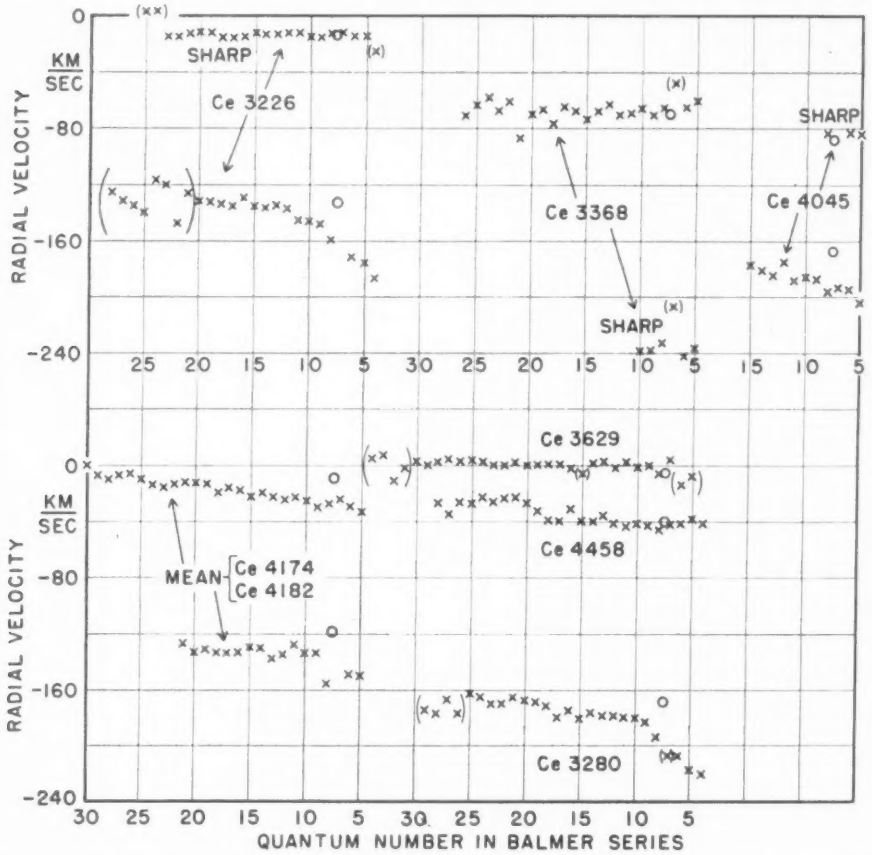

FIG. 3.—Radial velocities measured with high dispersion. Lines of *H* are represented by crosses; those of *Ca* II (stellar) by circles. The interstellar lines of *Ca* II yield a radial velocity of +23 km/sec (not plotted).

of the lines and on blending, is shown by the scatter of the points. Except for the weakest or most diffuse lines, the measurements provide reliable data on the behavior of the series. The radial velocities recorded in Table 2 were read from smooth curves drawn through the plotted points.

Many series show a progression toward algebraically larger displacements (smaller velocities outward from the photosphere) with increasing quantum number. The progressions appear to be of two types: (A) a fairly uniform change in velocity extending over all the lines measured and (B) a rapid change from $H\beta$ (No. 4) to No. 10 or No. 12, with a much slower change thereafter. Well-marked examples of type A are C 7443 (Fig. 1), Ce 4045 shortward component, and Ce 4174, 4182 longward component (Fig.

3). Examples of type B are C 7227 (Fig. 1), Ce 3226 shortward component, Ce 3280 single (Fig. 3), and Ce 4929 shortward component. Series not showing progression are the longward components of Ce 3226, 3368, 4929, and the single component of Ce 3629 (Fig. 4); with the exception of Ce 3368 (radial velocity, −68 km/sec), the displacements of these series are small. On plates Ce 4107, 4132, 4140, a few lines in series with large displacements indicate little or no progression.

The progression in the Balmer series indicates that the atmospheric layer in which the lines originate is not homogeneous. If the layer is thick, as it must be, the pressure at the top should be less than at the bottom. The apparent Balmer decrement is probably less rapid for low pressure than for high; hence the lines toward the limit of the series may represent a higher atmospheric level than the lines of longer wave length. On this hypothesis a progression of type A represents an acceleration within the stratum where hydrogen lines are formed. In HD 45910 the acceleration appears to be toward the center of the star, although the motion is outward; hence it may be due to gravity. In 48 Librae[6,7] the net acceleration during a prolonged oscillation has been outward whether the motion was outward or inward.

The rapid progressions of type B may be due in part to the effect of emission, but it is by no means certain that this is the whole cause; differences in velocity may be involved here also.

On plates with double hydrogen lines the relative intensity of the two components may change considerably from line to line along the series. From about $H\zeta$ toward the limit of the series, the Balmer decrement of intensity may differ systematically for the two components, causing a gradual but cumulative shift in relative intensity. From $H\beta$ to $H\zeta$ the changes are more rapid and more complicated; here emission probably has a considerable effect. A diffuse component may have a slower decrement than a sharp component; components about equally diffuse may have different decrements. These facts indicate that saturation does not play a dominant role.

Microphotometer tracings of these spectrograms would yield a large amount of reasonably accurate data. These data could supply quantitative checks on hypotheses of the structure of the stellar atmosphere that might be developed in the future. Figures 4 and 5, together with the data in Table 3 and Figure 6, may serve to illustrate the possibilities.

Lines of ionized calcium.—The H and K lines of *Ca* II behave much like those of the Balmer series. If the hydrogen series has no progression in velocity, the common velocity is very nearly the same as that yielded by the corresponding components of H and K; if there is a progression, the H and K velocities agree with those from hydrogen lines of the higher quantum numbers (see Table 2). This interesting phenomenon has been found previously in the spectrum of 48 Librae.[6] The widths and relative intensities of the components also correspond to those of the hydrogen lines. On plate Ce 3226 the relative intensities resemble those of the lines *H* 8–*H* 11, although the radial velocities agree with those from *H* lines of higher quantum number. On this plate the percentage absorptions of the shortward and longward components are 50 and 56, respectively; the longward component is very sharp (see Figs. 2 and 5).

The strong interstellar H and K lines usually stand by themselves but on a few plates are on the longward edges of stellar components. They yield a radial velocity of $+22.7 \pm 0.23$ km/sec.

Lines of helium.—The lines of *He* I are normally very wide and shallow without large displacements. On a few plates, one or two of the strongest seem to show faintly a structure similar to that of the hydrogen lines.

Lines of ionized metals.—As previous observers have noted, lines of ionized metals are

[6] Merrill and Sanford, *Mt. W. Contr.*, No. 690; *Ap. J.*, **100**, 14, 1944.

[7] P. W. Merrill, *Pub. A.S.P.*, **60**, 258, 1948.

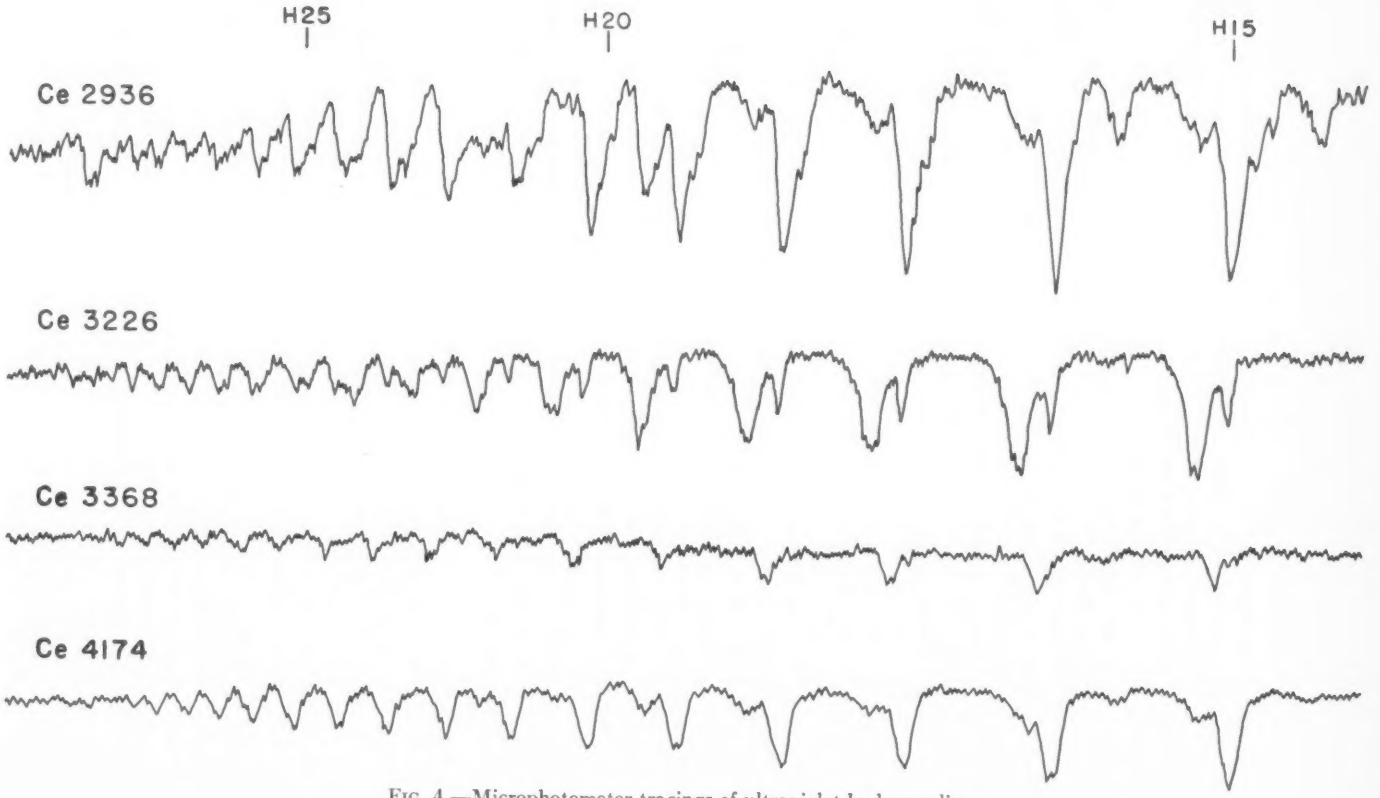

FIG. 4.—Microphotometer tracings of ultraviolet hydrogen lines

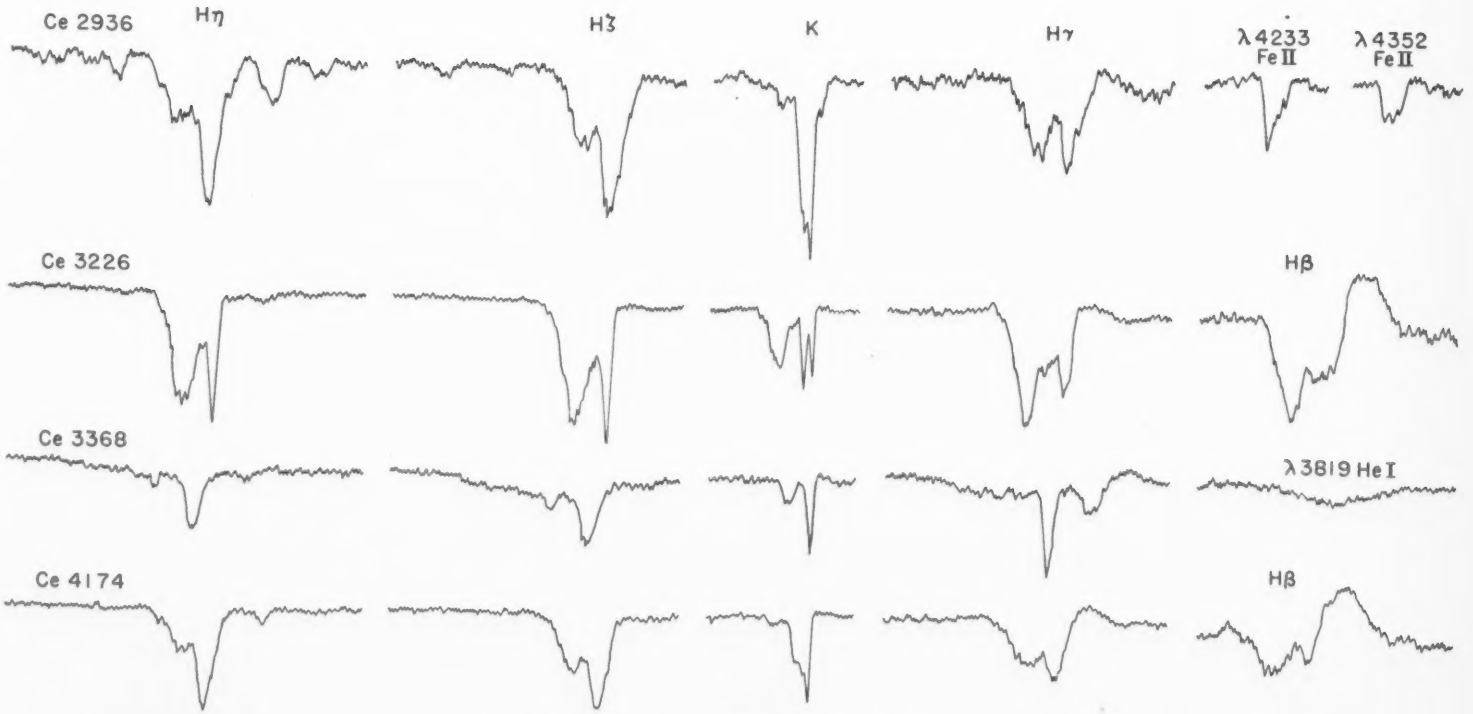

FIG. 5.—Microphotometer tracings of various lines

subject to radical variations in intensity and displacement. These lines are strong and numerous on three of the coudé plates and are faintly present on several others. With the exception of plate Ce 2936, the displacements (Table 4) agree reasonably well with those for hydrogen and *Ca* II. On plate Ce 3226, thirty-three sharp lines yield −12.8 km/sec, and five diffuse lines, −136 km/sec. When the lines are well defined the agree-

TABLE 3

DEPTHS OF THE COMPONENTS OF THE HYDROGEN LINES ON PLATE Ce 3226
(Percentage Absorption)

H	Shortward Component	Longward Component	*H*	Shortward Component	Longward Component
β	51	34*	13	59	50
γ	70	61	14	55	48
δ	69	66	15	52	36
ε	64	67	16	48	40
ζ	64	68	17	45	36
9	60	65	18	44	34
10	61	64	19	46	22
11	60	62	20	31	22
12	60	55	21	28	15

* At *Hβ*, and to a less extent at *Hγ* and *Hδ*, the tabulated absorption is too small, especially for the longward component, because no account was taken of the emission. The maximum of the emission, lying longward from both absorption components, rises above the level of the continuous spectrum by the following percentages: *Hβ*, 86; *Hγ*, 35; *Hδ*, 12.

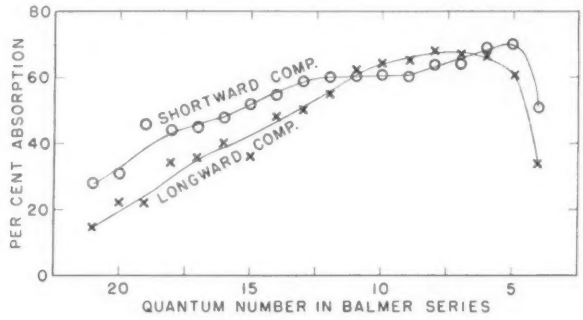

FIG. 6.—Depths of the components of the hydrogen lines on plate Ce 3226

ment between lines of various metals is good (Table 5). On plate Ce 2936, fifteen lines of *Mg* II, *Si* II, *Ti* II, *V* II, *Cr* II, and *Fe* II yield +51 km/sec. A few of the stronger lines, mainly of *Fe* II, yield +31 km/sec; these lines are about 1.7 A wide, with fairly sharp edges and faint emission borders.

Abnormal M-type spectrum.—On the only coudé spectrogram of the red region, Ce 4036, there appears a faint absorption-line spectrum resembling in many respects that of α Ceti, type M2. About a score of the most prominent lines have been identified with neutral metals, chiefly *Fe* I and *Ca* I; these yield a velocity of +60.2 ± 0.8 km/sec, a value quite different from that derived from either absorption component of *Hα*

(Table 2). An extraordinary peculiarity of this low-temperature spectrum is the absence of the D lines of sodium. In addition to the strong interstellar D lines, there is probably a weak, ill-defined pair displaced shortward 4 or $4\frac{1}{2}$ A, a displacement which might correspond to that of one of the hydrogen components toward the limit of the series; but no lines appear in the positions which correspond to a velocity of +60 km/sec.

TABLE 4

RADIAL VELOCITIES FROM LINES OF IONIZED METALS

Plate Ce	Radial Velocity (Km/Sec)	Plate Ce	Radial Velocity (Km/Sec)
2936	+ 31 or + 51	3368	(− 60) and .....
3226	−136 and − 13	3629	..... + 3
3257	(−174) (− 4)	4174	..... (+ 2)
3280	(−176) (+ 4)	4182	..... (−11)

TABLE 5

COMPARISON OF RADIAL VELOCITIES FROM LINES OF SEVERAL METALS

Element	Ce 3226		Ce 3629	
	Km/Sec	No.	Km/Sec	No.
Ti II	−14.0	8	+3.4	10
Cr II	−12.6	12	+1.9	7
Mn II	.....	.....	+1.8	5
Fe II	−12.6	11	+2.4	18
Ni II	−10.9	2	+4.1	6
Mean	−12.8	33	+2.8	46

It is hoped soon to obtain more information concerning this remarkable low-temperature spectrum in the red.

RADIAL VELOCITIES OF TWO STARS OF THE W URSAE MAJORIS CLASS*

DANIEL M. POPPER
Department of Astronomy, University of California, Los Angeles
Received July 27, 1948

ABSTRACT

Radial-velocity curves and elements are given for the following binaries:

VW Cephei.—$\gamma = -35$ km/sec; $K_1 = 75$ km/sec; $K_2 = 230$ km/sec.

TX Cancri.—$\gamma = +36$ km/sec; $K_1 = 112$ km/sec; $K_2 = 217$ km/sec. This star is a member of the Praesepe cluster.

Masses, luminosities, and radii of the components of these systems are uncertain because of difficulty in interpreting the light- and velocity-curves.

A collection of spectrographic data for seven W UMa stars reveals that in each case the observed mass ratio differs from unity more than one would predict from the luminosity ratio and that, for four of the five stars with unequal minima in the light-curve, the brighter and more massive star is the cooler.

VW CEPHEI[1]

VW Cephei is one of the brighter stars of the W Ursae Majoris class and one of the very few eclipsing binaries with a well-determined trigonometric parallax. C. M. Huffer[2] has studied the star photoelectrically and has analyzed all existing data on the times of minimum light. He has reduced his light-curve by standard Russell methods, assuming the luminosity ratio of the components to be 1.5.

On June 13 (U.T.), 1946, nineteen spectrograms of VW Cep were obtained with a dispersion of 26 A/mm at $H\gamma$. They cover a little more than one period of revolution. The exposure time was 20 minutes or 0.05 period. The magnitude, about 8.2 photographic, is such that ideal observing conditions are required if the exposure times are to be kept as short as this.

The heliocentric dates of observation[3] and measured velocities are given in Table 1. Ten of the spectrograms show double lines. The approximate times of light-minima may be obtained from the times of appearance and disappearance of line doubling. They are JD 2431984.715 and JD 2431984.855. Huffer's light-elements,

$$\mathrm{JD}_{\min} = 2424658.7574 + \frac{0.27831993 + 0.00000108 \cos 360E}{20{,}411} E,$$

predict minima at 0.688 and 0.827. At these times double lines are just disappearing, and hence they cannot pertain to the minima of our epoch. The difference is 0.027 days or 0.10 period. Further photometric and spectrographic data are required to determine

* *Contributions from the McDonald Observatory, University of Texas*, No. 155.

[1] HD 197433; Sp G5; mag. ptm. 7.6; $\alpha = 20^{h}39^{m}8$; $\delta = +75°13'$ (1900).

[2] *Ap. J.*, **103**, 1, 1946.

[3] Reduction of the times of observation to the sun may be simply carried out with the same quantities used in reducing the radial velocities to the sun with Herrick's table (*Lick Obs. Bull.*, No. 470, 1935). The reduction is

$$\Delta T \text{ (days)} = 0.000194\ (lY' - mX') .$$

The maximum error is about 3 per cent (twice the orbital eccentricity), which is satisfactorily small in nearly all applications. The quantities X' and Y' are the rectangular components of the earth's velocity, and l and m are the direction cosines of the star, all in the ecliptic system.

whether the velocity- and light-curves are not in phase or whether Huffer's formula cannot be extrapolated beyond his last observations, which are about six thousand revolutions earlier than my spectrograms. The phases in the table are with respect to primary minimum at JD 2413984.715.

The radial velocities yield the following elements, each of which is uncertain by about 10 km/sec:

$$\gamma = -35 \text{ km/sec}, \qquad K_1 = 75 \text{ km/sec}, \qquad K_2 = 230 \text{ km/sec}.$$

The measures and computed velocity-curves are shown in Figure 1. Six Victoria velocities, generously made available to me by Dr. R. M. Petrie, are also shown. They were obtained from spectrograms of one-half the dispersion and 50 per cent greater exposure

TABLE 1

RADIAL VELOCITIES OF VW CEPHEI

PLATE CG	HELIOC. DATE JD 2431984+	PHASE	VELOCITIES (KM/SEC)	
			I	II
4930	0.660	0^{p}797	−123	+199
4931	.676	.854	−118	+157
4932	.691	.908	.....	.....
4933	.706	.962	.....	.....
4934	.721	.016	.....	.....
4935	.737	.074	.....	.....
4936	.752	.128	.....	.....
4937	.767	.181	+ 40	−231
4938	.784	.243	+ 33	−265
4939	.799	.296	+ 28	−280
4940	.815	.354	+ 23	−178
4941	.830	.408	.....	.....
4942	.848	.472	.....	.....
4943	.865	.534	.....	.....
4944	.880	.587	.....	.....
4945	.895	.641	−119	+133
4946	.910	.695	−107	+179
4947	.925	.749	−111	+206
4948	0.940	0.803	−114	+208

time than those employed at McDonald. The time of observations is about sixteen hundred orbital revolutions (460 days) later than that of the McDonald plates. The discrepancy in the phases appears to be even greater than for my observations.

Since the brighter and more massive star recedes after primary minimum, it must be the cooler. The combined spectral type is G8–K0. If Huffer's surface-brightness ratio, 0.48, is valid, the spectral types of the components are K1 for the brighter star and G5 for the fainter. The photographic luminosity ratio shown by the spectrograms is in approximate agreement with the magnitude difference assumed by Huffer, 0.4 mag. for M_{pg} or 0.5 mag. for M_{pv}.

Mrs. Gaposchkin has suggested[4] that the variation of period of VW Cep is the result of motion about a third member of the system, this third member having about the same mass as each of the other components. The appearance of the spectrograms eliminates the possibility of the existence of a third star with a luminosity in the photographic region of the spectrum comparable to that of one of the observed components. While the

[4] *Pub. A.A.S.*, **10**, 127, 1941.

lines are much broadened and blended by rotation, they are no more badly blended than, and are just as deep as, those in the spectrum of 44 Boo B, for example.

It is doubtful whether a thorough discussion of the luminosities, masses, and radii of the components of VW Cep is justified, in view of the great difficulties in interpreting unambiguously the light- and velocity-curves of such highly distorted stars. Provisional values are derived in what follows.

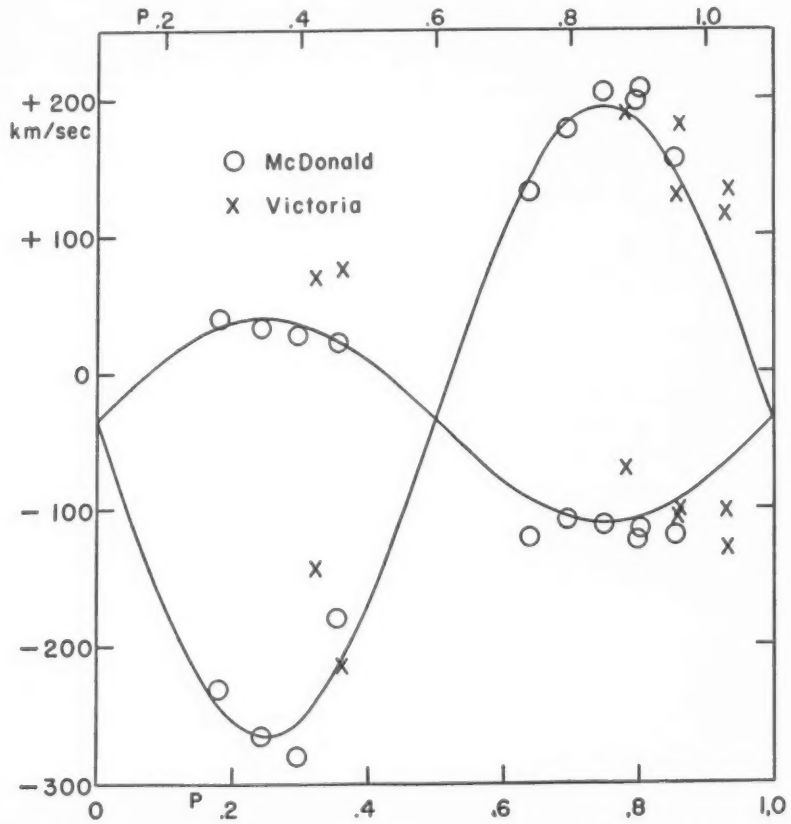

FIG. 1.—Spectrographic observations of VW Cephei. Zero points of abscissae: *below*, obtained from spectrograms; *above*, according to Huffer's light-elements.

The luminosities may be obtained directly from the apparent magnitude, trigonometric parallax, and magnitude difference. For the visual magnitude outside eclipse we adopt 7.45 (HD = 7.62; H_{pv} − HD = −0.2; $I_{pv} - H_{pv} = +0.10 + 0.06C$; correction for eclipse, ∼0.1). The parallax is 0″.053; hence M_{pv} is 6.07, and we have the values shown in the accompanying tabulation.

	M_{pv}	M_{bol}	log L
Brighter star	6.6	6.5	−0.8
Fainter star	7.1	7.0	−1.0

From the values of K_1, K_2, and the period we find

$$m_1 \sin^3 i = 0.62 , \qquad m_2 \sin^3 i = 0.20 .$$

Using the unreliable value of the orbital inclination obtained by Huffer, 63°, and applying a correction of 25 per cent for reflection[5] ($a_1/a = 0.52$), we obtain

$$m_1 = 1.10 , \qquad m_2 = 0.35 .$$

The discrepancy between the observed mass-ratio and that predicted by the luminosity ratio is even more extreme than in the case of 44 Boo B.[6] The sum of the masses of the components is in accordance with the luminosities.

The luminosities, together with Kuiper's effective temperatures[7] for types K1 and G5, lead to the following values of the radii:

$$\log R_1 = -0.22 , \qquad \log R_2 = -0.42 .$$

These values of the radii are probably more reliable than are those which could be derived from the light- and velocity-curves. Hence no attempt is made here to improve the scale of effective temperatures.

TX CANCRI[8]

The presence of an eclipsing variable of W UMa type in the Praesepe cluster was announced by Haffner.[9] The properties of the system have been discussed by Haffner[9,10] and by Tscherny.[11] In his later paper[10] Haffner made use of the radial-velocity observations published here.

Twenty-two spectrograms of this star, having a dispersion of 76 A/mm at $H\gamma$, were obtained at the McDonald Observatory. The average exposure time was 23 minutes, or 0.046 period. The nine spectrograms showing double lines are listed in Table 2. The phases, which were computed from an unpublished set of light-elements by Haffner,

$$\mathrm{JD}_{\min} = 2432615.452 + .3828806E ,$$

fit the velocity measures satisfactorily. The more massive and slightly brighter star recedes after zero phase. Since the two minima are of equal depth and result almost entirely from the ellipticity of the stars,[9] this observation is of little significance.

Approximate elements of the velocity-curves are

$$\gamma = +36 \text{ km/sec} , \qquad K_1 = 112 \text{ km/sec} , \qquad K_2 = 217 \text{ km/sec} .$$

The velocity-curve is shown in Figure 2. The systemic velocity, γ, agrees satisfactorily with the radial velocity of the cluster, +33 km/sec.

The spectral type of the combined spectrum is F8 V, compared to F6 derived from the color of the star by Haffner and Heckmann.[12] The photographic luminosity ratio is difficult to estimate from poor lines on low-dispersion spectrograms. The value 0.8 for L_1/L_2 cannot be greatly in error.

[5] G. P. Kuiper, *Ap. J.*, **88**, 498, 1938.

[6] D. M. Popper, *Ap. J.*, **97**, 497, 1943. [7] *Ap. J.*, **88**, 429, 1938.

[8] +19°2068; $\alpha = 8^h34^m3$; $\delta = +19°21'$ (1900); mag. pg. 10.5–10.8.

[9] *Zs. f. Ap.*, **14**, 285, 1937.

[10] *A.N.* (in press). A copy of the manuscript was kindly sent to me by Dr. Haffner in advance of publication.

[11] *A.J.*, **49**, 76, 1941. [12] *Göttingen Veröff.*, No. 55, 1937. TX Cnc is star 244.

TABLE 2

RADIAL VELOCITIES OF TX CANCRI

FILM	HELIOC. DATE JD 2430000+	PHASE	VELOCITIES (KM/SEC)	
			I	II
7883	1928.668	0P271	+157	−161
7884	1928.702	.360	+172	−144
9795	2304.615	.162	+128	−156
9807	2305.623	.795	− 79	+260
9818	2306.602	.352	+143	−150
9841	2308.657	.719	− 59	+267
9862	2310.601	.796	− 80	+250
9975	2322.622	.192	+110	−180
9977	2322.658	0.286	+140	−179

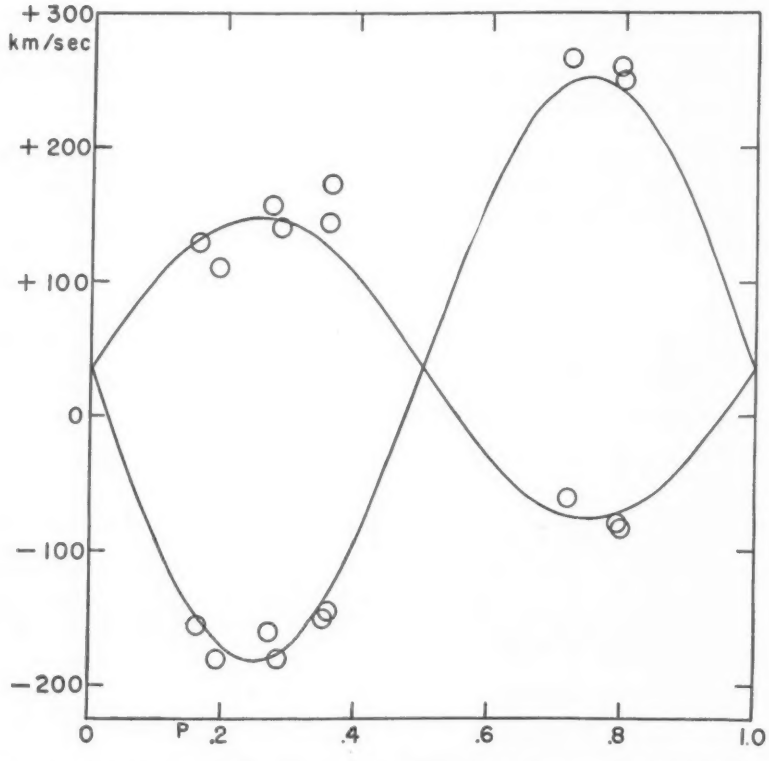

FIG. 2.—Spectrographic observations and computed velocity-curves of TX Cancri

From the known parallax of the cluster, 0".0070 and the apparent magnitude of TX Cnc, Haffner obtains for the luminosity of each star, on the assumption of equal components,

$$M_{pv} = 4.95 , \qquad M_{bol} = 4.9 , \qquad \log L = -0.08 .$$

Haffner has obtained the radii of the stars and the inclination of the orbit plane in an ingenious manner[10] with the help of the following assumptions: (*a*) The ellipticity of the stars may be obtained directly from the shape of the light-curve, i.e., the photometric and dynamical ellipticities are the same. (*b*) The projected disks of the two stars are precisely tangent at zero phase. (*c*) The two stars are identical in size and luminosity. Even if conditions *b* and *c* were fulfilled, it is doubtful whether *a* would lead to trustworthy results because of the effects of reflection, limb darkening, and gravity darkening for such close stars.[13] Haffner's values are

$$i = 59° , \qquad \frac{R_1}{a} = \frac{R_2}{a} = 0.27 .$$

TABLE 3

W UMA STARS WITH MEASURED RADIAL VELOCITIES

Star*	Spectrum	Period (Days)	Mass Ratio	$m_1 \sin^3 i$	$m_2 \sin^3 i$	M_{bol} (Mean)
W UMa	F8	0.334	1.4:	0.7:	0.5:	.....
TX Cnc	F8	.383	1.9	1.0	0.5	4.9
44 Boo B	G2	.268	2.0	0.8	0.4	6.5
ER Ori	G2	.423	1.6:	0.4:	0.3:	.....
YY Eri	G5	.321	1.5	0.7	0.5	.....
VW Cep	K0	.278	3.1	0.6	0.2	6.7
AH Vir	K0	0.408	2.4	1.3	0.6	.....

* References:
W UMa: A. H. Joy, *Ap. J.*, **49**, 358, 1919.
TX Cnc: This paper.
44 Boo B: D. M. Popper, *Ap. J.*, **97**, 407, 1943.
ER Ori: O. Struve, *Pub. A.S.P.*, **56**, 34, 1944.
YY Eri: O. Struve, *Ap. J.*, **106**, 92, 1947.
VW Cep: This paper.
AH Vir: Y. C. Chang, *Ap. J.*, **107**, 96, 1948.

From the values of K_1, K_2, and the period, we find

$$m_1 \sin^3 i = 0.95 , \qquad m_2 \sin^3 i = 0.48 .$$

Assuming Haffner's value of i and applying a correction of 3 per cent for reflection, we obtain for the masses

$$m_1 = 1.5 , \qquad m_2 = 0.8 .$$

Once more we have the anomaly in a W UMa system of widely differing masses associated with stars of small magnitude difference.

The luminosity of the mean component, together with the effective temperature for spectral type F8, leads to a value of the mean radius,

$$\log R = -0.12 .$$

As in the case of VW Cep, further discussion is probably unwarranted without more adequate theories.

[13] Cf. H. N. Russell, *Ap. J.*, **94**, 159, 1941.

DISCUSSION

Radial velocities have been published for seven W UMa stars with periods less than 0.5 days and with the spectra of both components visible. Data for these stars are collected in Table 3. The mass ratios of W UMa and ER Ori are poorly determined and are lower limits. In both cases, velocities of the secondary which lead to larger ratios have been discarded. Absolute magnitudes are listed for those stars with reliable geometrical parallaxes.

For every star of this list the observed mass ratio exceeds, and in four cases greatly exceeds, that expected for normal stars of the observed luminosity ratio. The luminosity ratio of the components as shown by the spectrum lines cannot exceed 2 in any case and probably ranges between 1.5 and 1. In each case where a luminosity difference is indicated, the more massive star is also the more luminous.

In the cases of 44 Boo B, YY Eri, VW Cep, and AH Vir, the brighter and more massive star recedes after primary minimum and hence is the cooler. Only in the case of ER Ori is the fainter star the cooler. The light-curves of W UMa and TX Cnc do not show a difference in surface brightness between the components.

For TX Cnc, YY Eri, VW Cep, and AH Vir there is evidence that the relative strengths of the spectrum lines show a systematic variation with phase, being more nearly equal for the two components when the fainter star approaches. The existence of this phenomenon in spectroscopic binaries has been emphasized by Struve.[14]

The most significant characteristic of these systems appears to be the set of large observed mass ratios. Our understanding of the light- and velocity-curves is as yet insufficient to enable us to decide whether the effect is real or results from a misinterpretation of the observations.

[14] *Ap. J.*, **102**, 74, 1945.

SPECTROGRAPHIC OBSERVATIONS OF THE ECLIPSING BINARIES RZ COMAE, V 502 OPHIUCHI, RV CORVI, AND BF VIRGINIS*

O. STRUVE AND L. GRATTON†
Yerkes and McDonald Observatories
Received July 27, 1948

ABSTRACT

Two systems of the W UMa type—RZ Com and V 502 Oph—show double lines which lead to mass ratios of $a = 2.1$ and $a = 2.5$, respectively. The individual mass functions are: for RZ Com, $m_1 \sin^3 i = 1.58 \odot$, $m_2 \sin^3 i = 0.75 \odot$; for V 502 Oph, $m_1 \sin^3 i = 1.22 \odot$, $m_2 \sin^3 i = 0.49 \odot$. The large values of a show that one or possibly both components of the W UMa systems depart from the mass-luminosity relation.

The other two systems—RV Crv and BF Vir—have single lines, and their mass functions are $f(m) = 0.033 \odot$ and $0.025 \odot$, respectively. These mass functions are small, and they show that even for periods as short as 0.75 and 0.64 day, respectively, we encounter the same difficulty of reconciling the Algol-type binaries with the "normal" spectroscopic binaries as we encountered previously for systems of longer periods. The former have systematically much smaller values of K_1 than do the ordinary spectroscopic binaries. This, in turn, leads to the conclusion that very often the fainter companions of the typical Algol systems depart appreciably from the mass-luminosity relation: they are either too luminous for their mass or not sufficiently massive for their luminosity.

Previous investigations of the velocity-curves of short-period eclipsing binaries had led to several interesting conclusions.[1] The four stars investigated in May and June, 1948, at the McDonald Observatory were chosen from N. L. Pierce's *Finding List of Eclipsing Variables*.[2] The first two stars, RZ Comae and V 502 Ophiuchi, are apparently systems of the W Ursae Majoris type. The other two, RV Corvi and BF Virginis, have earlier spectral types, slightly longer periods, and greatly different depths of minima. All the spectrograms were obtained on 103*a*-O film with the $f/2$ Schmidt camera and two glass prisms in the standard Cassegrain spectrograph attached to the 82-inch reflector. The dispersion was 76 A/mm at $H\gamma$; the slit width was usually 0.10 mm and the length of the slit was 2.5 mm. The projected width of the slit on the film was usually 0.018 mm. RZ Comae is so faint and so red that it was sometimes necessary to increase the slit width to 0.15 or 0.20 mm.

Table 1 gives the observing program, together with the relevant data from Pierce's catalogue. Table 2 contains in the third and fourth columns the photometric elements given in Schneller's last catalogue and used for the computation of the phases. The fifth and sixth columns give for comparison the elements from the first edition of the new Kukarkin and Parenago (1948) catalogue, which arrived too late to be used in this study. Photometric orbits are available for only the first two stars. That of RZ Comae was obtained by S. Gaposchkin.[3] He found $L_b = L_f = 0.50$; $r_b = r_f = 0.34$; $i = 81°$. The eclipse is partial, and the ratio of the surface brightnesses is 1.0. The photometric orbit of V 502 Ophiuchi was obtained by A. Nekrassova.[4] She found: $L_b = 0.73$; $L_f = 0.27$; $r_b = 0.51$; $r_f = 0.35$; $i = 75°$. The ratio of the surface brightnesses is 1.4.

* *Contributions from the McDonald Observatory, University of Texas*, No. 156.

† Fellow of The Italian National Research Council.

[1] *Ap. J.*, **106**, 92, 1947; *Ann. d'ap.*, **11**, 117, 1948. D. M. Popper has independently reached similar conclusions for the W Ursae Majoris stars. (See his paper in this issue.)

[2] *Contr. Princeton U. Obs.*, No. 22, 1947.

[3] *Variable Stars* ("Harvard Monograph," No. 5 [Cambridge: Harvard University Press, 1938]), p. 70.

[4] *Astr. Circ. Acad. Sci. Soviet Union*, No. 21, p. 8, 1943.

The radial velocities of the first and fourth stars were measured by Struve. Those of the second and third by Gratton. The results are listed in Table 4. The scatter of the measurements is large in all four cases, and the material warrants only the determination of circular orbits. These are listed in Table 5.

TABLE 1

THE OBSERVING PROGRAM

No.	Star	1950		Period (Days)	Magnitude			D (Hours)	d (Hours)	Sp	Remarks	No. of Spectrograms
		α	δ		M	A_1	A_2					
1	RZ Com	$12^h32^m35^s$	$+23°37'$	0.34	10.0	0.7	0.7	.....	.....	.....	Ellipticity	33
2	V 502 Oph	16 38 48	+ 0 36	.45	8.0	0.5	.4	.....	.....	.....	Refl., ellipt.	31
3	RV Crv	12 34 09	−19 18	.75	9.0	1.0	.6	.....	.....	F0	*P*?	26
4	BF Vir	13 45 18	− 0 20	0.64	9.5	0.5	0.1	4	0	A0	*P*? ellipt.	29

TABLE 2

PHOTOMETRIC ELEMENTS

No.	Star	Epoch JD	Period (Days)	Epoch JD	Period (Days)
1	RZ Com	2425005.524	0.3385057	5005.522	0.33850534
2	V 502 Oph	28684.493	.453405	Same	0.453419
3	RV Crv	29703.284	.74728	Same	Same
4	BF Vir	28313.306	0.639599	Same	Same

TABLE 3

LIST OF STAR LINES

Element	λ	No. of Star	Element	λ	No. of Star
Ca II	3933.67	3, 4	*Sr* II	4215.52	3
Fe I	4005.25	3	*Ca* I	4226.73	1, 2, 3, 4
Fe I	4045.82	1, 2, 3, 4	*Sc* II+*Fe* I	4325.39	2, 3
Fe I	4063.60	1, 2, 4	*Hγ*	4340.47	1, 2, 3, 4
Fe I	4071.75	1, 2, 4	*Fe* II	4351.77	3
Sr II	4077.71	1, 2, 3, 4	*Fe* I	4383.55	3
Hδ	4101.74	1, 2, 3, 4	*Mg* II	4481.23	3, 4
Fe II	4178.34	3			

The spectral type of RZ Comae is approximately K0. The lines are exceedingly diffuse, but two spectra can be clearly discerned at the elongations. The material is not suitable for a critical determination of the spectral types of the two components. If there is a difference, it is not large. However, there appears to be a fairly pronounced variation in the intensities of the two components at the elongations. This phenomenon resembles that previously seen in the case of YY Eridani[1] and AH Virginis.[5] In the case of RZ Comae this phenomenon produces a tendency of the violet-displaced components to appear relatively stronger than the red-displaced components. There is a suggestion that the relative intensities of the two components are not always precisely the same in dif-

[5] Y. C. Chang, *Ap. J.*, **107**, 99, 1948.

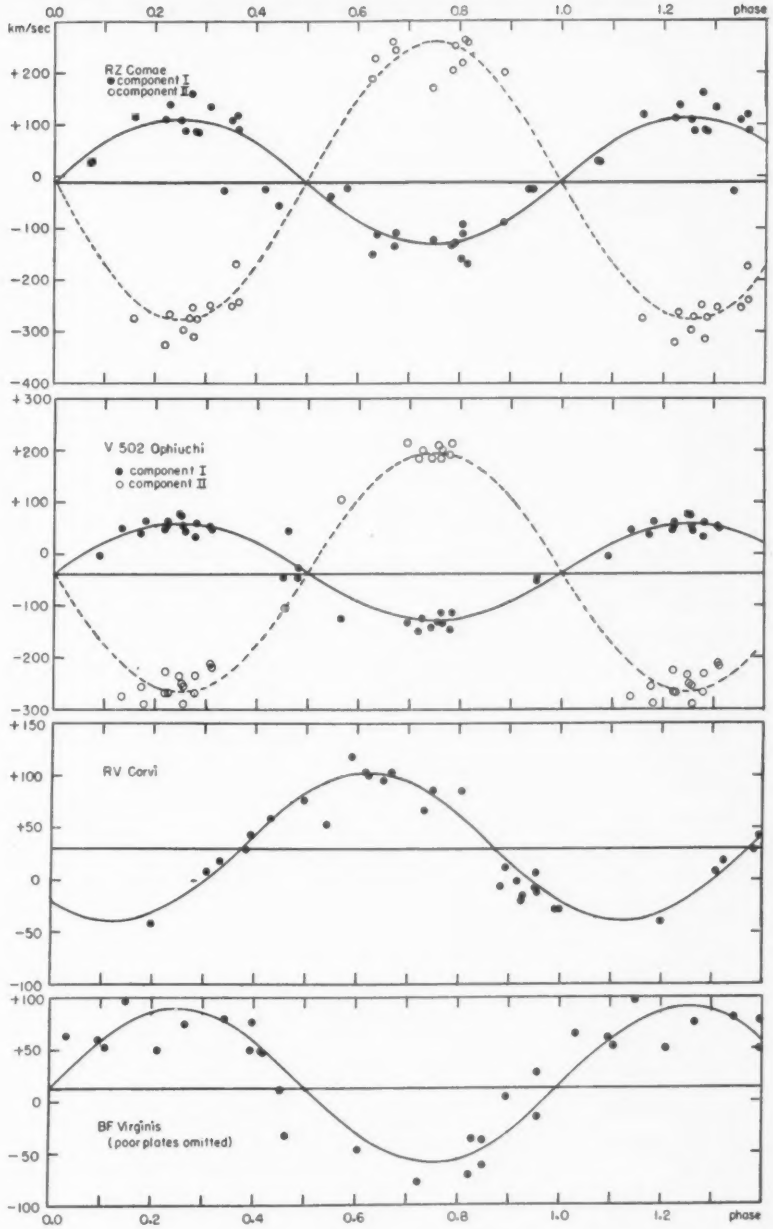

FIG. 1—Velocity-curves of four eclipsing binaries

TABLE 4

RADIAL VELOCITIES

RZ COMAE

PLATE	DATE (1948)	U.T.	PHASE		VELOCITIES (KM/SEC)	
			In Days	In Period	I	II
10846	May 2	3:05	0.273	0.806	−110	+222
10847	2	4:06	.316	.934	− 23	.....
10848	2	5:16	.025	.074	+ 28	.....
10849	2	6:43	.086	.254	+108	−298
10850P	2	8:16	.150	.443	− 58	.....
10862	5	2:50	.216	.638	−119	+231
10896	9	3:34	.185	.547	− 39	.....
10897	9	4:36	.228	.674	−115	+251
10904	10	2:54	.142	.419	− 29	.....
10926	12	2:58	.114	.337	− 26	.....
10940	14	2:51	.078	.230	+133	−262
10942	15	3:10	.075	.222	+114	−322
10943	15	4:20	.124	.366	+ 90	−239
10988	19	3:26	.024	.071	+ 29	.....
11004	25	3:25	.268	.792	−131	+249
11005	25	4:39	.320	.945	− 29	.....
11010	26	3:57	.276	.815	−169	+262
11021	27	4:57	.301	.889	− 87	+199
11048	29	3:55	.227	.671	−142	+266
11054P	30	3:56	.213	.629	−156	+188
11060	31	3:55	.196	.579	− 21	.....
11081	June 5	4:00	.123	.363	+120	−170
11094	7	4:40	.119	.352	+111	−250
11099	8	4:25	.093	.275	+163	−251
11110	9	4:51	.096	.284	+ 90	−270
11123	11	4:35	.054	.160	+117	−274
11150	16	3:24	.266	.786	−139	+204
11165	17	3:59	.274	.809	− 91	+266
11181	18	4:18	.272	.804	−156	+261
11199	19	4:13	.253	.747	−128	+172
11264	28	3:38	.088	.260	+ 88	−272
11270	29	4:07	.094	.278	+ 91	−309
11281	30	4:45	0.104	0.307	+134	−249

V 502 OPHIUCHI

PLATE	DATE (1948)	U.T.	PHASE		VELOCITIES (KM/SEC)	
			In Days	In Period	I	II
10918	May 11	5:37	0.116	0.256	+ 43	−290
10929P	12	5:34	.207	.457	+ 41	−101
10930P	12	5:47	.216	.476	− 47	.....
10947	15	6:44	.082	.181	+ 62	−290
10962	16	5:19	.116	.256	+ 53	−256
10963	16	5:36	.127	.280	+ 60	−232
10964	16	5:56	.141	.311	+ 49	−216
10971	17	5:12	.204	.450	− 47	.....
10972	17	5:32	.218	.481	− 27	.....
10979	18	6:20	.345	.761	−114	+188
10990	19	6:10	0.431	0.951	− 44	.....

TABLE 4—*Continued*

V 502 OPHIUCHI—(*Continued*)

Plate	Date (1948)	U.T.	Phase		Velocities (Km/Sec)	
			In Days	In Period	I	II
11006P	May 25	5:39	0.061	0.135	+ 49	−273
11007P	25	6:03	.078	.172	+ 39	−255
11022	27	5:50	.256	.565	−125	+102
11036P	28	5:47	.347	.765	−131	+202
11050	29	5:32	.430	.948	− 50	.....
11055P	30	4:51	.041	.090	− 2	.....
11061P	31	4:40	.126	.278	+ 31	−269
11062	31	4:58	.139	.307	+ 53	−211
11072	June 3	3:10	.343	.756	−132	+212
11073	3	3:27	.355	.783	−111	+214
11082	5	3:43	.099	.218	+ 49	−225
11130	12	11:22	.325	.717	−151	+185
11131	12	4:38	.336	.741	−144	+185
11140	15	3:07	.100	.221	+ 54	−268
11141	15	3:24	.112	.247	+ 79	−233
11166	17	4:44	.353	.779	−148	+192
11207	22	3:32	.315	.695	−132	+216
11208	22	3:50	.328	.723	−125	+200
11223	24	4:48	.101	.223	+ 61	−270
11224	24	5:06	0.114	0.251	+ 75	−249

RV CORVI

Plate	Date (1948)	U.T.	Phase		Velocities (Km/Sec)
			In Days	In Period	
10852	May 4	2:55	0.405	0.542	+ 53
10853P	4	3:47	.441	.590	+117
10854	4	4:23	.466	.624	+100
10855P	4	5:10	.498	.666	+103
10863	5	3:42	.690	.923	− 20
10864	5	4:11	.710	.950	− 7
10889	8	2:42	.660	.883	− 6
10890	8	3:16	.683	.914	− 1
10891	8	3:58	.712	.953	− 11
10892	8	4:46	.746	.998	− 28
10914P	11	2:38	.668	.894	+ 12
10915	11	3:11	.691	.925	− 15
10927	12	3:59	.229	.306	+ 9
10959	16	3:14	.462	.618	+104
10960	16	3:47	.485	.649	+ 95
10968	17	3:10	.712	.953	+ 7
10969	17	3:51	.740	.990	− 28
10976P	18	3:45	.241	.322	+ 18
11074	June 3	4:01	.559	.748	+ 86
11095	7	5:37	.143	.191	− 41
11097	8	3:00	.286	.383	+ 29
11121	11	2:54	.293	.392	+ 43
11128	12	2:57	.548	.733	+ 66
11164	17	3:06	.323	.432	+ 58
11221P	24	3:12	.601	.804	+ 85
11269	29	3:14	0.372	0.498	+ 77

TABLE 4—*Continued*

BF VIRGINIS

Plate	Date (1948)	U.T.	Phase		Velocities (Km/Sec)
			In Days	In Period	
10865	May 5	5:04	0.061	0.095	+ 60
10866	5	5:51	.094	.147	+ 97
10893	8	5:37	.525	.821	− 71
10898	9	5:46	.252	.394	+ 50
10905	10	4:01	.539	.843	− 37
10906	10	4:48	.572	.894	+ 4
10907	10	5:42	.610	.954	+ 28
10916P	11	4:02	.261	.408	− 24
10917	11	4:52	.296	.463	− 32
10928	12	4:57	.020	.031	+ 65
10941P	14	4:47	.094	.147	+ 66
10961	16	4:40	.170	.266	+ 75
10970	17	4:36	.529	.827	− 36
10977	18	4:42	.254	.397	+ 77
10978	18	5:34	.290	.453	+ 11
10989	19	5:16	.637	.996	+ 35
11049	29	4:52	.387	.605	− 46
11075	June 3	4:47	.267	.417	+ 47
11080P	4	3:23	.569	.890	− 78
11086	6	4:46	.069	.108	+ 52
11109P	9	3:21	.451	.705	− 30
11122	11	3:37	.543	.849	− 61
11129	12	3:40	.266	.416	+ 49
11133	13	3:17	.611	.955	− 15
11137P	14	4:17	.372	.582	− 53
11151	16	4:26	.461	.721	− 77
11198	19	3:23	.219	.342	+ 80
11222	24	4:09	.134	.210	+ 50
11280P	30	3:34	0.354	0.553	+ 4

TABLE 5

ELEMENTS OF CIRCULAR SPECTROGRAPHIC ORBITS

No.	Star	Period (Days)	V (Km/Sec)	K_1 (Km/Sec)	K_2 (Km/Sec)	T_1 (Min. Vel.)	$f(m)$ ⊙	m_1 ⊙	m_2 ⊙	$a_1 \sin i$ (Km)	m_1/m_2
1	RZ Com	0.34	−12	130	270	0.75 P	0.078	1.58	0.75	0.61×10^6	2.1
2	V 502 Oph	.45	−37	95	235	.75 P	.040	1.22	0.49	$.59\times10^6$	2.5
3	RV Crv	.75	+30	75	.....	.12 P	.033	.....	.....	$.77\times10^6$	.....
4	BF Vir	0.64	+13	72	.....	0.70 P	0.025	.....	.....	0.63×10^6	.....

ferent cycles, even though the phases within the cycle may be identically the same. The possibility of such a variation was suspected in the course of the observations, but there was no time to secure additional material to study it adequately. From the velocity-curve it will be seen that the more massive component is being eclipsed during the secondary minimum. Since in the case of this star the depths of the minima are very nearly the same, this is, of course, not physically significant. It is, however, important to know that the mass ratio of the two components is $\alpha = 2.1$. As in the cases of all other known

velocity-curves of W Ursae Majoris systems, this large ratio of the masses is incompatible with the mass-luminosity relation, because we know from the photometric orbits and from the appearance of double lines that the luminosities of the two components must be roughly the same, so that their masses cannot differ very greatly.

V 502 Ophiuchi has double lines which are appreciably broadened by rotation but are easier to measure than the lines of RZ Comae. The brighter star, which is in front at phase 0.0, is a G2 dwarf of class V: the fainter, which is in front at phase 0.5, is an F9 dwarf of class V. The hydrogen lines are quite strong but probably not unusually so for these spectral types. The velocity-curve resembles strikingly those of other stars of the W Ursae Majoris class. The more massive component is eclipsed at the secondary minimum; hence it is consistent with the photometric data that its spectral type should be later than that of the less massive component. The mass ratio $\alpha = 2.5$ is unusually large even among the W Ursae Majoris systems. Although in this system one component is always stronger than the other, the difference between the luminosities of the two stars is not nearly sufficient to account for the large mass ratio if the mass-luminosity relation is to be used.

The spectrum of RV Corvi is F0. There are no appreciable variations in spectral type with phase. The velocity-curve shows a pronounced shift in phase from that computed with the elements of Table 2. A small correction in the period would suffice to produce the desired shift, which amounts to about 0.13 day. The spectrum of only one component is visible, and it is this component which undergoes eclipse at the phase nearest to zero.

The spectral type of BF Virginis is approximately A2. The *H* lines and *Ca* II are very strong. *Ca* I, *Mg* II 4481, and *Fe* I are fairly pronounced, but the lines of *Fe* II are very weak. The star is thus a representative of the group of relatively not very luminous A-type stars similar to those found in all other short-period systems of type A. The spectrum of only one component is visible. It is important to note that this component undergoes eclipse not at primary minimum, whose depth is 0.5 mag., but at secondary minimum, whose depth is only 0.1 mag. This phenomenon might tend to connect BF Virginis with the W Ursae Majoris systems, in which the same anomaly occurs whenever there is a measurable difference in the two photometric minima. The mass function of BF Virginis is small, as is that of RV Corvi. It is probable that there is no blending with the spectrum of the fainter component, so that we may conclude that the unusual tendency of the eclipsing variables to have small mass functions persists even among binary systems of periods of the order of $\frac{2}{3}$ of a day.[6] The consequences of this tendency have been discussed elsewhere.[7] The representation of the observations would be improved by assuming a slightly shorter period.

[6] *Ap. J.*, **104**, 281, 1946.

[7] O. Struve, *Ann. d'ap.* **11**, 117, 1948.

A SPECTROSCOPIC STUDY OF BETA AURIGAE*

BURKE SMITH
McDonald and Yerkes Observatories
Received June 8, 1948

ABSTRACT

Twenty-six coudé spectrograms of β Aurigae, taken in 1943, were measured for radial velocity, and new orbital elements were computed. A total of 67 lines was measured, with dispersion of 2.2 A/mm at λ 4071 to 4.6 A/mm at λ 4630. The spectrograms were examined for possible variations in intensities and contours of spectral lines at or near eclipse phase and at times of maximum velocity, but the result was negative.

Since β Aurigae (mag. 2.07) consists of two A0 stars of nearly equal mass and has a reliable parallax, the determination of new, accurate orbital elements is desirable for the mass-luminosity relationship. In addition, the question of possible changes in the intensity and contour of spectral lines during or near the phase of eclipse and at times of maximum velocity is of interest, as some investigators have reported a change in the appearance of the lines with phase. Little has been published on the orbital elements since R. H. Baker's article in 1910,[1] in which he discussed the results of his own measurements and those of previous investigators. The present paper is based upon the results of measurements of coudé spectrograms which were taken with the 82-inch McDonald telescope in 1943. A total of fifty-one spectrograms was taken, primarily to detect possible changes in intensity or contour of spectral lines. On twenty-one of the plates the phase was such that it was possible to separate the lines of the two components so that their separate velocities could be measured and orbital elements computed. Of the remaining thirty plates, five were selected as being taken very near to phase 0.0 or 0.5, with coincidence of spectral lines, and were measured to determine γ, the velocity of the system. The dispersion varied from 2.2 A/mm at λ 4071 to 4.6 A/mm at λ 4630. All plates were of uniformly good quality, and with the high dispersion it was possible to obtain accurate measurements of velocities. Only lines which appeared to be free from blends were measured. The wave length in every case was computed by Hartmann's formula.

Table 1 shows, for the five plates, the wave length and identification of each line as given in the *Revised Multiplet Table*,[2] the number of plates measured, and the average O−C, which is, for each line, the observed velocity minus the mean plate velocity as calculated from the *R.M.T.* wave lengths, the result for each line being averaged over the number of plates measured. Some of the lines show rather large departures, which may be due to blends. A total of sixty-seven lines was measured on these plates. Corrections, based on Table 1, were made to the measured velocities of the lines which showed the highest O−C, averaged on three or more plates: *Fe* I 4045.815, *Fe* I 4066.979, *Mg* II 4390.585, *Ti* II 4450.487, *Fe* II 4555.890, *Cr* II 4634.11. The measured plate velocities for the five plates are shown in Table 2. The phase was measured from the epoch of mid-eclipse (coincidence of lines) of the less massive component, which was assumed to occur on December 16.239, 1943, JD 2431074.739, as determined from the solution for the orbital elements.

* *Contributions from the McDonald Observatory, University of Texas*, No. 154.

[1] *Pub. Allegheny Obs.*, 1, 163, 1910.

[2] C. E. Moore, *A Multiplet Table of Astrophysical Interest, Revised Edition* [*R.M.T.*] (*Contr. Princeton U. Obs.*, No. 20, 1945).

TABLE 1

WAVE LENGTHS AND RESIDUALS

λ	Element	Plates Measured	Average O−C		λ	Element	Plates Measured	Average O−C	
			ΔV (Km/Sec)	$\Delta\lambda$ (Angstroms)				ΔV (Km/Sec)	$\Delta\lambda$ (Angstroms)
4035.631	*V* I	4	−0.98	−0.013	4369.404	*Fe* II	1	+1.16	+0.017
4045.815	*Fe* I	5	−3.98	− .054	4383.547	*Fe* I	5	−1.92	− .028
4053.814	*Ti* II	4	+2.18	+ .030	4390.585	*Mg* II	3	+2.77	+ .040
4063.597	*Fe* I	5	−2.16	− .029	4395.031	*Ti* II	5	+2.60	+ .038
4066.979	*Fe* I	5	+3.44	+ .047	4399.767	*Ti* II	4	+0.27	+ .004
4071.740	*Fe* I	5	+1.60	+ .022	4404.752	*Fe* I	5	+1.74	+ .025
4077.714	*Sr* II	4	+0.23	+ .003	4415.125	*Fe* I	5	−1.54	− .023
4118.549	*Fe* I	1	+0.49	+ .007	4416.817	*Fe* II	4	−0.65	− .010
4130.884	*Si* II	5	−2.54	− .035	4443.802	*Ti* II	2	−0.23	− .003
4132.060	*Fe* I	4	+1.46	+ .020	4450.487	*Ti* II	3	−3.75	− .056
4163.644	*Ti* II	5	−0.80	− .011	4459.121	*Fe* I	1	−1.98	− .029
4171.897	*Ti* II	2	+3.60	+ .050	4468.493	*Ti* II	5	−0.34	− .005
4173.450	*Fe* II	4	+0.25	+ .003	4481.228	*Mg* II	5	−1.50	− .022
4178.855	*Fe* II	5	+1.00	+ .014	4489.185	*Fe* II	2	−2.05	− .031
4181.758	*Fe* I	1	+0.64	+ .009	4491.401	*Fe* II	1	−1.09	− .016
4187.802	*Fe* I	1	−0.68	− .010	4501.270	*Ti* II	5	−1.94	− .029
4215.524	*Sr* II	5	−0.28	− .004	4508.283	*Fe* II	5	+0.98	+ .015
4219.364	*Fe* I	1	−3.14	− .044	4515.337	*Fe* II	5	+1.40	+ .021
4233.167	*Fe* II	5	+2.36	+ .033	4520.225	*Fe* II	5	+0.30	+ .004
4235.942	*Fe* I	3	+0.23	+ .003	4522.634	*Fe* II	5	−0.62	− .009
4242.38	*Cr* II	4	−0.60	− .008	4541.523	*Fe* II	1	+0.91	+ .014
4254.346	*Cr* I	3	−0.50	− .007	4555.890	*Fe* II	5	+3.92	+ .059
4258.155	*Fe* II	5	−2.18	− .031	4558.659	*Cr* II	5	+0.48	+ .007
4260.479	*Fe* I	5	−1.85	− .026	4563.761	*Ti* II	5	+0.86	+ .013
4261.92	*Cr* II	5	+0.50	+ .007	4571.971	*Ti* II	5	+0.96	+ .015
4273.317	*Fe* II	4	+2.52	+ .036	4576.331	*Fe* II	4	+0.45	+ .007
4294.101	*Ti* II	5	−0.24	− .003	4583.829	*Fe* II	5	+1.92	+ .029
4296.567	*Fe* II	5	+1.52	+ .022	4588.217	*Cr* II	5	−1.42	− .022
4300.052	*Ti* II	5	+0.67	+ .010	4592.09	*Cr* II	4	+1.03	+ .016
4301.928	*Ti* II	5	+2.08	+ .030	4616.64	*Cr* II	4	+1.06	+ .016
4303.166	*Fe* II	5	−2.48	− .035	4618.83	*Cr* II	4	−0.65	− .010
4325.765	*Fe* I	5	−2.25	− .032	4629.336	*Fe* II	5	−1.66	− .026
4340.468	*Hγ*	5	−0.28	− .004	4634.11	*Cr* II	5	−3.28	−0.051
4367.657	*Ti* II	1	+1.11	+0.016					

TABLE 2

Plate No.	Date (1943)	U.T.	Phase		Velocity (Km/Sec)	No. of Lines (Msd.)
			Days	Decimals		
562	Dec. 16	6:25	0.028	0.007	−16.75±0.19	66
459	Nov. 20	12:11	1.971	.498	−17.26±0.20	52
524	Dec. 6	9:13	1.935	.489	−17.17±0.24	53
559	Dec. 16	4:37	3.913	.985	−17.36±0.28	55
560	Dec. 16	5:12	3.938	0.994	−16.46±0.23	55

From the average of these plates, the velocity of the system was found to be

$$\gamma = -17.00 \pm 0.11 \text{ km/sec} . \quad (1)$$

From the remaining twenty-one plates (Table 3) the radial velocity of each component was determined. Although the observations were not well distributed in phase, this was made up for in part by the high quality of the lines and the high dispersion. The average number of lines measured per plate was thirty-two. The probable error of the mean for a single plate varied from ± 0.4 to ± 0.7 km/sec.

TABLE 3

MEASURED VELOCITIES

Plate No.	Date (1943)	U.T.	Phase (Days)	Primary		Secondary	
				Velocity (Km/Sec)	Lines	Velocity (Km/Sec)	Lines
567	Dec. 16	9:36	0.161	+ 11.02	22	− 46.25	22
568	Dec. 16	10:12	0.186	+ 16.10	29	− 51.61	30
569	Dec. 16	10:48	0.211	+ 19.02	26	− 52.45	26
570	Dec. 16	11:26	0.237	+ 20.56	36	− 57.31	37
571	Dec. 16	12:06	0.265	+ 24.70	34	− 60.81	33
572	Dec. 16	12:48	0.294	+ 29.71	33	− 65.77	33
452	Nov. 19	5:33	0.712	+ 77.91	39	−117.83	32
453	Nov. 19	6:26	0.749	+ 81.73	30	−120.00	27
498	Dec. 1	7:54	0.930	+ 91.01	39	−127.07	40
574	Dec. 17	4:22	1.043	+ 88.46	36	−128.18	34
456	Nov. 20	6:40	1.759	+ 21.09	30	− 56.17	30
516	Dec. 6	3:58	1.806	+ 17.03	37	− 52.29	41
479	Nov. 28	6:09	1.817	+ 16.64	19	− 48.94	21
503	Dec. 2	5:22	1.825	+ 13.62	27	− 45.50	26
517	Dec. 6	4:40	1.835	+ 11.52	29	− 43.13	27
465	Nov. 21	10:18	2.910	−123.41	32	+ 92.52	36
468	Nov. 21	12:43	3.011	−126.26	37	+ 93.16	40
549	Dec. 15	8:45	3.086	−123.36	43	+ 92.99	45
552	Dec. 15	10:31	3.159	−120.13	34	+ 89.10	32
554	Dec. 15	12:42	3.250	−114.10	35	+ 82.19	36
509	Dec. 4	4:41	3.796	− 49.67	31	+ 16.42	34

The period, P, was found by earlier observers to be around 3.96 days. Baker,[1] in 1910, from a review of all previous determinations and his own measurements, concluded that the period was increasing, and gave $P = 3^d.960027 + 0^d.000010\ (t - 1906)$ as the best determination. A later determination by M. V. Berg[3] from observations at Poulkova in 1913–1925 gave $P = 3^d.960027 + 0^d.0000035\ (t - 1906)$. I have collected in Table 4 the times of coincidence of spectral lines (mid-eclipse of the primary, more massive, component), as given in the literature, for eight different epochs, beginning with January 27.708, 1904, which was based on Potsdam and Poulkova observations previous to that date, as reported by Vogel,[4] and including the epoch of December 18.219, 1943, JD 2431076.719, which was derived from the determination of the orbital elements as given below. Table 4 shows, for each date, the epoch of mid-eclipse of the primary, the interval in days from one epoch to the next, and the mean computed period for each interval. A simple average of the seven computed periods gives, for the interval 1904–1943,

$$P = 3.9600421 \pm 0.0000013 \text{ days} . \quad (2)$$

[3] *Poulkova Obs. Circ.*, No. 18, 1936.

[4] *Ap. J.*, 19, 360, 1904.

For the interval 1904–1925 the average is 3.960022 days, and for 1925–1943 it is 3.960074 days. These data would seem to indicate a slight increase in the average period over the last forty years, or perhaps during the last twenty years. However, it would hardly be safe to conclude definitely that the period has changed.

The remaining orbital elements were determined by computing an orbit by least squares, using the velocities shown in Table 3. Since it is known that e is very small, a preliminary circular orbit was first computed, using $\gamma = -17.00$, $e = 0$, and $K = 108$ km/sec. This showed slight systematic differences between observed and computed velocities near phases 0.0 and 0.5, which seemed large enough to justify a solution for an

TABLE 4

DETERMINATION OF AVERAGE PERIOD P

Coincidence of Spectral Lines (Primary Mid-eclipse)		Interval (Days Elapsed from Previous Epoch)	No. of Cycles (P=3.9600)		Computed Period P for Each Interval (Days)	Source
Date	JD 24+		Computed	Rounded Off		
1904.08	16,507.708	.....	.....	.....	.....	Vogel, *Ap. J.*, **19**, 370, 1904
1905.70	17,101.722	594.014	150.0035	150	3.9600933	Baker's definitive orbit, *Pub. Allegheny Obs.*, Vol. 1, No. 22, 1910
1908.90	18,273.888	1172.166	296.0015	296	3.9600203	*Ibid.*
1910.81	18,966.907	693.019	175.0048	175	3.9601086	Stebbins' light-elements, *Ap. J.*, **34**, 123, 1911
1914.01	20,135.103	1168.196	294.9990	295	3.9599864	M. V. Berg, *Poulkova Obs. Bull.*, **11**, 359, 1927–29
1919.16	22,016.096	1880.993	474.9982	475	3.9599853	*Ibid.*
1925.19	24,225.791	2209.695	558.0038	558	3.9600269	*Ibid.*
1943.96	31,076.719	6850.928	1730.0323	1730	3.9600740	McDonald 1943 plates

elliptic orbit. Sterne's second method for computing an orbit,[5] using differential corrections, was therefore employed. The measured velocities of all plates were used as normal points, each with weight 1. The differential correction, ΔV, for each normal point was computed from the preliminary circular orbit and the observed velocities. The solution gave, for the elements of the primary component,

$$\begin{aligned} e &= 0.011 \pm 0.004 , & K &= 107.34 \pm 0.59 \text{ km/sec} , \\ \omega &= 204^\circ.35 \pm 34^\circ.8 , & a \sin i &= 5{,}845{,}000 \text{ km} . \\ T &= 3.246 \pm 0.38 \text{ days} , \end{aligned} \qquad (3)$$

For the secondary component,

$$K_s = 110.70 \pm 0.39 \text{ km/sec} , \qquad a_s \sin i = 6{,}028{,}000 \text{ km} . \qquad (4)$$

The epoch of primary eclipse (coincidence of the lines) was fixed at 1943.96, JD 2431076.719.

[5] *Proc. Nat. Acad. Sci.*, **27**, 175, 1941.

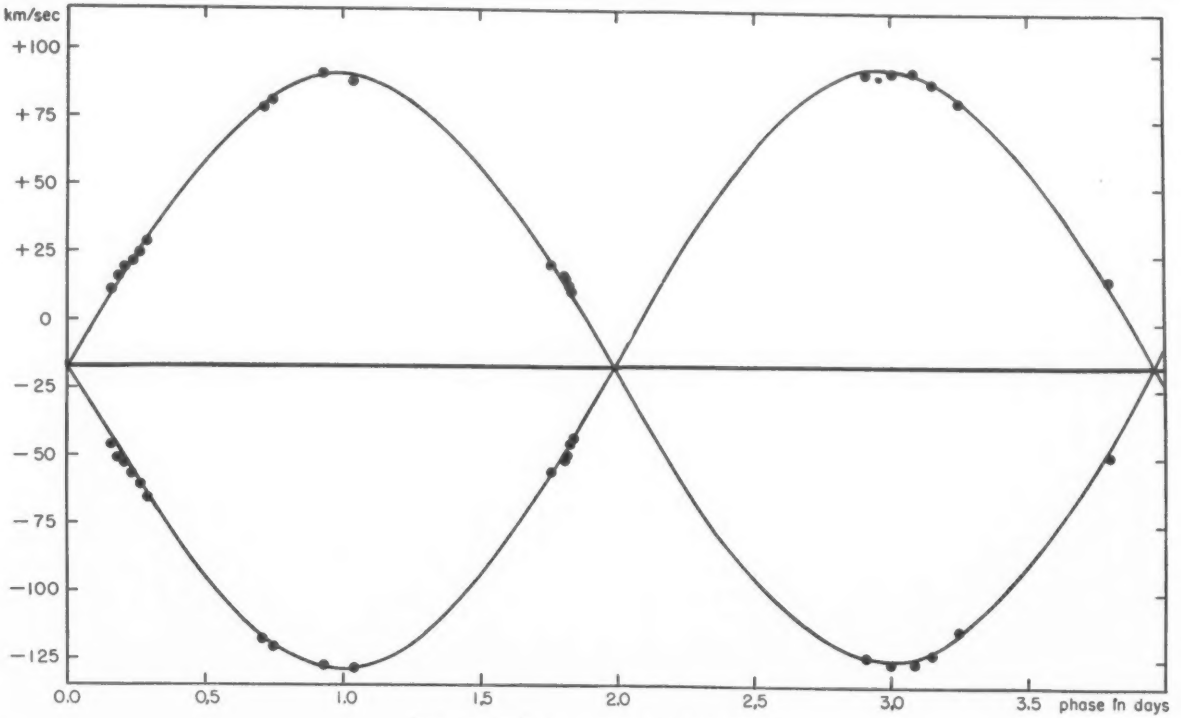

FIG. 1.—Velocity-curves of β Aurigae

On account of the smallness of e, the values obtained for T and ω are of little significance, as indicated by their probable errors. In fact, the value obtained for e may not have any real significance, in view of the poor distribution of the observations in phase. A final solution by least squares, based upon circular elements, was therefore carried through, which gave:

$$\begin{aligned} K &= 107.46 \pm 0.39 \text{ km}, & K_s &= 111.49 \pm 0.37 \text{ km}, \\ a \sin i &= 5{,}851{,}000 \text{ km}, & a_s \sin i &= 6{,}071{,}000 \text{ km}. \end{aligned} \tag{5}$$

Until more material is available, it is believed that these elements are more reliable than the elliptical elements (3) and (4). In Figure 1 the observed velocities are plotted, along with a smooth curve representing the circular elements from equations (5).

The ratio of masses of primary and secondary components, M/Ms, and the system velocity, γ, may be determined from the relation, $M/Ms = 1 + x = (V_s - \gamma)/(\gamma - V)$, where V and V_s are the observed velocities of the primary and secondary. By putting $\gamma = -17.00 + \Delta\gamma$, neglecting the term $x\Delta\gamma$, and solving for the two unknowns, x and $\Delta\gamma$ by least squares, we obtain, using the twenty-one measured plate velocities,

$$x = 0.0303 \pm 0.007, \quad \gamma = -17.06 \pm 0.27 \text{ km/sec}, \quad \frac{M}{Ms} = 1.0303 \pm 0.0075.$$

This compares with results by Ludendorff,[6] $M/Ms = 1.0105 \pm 0.0087$, and Baker,[7] $M/Ms = 1.022 \pm 0.0078$. The value of γ is in satisfactory agreement with that already obtained (eq. [1]), in view of the larger probable error.

The question of variation in the intensities of spectral lines in components of certain spectroscopic binaries as each component approaches or recedes from the sun has been studied by a number of investigators.[8] Berg reported observing such a variation in β Aurigae. However R. M. Petrie,[9] in an investigation of the spectra of several stars with the relatively high dispersion of 11 A/mm, was unable to find definite evidence of the effect in the case of β Aurigae. In the present study, all the fifty-one plates were examined by both the author and Dr. Struve in an effort to detect any variation in either intensity or contour of lines at times of maximum velocity or near or during eclipse phase. Only eye estimates were made, and the results were negative.

In view of the comparatively high dispersion of the McDonald plates and those analyzed by Petrie, this would seem to indicate that, if such an effect is present in β Aurigae, it must be very small.

My thanks are due to Dr. O. Struve for the use of the spectrograms and for his kind advice and encouragement, and also to him and Dr. W. A. Hiltner, for obtaining the spectrograms. I am also indebted to Dr. G. P. Kuiper for helpful suggestions, and to Dr. Petrie for communicating some unpublished observations of β Aurigae taken at the Dominion Astrophysical Observatory.

[6] *A.N.*, **183**, 113, 1909.

[7] *Op. cit.*, p. 174.

[8] Struve and Ebbighausen, *Ap. J.*, **80**, 371, 1934; Struve, *Ap. J.*, **85**, 41, 1937; Berg, *op. cit.*; M. K. Aly, *Observatory*, **66**, 343, 1946.

[9] Privately communicated to the author, from results given by Petrie at the sixty-sixth meeting of the A.A.S., 1941.

A STUDY OF THE ORBIT OF BETA AURIGAE

S. L. PIOTROWSKI
Harvard College Observatory
Received June 11, 1948

ABSTRACT

The elements of the system β Aurigae are determined by an analytic method developed recently by the writer. The basic observational data are Stebbins' photoelectric observations and Petrie's spectroscopic determination of the ratio of luminosities. The methodological questions, in particular those arising in connection with the determination of elements from combined photometric and spectroscopic data, are given an exhaustive treatment.

INTRODUCTION

The aim of the present study is twofold. On the basis of the photometric data obtained by J. Stebbins[1] and of the ratio of brightnesses of the two components determined by R. M. Petrie,[2] the orbital elements of β Aurigae are evaluated. The mere determination of elements is, however, not the sole aim of this paper. An equally important one is a thorough presentation of the essentially analytic method for the determination of the elements. The method employed is, in principle, the one described by Kopal,[3] improved and extended recently by the present writer.[4] Its salient feature is the fact that the fundamental equation of the problem is applied directly to the observed normal points. The corrections to the provisionally adopted depths of the minima are introduced into the equations as unknowns from the outset. The individual equations are properly weighted. The elements are determined by the least-squares method, which furnishes their mean errors. Errors arising from the uncertainty in the assumed degree of darkening, in the maximum brightness of the system, and in the spectroscopically determined ratio of luminosities of the components are duly taken into account.

In what follows, the methodical questions are treated exhaustively, and some points are developed beyond the actual requirements for a successful application to the case of β Aurigae.

RECTIFICATION OF THE LIGHT-CURVE

The rectification was performed in the manner described recently by Russell.[5] A harmonic analysis of the observations between minima yielded[6] for the variations of light of the uneclipsed stars

$$B_0+B_1\cos\theta+B_2\cos^2\theta \equiv \begin{array}{ccccc} 1.0025 & - & 0.0007\cos\theta & - & 0.0101\cos^2\theta\,, \\ \pm 0.0015 & & \pm 0.0016 & & \pm 0.0031\,(\text{p.e.}) \end{array}$$

with light-unity corresponding to $\Delta m = 0.350$ mag. We remove the ellipticity by dividing the light-intensity l by $B_0 + B_2\cos^2\theta$. In order to account for the effect of reflection, we first add to the result of division the term $B_1\cos\theta$ with reversed sign (the terms of the order of squares and cross-products of $B_0 - 1$ and B_2 being neglected). The remaining terms arising from the reflection cannot be determined in the case of β Aurigae from the

[1] *Ap. J.*, **34**, 112, 1911.

[2] *Pub. Dom. Ap. Obs., Victoria*, Vol. **7**, No. 12, 1941.

[3] *Introduction to the Study of Eclipsing Variables* (Cambridge: Harvard University Press, 1946), pp. 62 ff.

[4] *Ap. J.*, **106**, 472, 1947; **108**, 36, 1948.

[5] *Ap. J.*, **102**, 1945; **104**, 153, 1946.

[6] This result was kindly communicated to the writer by Dr. Zdenek Kopal.

analysis of light between the minima and must be found from a preliminary, approximate knowledge of elements of the system. These terms are of the form[7]

$$K r_1 r_2 (0.28 + 0.07 \cos 2\theta), \tag{1}$$

where r_1 and r_2 are the radii of the larger and smaller component and the expression for the factor K is given in Russell's paper quoted above. In case of nearly equally large and equally bright components, K is very close to unity. The determination of elements of β Aurigae by Shapley[8] made it plausible to put $K = 1$ and $r_1 r_2 = 0.02$. In order to reduce the light-intensity outside eclipses to unity, we have still to perform one division, viz., by $1 + K r_1 r_2 (0.28 + 0.07 \cos 2\theta)$. The light-intensity rectified for both ellipticity and reflection, l_{rect}, is then obtained by performing the operations indicated below:

$$\begin{aligned} l_{\text{rect}} &= \frac{\dfrac{l}{(B_0 + B_2 \cos^2 \theta)} - B_1 \cos \theta + K r_1 r_2 (0.28 + 0.07 \cos 2\theta)}{1 + K r_1 r_2 (0.28 + 0.07 \cos 2\theta)} \\ &\cong \left\{ \frac{l}{(B_0 + B_2 \cos^2 \theta)} - B_1 \cos \theta + K r_1 r_2 (0.28 + 0.07 \cos 2\theta) \right\} \frac{1 - l}{B_0 + B_2 \cos^2 \theta}. \end{aligned} \tag{2}$$

The product of the two brackets factored by $K r_1 r_2$ in the right-hand side of equation (2) is a small quantity of the second order outside eclipses, if $B_0 - 1$, B_1, B_2, and $r_1 r_2$ are regarded as small quantities of the first order.

Since the components of the system β Aurigae are of nearly the same size and, moreover, since this size is small as compared with their separation, it is very likely that the rectification just performed will not need any further improvement. Should we, however, plan to allow for the photometric effects arising from the higher-order distortions and to take exact account of the gravity darkening, the inclusion of the terms given by equation (1) in the rectification of the light-curve does not seem to be advisable.[9] The constant term in expression (1) does not change anything in the light-curve considered in the $(n_1 \sin^2 \theta)$ plane and enters into the equations of the problem only through the luminosities of the components. In the case of a total (annular) eclipse we get the same geometrical elements, whether or not we include the constant part of equation (1). The small term factored by $\cos 2\theta$ can be conveniently accounted for, together with other perturbations, in the final adjustment of elements.

Since the components of β Aurigae are very nearly equal in masses[10] and evidently also in radii, the dynamical value of ellipticity ϵ will be,[11] to a good approximation, equal to $(\frac{3}{2})r^3$. and, with $r \cong 0.15$,[8] this leads to

$$\epsilon \cong 0.005 , \qquad z = 2\epsilon \sin^2 i \cong 0.01 ,$$

where i, as usual, denotes the inclination of the orbit. From several good determinations[12] of the coefficient of limb darkening for A0 stars (both components of β Aurigae are of this type), we conclude that the assumption that limb darkening, u, is equal to 0.5 for both components is not far from the truth. The observed value of the photometric ellipticity C is equal (approximately) to $-B_2$ plus twice the coefficient of $\cos 2\theta$ in expression (1); hence,

$$\begin{aligned} C_{\text{obs}} = \quad & 0.0101 \quad + \quad 0.0028 = \quad 0.0129 \\ & \pm 0.0031 \text{ (p.e.)} \qquad\quad \pm 0.0031 \text{ (p.e.)} \end{aligned} .$$

[7] Cf. Russell's eq. (20) (*Ap. J.*, **104**, 157, 1946).

[8] *Contr. Princeton U. Obs.*, No. **3**, 1915.

[9] This suggestion comes from Dr. Kopal.

[10] R. H. Baker, *Pub. Allegheny Obs.*, **1**, 163, 1910.

[11] Cf. eq. (7), *Ap. J.*, **102**, 4, 1945.

[12] Cf. Table 5, *Ap. J.*, **106**, 111, 1947.

From the equation[5]

$$C = \epsilon \frac{(1+y)(15+u)}{15-5u},$$

where y is the coefficient of gravity darkening, we obtain, with $\epsilon = 0.005$, $u = 0.5$ and, adopting $y = 1.8u$,

$$C = 0.0118,$$

which agrees very well with C_{obs} within the limits of its uncertainty. Therefore, the value 0.01 for the constant z which occurs in the equations of the problem was accepted.

SPECTROSCOPIC DETERMINATION OF k

The minima of β Aurigae are so shallow that a determination of the ratio of radii k from the light-curve alone would be an utterly hopeless task. From the combined spectroscopic and photometric evidence it is clear that k is not far from unity, and this value was previously accepted in the solution.[8] Fortunately, we now have a fairly reliable determination of the ratio of luminosities of the components as obtained spectroscopically by R. M. Petrie.[2] He gives the difference of brightnesses of the two components Δm (in stellar magnitudes) as being equal to 0.13 ± 0.02 (p.e.). The Stebbins "minimum I" corresponds, furthermore, to the eclipse of the brighter component.[13] Since the amplitude of the "minimum II" is slightly greater than that of minimum I, we infer that the latter corresponds to a transit. Denoting by L_l and L_s the luminosities of the larger and smaller component, respectively, and by $1 - \lambda_I$ and $1 - \lambda_{II}$ the amplitudes of the minima I and II, we have

$$k^2 = \frac{L_s}{L_l} \frac{1-\lambda_I}{1-\lambda_{II}} (k^2 Q) \tag{3}$$

where Q is a known function of the limb darkening, k and p_0; p_0, as usual, denotes the maximum value of the geometric phase p of the eclipse. From spectroscopic observations we have $L_s/L_l = 0.887 \pm 0.016$ (p.e.). The product k^2Q is very nearly equal to 1. In the case of uniformly bright disks it is equal to 1. In the present case (using the approximate values of elements from Shapley's solution[8]) we find $k^2Q = 1.01$. From the rectified light-curve I estimated the amplitudes of the minima, finding

$$1 - \lambda_I = 0.0627; \qquad 1 - \lambda_{II} = 0.0716,$$

and hence, from equation (3), $k = 0.886$. Differentiating logarithmically equation (3), we find (regarding k^2Q as a constant equal to 1)

$$\delta k = \frac{k}{2} \left[0.921\, \delta(\Delta m) + \frac{\delta(1-\lambda_I)}{1-\lambda_I} - \frac{\delta(1-\lambda_{II})}{1-\lambda_{II}} \right]. \tag{4}$$

With the root-mean-square values of $\delta(1 - \lambda_I)$ and $\delta(1 - \lambda_{II})$ estimated roughly from the dispersion of individual normal points near the minima as ± 0.003 (p.e.), we get ± 0.03 from equation (4) as probable error of k.

EQUATIONS OF CONDITION

FIRST APPROXIMATION

The fundamental equation of the problem which we shall apply to each normal point during the minima I and II has the form[14]

$$\sqrt{w_i}\,[p_i^2(1 - z\cos^2\theta_i) - p_0^2(1-z)]\,x' + 2\sqrt{w_i}\,[p_i(1 - z\cos^2\theta_i) - p_0(1-z)]\,y' + n_i d(1-\lambda) = \sqrt{w_i}\sin^2\theta_i, \tag{5}$$

where p, p_0, and z have their usual meaning and θ denotes the phase angle. The subscript i refers to the number of the respective normal point. The constants x' and y' are parame-

[13] This information was communicated in a letter by R. M. Petrie to Z. Kopal.

[14] Cf. *Ap. J.*, **108**, 36, 1948.

ters denoted by D_1 and D_2 in Kopal's monograph[15] and are related to equatorial radii of the components and to the inclination of the orbit by the equations

$$\frac{x'^2}{x' + zy'^2} = x = r_2^2 \csc^2 i\,, \tag{6}$$

$$\frac{x'y'}{x' + zy'^2} = y = r_1 r_2 \csc^2 i\,. \tag{7}$$

Furthermore, $\sqrt{w_i}$ denotes the square root of the weight. In the case of β Aurigae the amplitudes of the minima are so small that it makes practically no difference whether we assume that the errors are equal on the magnitude scale or on the light-intensity scale. For the sake of simplicity we assume that they are equal on the light-intensity scale, and therefore we have[14]

$$\sqrt{w_i} = -\frac{dn}{d \sin^2 \theta}(1 - \lambda)\,. \tag{8}$$

In addition, the definition of k provides us with a relation of the form

$$x' - ky' = 0\,. \tag{9}$$

Substituting, in equation (9), k from the spectroscopic determination, we can treat (9) as an additional equation of condition for x' and y'. The mean error to be expected in its right-hand side is $\pm y'_{tr}\sqrt{(\delta k)^2}$, where y'_{tr} denotes the true value of y'. Since, by equation (8), $\sqrt{w_i}$ is nothing else but the inverse of $d \sin^2 \theta/dl$, the mean error of the right-hand side of equation (5) is equal to the mean error of the observed light-intensity, l. We found previously that the probable error of spectroscopic k is ± 0.03. From Stebbins'[1] Table V we infer that the probable error of l is ± 0.005. Shapley's determination[8] of elements of β Aurigae makes it plausible to put $y'_{tr} = 0.02$, and hence the probable error of the right-hand side of equation (9) is $\cong \pm 0.0006$. In consequence, the square root of the weight of equation (9) comes out 10.

The rectified brightnesses of the normal points used in the solution are given in the second column of Table 1. From the points occurring in the first and second part of Stebbins' Table IV, the first and the last point from the first part and the last point from the second part were not used in the solution (and do not figure in Table 1) because they evidently fall outside eclipses. In order to avoid very large residuals, the second and the eighth from the points referring to minimum II were combined into one, and consequently the square root of weight of the relative equation of condition and the coefficient of $d(1 - \lambda)$ in it were multiplied by $\sqrt{2}$. The phases given in the first column of Table 1 were computed with the period 3.96 days; they are reckoned for both minimum I and minimum II from the mid-eclipse and are shifted by $-^{\circ}.40$ with respect to phases used by Stebbins. This small correction was determined from careful examination of minimum I. The square roots of weights were taken directly from the free-hand curve as equal to $dl/d \sin^2 \theta$.

Let a'_0 and a''_0 denote the photometric phases of the deepest eclipse for the occultation and transit and, furthermore, let the superscripts U and D denote the values corresponding to the hypotheses of a uniform brightness and of a complete limb darkening. We have

$$a'_0 = 1 - \lambda_{II} + (1 - \lambda_I)\frac{(1 - \bar{x})\, a_0^U + \bar{x}\, a_0'^D}{k^2\left[(1 - \bar{x})\, a_0^U + \frac{3}{2}\bar{x}\Phi(k)\, a_0''^D\right]}\,, \tag{10}$$

$$a''_0 = \frac{(1 - \bar{x})\, a_0^U + \frac{3}{2}\bar{x}\Phi(k)\, a_0''^D}{1 - \bar{x} + \frac{3}{2}\bar{x}\Phi(k)}\,,$$

[15] P. 197.

with

$$\bar{x} = \frac{2u}{3-u}.$$

Here $\Phi(k)$ is a known (tabulated) function of k. The limb darkening, u, is assumed to be equal for both components, that is, 0.5. Making a hypothesis (very close to the truth) that k in equations (10) and in p_i's is equal to 0.9, we get a_0' and a_0'', and, with the aid of the data given in Table 1, we form the system of equations of condition of the form (5).

TABLE 1

RECTIFIED BRIGHTNESSES OF NORMAL POINTS

PHASE	RECTIFIED BRIGHTNESS	O−C (MAG.)
	Minimum I	
9°83	0.9798	+0.019
6.27	.9711	− .004
2.18	.9313	+ .004
0.29	.9442	− .014
2.26	.9364	− .001
4.19	.9502	− .002
6.08	.9666	− .001
7.22	.9810	− .006
8.32	.9684	+ .019
9.76	.9889	+ .008
11.12	0.9906	+0.010
	Minimum II	
13.39	0.9953	+0.005
9.26	.9958	− .003
6.04	.9733	− .011
3.46	.9316	+ .008
1.68	.9282	+ .001
0.02	.9308	− .005
2.14	0.9308	+0.000

We solve this system together with equation (9) multiplied by 10 by the method of least squares and obtain the normal equations

$$\begin{aligned} 102.0488x' - 85.3075y' + 1.0339d(1-\lambda_{\mathrm{I}}) + 0.3762d(1-\lambda_{\mathrm{II}}) &= 0.10883, \\ + 83.8336y' + 1.7920d(1-\lambda_{\mathrm{I}}) + 0.6516d(1-\lambda_{\mathrm{II}}) &= 0.17619, \\ + 4.6563d(1-\lambda_{\mathrm{I}}) &= 0.07944, \\ + 3.9349d(1-\lambda_{\mathrm{II}}) &= 0.82807 \end{aligned}$$

the solution of which is

$$x' = 0.0177; \quad y' = 0.0200 \cdot \quad d(1-\lambda_{\mathrm{I}}) = +0.0054; \quad d(1-\lambda_{\mathrm{II}}) = +0.0021.$$

The inverse of the matrix of coefficients of normal equations is[16]

$$\{Q_{ij}\} = \begin{Bmatrix} +0.0758, & +0.0783, & -0.0470, & -0.0202 \\ * & +0.0929, & -0.0531, & -0.0229 \\ * & * & +0.2456, & +0.0133 \\ * & * & * & +0.2599 \end{Bmatrix}.$$

The mean error of an observation of unit weight was found to be ± 0.0062. From the numerical results given above we get, for the corrected amplitudes of the minima,

$$1 - \lambda_{\mathrm{I}} = 0.0681 \; ; \qquad 1 - \lambda_{\mathrm{II}} = 0.0737 \; .$$

Dividing x' by y', we get $k = 0.886$. As we see, this value is identical with the one introduced into the equations of condition from spectroscopic evidence. This outcome could be predicted a priori, since with shallow minima the photometric observations can give very little information—if any—about the relative sizes of the components.

SECOND APPROXIMATION

As the corrections to the depths of the minima are considerable, we repeat the solution with the corrected values of the amplitudes. From equation (3), with $k^2Q = 1.014$ (from the first approximation), we get $k = 0.912$. We determine the mean error of k from equation (4) with the aid of the values of Q_{ij}'s and of the mean error of unit weight found in the first approximation. We get a mean error of $k = \pm 0.03$. The mean error of the right-hand sides of equation (5) is found, from the residuals, as equal to ± 0.0064, and hence the square root of weight[17] of equation (9) becomes 11. With the new values of amplitudes, the n_i's were recomputed, and the equations of condition of the following form[5] were formed. For minimum I,

$$\sqrt{w_i}\,[p_i^2(1 - z\cos^2\theta_i) - p_0^2(1 - z)]\,x' + 2\sqrt{w_i}\,[p_i(1 - z\cos^2\theta_i) - p_0(1 - z)]$$

$$\times y' - n_i(d\lambda_{\mathrm{I}}) + (n_i - 1)\,dU + \frac{1 - \lambda_{\mathrm{I}}}{a_0''\,[1 - \bar{x} + \frac{3}{2}\bar{x}\Phi(k)]}\,n_i\left[\frac{\frac{3}{2}\Phi(k)\,a_i''^{D} - a_i^{U}}{n_i}\right.$$

$$\left. - \tfrac{3}{2}\Phi(k)\,a_0''^{D} + a_0^{U}\right] d\bar{x} = \sqrt{w_i}\sin^2\theta_i ,$$

while for minimum II we have $(d\lambda_{\mathrm{II}})$ instead of $(d\lambda_{\mathrm{I}})$, and the term with $d\bar{x}$ is

$$+\frac{1 - \lambda_{\mathrm{II}}}{a_0'}\,n_i\left[\frac{a_i'^{D} - a_i^{U}}{n_i} - (a_0'^{D} - a_0^{U})\right] d\bar{x} .$$

Again, in equations (10) and in the p_i's, k was taken to be 0.90 and hence $p_0 = 0.4515$. The terms with the correction of the unit of light dU and with $d\bar{x}$ were transposed to the

[16] The numbers Q_{ii} are the inverse weights of the unknowns. The Q_{ij}'s $(i \neq j)$ are prerequisite for the computation of the mean error of any function of the unknowns. Since $Q_{ij} = Q_{ji}$, asterisks were used to avoid the re-writing of the same numbers.

[17] The error of spectroscopic k as given by eq. (4) is dependent on the error not only of spectroscopic determination of L_s/L_l but also, through $1 - \lambda_{\mathrm{I}}$ and $1 - \lambda_{\mathrm{II}}$, of the errors of photometric observations. Therefore, it is not quite correct to weight eq. (9), when combining it with eqs. (5), according to the mean error of k and l_i's. A more rigorous way would be to use, instead of eq. (9), an equation of the form $x' - (k + \delta k)y' = 0$, substitute in this equation δk from eq. (4), and keep $d(1 - \lambda_{\mathrm{I}})$ and $d(1 - \lambda_{\mathrm{II}})$ as unknowns. The weight should be then taken according to the error in spectroscopic Δm (and in the l_i's).

right-hand sides of equations of condition and the solution for x', y', $(d\lambda_{\mathrm{I}})$, and $(d\lambda_{\mathrm{II}})$ was obtained by the least squares. It yielded the normal equations

$$\begin{aligned}
123.3314x' - 106.4717y' - 1.2573(d\lambda_{\mathrm{I}}) - 0.4710(d\lambda_{\mathrm{II}}) &= 0.11724 \\
&\quad + 3.5939dU + 0.02484d\bar{x}\,. \\
+ 106.9294y' - 2.2899(d\lambda_{\mathrm{I}}) - 0.8728(d\lambda_{\mathrm{II}}) &= 0.19371 \\
&\quad + 5.8277dU + 0.04212d\bar{x}\,, \\
+ 3.9424(d\lambda_{\mathrm{I}}) &= -0.07312 \\
&\quad - 1.8056dU - 0.01905d\bar{x}\,, \\
+ 3.7152(d\lambda_{\mathrm{II}}) &= -0.02728 \\
&\quad - 0.6068dU - 0.00630d\bar{x}\,,
\end{aligned}$$

the solution of which is

$$\begin{aligned}
x' &= 0.0175 + 0.179dU + 0.0035d\bar{x}\,; \\
y' &= 0.0192 + 0.177dU + 0.0039d\bar{x}\,; \\
(d\lambda_{\mathrm{I}}) &= -0.0018 - 0.298dU - 0.0015d\bar{x}\,; \\
(d\lambda_{\mathrm{II}}) &= -0.0006 - 0.099dU - 0.0003d\bar{x}\,.
\end{aligned} \tag{11}$$

The mean error of the unit weight came out ± 0.0063, and the inverse of the matrix of coefficients of normal equations is

$$\{Q_{ij}\} = \begin{Bmatrix} 0.0735\,, & 0.0748\,, & 0.0669\,, & 0.0269 \\ * & 0.0857\,, & 0.0736\,, & 0.0296 \\ * & * & 0.3178\,, & 0.0258 \\ * & * & * & 0.2795 \end{Bmatrix}.$$

Hence the mean errors of the unknowns (if dU and $d\bar{x}$ are ignored) are

$$\begin{aligned}
&\text{m.e. of } x' = \pm 0.0017\,; \qquad \text{m.e. of } y' = \pm 0.0019\,; \\
&\text{m.e. of } (d\lambda_{\mathrm{I}}) = \pm 0.0036\,; \qquad \text{m.e. of } (d\lambda_{\mathrm{II}}) = \pm 0.0034\,.
\end{aligned} \tag{12}$$

As we see, the corrections to the depths of both minima are smaller than their mean errors. Consequently, we are justified in accepting the approximation just performed as final. In order to ascertain the effect of our assumption regarding k in equations (10) and in p''s on the solution, I recomputed x', y', $(d\lambda_{\mathrm{I}})$, and $(d\lambda_{\mathrm{II}})$ with $k = 0.95$. The differences came out negligible in comparison with the mean errors: e.g., x' was found to be 0.0179, and hence the difference was 0.0004. We infer, therefore, that the additional uncertainty introduced into the determination of elements by the uncertainty of k in the coefficients of the equations of condition is negligible.[18]

Having the solution for the auxiliary constants in the form given by equations (11), it is easy to estimate the amount of uncertainty introduced into the elements by the uncertainty of the maximum light and of the (assumed) degree of darkening. The representation of fourteen normal points falling outside eclipses with the aid of the formula $B_0 + B_1 \cos\theta + B_2 \cos^2\theta$ gave a root-mean-square residual of ± 0.0054, and therefore the uncertainty of light-unity is approximately $\pm 0.0054/\sqrt{14} = \pm 0.0014$. As to the

[18] Cf. eq. (9′), *Ap. J.*, **106**, 475, 1947.

uncertainty of the coefficient of limb darkening, we can reasonably expect from other physical evidence[12] that for both A0 components it deviates from 0.5 not more than ± 0.1. On using equations (11) we find that, compared with the mean errors given by equations (12), the additional errors arising from the uncertainties of the light-unity and of the degree of darkening are negligible.

THE ELEMENTS AND THEIR MEAN ERRORS

From the values of the auxiliary parameters x', y', and p_0, we find in a usual way the elements i, r_1, and r_2. Some explanations are in place as to the manner in which the mean errors of these quantities were determined. We have to express the error of any one element i, r_1, or r_2 as a linear function of the errors of x', y', λ_I, or λ_{II}. First of all, because of the smallness of the ellipticity, we can safely assume that $\delta x = \delta x'$, $\delta y = \delta y'$. Neglecting the changes in the quantity (k^2Q), we find

$$\delta a_0' = -\delta(d\lambda_{II}) - \delta(d\lambda_I)\frac{(k^2Q)}{k^2} - 2(1-\lambda_I)\,k^{-3}(k^2Q)\,\delta k\,;$$

and, by numerical differentiation, from tables of the function p, we obtain

$$\delta p = \frac{\partial p}{\partial k}\,\delta k + \frac{\partial p}{\partial a}\,\delta a\,.$$

With the aid of the two last equations, substituting in them $\delta k = (\delta x - k\delta y)/y$, we find δp_0 as a linear function of $\delta(d\lambda_I)$, $\delta(d\lambda_{II})$, . . . The expression of δr_1, δr_2, and δi as linear functions of errors of the auxiliary parameters x, y, . . . , offers no difficulty. The following final values of elements and of their mean errors were found

$$i = 78^\circ.5 \pm 0^\circ.6\,(\text{m.e.}), \quad r_1 - 0.142 \pm 0.007\,(\text{m.e.}), \quad r_2 = 0.130 \pm 0.006\,(\text{m.e.}).$$

It should be mentioned that the above value of the inclination has been corrected for polar flattening by means of the equation[19]

$$\tan i = \frac{b}{c}\tan j\,,$$

where j is the value of the inclination derived from the solution and b/c is the ratio of the minor equatorial to the polar radius of the stars. With $\epsilon = 1 - (b/a) = 0.005$ and[19] $a - c = (3/2)(a - b)$, we have $b/c = 1.002$.

The spectroscopic ratio of luminosities of both components refers, in all probability, to the moment of greatest separation of the spectral lines, which is presumably at the quadratures. Since the components are nearly equal in brightness as well as in dimensions and, moreover, since their separation is considerable, we can safely assume that, at quadratures, this ratio is very nearly equal to the ratio of luminosities freed from the reflection effect. Denoting by L_l' and L_s' the luminosities at quadratures freed from reflection of the larger and smaller component, we have

$$\frac{L_s'}{L_l'} = 0.887 \pm 0.016\,(\text{p.e.}).$$

If we equalize the theoretical and observed expressions for the uneclipsed light of the system, we get, at quadratures,

$$B_0 = (L_l' + L_s')\,[1 + K r_1 r_2 (0.28 - 0.07)] = (L_l' + L_s')\,1.0042\,,$$

[19] Cf. Kopal, *op. cit.*, p. 195.

where $B_0 = 1.0025 \pm 0.0015$ (p.e.) and the light-unity corresponds to $\Delta m = 0.350$ mag. (β Tauri was used as comparison star). From the last two equations we get

$$L'_s = 0.469 \pm 0.007 \text{ (m.e.)},$$

$$L'_l = 0.529 \pm 0.007 \text{ (m.e.)}.$$

With aid of elements obtained in the second approximation the theoretical light-curve was drawn and the values of O − C given in the third column of Table 1 were formed.

The author is indebted to Dr. Zdeněk Kopal for much helpful discussion in connection with this study and for careful preview of the manuscript.

A PHOTORED STUDY OF THE ECLIPSING VARIABLE QY AQUILAE

BALFOUR S. WHITNEY
University of Oklahoma Observatory
Received June 28, 1948

ABSTRACT

Relative dimensions of the components are found from a light-curve based on 1390 photored observations, which agree, within the limits of the relative errors, with dimensions obtained 3 years ago from a photographic curve. Secondary minimum occurs at phase 0.487. The direction of the displacement is in accordance with Struve's spectrographic results.

This investigation was undertaken as a check on the results published three years ago,[1] in which wide differences were found between the dimensions of the components as determined from photographic and visual light-curves. The visual curve was not accurate enough to warrant much confidence in the reality of these differences.

Eastman 103-E and 103*a*-E plates were used with a No. 28 Wratten filter. Exposures (1390 in number) varied from 3 minutes in maxima to 10 or 12 minutes in minima.

TABLE 1

PHOTORED MAGNITUDES OF COMPARISON STARS

a	10.60	*e*	10.81	*k*	12.87	7.1 E., 1.9 N.	10.82
b	10.16	*f*	12.12	*l*	12.63	6.6 E., 3.1 S.	11.18
c	12.22	*g*	12.21	*w*	11.04	3.7 W., 0.8 N.	11.45
d	12.28	*h*	12.81	*x*	11.17		

Photored magnitudes of comparison stars, determined from 14 comparisons with the pole, using the Harvard magnitudes[2] as standards, are listed in Table 1, in which the letters refer to the chart in Paper I. The co-ordinates for the last three are measured from the variable. The mean internal probable error was ± 0.030 mag.

Phases were computed from the elements[3]

$$\text{JD}\odot 2430223.615 + 7.229617E\,.$$

Recent normal minima from the photored plates, with residuals computed with these elements, are listed in Table 2. The residuals from the first three minima in Table 4 of Paper I are large (-0.12, -0.045, and -0.057 day).

Normal points of ten estimates each are listed in Table 3, in which the residuals, O−C, were read from a plot of the final theoretical curve (Fig. 1).

For the solution, the normals in the partial phases of primary minimum were reflected on one branch, and means of groups of three were formed. These thirty-point normals, with the square roots of the weights computed, roughly, by Piotrowski's method,[4] are shown in Table 4. Thirty-point normals in maximum light were used for the partial rectification. The coefficients in the equation

$$l_1 + l_2 = 0.989\,(\pm 0.003) - 0.019\,(\pm 0.001)\cos\theta - 0.020\,(\pm 0.003)\cos 2\theta$$

[1] *Ap. J.*, **102**, 202, 1945; referred to hereafter as "Paper I."

[2] *Harvard Ann.*, **89**, 99, 1935.

[3] *A.J.*, **50**, 131, 1943.

[4] *Ap. J.*, **106**, 472, 1947.

TABLE 2

OBSERVED MINIMA

JD ⊙	Weight	Epoch	O−C	JD ⊙	Weight	Epoch	O−C
2430000+				2430000+			
1705.688	1	205	+0.002	2399.725	3	301	−0.005
1777.979	1	215	− .004	2421.418	2	304	− .001
1980.409	3	243	− .003	2435.876	4	306	− .002
1987.640	3	244	− .002	2486.472	1	313	−0.013
2088.863	2	258	+0.007				

TABLE 3

NORMAL POINTS

Phase	m_{pr}	O−C	Phase	m_{pr}	O−C	Phase	m_{pr}	O−C	Phase	m_{pr}	O−C
+0ᵖ0000	12.83	+ 1	+0ᵖ124	10.96	+13	+0ᵖ490	11.00	+4	+0ᵖ905	10.82	−3
+ .0035	12.84	+ 2	+ .131	10.88	+ 5	+ .494	10.95	−1	+ .907	10.77	−8
+ .0065	12.80	− 2	+ .141	10.81	− 2	+ .502	11.01	+6	+ .909	10.80	−5
+ .0097	12.74	0	+ .156	10.85	+ 2	+ .507	10.91	−4	+ .913	10.83	−2
+ .0120	12.67	+ 5	+ .171	10.81	− 1	+ .508	10.94	0	+ .916	10.79	−6
+ .0130	12.57	+ 1	+ .188	10.86	+ 5	+ .512	10.88	−5	+ .920	10.88	+2
+ .0150	12.50	+ 7	+ .191	10.82	0	+ .514	10.93	0	+ .925	10.88	+3
+ .0170	12.34	+ 2	+ .194	10.82	0	+ .516	10.91	0	+ .929	10.89	+3
+ .0191	12.15	− 4	+ .205	10.83	+ 2	+ .522	10.87	−2	− .0692	10.87	+1
+ .0202	12.18	+ 5	+ .248	10.74	− 6	+ .552	10.85	+3	− .0682	10.88	+2
+ .0212	12.17	+10	+ .258	10.78	− 1	+ .574	10.82	0	− .0670	10.89	+2
+ .0228	12.05	+ 8	+ .262	10.74	− 5	+ .578	10.80	−2	− .0646	10.88	0
+ .0245	11.86	− 1	+ .271	10.81	+ 2	+ .580	10.83	+1	− .0634	10.89	0
+ .0257	11.79	− 3	+ .288	10.77	− 3	+ .583	10.81	0	− .0619	10.83	−8
+ .0270	11.75	0	+ .294	10.81	+ 1	+ .590	10.82	+1	− .0601	10.86	−5
+ .0299	11.56	− 6	+ .313	10.78	− 2	+ .596	10.80	−1	− .0589	10.87	−5
+ .0326	11.45	− 7	+ .318	10.78	− 2	+ .599	10.79	−2	− .0578	10.84	−9
+ .0347	11.37	− 8	+ .325	10.81	+ 1	+ .600	10.77	−4	− .0542	10.97	−1
+ .0369	11.36	− 1	+ .352	10.86	+ 6	+ .606	10.84	+3	− .0473	11.15	+3
+ .0405	11.33	+ 7	+ .366	10.84	+ 4	+ .632	10.82	+1	− .0411	11.24	0
+ .0439	11.22	+ 4	+ .370	10.83	+ 3	+ .643	10.80	0	− .0378	11.36	+1
+ .0479	11.11	0	+ .379	10.77	− 3	+ .659	10.80	0	− .0356	11.39	−2
+ .0499	11.08	+ 1	+ .412	10.84	+ 3	+ .674	10.82	+2	− .0339	11.48	0
+ .0520	11.06	+ 3	+ .416	10.80	− 1	+ .683	10.82	+2	− .0322	11.53	−1
+ .0549	10.94	− 3	+ .420	10.78	− 4	+ .701	10.84	+4	− .0296	11.71	+5
+ .0567	10.94	0	+ .426	10.89	+ 6	+ .709	10.79	−1	− .0267	11.76	0
+ .0582	10.96	+ 4	+ .432	10.81	− 3	+ .715	10.78	−2	− .0245	11.78	−5
+ .0593	10.99	+ 8	+ .435	10.77	− 7	+ .725	10.78	−2	− .0224	12.03	+3
+ .0609	10.91	+ 1	+ .438	10.89	+ 4	+ .754	10.79	−1	− .0198	12.12	−3
+ .0718	10.92	+ 5	+ .440	10.94	+ 8	+ .773	10.80	0	− .0177	12.25	−1
+ .0856	10.87	+ 3	+ .443	10.90	+ 3	+ .803	10.80	−1	− .0148	12.42	−3
+ .0894	10.88	+ 3	+ .449	10.82	− 6	+ .834	10.77	−6	− .0122	12.61	+2
+ .0974	10.83	− 2	+ .451	10.79	−10	+ .874	10.79	−4	− .0094	12.73	−3
+ .1007	10.87	+ 2	+ .453	10.87	− 3	+ .878	10.85	+1	−0.0051	12.80	−2
+0.104	10.82	− 3	+0.478	10.89	− 6	+0.885	10.83	−1			

were small enough that more complete rectification was not required. Moreover, only the normals between primary and secondary showed any appreciable indications of curvature. Those following secondary would have been fitted better by a straight line. The ellipticity is too poorly determined to warrant further consideration.

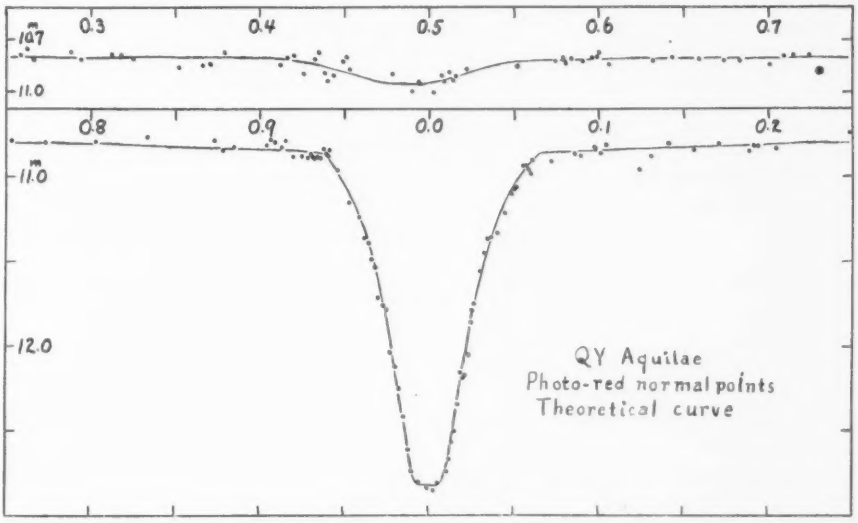

FIG. 1.—The light-curve of QY Aquilae. The normal points are means of 10 observations each

TABLE 4

THIRTY-POINT REFLECTED NORMALS IN PRIMARY MINIMUM

Phase	$\sqrt{w}$	m_{pr}	Phase	$\sqrt{w}$	m_{pr}	Phase	$\sqrt{w}$	m_{pr}
0^{p}0085	7	12.76	0^{p}0265	5	11.76	0^{p}0484	3	11.11
.0124	8	12.62	.0306	5	11.60	.0537	2	10.99
.0156	8	12.43	.0337	4	11.43	.0576	2	10.91
.0189	6	12.17	.0368	3	11.37	.0594	1	10.91
.0213	6	12.13	0.0418	3	11.26	0.0621	1	10.88
0.0239	7	11.90						

Secondary minimum occurs at phase 0.487 period. The displacement is in the direction indicated by Struve's spectrographic orbit[5] but is somewhat smaller in amount. The effect of the eccentricity on the light-curve in minimum was found to be negligible.

Solution of the rectified curve was effected by Kopal's second method.[6] Convergence was so slow that six solutions were required. Successive values of k were 0.70, 0.90, 0.723, 0.781, 0.764, 0.771, and 0.768. The final values of the C's were: $C_1 = 0.0341 \pm 0.0018$, $C_2 = 0.0445 \pm 0.0007$, $C_3 = 0.00167 \pm 0.00057$.

The mass-ratio in Table 5 was computed from relative luminosities obtained by ap-

[5] *Ap. J.*, **103**, 86, 1946.

[6] *An Introduction to the Study of Eclipsing Variables* (Cambridge: Harvard University Press, 1946).

plying radiometric corrections[7] to the visual maxima and minima. The spectrum of the fainter star was assumed to be K2, on the basis of color indices. This mass-ratio was used, as in Paper I, to find the densities. The same mass-ratio and densities followed from the simpler formula:

$$\frac{m_b}{m_f} = \left(\frac{L_b}{L_f}\right)^{2/5},$$

using the photored relative luminosities.

TABLE 5

THE SYSTEM OF QY AQUILAE

Relative Elements (Darkening Coeff., 0.7)		Photored Light-Curve	
k	0.768 ± 0.028*	Maximum	$10^m.80$
L_b	0.835	A_1	2.02
L_f	0.165	A_2	0.16
r_b	0.185 ± 0.005*	D	$0^p.1392 = 1^d.006$
r_f	0.240 ± 0.006*	d	$0^p.0132 = 0^d.095$
i	$87°.8 \pm 2°.0$*	Phase of secondary min.	$0^p.487$
Mass ratio $\left(\frac{m_b}{m_f}\right)$	1.9	Blue-red indices	
ρ_b	0.027	Maximum	$0^m.63$
ρ_f	0.014	Minimum	1.76
e	0.020 ± 0.006†		
J_b/J_f	8.58		

* Relative errors computed from probable errors in the C's.

† Relative error, based on assumed uncertainty of $\pm 20°$ in ω, $\pm 0^p.002$ in phase of secondary minimum.

A comparison of the accuracy of the photored and the photographic observations shows little difference between the two. The means of the residuals of single estimates from the ten-point normals were 0.064 (pr) and 0.061 (pg) mag. The mean residual of the ten-point normals from the theoretical curves was 0.030 mag. in both cases.

The differences between the relative radii from the two curves are within the ranges of the relative errors. Observations of much greater precision than can be reached with methods now available at this observatory will be required to demonstrate the reality of such differences, if they exist.

The hope, entertained at the beginning of this study, that it would be possible to determine the degree of limb darkening by comparing the two light-curves was nullified by the scattering of the photored normal points on the shoulders of primary minimum.

[7] Russell, Dugan, and Stewart, *Astronomy* (Boston: Ginn & Co., 1938), p. 736.

ASSOCIATION OF CORONA WITH PROMINENCE

WALTER ORR ROBERTS*

Received April 9, 1948

ABSTRACT

A coronal spectrogram, taken on June 14, 1947, shows a striking association between λ 6374 of the corona and λ 6563 of an active prominence; at the same position the rarely observed unidentified coronal line λ 5694 shows clearly. The positions of sharp maxima of the prominence spectrum and of the coronal spectrum coincide precisely for the two brightest parts of the prominence. Some likelihood appears to exist that the occurrence of λ 5694 is generally associated with the occurrence at the same place on the sun of rapidly moving prominences of the "sun-spot" type.

A routine spectrogram made at the Climax station on June 14, 1947, displayed an apparent association between the corona of the sun and a brilliant prominence at the same position angle on the solar limb. The spectrogram was made on an Eastman type 103-F spectroscopic plate exposed in the Littrow spectrograph of the High Altitude Observatory coronagraph at Climax, Colorado. Its appearance suggests a direct physical association between the corona and an active prominence. None of our previous records displays this effect.

The spectrogram was taken with a curved slit and with the region just beyond the limb focused on the slit. The plate was centered at 90° apparent position angle (east) on the sun, and the phenomenon appeared between 90° and 95° apparent position angle, near the center of the plate. We did not discover the unusual phenomenon until the plate had been processed after sunset and thus were not able to make special photographs of the effect.

Our usual spectrograms, taken for routine estimates of the sun's coronal intensity in λ 5303 and λ 6374, display also the coronal line at λ 6704 and the prominence lines at $H\alpha$ (λ 6563) and D_3 (λ 5875). Occasionally, with bright prominences, several other lines show, including those of sodium, magnesium, and iron.

This particular spectrogram showed a striking brightening of the λ 6374 red coronal line (*Fe* X, Edlén[1]) at the positions (91° and 93½°) of the two brightest parts of the $H\alpha$ emission from the prominence. Both prominence and coronal emission lines showed the extraordinary broadening that one usually associates with a wide range of line-of-sight velocities. The red coronal line appeared, as well, to show a significant displacement of the center of gravity, though the faintness of the line makes this observation a bit dubious. In addition, the plate showed, at the same positions, emission from the relatively rare line λ 5694 discovered by Lyot[2] and generally ascribed to the corona. The atomic origin of this line is not yet known, though it has been very tentatively identified as *Ca* XV by Edlén.[1] Some suggestion of continuous emission showed on the plate, but for a number of reasons we can feel no great confidence in this observation.

The prominence with which the corona was associated was extremely intense and also of a very active type, with bright surges and loops, perhaps most nearly like III-b in Pettit's[3] classification. The prominence quite evidently was of the strikingly active character not unusual at this phase of the solar activity cycle, with intense, rapidly rising and falling surges and jets and with small, changeable loops. A sun-spot group of no spec-

* High Altitude Observatory of Harvard University and University of Colorado, Climax, Colorado.

[1] *Zs. f. Ap.*, **22**, 30, 1942. See also summary by P. Swings, *Ap. J.*, **98**, 116, 1943.

[2] *M.N.*, **99**, 580, 1939.

[3] *Ap. J.*, **98**, 6, 1943.

tacularly unusual nature showed at approximately the same latitude and longitude the following day, which suggests that we should regard the two phenomena as associated.

A photograph of the prominence taken at approximately 14^h35^m, G.C.T., is shown in Figure 1. The black line represents the approximate position of the spectrograph slit. The spectrogram was obtained at 13^h51^m, G.C.T., so that considerable change in

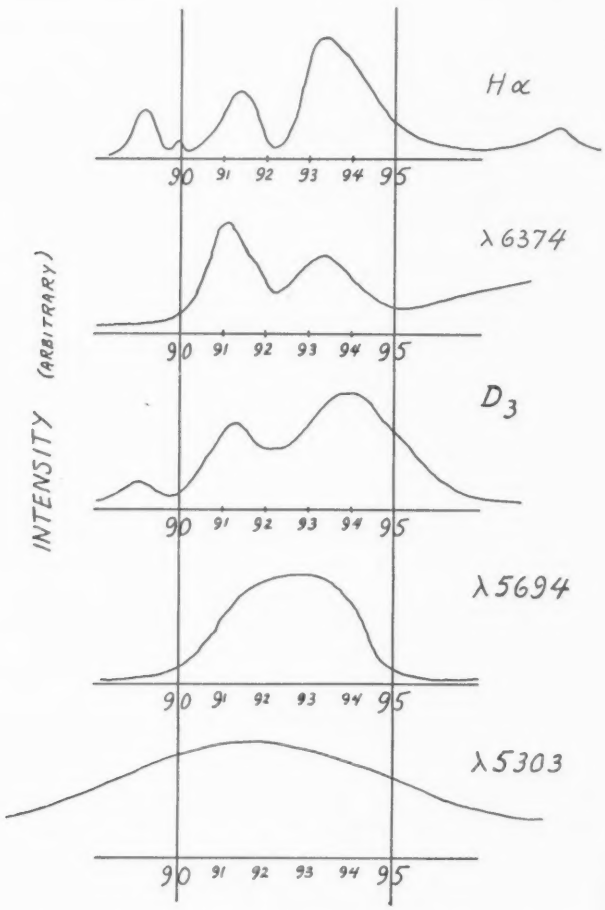

FIG. 3.—Intensities of coronal and prominence lines at 13:51 G.C.T. as a function of apparent position angle. Vertical scales are arbitrary and independent of each other. South is to right. Intensities were evaluated by estimate from the original plate.

details of the prominence structure may have occurred in the interval separating the photograph from the spectrogram.

No significant effect showed in λ 5303, the well-known green coronal line (*Fe* XIV, Edlén[1]), though a broad maximum appeared in the general latitude of the λ 6374 knots.

Figure 3 shows hand-drawn intensity graphs for the coronal lines λλ 6374, 5694, 5303, and for the prominence lines *Hα* and D_3. The vertical scale is arbitrary intensity, subjectively evaluated. The horizontal scale is apparent position angle.

In Figure 2, prints from the spectrogram of each of the lines are reproduced. The various effects also showed, but with less certainty, on an adjacent spectrogram, where the

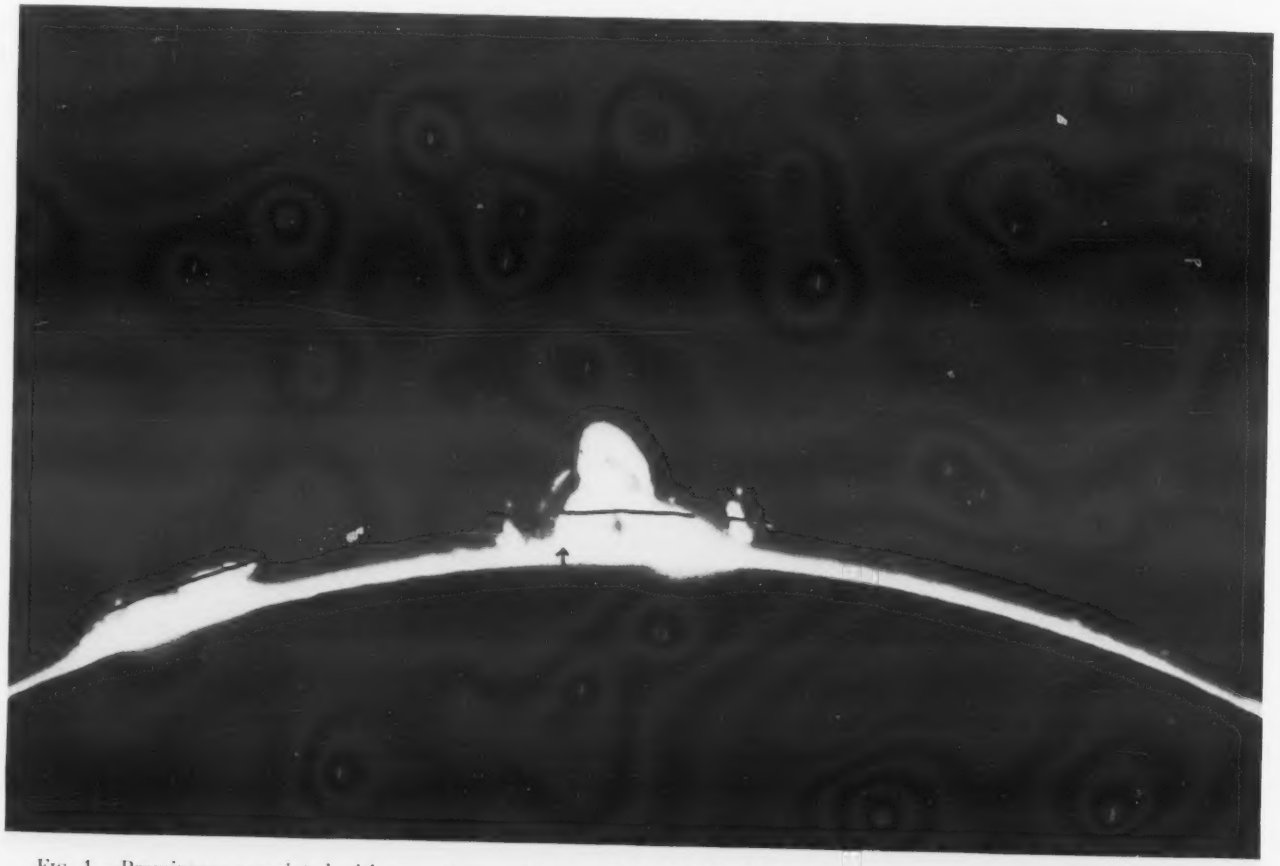

FIG. 1.—Prominence associated with coronal line, shown at 14:35 G.C.T. Photograph in *H*-alpha. Black line shows approximate position of the slit for photographs of Fig. 2. Arrow shows 90° apparent position angle. South is to the right.

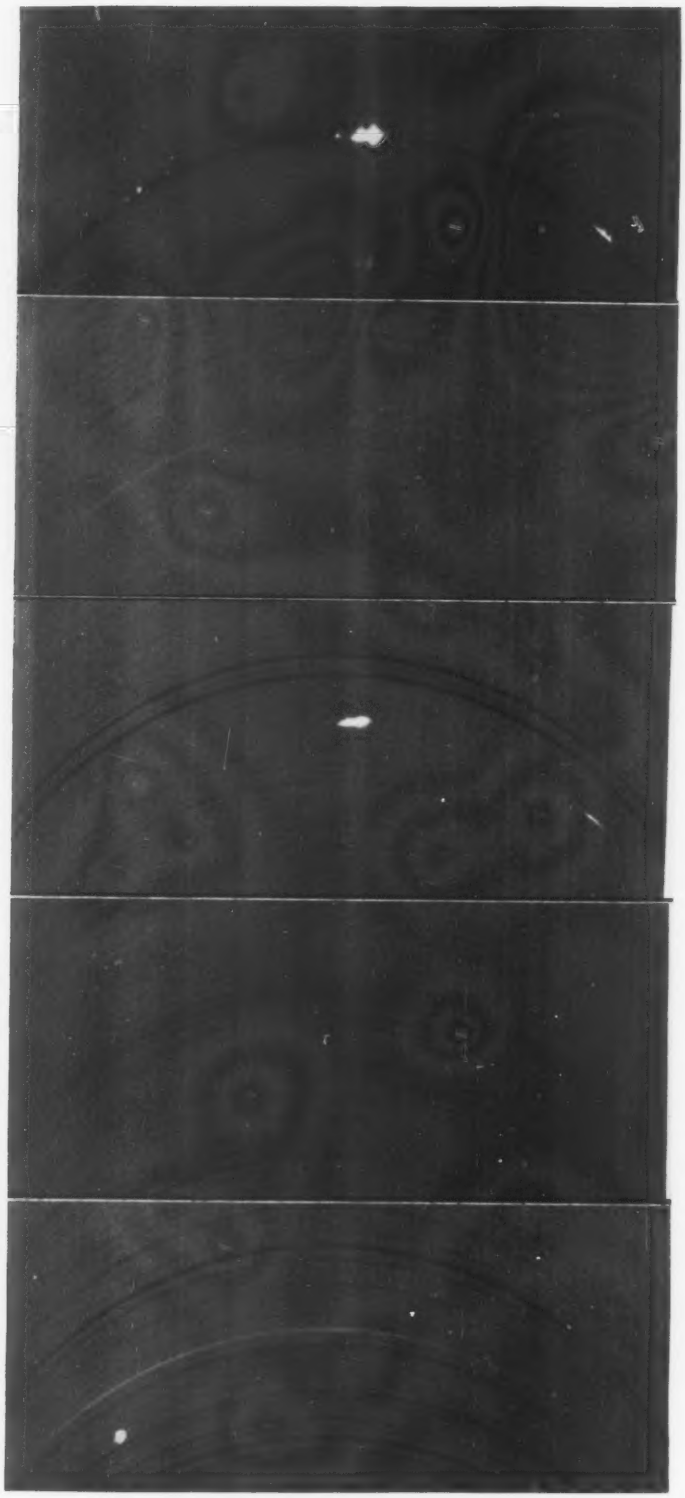

FIG. 2.—Photographs of spectrum lines graphed in Fig. 3. Each line is shown in a small segment of the whole spectrum.

phenomena were near the edge of the field of the slit rather than near the center. Unfortunately, a coronagraph, because it uses a nonachromatic objective lens, can be focused for one wave length only; hence the focus, though good at λ 6563, is noticeably poor at λ 5694 and λ 5303.

The observations lead one to suspect that the line λ 5694 ascribed to the corona is perhaps more closely associated with prominences than has hitherto been suspected. It also suggests, possibly, that we should again search the lower excitation potentials intermediate between *Fe* X and prominence lines for an explanation of λ 5694 rather than the high excitation of Edlén's tentative identification as *Ca* XV.

It also hints at a possible interaction between corona and prominences which identification of λ 5694 might help clarify. Possibly a further investigation of the effect may disclose direct relationships between prominences and the formation of the corona, especially if, as this observation perhaps intimates, high-velocity prominences are, in general, significantly associated with the λ 5694 emission. Results offered by Waldmeier[4] also point out the association of λ 5694 with the active "spot-type" prominences.

Observers with suitable apparatus should certainly investigate more closely the relative intensities, line widths, and distributions of coronal lines near brilliant, active prominences which have high velocities in the line of sight, and especially should this be done with higher-resolution apparatus. Coronagraphs capable of producing achromatic final images would greatly facilitate studies of this sort.

[4] *Zs. f. Ap.*, **20**, 172, 1940; *Astronomische Mitteilungen der Eidgenössischen Sternwarte Zürich*, No. 146.

THE SPECTRUM OF COMET 1947n*

P. SWINGS AND THORNTON PAGE
McDonald Observatory
Received August 12, 1948

ABSTRACT

The spectrum of Comet 1947n has been observed from heliocentric distance $r = 0.504$ to $r = 1.135$ between λ 3000 and λ 8900. The *OH* band is unusually weak relative to *NH*. The (0, 0) band of *CN* reveals a complex rotational structure due to fluorescence, similar to that observed in previous comets. Features appearing within the Swan bands are described and discussed. The red region is mainly due to NH_2. Two intense infrared emissions have been found for the first time at λ 7906 and λ 8106. A detailed discussion seems to indicate that they may be attributed to the red system of *CN*. This *CN* emission in the infrared does not result from fluorescence but probably from the photodissociation of a parent-molecule. No atomic lines have been found other than the D lines of *Na*. The two components of the nucleus reveal exactly the same spectrum.

The solution of a number of important problems in cometary physics must await the apparition of bright comets. Hence, when news was received that an extremely bright comet had been seen in the Southern Hemisphere, a special effort was made at the McDonald Observatory to observe this object, in spite of the difficulties caused by the proximity of the comet to the sun. The comet was first seen a few minutes before setting on December 14.05 (U.T.). We decided to try, first, to obtain some information on the infrared part of the spectrum.[1]

A plane-grating spectrograph equipped with a solid Schmidt $f/0.65$ camera and focused for the region λλ 7000–9000 was installed at the prime focus of the 82-inch reflector. The first spectrogram, obtained on December 15.05 (U.T.)[2] on ammonia hypersensitized IN emulsion, revealed two emission bands near λ 7906 and λ 8106. As far as we know, these cometary radiations have not been observed previously. Other spectrograms on Eastman IN film, obtained with the same instrument on several of the following evenings, confirmed the presence of these intense emissions. For three of the exposures, a Wratten *a* filter, the complete absorption of which between λ 3100 and λ 5200 had been checked, was placed on the slit, in order to absorb the second-order violet which would have been superposed on the infrared emission. On two evenings an attempt was made to extend the spectral range beyond the limit of the IN emulsion by using hypersensitized IM emulsion, but without success. On December 18.06 and 20.05, two grating spectrograms were obtained on Eastman 103*a*-F emulsion, with excellent definition from λ 4400 to λ 6700 (see Fig. 1, *a*).

During the period of spectrographic observation at the prime focus, December 15–23, it was impracticable to obtain the individual spectra of the two components of the nucleus,[3] and we guided on the brighter component. On December 24 we started a series of exposures at the Cassegrain focus, in order to cover the ultraviolet and visual regions. By that time the comet had faded to about the sixth magnitude; and, since the exposure could not exceed 90 minutes under the best conditions, only fairly low dispersions could

* *Contributions from the McDonald Observatory, University of Texas*, No. 157.

[1] It has been recognized that observations of comet spectra in the red and the infrared are especially desirable (see N. T. Bobrovnikoff, *Rev. Mod. Phys.*, **14**, 164, 1942, at 172; P. Swings, *M.N.*, ~~**86**, 103~~, 1943, at 109).

[2] At that time the comet was no longer extremely bright; its visual magnitude was about 3–4.

[3] The duplicity of the nucleus was discovered on December 10, by W. H. van den Bos, at the Union Observatory, Johannesburg, South Africa. We observed it independently on December 19.

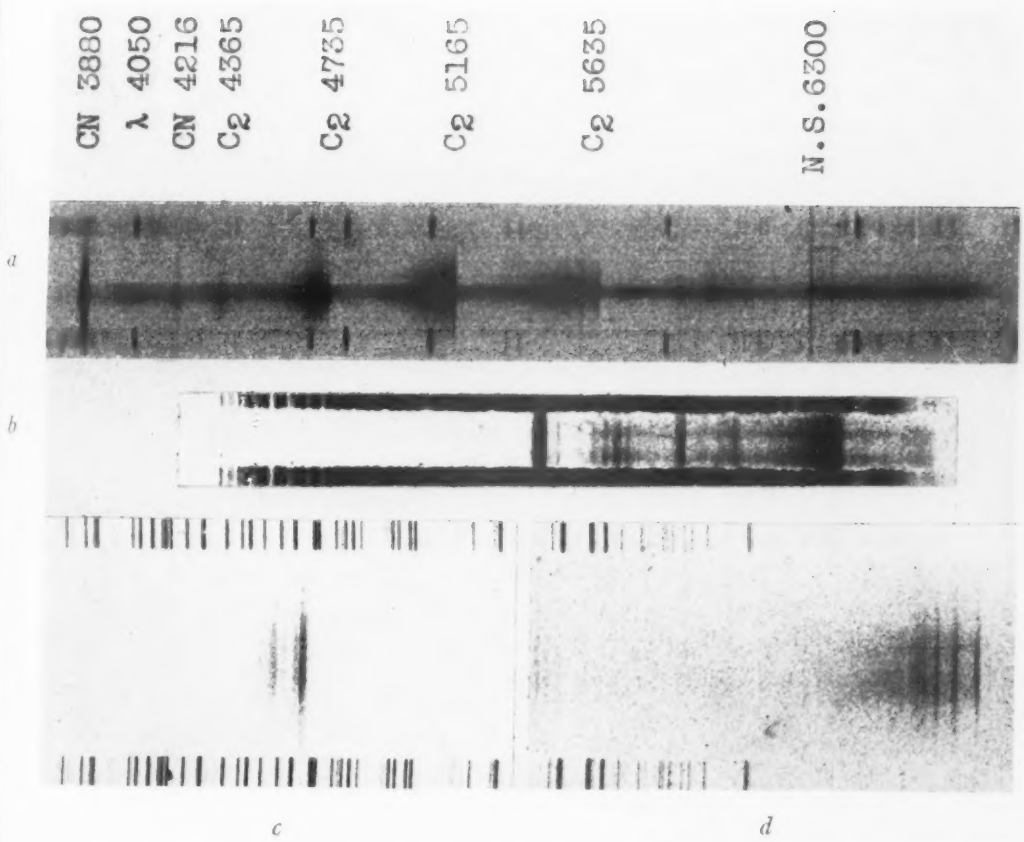

FIG. 1.—The spectrum of Comet 1947n. *a*) Grating spectrogram of 1947, December 20.054 U.T. *b*) Quartz-prism spectrogram of 1948, January 04.065 U.T., showing spectra of two components. *c*) Glass-prism spectrogram of 1947, December 27.065 U.T., showing structure of *CN* (0, 0) band near λ 3880. *d*)Glass-prism spectrogram of December 27.065 U.T., showing structure of C_2 ($\Delta v = +1$) bands near λ 4735.

be used. On all the exposures after December 23, the slit was placed in the position angle of the two components of the nucleus, hence revealing the spectra of both these components (Fig. 1, *b*). The list of observations, including the essential optical data, is given in Table 1.

Except for the difference in total intensity, the spectra of the components are practically identical. The separation between the two spectra is well marked in the case of bands such as those of CH, CH_2, and NH_2, which are concentrated close to the nucleus. On the other hand, the bands of CN, C_2, and NH, which always extend far into the head, show only an inconspicuous intensity drop between the two nuclei. As far as can be ascertained by visual examination of the spectrograms, not only are the relative intensi-

TABLE 1

SPECTROGRAMS OF COMET 1947n OBTAINED AT THE MCDONALD OBSERVATORY

U.T. Date*	Heliocentric Distance (r)	Dispersion in A/mm at			Projected Slit Width at			Eastman Emulsion	Quality of Spectrogram
		λ 3880	λ 6300	λ 8000	λ 3880	λ 6300	λ 8000		
1947, Dec.									
15.049	0.504 A.U.	.....	.....	320	.....	.....	28 A	IN†	Good in I.R.
16.050	0.534	.....	.....	320	.....	.....	28	IN†	Fair; sky strong
18.058	0.594	410	339	.....	7.1 A	5.9 A	.....	103*a*-F†	Good
19.054	0.622	.....	.....	320	.....	.....	21	IN†	Good in I.R.
20.054	0.649	410	339	.....	14	12	.....	103*a*-F†	Good
21.054	0.676	.....	.....	320	.....	.....	45	IN†	Weak (clouds)
22.052	0.703	.....	.....	320	.....	.....	34	IN†	Weak (clouds)
24.062‡	0.757	(130)§	.....	.....	(2.3)§	.....	.....	103*a*-O	Good in U.V.
25.06‡	0.782	115	.....	.....	2.7	.....	.....	103*a*-O	Good
26.06‡	0.807	46	.....	.....	0.83	.....	.....	103*a*-O	Good at λ 3880
27.065‡	0.832	46	.....	.....	0.83	.....	.....	103*a*-O	Very good
1948, Jan.									
02.06‡	0.976	91	610	.....	2.0	13.7	.....	103*a*-F†	Fair
04.065‡	1.022	222	.....	.....	4.0	.....	.....	103*a*-O	Fair
06.065‡	1.068	.....	610	.....	.....	11.0	.....	103*a*-F†	Good
09.06‡	1.135	.....	610	.....	.....	13.7	.....	103*a*-F†	Poor

* Two spectrograms on IM emulsion, exposed on December 17.052 and 23.061, were too weak and did not show any infrared emission.

† The emulsion was hypersensitized in ammonia.

‡ After December 24, all spectrograms were taken with the slit across both components of the comet.

§ At λ 3370.

ties of the different bands (NH, CN, CH_2, CH, C_2, NH_2) the same in both components, but also the rotational intensity distributions within the individual bands are identical. On all exposures begun late enough to avoid twilight the solar spectrum is extremely weak.

The absolute magnitude of Comet 1947n is approximately[4] $M = 6.2$. Since absolute magnitudes of comets have been observed from 0 to 15,[5] the present object should be considered of average luminosity.

ULTRAVIOLET AND VIOLET REGION OF THE SPECTRUM

The OH band near λ 3090 is extremely weak. In fact, it is much weaker, relative to NH, than in Comet Cunningham, 1941 I, which was observed at the McDonald Observatory under nearly the same conditions of heliocentric distance, zenith distance, season,

[4] L. E. Cunningham, *Pub. A.S.P.*, **60**, 27, 1948.

[5] B. A. Vorontsov-Velyaminov, *A.J. Soviet Union*, **22**, 317, 1945.

weather, and instrument. Of the seven comets for which ultraviolet spectrograms have been obtained at the McDonald Observatory, only Comet de Kock–Paraskevopoulos, 1941 IV, observed at heliocentric distance 0.9 A.U., reveals such weak *OH* emission relative to *NH*. Comet 1941 IV is the only comet, besides 1947n, which was observed after perihelion passage. However, its perihelion distance ($q = 0.79$ A.U.) was large compared with that of 1947n ($q = 0.1$ A.U.).

The (0, 0) band of *NH*, transition $^3\Pi \rightarrow {}^3\Sigma$ near λ 3360, shows strongly. It is not so well resolved as in Comet 1941 I. Four components appear, as indicated in Table 2.

The (1, 0) band of *CN*, transition $^2\Sigma \rightarrow {}^2\Sigma$ near λ 3580, is too weak to show any structure. The (0, 0) band of *CN*, near λ 3880, was obtained with a projected slit width of 0.83 A (Fig. 1, *c*). Since the intervals between successive lines of the *R* branch are about 0.7–0.8 A, the present resolution is unable to bring out completely the individual lines of the *R* branch, as McKellar succeeded in doing for Comet 1943 I.[6] The profile of the

TABLE 2

NH LINES IN COMET 1947n

λ*	Int.	Identification	λ*	Int.	Identification
3349.6	1	$R_2(1)$	3365.0	1	$P_2(2)$
3353.7	2	$R_2(0)+R_1(1)$	3369.3	1	$P_1(2)$
3358.1	10	$R_1(0)+Q_2(2)$			

* From micrometer measures on spectrograms and from measurement of separate microphotometer tracings of the brighter and fainter components of the comet.

(0, 0) band presents the same type of complexity as that observed previously. On the spectrogram of December 27.065, sharp maxima are observed at:

P branch: λ 3876.9 (int. 18); λ 3877.6 (20); λ 3879.9 (40); λ 3881.4 (30);
R branch: λ 3872.8 (6); λ 3871.9 (5); λ 3868.9 (20); λ 3867.4 (15); λ 3865.0 (6); λ 3862.8 (5); λ 3862.1 (4)

and sharp minima at:

P branch: λ 3878.7 (15)
R branch: λ 3871.3 (2); λ 3865.6 (4); λ 3864.0 (2).

This profile may be explained, as in previously published cases,[7] by the influence of the solar absorption lines on the resonance fluorescence spectrum excited by the solar radiation in the *CN* molecules of the comet. Owing to the peculiar rotational intensity distribution, several sharp peaks observed in the *R* branch (for example, λ 3865.0) are actually individual rotational lines.

The measurements of the spectrograms of December 27.06 and December 26.06 are in good agreement. On a spectrogram of lower resolution obtained on December 25.06, the *R* branch appears to extend to λ 3847, maxima being observed on a tracing at λλ 3859.7, 3854.2, and 3850.6, beyond the limits found on December 26 and 27. These maxima can barely be recognized on the original film.

Nothing unusual appears in the "λ 4050 group,"[8] the (0, 1) band of *CN* near λ 4216, the *CH* lines near λ 4313, and the C_2 sequence near λ 4382.

[6] *Ap. J.*, **99**, 162, 1944.

[7] P. Swings, *Lick Obs. Bull.*, **19**, 131, 1941, and *M.N.*, **103**, 86, 1943; A. McKellar, *Rev. Mod. Phys.*, **14**, 179, 1942, and *Ap. J.*, **99**, 162, 1944.

[8] Tentatively identified as CH_2 by G. Herzberg, *Ap. J.*, **96**, 314, 1942.

VISUAL REGION OF THE SPECTRUM

The best material from λ 4400 to λ 6700 is provided by the two grating spectrograms of December 18 and 20 and by the glass-prism spectrogram of December 27; however, the latter extends only to approximately λ 5000.

Interesting features are observed on the glass-prism spectrogram of December 27 in the region of the $\Delta v = +1$ Swan bands (projected slit width at λ 4700: 1.87 A; see Fig. 1, *d*). These features are listed in Table 3. The measured wave lengths are those of intensity maxima, not of edges; hence they have not been corrected for projected slit width.

The maxima observed between the main Swan bands have, for the most part, been mentioned previously,[9] although possibly not so completely as in Table 3. It may be significant that the two doublets, λλ 4708.8–4704.0 and λλ 4692.6–4687.7, have practically the same separation. The weak feature at λ 4742.9 is distant from the (1, 0) band, λ 4734.9, by the amount expected for the (1, 0) band of $C_{12}C_{13}$; it is probably a faint isotopic carbon band.

TABLE 3

FEATURES IN THE REGION λλ 4665–4750

λ	Int.	Identification	λ	Int.	Identification
4669.5	8	$?C_2(6,5)$	4708.8	10	.....
4676.2	15	$C_2(5,4)$	4713.2	30	$C_2(2,1)$
4682.7	15	$C_2(4,3)$	4719.0	3	.....
4687.7	8	.....	4728.1	3	.....
4692.6	10	.....	4734.9	20	$C_2(1,0)$
4695.5	25	$C_2(3,2)$	4742.9	1	$?C_{12}C_{13}(1,0)?$
4704.0	5	.....	4746.4	2	.....

On the two grating spectrograms of December 18 and 20, the Swan bands are very intense, and emission features are observed to the violet of λ 4670. Those extending from λ 4504 to λ 4662 may be found in Table 4, in which the measurements of the two grating spectrograms have been tabulated. However, Table 4 does not contain the region λλ 4670–4746, which is better represented on the prism spectrogram (wave lengths in Table 3). Table 4 shows that emission features appear in addition to the usual Swan bands, violetward of (2, 2); between (0, 0) and (1, 1), (2, 3) and (3, 4), and (3, 4) and (4, 5).

It is not clear at present whether the origin of these fairly sharp features in the region of the Swan bands is due to some emission by an as yet unidentified molecule[10] or whether some effect of the solar absorption lines on the fluorescence excitation is responsible. For example, abnormal emission features between the (1, 0) and (2, 1) bands could be due to an abnormal distribution among the rotational levels of the $v' = 1$ state. This state is reached by absorption of solar radiation within the (1, 0) λ 4737, (1, 1) λ 5129, and (1, 2) λ 5586 bands. While solar absorption lines are not so numerous in these three regions as in the λ 3880 region of *CN*, they may be able to affect appreciably the profile of the Swan bands. It would be interesting to draw the synthetic profiles, in order to separate the emissions due to the excitation mechanism from those due to molecules other than C_2.

[9] See N. T. Bobrovnikoff, *Ap. J.*, **99**, 173, 1944, Pl. VI and Table 1, and *Pub. Lick Obs.*, **17**, 436, 1931; A. McKellar, *Rev. Mod. Phys.*, **14**, 179, 1942, Fig. 7, and *Ap. J.*, **99**, 162, 1944.

[10] Nothing is known of the spectra of NH^+, CN^+, and C_2^+, which may be present in comets.

TABLE 4*

EMISSION LINES IN COMET 1947n, λ>4400

Comet 1947n						Adopted λ	Earlier Measures McD. and Mt.W.	Victoria Measures	Comet 1911 V	Nuclear Features	Comets 1910 II and 1941 I	Lyon Measures	Identification
Dec. 18.058			Dec. 20.054										
I (1)	*l* (2)	λ (3)	I (4)	*l* (5)	λ (6)	(7)	(8)	(9)	(10)	(11)	(12)	(13)	(14)
1	5	4414.6	2	20n	19.0	4416.8	19.2	.....	.....	12.–21.	13.3	.....	.....
			1	20s	84.5	4484.5	74.8–86.0 –96.8	85.6	.....	77.–86.	85.	.....	.....
1	10	4503.	1	20n	04.7	4504.	10.6	.....	.....	.....	.....	.....	NH_2?
1	25	4541.	.....	.....	.....	4541.	40.8	42.3	47.(tail)	.....	.....	.....	NH_2
1	25	4573.	1	20	67.5	4570.2	75.0	.....	72.(tail)	.....	69.	.....	CN (0, 2)?†
			1	20	85.9	4585.9	89.1	89.1	.....	.....	90.	.....	CN (0, 2)?†
2	30	4597.	1	20	98.7	4598.	03.6	.....	.....	.....	.....	.....	.....
			1	20	12.9	4612.9	07.3–17.0	08.1–15.0	08.	14.	07.4	.....	CN (0, 2)
2	40	4625.1	2	40	32.3	4628.7	29.8	.....	.....	31.	.....	.....	.....
2	50	4645.	2	50	53.7	4645.	.....	.....	.....	45.6	46.8	.....	.....
3	60	4662.2				4662.2	.....	.....	60.	61.3	60.7	.....	C_2(6, 5)?
			0.5	20n	91.	4791.	.....	.....	.....	91.9	.....	85.2–94.6	NH_2?
1	10n	4841.5	1	20n	37.2	4839.4	38.9	36.3	37.8	40.4	.....	38.8	NH_2 plus C_2
1	10	4868.1	1	20n	76.6	4872.4	68.2–76.0	.....	.....	74.–79.5	73.0	68.2–75.3	NH_2
1	10	4898.2	.....	.....	.....	4898.2	.....	.....	.....	.....	.....	.....	.....
1	10	4925.6	2	20n	23.0	4924.3	25.7	.....	25.5	28.5	.....	25.9	NH_2
2	10	4997.	.....	.....	.....	4997.	.....	.....	.....	.....	.....	.....	.....
0.5	50n	4997.	.....	.....	.....	4997.	.....	.....	.....	.....	.....	.....	.....
.....	.....	.....	3‡	20s	07.6	5007.6	07.0	.....	.....	08.	.....	07.1	.....
.....	.....	.....	3‡	20s	29.0	5029.0	.....	.....	.....	33.0	.....	.....	.....
.....	.....	.....	2‡	50	54.4	5054.4	.....	.....	.....	50.9	.....	.....	.....
.....	.....	.....	2‡	60n	69.	5069.	.....	.....	.....	.....	?81.2	.....	.....
4	50	5097.6	2	60s	97.0	5097.3	.....	.....	94.	.....	01.4	.....	C_2(2, 2)
5	70	5130.2	3	70	26.2	5128.2	.....	.....	28.0	.....	27.1	.....	C_2(1, 1)
.....	.....	.....	1	60	44.0	5144.0	.....	.....	.....	.....	.....	.....	C_2(0, 0)§
8	100s	5167.4	5	100	62.4	5164.9	.....	.....	64.0	.....	67.4	.....	C_2(0, 0)
.....	.....	.....	1	20s	82.4	5182.4	86.5	.....	78.	78.	.....	.....	.....
.....	.....	.....	1	20s	01.1	5201.1	.....	.....	.....	.....	.....	.....	.....
.....	.....	.....	1	20n	49.1	5249.1	43.1–59.0	.....	.....	.....	.....	43.1–58.9	NH_2
.....	.....	.....	1	20n	83.7	5283.7	83.5	.....	.....	.....	.....	.....	.....
.....	.....	.....	1	30	16.0	5316.0	18.5	.....	.....	.....	.....	19.2	N_2?
.....	.....	.....	1	40	32.7	5332.7	36.5	.....	.....	.....	.....	31.0	N_2?
1	20n	5349.9	1	40n	53.2	5351.6	55.3	.....	.....	.....	.....	54.4	.....

TABLE 4—*Continued*

.....	.....	.....	1	30	16.0	5316.0	18.3	.....	.....	.....	.....	31.0	N_2?
.....	.....	.....	1	40	32.7	5332.7	36.5	.....	.....	.....	.....	54.4	.....
1.....	20n	5349.9	1	40n	53.2	5351.6	55.3	.....	.....	.....	.....		

TABLE 4—*Continued*

Comet 1947n							Earlier Measures McD. and Mt.W.	Victoria Measures	Comet 1911 V	Nuclear Features	Comets 1910 II and 1941 I	Lyon Measures	Identification
Dec. 18.058			Dec. 20.054			Adopted λ							
I (1)	*l* (2)	λ (3)	I (4)	*l* (5)	λ (6)	(7)	(8)	(9)	(10)	(11)	(12)	(13)	(14)
1.....	20n	5379.9	1	20s	82.2	5381.1	86.4	.....	.....	.....	.....	85.9	NH_2
0.5...	15s	5416.9	.....	.....	.....	5416.9	18.3	.....	18.5	18.5	.....	18.2	NH_2
1.....	40s	5429.1	1	30s	26.8	5427.9	28.0	.....	28.3	.....	.....	27.7	NH_2‖
1.....	30s	5445.6	1	40s	42.7	5444.2	45.0	.....	.....	.....	.....	49.7	NH_2‖
1.....	30	5464.2	2	50s	68.2	5466.2	.....	.....	70.	.....	.....	.....	C_2(4, 5)
1.....	30	5478.8	1	50s	87.3	5483.1	.....	.....	.....	.....	.....	.....	C_2§
2.....	50	5498.3	2	60s	99.5	5498.9	.....	.....	.....	.....	.....	.....	C_2(3, 4)
1.....	40	5519.2	1	50s	18.0	5518.6	.....	.....	.....	.....	?05.8	.....	C_2 plus NH_2?§
3.....	50	5538.8	2	60s	38.3	5538.5	.....	.....	40.0	.....	39.4	.....	C_2(2, 3)
4.....	60	5582.8	3	100	81.8	5582.3	.....	.....	84.8	.....	89.5	.....	C_2(1, 2)
4.....	50	5634.5	4	80	33.8	5634.1	.....	.....	34.8	.....	39.3	.....	C_2(0, 1)
.....	.....	.....	1	20s	79.0	5679.0	87.1	94.6	92.5	92.5	.....	88.–96.3	NH_2
2.....	15n	5702.7	2	30s	01.7	5702.2	01.5	04.0	05.	05.	.....	08.2	NH_2
1.....	15n	5732.8	2	20n	32.2	5732.5	31.2–39.6	31.4	32.	32.	.....	?42.7	NH_2?
.....	.....	.....	1	10s	97.8	5797.8	05.0	.....	.....	.....	.....	04.	NH_2?
.....	.....	.....	1	10s	17.4	5817.4	.....	.....	.....	.....	.....	.....	NH_2?
.....	.....	.....	1	10s	36.2	5836.2	.....	.....	.....	.....	.....	.....	.....
.....	.....	.....	1	10s	68.9	5868.9	.....	.....	.....	.....	.....	.....	NH_2
2.....	20n	5888.8	3	30n	90.4	5889.6	92.8	88.3	(*Na*)	.....	.....	92.5	*Na* plus NH_2
.....	.....	.....	1	30s	33.4	5933.4	.....	.....	.....	.....	.....	.....	NH_2
.....	.....	.....	1	40s	59.6	5959.6	49.	.....	.....	.....	.....	.....	NH_2 plus C_2(4, 6)
2.....	15s	5973.2	2	40s	76.6	5974.9	77.7	76.6	77.	77.	72.	77.4	NH_2
1.....	15s	5990.2	.....	.....	.....	5990.2	.....	.....	94.	94.	92.	93.4	NH_2?
0.5...	15s	5999.8	2	40s	96.1	5998.0	96.0	95.8	.....	.....	.....	.....	NH_2 plus C_2(3, 5)
1.....	15s	6015.8	1	40s	18.6	6017.2	19.4	13.1–20.2	20.5	20.5	.....	19.8	NH_2
0.5...	15s	6034.0	1	20s	33.6	6033.8	36.9	36.5	.....	.....	.....	31.4	NH_2
1.....	15s	6052.6	1	20s	56.1	6054.4	53.5	59.5	.....	.....	.....	.....	NH_2 plus C_2(2, 4)
1.....	15s	6092.9	2	30s	96.6	6094.8	98.7	96.9	.....	.....	.....	99.4	NH_2
1.....	15s	6106.6	.....	.....	.....	6106.6	10.3	10.0	.....	.....	.....	.....	NH_2
1.....	15s	6116.7	2	30s	19.2	6118.0	20.9	20.9	.....	.....	.....	.....	NH_2 plus C_2(1, 3)
1.....	15n	6157.1	.....	.....	.....	6157.1	48.6–70.6	47.6	.....	.....	.....	.....	NH_2
1.....	15n	6185.9	1	60?	87.2	6186.5	.....	84.8	.....	.....	.....	.....	NH_2 plus C_2(0, 2)
3.....	¶	6296.1	3	¶	98.4	6297.3	98.0	00.7	00.	00.	.....	98.8	NH_2
0.5...	20n	6327.	2	30s	31.9	6329.5	33.2	35.2	.....	.....	20.	29.4	NH_2
.....	.....	.....	2	50	45.2	6345.2	45.6	45.7	.....	.....	.....	45.4	NH_2**
1.....	¶n	6359.	1	¶	62.1	6360.6	64.1	64.3	.....	.....	.....	54.	NH_2

TABLE 4—*Continued*

Comet 1947n							Earlier Measures McD. and Mt.W.	Victoria Measures	Comet 1911 V	Nuclear Features	Comets 1910 II and 1941 I	Lyon Measures	Identification
Dec. 18.058			Dec. 20.054			Adopted λ							
I (1)	*l* (2)	λ (3)	I (4)	*l* (5)	λ (6)	(7)	(8)	(9)	(10)	(11)	(12)	(13)	(14)
2.....	50n	6541.1	1	20n	36.	6538.6	46.	.....	.....	.....	29.	39.7	NH_2††
2.....	50s	6556.4	1	20	57.6	6557.0	.....	.....	.....	.....	.....	59.5	NH_2
2.....	50n	6571.9	.....	.....	.....	6571.9	.....	.....	.....	.....	.....	79.8	NH_2
1.....	40n	6583.9	2	20	76.8	6580.3	81.	79.5	78.	78.	.....		NH_2
2.....	30n	6594.7	2	30	98.3	6596.5	98.	97.0	98.	98.	.....	.....	NH_2††
3.....	15s	6614.1	3	40	17.0	6615.6	22.	19.8	19.	19.	.....	.....	NH_2
1.....	30s	6636.5	2	20	37.3	6636.9	42.	41.6	.....	.....	35.	.....	NH_2
1.....	15s	6668.1	2	20n	72.	6670.	.....	74.6	.....	.....	77.	.....	NH_2††
2.....	5s	6722.1	.....	.....	.....	6722.1	.....	.....	.....	.....	.....	.....	NH_2
2.....	10s	6748.8	2	20n	48.6	6748.7	.....	.....	.....	.....	.....	.....	NH_2
2.....	7s	6762.1	.....	.....	.....	6762.1	.....	.....	.....	.....	.....	.....	NH_2

* The columns list the following:
1 and 4 are intensity estimates on a scale from 0 to 5.
2 and 5 are estimated lengths of lines, in seconds of arc, together with a description: "s" = sharp, "n" = broad.
3 and 6 are measured wave lengths, corrected for radial velocity and line curvature.
7 contains the means of wave lengths in cols. 3 and 6.
8 contains mean values of earlier measurements made at the McDonald and Mt. Wilson observatories on spectra of the following: Comet Cunningham, 1941 I (P. Swings, *Ap. J.*, **98,** 142, 1943, and unpublished), Comet 1943 I (R. Minkowski, *Ap. J.*, **98,** 142, 1943; and P. Swings and O. Struve, *Pub. A.S.P.*, **55,** 150, 1943), Comet Peltier, 1936 II (W. Baade and R. Minkowski, *Pub. A.S.P.*, **48,** 227, 1936), Comet Finsler, 1937 V (R. Minkowski, *Pub. A.S.P.*, **49,** 276, 1937). For the region λλ 4419–4839, only the unpublished measurements of Comet 1941 I by P. Swings are listed.
9 contains mean values of measurements made at Victoria in the spectra of Comet Cunningham, 1941 I (A. McKellar, *Ap. J.* **98,** 142, 1943), Comet 1943 I (*ibid.*, and *Ap. J.*, **99,** 162, 1944).
10 contains wave lengths measured in the spectrum of Comet Brooks, 1911 V, by W. H. Wright, *Lick Obs. Bull.*, **7,** 8, 1912.
11 contains mean wave lengths of nuclear emissions, measured or compiled by F. Baldet, *Ann. Obs. Astr. Phys. Paris*, **7,** 1926. (Many of Baldet's features were taken from Wright's list of lines in Comet Brooks.)
12 contains the means of wave lengths measured in the spectra of Comet Halley, 1910 II, and Comet Cunningham, 1941 I (N. T. Bobrovnikoff, *Pub. Lick Obs.*, **17,** 309, 1930; and *Ap. J.*, **99,** 173, 1944).
13 contains the means of wave lengths measured in the spectra of Comet Peltier, 1936 II, Comet Encke, 1937 VI, Comet Finsler, 1937 V, Comet 1943 I, and Comet 1939 III by J. Dufay, *C.R.*, **222,** 51, 1946.
14 contains identifications. For the wave lengths of the NH_2 lines see P. Swings, A. McKellar, and R. Minkowski, *Ap. J.*, **98,** 142, Table 3, 1942.

† Feature in *R* branch.
‡ Complex structure.
§ Feature in Swan bands.
‖ Identification not satisfactory, since the cometary line is long.
¶ Estimation of length impossible because of night sky line.
** Doubtful minor contribution from *CN* (red system).
†† Possible minor contribution from C_2.

It is possible but not probable that some of the faint features listed in Table 4 are spurious. Although the blue region may not be so well resolved as on previously investigated prism spectrograms, the measured wave lengths agree well with earlier results. Since the projected slit widths are 7 A and 14 A, respectively, the resolution is limited. However, in the red region the resolution is better than in most lists of wave lengths previously published.

Besides C_2, the only certain identification in the red region is that of the a band of ammonia, presumably due to NH_2. It is interesting to note that, except for weak and doubtful C_2 contributions, the whole region $\lambda > 6000$ appears due to NH_2. A laboratory analysis of the NH_2 spectrum is urgently needed.

Table 4 reveals a certain number of emissions still unidentified. A systematic examination reveals coincidences with the spectra[11] of NO, NO_2, Na_2, O_2^+, formaldehyde, benzene derivatives, and various oxides, for example, CaO and MgO. However, it is felt that these coincidences may be accidental. It is planned to extend this work in the visual region with the same spectrograph to other comets; such material has recently been secured for Comet Bester (1947k). Table 4 differs appreciably from previously published lists, such as the one by Swings, McKellar, and Minkowski.[11] It is noted that most of the lines listed by these authors above λ 6300, and not present in our Table 4, are unidentified features; this points toward the presence of some as yet unidentified compound. Since Table 4 applies to small heliocentric distances, differences should be expected from the table by Swings, McKellar, and Minkowski, which combines observations at both small and large heliocentric distances.

Special attention was given to possible identifications of NH_3, HCN, and C_2H_2, which were expected as parent molecules and possibly as the source of the infrared bands. Ammonia has a weak vibration rotation band $5\nu_1$, with a maximum near λ 6440. Lists of individual lines have been published by R. M. Badger[12] and by S. H. Chao.[13] A comparison shows that these lines are absent from Comet 1947n.[14] Hydrogen cyanide and acetylene, which also have vibration rotation bands in the red region, lead to the same conclusion. The result of this simple comparison is confirmed by synthetic low-temperature profiles[15] for the red bands of NH_3, HCN, and C_2H_2.

INFRARED REGION OF THE SPECTRUM

When no red filter is interposed, the spectrograms on IN emulsion show the second order of the CN band at λ 3880 in addition to the emissions at λ 7906 and λ 8106. This second-order band appears less intense than λ 7906. Yet the IN emulsion is very sensitive to violet light—in fact, more sensitive than to λ 8000.[16] This indicates that the

[11] Striking coincidences with the O_2^+ bands (0, 1) and (0, 0) and (2, 0) at low temperatures are found in the list of lines of the visual region compiled by Swings, McKellar, and Minkowski (*Ap. J.*, **98**, 142, Table 3, 1943).

[12] *Phys. Rev.*, **35**, 1038, 1930.

[13] *Phys. Rev.*, **50**, 27, 1936.

[14] Some coincidences are found in the comets 1941 I and 1943 I, but they are not sufficient to warrant an identification.

[15] These synthetic profiles, as well as those for the molecules considered in the next section, were kindly drawn by Dr. J. Hunaerts, of Uccle.

[16] Three other factors affect this ratio: the grating efficiency, the dispersion, and the transmission of the UV glass block in the Schmidt camera. Calculations from the Rowland formula (*Phil. Mag.*, **5–35**, 397, 1893) show that the grating efficiency in the first-order spectrum should be very closely the same at λ 3880 and at λ 7900 but that the second-order λ 3880 should be reduced to one-fifth of its normal intensity relative to the first-order λ 7900. Deviations from the theoretical formula might increase this factor to one-fourth. The dispersion in the second order is twice that in the first-order spectrum. The transmission of the UV glass at λ 3880 is over eight-tenths of that at λ 7900. The IN emulsion is about one-sixteenth as fast at λ 7900 as it is at λ 3880, but hypersensitization increases this to about one-third.

** Doubtful minor contribution from CN (red system).
†† Possible minor contribution from C_3.

radiations at λ 7906 and λ 8106 are actually very strong, comparable in intensity with the strongest violet emission, that of *CN*.

Only λ 7906 and λ 8106 are considered in this paper. There may be other, much weaker emissions near λλ 7088, 7381, 8242, and 8783; but these are uncertain and should be confirmed before identifications are attempted.[17]

The λ 7906 emission is stronger than λ 8106 by a factor of 2 or 3. The blue edge of the λ 7906 band is around λ 7858, and the red edge near λ 7957. In addition to a strong sharp peak at λ 7906, there is a secondary shallower maximum in the blue wing, near λ 7876. The emission centered at λ 8106 appears shallower than at λ 7906; it extends from λ 8046 to λ 8164 and does not reveal any structure. However, this lack of structure may be only apparent, resulting from the weakness of the emission and the wide slit employed.

The identification of the two infrared emissions is fraught with difficulties, one reason being the low resolution used and the other the scarcity of laboratory information in this region. Attention has been given to polyatomic, as well as to diatomic, molecules.

IDENTIFICATION WITH POLYATOMIC MOLECULES

The wave length λ 7906 is near the maximum of a vibration rotation band of NH_3, which is very prominent in absorption in the spectrum of Jupiter.[18] Further, NH and NH_2 are strong in Comet 1947n, and we may expect that these radicals result from the photodissociation of ammonia, which, being a chemically stable compound, may be present as a solid or an occluded gas in the meteorites forming the cometary solid nucleus. The λ 7906 band is concentrated close to the nucleus, as are the identified polyatomic molecules CH_2 and NH_2. Moreover, the NH_3 band should have a secondary maximum on the blue side of the main peak. For these various reasons, the identification with ammonia appeared promising. A synthetic low-temperature profile cannot be accurately computed, since the individual lines of the NH_3 band have not yet been classified, doubtless because of the complexity of the band, which is a superposition of several vibrational transitions. Rough sketches of the synthetic profile, based on laboratory and theoretical intensities, show a principal maximum near λ 7914, with a secondary peak near λ 7950 and a much lower (probably unobservable) maximum in the red wing. Considering the absence of data on the rotational temperature of the NH_3 molecules, the identification of the observed profile of λ 7906 with the synthetic profile of the NH_3 band seemed a possibility.

However, Dr. G. Herzberg[19] has raised a serious objection. The absorption intensity of the NH_3 band near λ 7910 is so small that it would be surprising to find the band in

---

Combining these factors with the approximate intensity ratio from the IN spectrograms, we estimate that the intensity per angstrom at λ 7900 is equal to that in the *CN* 3880 band within a factor of 2.

As a check, the intensities of 103*a*-F films and IN films can be compared very roughly, the latter having about one-tenth as great sensitivity at λ 3880. The IN exposure times and slit widths (combined) were three times larger than those used on 103*a*-F, yet the recorded intensity of λ 3880 on 103*a*-F is about ten times that of λ 7900 on IN. Combining these factors with the dispersions, we find again that the intensity per angstrom at λ 7900 is very nearly equal to that at λ 3800. The total intensity of the λ 7906 band, extending over 100 A, must therefore be greater than that of *CN* 3880, which extends over 30 A or less.

[17] It is often stated that one should expect to find the resonance doublet of potassium λλ 7665–7699, when the comet is close enough to the sun to reveal the D line of sodium, as the boiling-point of *K* is only 762° C, against 877° C for *Na*. There is no trace of the potassium doublet on our infrared spectrograms taken at heliocentric distance 0.5. However, this may be due to the relatively low sensitivity of the IN emulsion. Atmospheric absorption would not affect λ 7699 appreciably and would decrease the intensity of λ 7665 only moderately.

[18] For a good reproduction of this NH_3 band see T. Dunham, Jr., *Pub. A.S.P.*, **51**, 269, Pl. XXXI, 1939.

[19] Private communication.

emission when there are much stronger absorption bands in the ultraviolet that would lead to photodissociation. This objection applies to any vibration rotation band likely to appear in this spectral region, including other possibilities discussed below.

Hydrogen cyanide, *HCN*, has also a vibration rotation band in the λ 7900 region.[20] However, this identification is not plausible. The synthetic profile—which, unlike that of NH_3, may be computed with a fair amount of confidence—has a primary peak near λ 7897 and a secondary one in the red wing near λ 7930; this is quite different from the observed profile. Moreover, another band of *HCN* near λ 8563 is not observed in the comet. It is true that this other band should be weaker than that near λ 7900, but an emission three or four times weaker than the observed one at λ 7906 could have been detected.

Other polyatomic molecules having bands near λ 7900 are acetylene (C_2H_2, strong band) and carbon dioxide (CO_2, weak band), but their synthetic profiles do not agree with the observed one. Moreover, Herzberg's objection applies to these molecules as well as to NH_3 and *HCN*.

IDENTIFICATION WITH DIATOMIC MOLECULES

Two molecules present themselves for possible identification, C_2 and *CN*. Herzberg and Phillips have recently found[21] a new system of C_2, which is a $^1\Pi_u \rightarrow {}^1\Sigma_g^+$ transition, between the lower levels of the $^1\Pi \rightarrow {}^1\Pi$ Deslandres-d'Azambuja system and the $^1\Sigma \rightarrow {}^1\Sigma$ Mulliken system. In the region considered here, four bands are present, the wave lengths of their heads being λ 7715, (3, 0), int. 5; λ 7908, (4, 1), int. 3; λ 8108, (5, 2), int. 1; and λ 8751, (2, 0), int. 10. These bands are degraded to the red. The coincidences of the (4, 1) and (5, 2) wave lengths with λ 7906 and λ 8106 are striking.

However, there are several reasons why the cometary bands could not belong to the new system of C_2. The IN emulsion is sensitive up to λ 8800 (the comparison line λ 8781 of *Ne* appears strongly); yet there is no trace of cometary emission near λ 8751, where the strongest band of the new C_2 system should be found. The comet emission λ 7906 is two or three times stronger than λ 8106. Yet no trace of emission near λ 7715 appears,[22] although one would expect the (3, 0) transition to be stronger than (4, 1) and (5, 2) in the $\Delta v = 3$ sequence, unless extremely improbable, peculiar excitation conditions prevail. The Swan systems of C_2 show the same intensity distribution in comets as they do in the laboratory. It would seem probable that this would also be true for the new C_2 bands. However, there is no trace of degradation toward the red for λ 7906 and λ 8106 in the comet.

It should be noted that the solar spectrum is very poor in absorption lines near λλ 7715, 7908, 8108, and 8750, so that the fluorescence spectrum should not be distorted if the exciting process of absorption takes place in the singlet system of C_2. A fluorescence excitation of the new system (singlet states) would be weak compared with the Swan bands (triplet states). If the primary absorption of solar radiation takes place in the new system, it affects only molecules which are in an excited state. It is true that the latter would be metastable; yet the population in it would be lower than in the ground state. If the primary absorption takes place from the ground state, one would expect the intercombination transition to have a low probability.

Finally, the infrared emission is concentrated near the nucleus, while the Swan bands of C_2 extend far into the head. All these reasons seem to rule out C_2.

The other diatomic molecule which should be considered is *CN*, whose red system has

[20] R. M. Badger and J. L. Binder, *Phys. Rev.*, **37**, 800, 1931.

[21] Communicated at the meeting of the A.A.S., December, 1947.

[22] The atmospheric *A* band does not absorb appreciably at this wave length.

its (2, 0) and (3, 1) transitions[23] in the regions of λ 7900 and λ 8100. The (2, 0) band has an R_2 head at λ 7874 and three other heads (R_1 and Q_1 being stronger than R_2) at longer wave lengths, so that a profile with maximum near λ 7906 is plausible. Similarly, the (3, 1) transition could have a maximum near λ 8106.

A synthetic profile of the red *CN* bands $\Delta v = +2$ has been prepared by Dr. Hunaerts for $T = 430°$ K. A sharp primary maximum appears at λ 7910 and a shallow one at λ 7880. These two wave lengths agree reasonably well with the observed ones; the general appearance of the synthetic profile is also very similar to that of the observed band.

On the other hand, spectrograms of these *CN* bands have been obtained in the Yerkes Observatory laboratory with the help of Mr. Rao, with the same spectrograph and slit width as used in the observations of the comet. The laboratory profiles do not agree well with the cometary ones. In the comet the secondary (lower) maximum of the λ 7906 band occurs in the blue wing, while it is on the red side of the main peak in the laboratory spectrograms. The distance between the two maxima of the laboratory emission near λ 7900 is about 45 A, while it is only 30 A in the comet. However, there may be some effect of temperature on the rotational intensity distribution; this factor could also explain why the cometary bands are narrower than the laboratory ones.

The *f*-value of the (2, 0) transition is small.[24] If the red system of *CN* is excited by fluorescence only, as is the case for the blue system, we should expect the λ 7900 band to be very weak compared with λ 3880, while in the comet the infrared radiation is as strong or stronger. From the intensity behavior in the blue system it is known that most *CN* molecules in the ground state $^2\Sigma$ are in the vibrational level $v'' = 0$. To reach the level $v' = 2$ of $^2\Pi$ from $^2\Sigma$, therefore, requires absorption in the (2, 0) band of low *f*-value, if the cometary emission results from fluorescence excitation.

However, it is possible that the *CN* molecules in the excited $^2\Pi$ level are actually formed in the process of photodissociation of a parent-molecule. In this case it would not be surprising to find a fairly high population on the level $v' = 2$. It would also be understandable that the red system does not extend so far out into the head as does the blue system.

On the whole, it appears very probable that the observed bands are actually the (2, 0) and (3, 1) transitions of the red system of *CN*, the *CN* molecules being excited to the $^2\Pi$ level in a process of photodissociation of a parent-molecule.

Our thanks are due to Dr. G. Herzberg for helpful suggestions and discussions and to Dr. J. Hunaerts for drawing the synthetic profiles. We want to acknowledge especially the considerable amount of observational help given by Dr. Jose, at the McDonald Observatory.

[23] These bands were hitherto numbered (1, 0) and (2, 1). Herzberg and Phillips have recently shown (private communication) that the vibrational numbering in the upper state must be shifted upward by one unit, the (0, 0) band being actually at 1.05 μ.

[24] A. S. King and P. Swings, *Ap. J.*, **101**, 6, 1945. The recent work by Herzberg and Phillips shows that the (0, 0) band at 1.05 μ is very strong, so that the total *f*-value of the whole red system may be of the same order as that of the blue system. However, here we are interested only in the *f*-value of the (2, 0) transition.

NOTES

A NOTE ON THE SPECTRUM OF 27 CANIS MAJORIS

The spectrum of 27 Canis Majoris was photographed with the quartz Cassegrain spectrograph of the McDonald Observatory on December 1, 1947. Figure 1 shows the region centered on the line *He* I 3888.65 and $H\zeta$ 3889.05. The interesting feature of this spectrum is the great intensity of the sharp *He* I line which arises from the metastable 2^3S level. This line is unsymmetrically superposed over the absorption line $H\zeta$, but the displacement of the *He* I line to the violet of the center of the broad $H\zeta$ line is considerably greater than 0.4 A. Another new feature is the unsymmetrical appearance of the higher members of the Balmer series. *H*9, *H*10, and *H*11 all have sharp components superposed unsymmetrically over broad and diffuse hydrogen wings. The cores of the hydrogen lines give, on the average, a radial velocity of −43 km/sec. The *He* I lines give, on the average, −44 km/sec. There is no convincing evidence of a difference in the velocities of lines belonging to different series, so that we must probably attribute the relatively broad *He* lines 3820, 4026, 4471, etc., to the same shell which gives rise to λ 3889; and this shell must be identical with the one that is responsible for the unsymmetrical cores of the hydrogen lines. The broad wings of the latter give a radial velocity which is about 83 km/sec greater than that of the sharp cores. Hence, we must recognize in 27 Canis Majoris the existence of two layers of gas: an inner reversing layer, whose radial velocity is about +40 km/sec, and an outer shell, whose radial velocity is about −43 km/sec. It is probable that this outer expanding shell was responsible for the negative radial velocities of 27 Canis Majoris observed in former years.[1]

The weakness of *He* I 3965 is somewhat unexpected. This line has a lower metastable level, 3^1S; and we should have expected that the ratio of atoms in the two metastable levels, 3^3S and 3^1S, would be approximately constant in all shells. In all probability this is an effect produced by turbulent motions which cause the curve of growth of the shell lines in 27 Canis Majoris to be different from the curve of growth of some of the other shells.

O. Struve
Shu-Koo Kao

Yerkes and McDonald Observatories
August 4, 1948

[1] *Ap. J.*, **104**, 459, 1946.

A NOTE ON THE SPECTRUM OF HD 698 (J. A. PEARCE'S STAR OF LARGE MASS)

In 1932, J. A. Pearce published the spectrographic orbit of the binary HD 698.[1] The period as given by him is 55.904 days; the eccentricity is very small; two components were observed, the stronger having a semi-amplitude of $K_1 = 85.5$ km/sec and the fainter one of $K_2 = 215.5$ km/sec. The conventional mass function as derived from the radial velocity of the stronger component is $f(m) = 3.6\ \odot$. This value is large, but not excessively so. If the mass ratio were close to 1, the minimum masses of the two components would be of the order of fifteen times the mass of the sun. Considering that the

[1] *M.N.*, **92**, 877, 1932.

star has bright lines of hydrogen and that its spectral type is B9, this would be consistent with the masses of other, fairly luminous stars of similar spectroscopic characteristics. However, in view of the very large mass ratio of $a = 2.5$, the individual mass functions are

$$m_1 \sin^3 i = 113\odot ,$$
$$m_2 \sin^3 i = 45\odot .$$

The star is not known to be an eclipsing variable, and the values of the true masses must, therefore, be even larger than those given by the mass functions.

The spectrum was characterized by Pearce as being typical of class B9 stars of high luminosity, containing, in addition to a strong *He* spectrum, a well-developed metallic spectrum usually associated with early class A stars. He suggested that the quality of the lines justified the designation of the spectrum by means of the letter "c." This fact and the emission characteristics of $H\alpha$ and $H\beta$ suggested to him that the star is one of high intrinsic luminosity.

The secondary spectrum, according to Pearce, is faint and measurable only at times of maximum separation of the lines. He classified it as B5, containing the usual lines of *H*, *He* I, *Mg* II, *C* II, and *Ca* II.

The question of the luminosity of HD 698 is somewhat puzzling. McDonald Observatory spectrograms, which extend far into the ultraviolet, show that the Balmer absorption lines and the *He* I lines ($2^3P^\circ - n^3D$ and $2^1P^\circ - n^3D$) have wings produced by Stark broadening. These lines are completely different from the lines that are usually associated with very high luminosity. They are, in fact, visible only as far as *H* 21, and this, in accordance with a previous investigation,[2] would place HD 698 very slightly above the stars of the main sequence and certainly not among those of the supergiant branch. The absolute magnitude, as inferred from the number of *H* lines would therefore be of the order of -2 and would not be anywhere near the value of -8 on the visual scale, which it would have to be if the star obeyed the mass-luminosity relation. The *H* absorption lines are, however, weaker and therefore somewhat narrower in HD 698 than in the B9 star ϕ Her and the B8 star γ Crv, while the sharp lines of *Si* II, *Fe* II, *Ca* II, etc., are much stronger, as are also the lines of *He* I. The intensities of the lines suggest a certain resemblance to the supergiants 4 Lac (B8 I*b*) and 67 Oph (B5 I–II), but the Stark-effect wings of the *H* lines suggest a luminosity not greatly in excess of the Morgan class III, which, at about B8, would correspond to a visual absolute magnitude between -2 and -3.

The interstellar *Ca* II lines are strong, according to Pearce's and our own spectrograms. Pearce estimates that the absolute magnitude of the B9 component, as found from the intensities of these lines, is -3.1. This would be consistent with the mass function if a were only slightly larger than 1. But it would not be consistent with a mass of more than 100 $\odot$. On the other hand, there would still be a small discrepancy between even this value and the one derived from the number of Balmer absorption lines.

The question arises as to whether HD 698 departs by at least 5 mag. from the mass luminosity-curve or whether the exceptionally large mass found by Pearce may be explained as the result of some other factor. It should be emphasized that this very large mass rests entirely upon the value of a and is thus directly dependent upon Pearce's measurements of the velocity of the fainter component. If, for example, the mass ratio were $a = 1$, so that the minimum mass of each component were about 15, then, in accordance with the usual mass luminosity-curve, the absolute bolometric magnitude of each component would be approximately -4. The bolometric correction would change this to about -3 vis. The star would then not seem to be unusually massive for its spectrum.

[2] Unsöld and Struve, *Ap. J.*, **91**, 365, 1940.

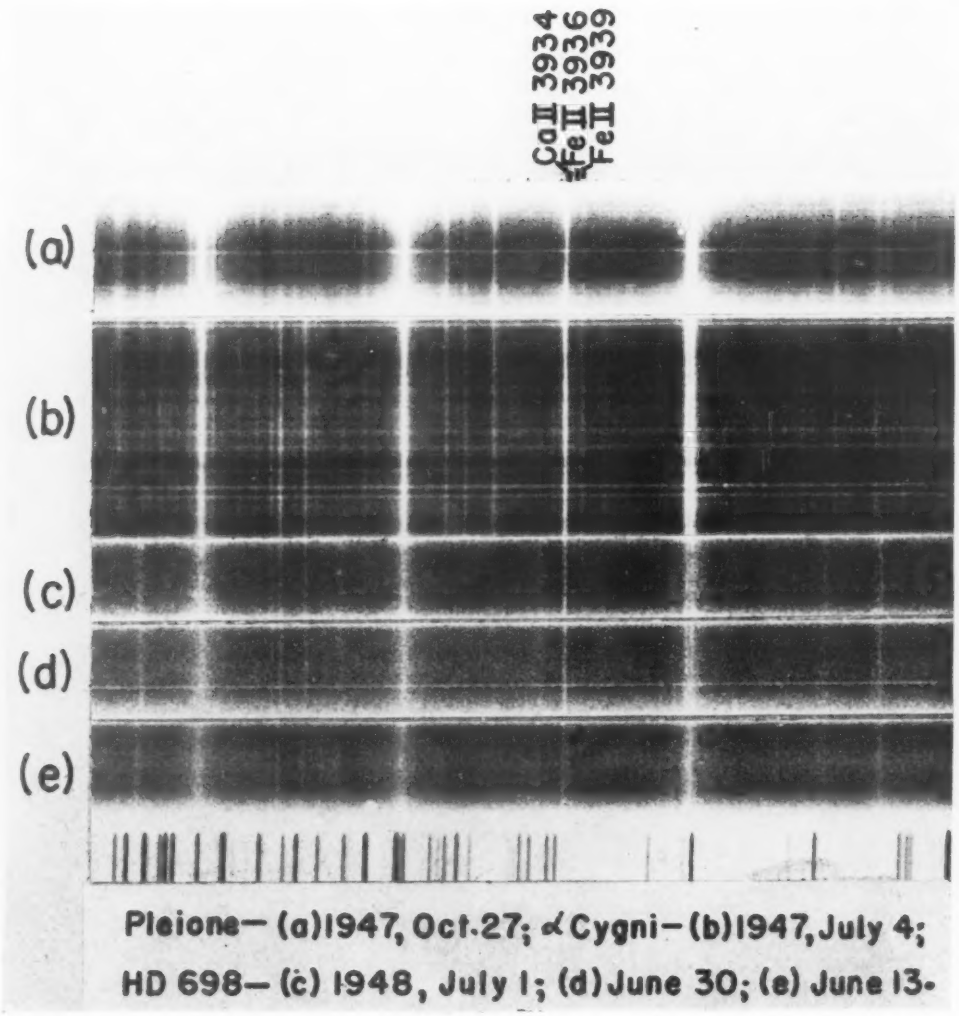
CaII 3934
FeII 3936
FeII 3939
(a)
(b)
(c)
(d)
(e)
Pleione— (a) 1947, Oct. 27; α Cygni— (b) 1947, July 4;
HD 698— (c) 1948, July 1; (d) June 30; (e) June 13.

FIG. 1

Pearce has published in his article an illustration showing the fainter component in the case of *Ca* II 3934 and *Mg* II 4481. On these two spectrograms the velocity of the stronger component was not far from its greatest value of approach. The lines are clearly shown in the reproduction.

In order to secure additional information concerning this remarkable object, we have observed HD 698 at the McDonald Observatory with the Cassegrain spectrograph attached to the 82-inch reflector. Two quartz prisms were used with a 500-mm UV camera. The dispersion was 40 A/mm at λ 3934. Our purpose was to duplicate as nearly as possible those observations which were shown in Pearce's reproduction. The results of our measurements of the radial velocity are given in Table 1. The phases were computed in accordance with Pearce's results. They agree closely with the negative branch of his velocity-curve for the stronger component. A small change in the period[3] is suggested, giving $P = 55.935$ days. When the principal component is displaced to the violet, we clearly see the interstellar component, and we also see an additional faint feature. On two plates—CQ 7017 and CQ 7024—the displacement between the strong *Ca* line of the first component and the weak feature on the red side of the interstellar component is 4.84 A (Table 2). There is also present a weak feature at a distance of about 2.4 A from the strong component of *Ca* II. The former would have given a velocity of the order of +260 km/sec, the latter one of +80 km/sec. Neither agrees with Pearce's velocity-curve for the fainter component, which is about +200 km/sec. Both of these features are undoubtedly to be identified with the *Fe* II lines of the principal component λ 3935.94 and λ 3938.24 + λ 3938.99. The latter two *Fe* II lines form a blend. Both are strong in α Cyg and in such shell stars as Pleione. They are present when the radial velocity of the principal component of HD 698 is approximately equal to the velocity of the system as a

TABLE 1

RADIAL VELOCITIES OF HD 698

Plate No. (CQ)	Date 1948	U.T.	Phase (Days)	Velocities (Km/Sec)	Plate No. (CQ)	Date 1948	U.T.	Phase (Days)	Velocities (Km/Sec)
6976	May 31	11:08	24.280	− 12.4	7055	June 25	10:05	49.236	−43.7
6994	June 5	9:22	29.206	− 74.9	7059	27	11:10	51.281	−42.7
7017	13	9:46	37.223	−108.0	7064	30	10:55	54.271	−14.4
7024	14	11:05	38.278	−112.1	7068	July 1	10:53	55.270	−11.6
7046	19	10:59	43.274	− 96.4					

TABLE 2

DIFFERENCES IN WAVE LENGTH OF TWO LINES OF *Fe* II AND *Ca* II K

CQ 7017	.....	+4.82A
7024	.....	+4.86
7059	+2.57	+5.18
7064	+2.25	+5.18
7068	+2.29	+5.14
Mean values	+2.37	+5.04
Differences of lab. meas.	+2.28	+4.88

[3] We have made no attempt to test the observations for periods of about one day.

whole (Fig. 1). The presence of these two *Fe* II lines may have caused some blending on Pearce's spectrograms, with a consequent distortion of the velocity-curve of the fainter component. They cannot be seen in his illustration.

In the case of *Mg* II 4481, the distance between the two components in Pearce's illustration corresponds to 3.9 A. Our plates do not show this region clearly, but the list of lines in α Cyg shows no suspicious blends near λ 4485, the closest being *Fe* II 4489.18 and *Ti* II 4488.32. Several lines of *Fe* I at wave lengths close to λ 4484 and λ 4485 are probably not present in this B9-type spectrum.

Additional evidence may be derived from the strong lines of *He* I and *Si* II in the ultraviolet region. In this part of the spectrum our dispersion matches that of Pearce. Our exposures were short, and the quality of the spectrograms is particularly fine. *He* I λ 3820 is perhaps the best line to examine, since, according to Pearce, *He* is present in the fainter star. The evidence is not convincing. There is certainly nothing at a separation of about 4 A from the principal component that cannot be explained in terms of *Fe* II absorption lines of the primary component.

To summarize our results we may state that in the case of *Ca* II 3934 there may be some blending of the secondary component which, according to Petrie, is about 3 mag. fainter than the primary. We have not succeeded in throwing doubt upon the second component of *Mg* II 4481, and we must leave undecided the question of a weaker component associated with *He* I 3820.

In view of the very great importance of this problem, it would be desirable to have additional information. At present we can only restate our conviction that there exists a strange discrepancy between the mass as derived with the help of Pearce's large value of α and the appearance of the spectrum which suggests a more moderate luminosity. This discrepancy, if it were real, would throw very grave doubt upon many applications of the mass-luminosity relation that are being constantly made in astrophysical research. The differences between the two *Fe* II lines and the strong component of *Ca* II 3933.66 are given in Table 2.

O. STRUVE
M. RUDKJØBING

YERKES AND MCDONALD OBSERVATORIES
July 26, 1948

ON THE SPECTRUM OF HD 193576 = V 444 CYGNI

The eclipsing system V 444 Cygni has been the object of several spectroscopic studies.[1] It seems, however, that the spectrum of this interesting binary, during the partial phases of primary minimum, shows a remarkable feature which has not been specifically mentioned in previous investigations.

The spectra reproduced in Figure 1 were taken with the 82-inch McDonald reflector,[2] around the primary minimum of the system, which occurred on May 17, 9^h25^m U.T., 1948.[3] The comparison of the absorption lines due to the O-component in spectrum *1* (see esp. λ 3889), taken outside eclipse, and in spectra *2*, *3*, and *4*, taken in the partial phases of the eclipse, shows that, with the exception of the line λ 3870, all become appreciably shallower and broader when the O star is eclipsed. The fact that these absorption lines, undoubtedly belonging to the O-component, are visible in phases quite close to totality is in qualitative agreement with the interpretation of the light-curve by

[1] Cf. O. C. Wilson, *Ap. J.*, **91**, 379, 1940, and **95**, 402, 1942; also C. S. Beals, *M.N.*, **104**, 205, 1944.

[2] I am indebted to Dr. O. Struve for securing these spectrograms.

[3] Dr. G. E. Kron has kindly made available to the writer unpublished information relating to the time of minima.

FIG. 1.—Spectra of HD 193576 = V 444 Cygni in the near ultraviolet at primary minimum. The phases were computed in days from May 17.392, 1948, as time of primary minimum.

Kopal and Mrs. Shapley,[4] according to which the O-type star is eclipsed by the semi-transparent extended envelope of the Wolf-Rayet component. Moreover, if the lines are broader and shallower than one would expect if the light of the O star were simply reduced by a constant factor independent of wave length, we may tentatively identify the mechanism of continuous opacity and line broadening in the Wolf-Rayet envelope as being scattering by free electrons in thermal motion—again in agreement with the hypothesis of Kopal and Mrs. Shapley. This identification should, of course, be quantitatively justified by analyzing the contours outside and during eclipse, on the basis of the theory of line broadening by electron scattering recently developed by the author.[5] It is planned to attempt a detailed analysis of the phenomenon in the future, with new observational material more suitable for spectrophotometric study. At the present time it is appropriate to recall that the study by O. C. Wilson[6] of the contours of $H\gamma$ in V 444 Cygni shows the line shallower and broader at phases near primary minimum.

The behavior of the absorption feature at λ 3870 is quite different from that of the other absorption lines visible in the spectrum, for it is much stronger in the phases near minimum light than outside eclipse. This feature can only be identified as *He* I 3888.65 displaced by 1500 km/sec. If this identification is correct, we have to conclude that the line has been formed in the expanding envelope of the Wolf-Rayet component. In view of the observation by Beals[7] that the line *He* I 4471 of this star was displaced by −700 km/sec, our plates were carefully inspected; but no trace of this line was found. In this connection it should be remembered that W. A. Hiltner[8] has called attention to the apparently nonperiodic appearances of displaced lines of *He* I at λ 3889 and λ 4471 in other binary systems which have a Wolf-Rayet component, as well as nonperiodic changes in the dilution of the radiation field present in the material producing such displaced lines.

GUIDO MÜNCH

YERKES OBSERVATORY
July 26, 1948

NOTE ON W URSAE MAJORIS STARS

Recent papers by Popper and Struve have called attention to two facts that appear paradoxical for binaries composed of two main-sequence stars:

a) The primaries either follow the empirical mass-luminosity relation or are somewhat too faint; but many of the secondaries are much too bright for their (small) masses.

b) In the majority of the cases investigated, the brighter and more massive star has the lower surface brightness; in some cases they are about equal in surface brightness.

A direct interpretation in terms of two independent stars appears impossible. The paradox may be removed if the energy emitted by the photosphere of the secondary does not derive mostly from the star's own interior but from the primary. This is possible if the pair has a common envelope and if strong currents convey photospheric material from one star to the other. This process is expected to take place in W UMa stars with unequal masses.[1]

If the masses differ by more than a factor of 2, the energy generation of the secondary should be negligible compared to that of the primary. The total energy output of the pair should then correspond to the mass of the primary. The observations under *a* indicate that this condition is approximately fulfilled, though no very accurate test is possible.

[4] *Ap. J.*, **104**, 160, 1946.

[5] *Ap. J.*, **108**, 116, 1948.

[6] *Ap. J.*, **95**, 402, Fig. 1, 1942.

[7] *Op. cit.*

[8] *Ap. J.*, **101**, 356, 1945, and **99**, 273, 1944.

[1] G. P. Kuiper, *Ap. J.*, **93**, 146 and 172, 1941.

A second test of the hypothesis should be a demonstration that currents extending to a plausible depth in the common envelope contain enough energy to permit undiminished photospheric radiation for at least a complete current cycle. The duration of this cycle will be comparable to the length of the orbital period ($\backsim 10^5$ sec). The heat content of the gas in circulation will be

$$U = c_v \bar{T} M_c ,$$

in which M_c is the mass of the current and $\bar{T}$ its mean temperature. From inspection of Figure 3 (*op. cit.*) it follows that the greatest depths to which the current system may extend exceeds one-tenth of the radius of the primary. Hence $\bar{T}/T_{\text{central}}$ may be as large as 0.02, or $\bar{T} = 4.10^5$ degrees; and M_c/M_{star} about 2.10^{-5}, or $M_c = 4.10^{28}$ gm. With $c_v = R/\gamma - 1$ per mole and $\gamma = 5/3$, or $8.3 \times 10^7/\frac{2}{3}\,\mu$ per gram,

$$U = 1.3\ 10^{42} \text{ ergs (upper limit)} .$$

Since $L\odot = 4.10^{33}$ ergs, the upper limit of U suffices for 3.10^8 seconds (10 years) if all the heat energy could be made available, which, of course, is never quite the case. There appears no difficulty, then, in letting it suffice, without replenishment, for about a day, as required by the hypothesis. The surface brightness of B would be expected to be nearly equal to that of A, in view of the near-equality of the surface gravities; but for large mass ratios (large turbulence) B might conceivably be brighter than A.

We conclude that currents in W UMa stars enveloping both components appear capable of producing the observed anomalies.

GERARD P. KUIPER

YERKES OBSERVATORY
July 27, 1948

A NEW BRIGHT DOUBLE STAR

The star 1 Geminorum, 5^h58^m0; $+23°16'$ (1900); 4.30 G5, was found to be double: 1948.820; 186°.8; 0".21; $\Delta m = 0.3$. At present this star is located close to Uranus, and it was found to be double in the 82-inch telescope when used for focusing purposes. It had been known to be a spectroscopic binary ($P = 9.59$ days).

A spectrum was obtained for the region 3500–6600 A with the Cassegrain spectrograph. The HD type is confirmed, but the metallic lines are shallow, indicating that the spectrum is composite. The two types are not very different and are difficult to assign with precision; they may be about G8 and G0, or K0 and F8. Evidently both visual components are giants with one (probably the later-type component) double once more.

GERARD P. KUIPER

McDONALD OBSERVATORY
November 10, 1948

REVIEWS

Atomic Energy Levels, as Derived from Analyses of Optical Spectra. By CHARLOTTE E. MOORE. Vol. I, Sec. 1. Circular 467. Washington, D.C.: National Bureau of Standards, U.S. Government Printing Office, 1948. Pp. iii+75. $0.50.

Twenty-six years ago Catalán's discovery of multiplets opened the way for the analysis of complex atomic spectra and led to a period of intense activity. The simpler spectra, consisting of a few long series, had already been deciphered. For the rest, a vast mass of observational material—wave lengths, intensities, temperature classes, Zeeman effect, etc.—was available, and the recognition of new types of observed structure and their theoretical interpretation on quantum principles ran neck and neck. Within a few years, theory, for once, reached its goal and left "no more worlds to conquer." Hund's theory, since its publication in 1927, has sufficed to account for the most intricate cases, even among the rare earths, and recognition of the effects of other types of coupling among the quantized vectors has cleared up apparently aberrant instances and peculiarities of the Zeeman patterns, e.g., among the inert gases. A rational system of classification of the energy-levels in all atomic spectra is thus established.

During the same thrilling years, the principal spectral lines—the deeper energy-levels and those which combined with them—were identified for a large number of neutral and singly ionized atoms and for some in higher states of ionization, and much more extensive analyses were published for many of them. Progress was so rapid that in 1932 Bacher and Goudsmit's extremely useful compilation, *Atomic Energy States*, contained data (often scanty) for no less than 231 spectra, representing sixty-nine elements.

Despite the diversion of interest to more exciting topics, such as nuclear physics and cosmic rays, progress in the analysis of spectra has been steady, and the number of those in which structure has been recognized is now double that in 1932. A beginning at least has been made for all the eighty-three stable or long-lived elements except three or four of the heavier rare earths. Good analyses are available for two short-lived atoms—*Rn* and *Ra*—and should be possible for most of the others as security restrictions permit.

Progress in the near future is likely to be slower. The number of workers in the field is smaller; and the most difficult cases have naturally been left to the last. The spectra of many of the heavy metals are so rich in lines that wave numbers of great accuracy are required to distinguish real frequency differences from accidental coincidences. The differences themselves are much larger and harder to pick up.

The intervals and intensities in the wide multiplets often differ seriously from the familiar elementary theory, making their recognition more difficult. For elements of high boiling-point the temperature classification of the lines, which is of such value in picking out those which arise from low levels, is seriously restricted.

An unambiguous assignment of term-designations is often impracticable without observations of the Zeeman effect with very strong fields and high dispersion. Powerful equipment, capable of providing these data, exists in a few laboratories; but an adequate study of a complex spectrum demands a great deal of work.

In certain arc spectra the critical lines which are required for the location of energy-levels which do not combine with the deep-lying states lie in the infrared. Sources capable of producing these lines with sufficient strength, as well as recorders sensitive to their wave lengths, are necessary for a complete analysis of the spectrum.

For all highly ionized atoms the principal lines are in the remote ultraviolet. The technique of observation *in vacuo*—as successfully developed by Edlén and his associates—has permitted detailed analysis of many spectra of highly stripped atoms and recognition of the principal terms of many more. For heavier atoms with more complex spectra dense groups of lines are found on the plates, which may be assigned confidently to a given degree of ionization but have not yet yielded to analysis.

Spectroscopists have for some time realized the need for a new compendium. When it was learned that Bacher and Goudsmit had no intention of revising their book, the matter was con-

sidered at a meeting of the Committee of the National Research Council on Line Spectra of the Elements held in Washington in May, 1946; and the preparation of the work was approved under the auspices of the Bureau of Standards, which undertook to provide for both the compilation and the publication.

The new work deserves the epithet "monumental." It "will finally appear in bound volumes of about 500 pages each" (not less than three of them), but successive sections are to be published in pamphlet form as they become available, for the benefit of those interested. The present section consists almost exclusively of tabular material, but the Introduction to Volume I (which the reviewer has already seen in proof) will give full details for the benefit of the general reader—that is, the ordinary physicist or astronomer.

The work is definitely a critical study. All the relevant material for each spectrum has been checked, combined, when and as necessary, and reduced to a uniform system of notation and presentation. This enormous labor is in the hands of one person—and, fortunately, of the one person who is best fitted to perform it.[1] Readers of the *Journal* are sufficiently familiar with Mrs. Sitterly's *Multiplet Table* and her work on the solar spectrum to require no further evidence. The Division of Spectroscopy at the Bureau includes Drs. Meggers and Kiess and, for the present, Dr. Catalán, so that the start of the new work could hardly be more auspicious.

With the wholehearted co-operation which is universal among spectroscopists, great quantities of unpublished data have been made available by many investigators—notably by Professor Edlén and his associates—so that the table for each spectrum represents substantially the whole state of knowledge at the date assigned.

It was decided from the start to omit hyperfine structure arising from atomic nuclei, though references are given to investigations of this. The structures observed in *H* I and *He* II, which represent ordinary term-values, are included, as are also the terms of *D* I, where the effects arising from the mass of the nucleus are exceptionally great.

By general agreement the rational arrangement in order of atomic number replaces the alphabetic order of the chemical symbols. The advantage of this is clearly shown in section 1, which includes the elements from hydrogen to fluorine. These nine elements can theoretically produce forty-five spectra. Data for all but one of these (*F* IX) appear in the pamphlet, though for the higher spectra isoelectronic with *H* I and *He* I the lists are scanty.

Matters of form and notation, upon which opinions differed at the committee meeting, were referred by questionnaire to a long list of workers actively interested in spectra from various standpoints, and the majority opinion was adopted. The results are fully described in the forthcoming Introduction to Volume I but not in the brief Foreword to section 1. Some explanatory comments may therefore be in order.

The energy-levels of each spectrum are measured upward from the ground state as zero-point, odd terms being denoted as usual by italics. When two or more systems of levels, not connected by intercombinations, are known (such as the singlets and triplets of *C* III), those of the groups which are not yet connected with the ground state are listed, for example, as $52315.0 + x$, where the number represents the best available estimate of its position and x is a correction, the same for all levels of the system, but unknown even in sign. Estimates of its probable maximum value are given in the accompanying text.

The levels are grouped into terms, tabulated in order of the lowest level in each term, and the differences of successive components given in a separate column. Levels which have not been classified into terms are introduced in their appropriate places. This policy represents a majority decision on a debatable issue and is subject to the criticism that the order of the levels is an observed fact, while their grouping into terms involves an element of judgment—often uncertain in complex spectra. The inconvenience of looking through a long list of levels (sometimes of both parities) arranged in order, to pick out those which have been assigned to a given term, was regarded by the majority as more serious.

Another column gives the electron configuration for each term, including the limit-term to which it goes in the next spectrum. No attempt has so far been made to indicate which component of the higher term is the limit for each one of the lower, probably because very few clear cases of this occur in the spectra considered. In a clearly defined case, such as *Cu* I, this information can be given with no change in the form of the tables.

[1] A witty account of some of the problems involved is found in Shenstone's review (*Journal of the Franklin Institute*, **246**, 260, 1948).

This information, though complete, leads to too cumbersome a notation for general use. For example, the line 7947.56 of *O* I represents the transition $2s^22p^3(^2D^\circ)3s\ ^3D_3 - 2s^22p^2(^2D^\circ)3p\ ^3F^\circ_4$. For practical purposes an abbreviated notation must be used. For the lighter elements where almost all terms can be assigned to series and the number of different limits is not great, the notation already used and all too briefly described in the *Revised Multiplet Table*[2] has been adopted. Here the "running electron" is given and the different limits denoted by superscripts. Thus the oxygen line in question is described as $3s'\ ^3D^\circ_3 - 3p'\ ^3F_4$, while s would indicate the lowest limit-term $^4S^\circ$ in *O* II and s″ the next higher $^2P^\circ$.

Where there are only two limits, of opposite parity, no superscript is necessary, for the parity of the limit is the same as that of the term if the running electron is s or d and opposite if it is p or f.

All these points are explained fully in the forthcoming Introduction to Volume I.

The significance of the notation used for a given spectrum is obvious upon comparing two adjacent columns of the main table and is also shown in an auxiliary table showing what terms have been identified and the configuration assigned to each which is given for all but the simplest spectra.

A special notation taking account of the peculiar coupling is to be used for the first spectra of the inert gases and those isoelectronic with them, while for the heavier elements, from scandium onward, the accepted notation with a, b, c, . . . for the low terms, z, y, x, . . . for the middle terms combining with them, and e, f, g, for the high terms will be adopted.

Spectroscopic term-values may be obtained by subtracting the tabulated value of any energy-level from that of the appropriate limit measured from the same zero-point. The difference between the ground-level of each spectrum and that of the next (as determined from the best available data) is given in the tables in heavy type (and measures the principal ionization potential for the state considered). By adding the tabular level of the limit-term in the upper spectrum and subtracting that for the given level in the lower, the term-value is obtained.

The tables give also the Zeeman *g*-values for all terms for which they are known. Observational conditions are unfavorable for the lighter elements, and the only data available in section 1 are unpublished values for eleven levels in *N* I and four in *O* I contributed by Kiess and Shortley.

Passing to specific comment on the present section, we note that the tabular level-values have been derived from observation for all spectra except *H* I and those isoelectronic with it, for which the theoretical values have been preferred. For the later spectra of this sequence and of that beginning with *He* I only a few terms are known, and the observed wave lengths are less than 50 A.

Apart from these, the analyses of the spectra are fairly complete, except for *F* I, where some lines remain unclassified, and *B* I, where only lines arising from the ground-level and with $\lambda < 2500$ A have yet been observed. The strongest lines involving the next level, $3p\ ^2P^\circ$, lie between 12,000 and 16,000 A. They should be easily observable with lead-sulphide cells—provided that a suitable source can be found—and may appear faintly in the solar spectrum.

Work on the remainder of Volume I—which is planned to go as far as vanadium—is well forward. Whether the spectra of the heavier elements can be included in two more volumes is not stated. If the admirable work which is now going on in Holland can be matched by studies of other elements in this country, there is hope that, by the time the last volume is reached, the principal terms of the first and second spectra of all the stable elements may be known.

Of the spectra not yet adequately analyzed, the most important astrophysically are the third and fourth spectra of the more abundant metals. The complete success of Edlén and Swings with *Fe* III indicates that the completion of similar studies for the others is primarily a question of manpower. Astrophysicists hope earnestly that this will be available.

The appearance of this pamphlet marks the beginning, under most favorable circumstances, of a great work of reference which will be invaluable to all serious investigations of atomic spectra. They will owe a debt of gratitude to the writer (as Mrs. Sitterly modestly describes herself, leaving "author" to denote the makers of the analyses), to the whole fellowship of spectroscopists who have contributed to its completeness, and to the director and staff members of the Bureau of Standards who have given it all possible support. Its modest price, as a government publication, is a part of the latter debt.

HENRY NORRIS RUSSELL

Princeton University Observatory

[2] *Contr. Princeton U. Obs.*, No. 20, xvii, 1945.

The Solar Spectrum, λ 6600 to λ 13495. By HAROLD D. BABCOCK and CHARLOTTE E. MOORE. Carnegie Institution of Washington Publication 579. Washington, D.C., 1947. Pp. 95. Bound, $2.00; paper covers, $1.40.

This study of the photographic infrared spectrum of the sun represents the completion of a research program extending over twenty-two years. It supersedes and extends the infrared part of the *Revision of Rowland's Table of Solar Spectrum Wave-Lengths*, which appeared in 1928. How much farther the photography and analysis of the infrared spectra has been carried in the intervening years is illustrated by the fact that the supplementary table covering the region λ 7233 to λ 10,216 in the Revised Rowland listed less than 1700 lines, of which about 250 were identified, whereas the new table tabulates more than 3800 lines in the same region, with a higher percentage of identifications. For the longer wave lengths, out to the limit of the new table at λ 13,495, the only other published solar wave lengths are a few determined by Migeotte with a grating and thermocouple.

The table is based upon plates taken at either the Mount Wilson Observatory or the Hale Solar Laboratory in Pasadena. First-order spectra taken with 21-foot concave grating spectrographs were used except for the region beyond λ 13,000, where it was necessary to work with less dispersion. Since the *Utrecht Photometric Atlas of the Solar Spectrum* consists of microphotometer tracings of similar spectrograms (but taken on Mount Wilson only), it is natural to find that practically every line detectable in the *Atlas* can be found in the table. Actually the table contains a number of faint lines not visible in the *Atlas*, and careful intercomparison of plates taken under different conditions has insured the reality of almost all of these.

The data given for each line in the main table are the wave length in International angstroms, intensity in disk and spot, identification, and excitation potentials. Since one of the most important uses of the table will be as an aid in the identification of lines in stellar spectra, many astrophysicists will wish that the number of the multiplet to which the line belongs, as given in *A Multiplet Table of Astrophysical Interest (Revised Edition)*, had been included. Presumably the authors felt that multiplet numbers might be changed in the future, but this is a risk that most users of the table would probably have been willing to accept in exchange for the greater convenience in comparing behavior of lines of the same multiplet.

The line intensities are expressed in the scale of Rowland intensities for the λλ 6229–6500 region, and the estimates have been made with the aid of scale plates. Supplementary tables are provided to allow the estimated intensities to be converted to equivalent widths, and it is shown in the discussion preceding the tables that the "intensities maintain, after correction for small systematic errors, a linear relation to the logarithms of the measured equivalent widths." It should be noted that these intensities refer to the spectrum of the central part of the sun's disk; consequently, they are more representative of the G0 dwarf than of the spectral type of integrated sunlight—G2.

Everyone who has struggled with the problem of separating stellar lines from telluric bands and lines in this region of the spectrum will appreciate the completeness with which the atmospheric lines of H_2O and O_2 have been identified in the table. The authors have been able to effect this differentiation of solar from terrestrial lines by their thoroughness in applying two methods. "In the first method, a comparison of spectra from the eastern and western equatorial limbs of the sun provides a distinction between solar lines, which show displacements due to Doppler effect, and telluric lines, which are unmodified. . . . The second method is based on the comparison of spectra of the central part of the solar disk recorded at different solar zenith distances, or at similar zenith distances on days of high and of low humidity." Supplementary tables indicate the spectral ranges within which the atmospheric bands are most troublesome in observing solar features.

Some of the more important applications of the tabular data to astrophysical problems are discussed in the introductory text and the notes to the main table. Thus it is shown that the average fraction of photospheric radiation absorbed by the solar lines throughout the region λ 6600 to λ 8090 is 1.5 per cent. Then a comparison is made of the intensities of the solar lines with those in the spectra of the stars δ Oph, β Peg, and υ Sgr, and the relation of excitation potential to the strength of lines of different elements in the solar spectrum is discussed briefly. An additional table, based upon an analysis by C. E. Moore of all available solar data, lists the sixty-six elements which have now been recognized in the solar spectrum.

Altogether, the wealth of valuable data comprised in so compact a publication is remarkable.

The authors have produced a work that is definitive in its field and indispensable to astronomical spectroscopists.

P. C. KEENAN

Perkins Observatory

Making Your Own Telescope. By ALLYN J. THOMPSON. Cambridge, Mass.: Sky Pub. Corp., 1947. Pp. xi+211. $3.50.

This book had its origin in a series of articles published in *Sky and Telescope* magazine some time ago. The description is intended as a step-by-step guide in the construction of astronomical mirrors and telescope mountings. There are also sections on adjustment of the telescope and optical principles, and a Bibliography is included. It is the opinion of a professional mirror- and lens-maker of long experience that the present book is the best available in its field.

INDEX TO VOLUME 108

INDEX TO SUBJECTS

Algol, The System of. *Olin J. Eggen* 1

η Aquilae, On the Pulsation in the Atmosphere of. *M. Schwarzschild, B. Schwarzschild, and W. S. Adams* 207

QY Aquilae, A Photored Study of the Eclipsing Variable. *Balfour S. Whitney* . . . 519

β Aurigae, A Spectroscopic Study of. *Burke Smith* 504

β Aurigae, A Study of the Orbit of. *S. L. Piotrowski* 510

ζ Aurigae during Eclipses, Notes on the Spectrum of. *Dean B. McLaughlin* 237

Be Stars Showing Bright Lines of *Fe* II, Three. *Arne Slettebak* 156

44 i Bootis, The System of. *Olin J. Eggen* 15

C_2 Molecule, An Extension of the Swan System of the. *John G. Phillips* 434

Ca II in X Cygni, Emission Lines of. *A. Van Hoof* 160

27 Canis Majoris, A Note on the Spectrum of. *O. Struve and Shu-Koo Kao* 537

Carbon, Relative Transition Probabilities of the Swan Bands of. *Robert B. King* . . . 429

Carbon Stars, The Far Violet Region in the Spectra of the Cool. *Andrew McKellar* . . 453

P Cassiopeiae, Rapid Variations in the Spectrum of. *Jesse L. Greenstein* 78

AO Cassiopeiae, The Eclipsing Variable. *Frank Bradshaw Wood* 28

CN Bands, Infrared. *G. Herzberg and J. G. Phillips* 163

Colors of Extragalactic Nebulae, Six-Color Photometry of Stars. VI. The. *Joel Stebbins and A. E. Whitford* 413

RZ Comae, V 502 Ophiuchi, RV Corvi, and BF Virginis, Spectrographic Observations of the Eclipsing Binaries. *O. Struve and L. Gratton* 497

Comet 1947n, The Spectrum of. *Jorge Sahade* 159

Comet 1947n, The Spectrum of. *P. Swings and Thornton Page* 526

Corona with Prominence, Association of. *Walter Orr Roberts* 523

RV Corvi, and BF Virginis, Spectrographic Observations of the Eclipsing Binaries RZ Comae, V 502 Ophiuchi. *O. Struve and L. Gratton* 497

X Cygni, Emission Lines of *Ca* II in. *A. Van Hoof* 160

Double Star, A New Bright. *Gerard P. Kuiper* 542

Eclipsing Binaries from Accurate Observations, Preliminary Solutions for. *Henry Norris Russell* 53

Eclipsing Binaries RZ Comae, V 502 Ophiuchi, RV Corvi, and BF Virginis, Spectrographic Observations of the. *O. Struve and L. Gratton* 497

Eclipsing Binary Systems, Remarks on the Determination of Intermediary Orbits of. *Zdeněk Kopal* 46

Eclipsing Binary UX Ursae Majoris, The Spectrum of the. *Otto Struve* 153

Eclipsing Variable QY Aquilae, A Photored Study of the. *Balfour S. Whitney* . . . 519

Eclipsing Variable AO Cassiopeiae, The. *Frank Bradshaw Wood* 28

Eclipsing Variables, Idealized Models and Rectified Light-Curves for. *Henry Norris Russell* 388

Electron Scattering on the Line Spectrum of High-Temperature Stars, The Effect of. *Guido Münch* 116

γ Equulei, The Magnetic Field of. *Horace W. Babcock* 191

Fe II, Three Be Stars Showing Bright Lines of. *Arne Slettebak* 156

HD 698 (J. A. Pearce's Star of Large Mass), A Note on the Spectrum of. *O. Struve and M. Rudkjøbing* 537

HD 45910, The Balmer Series in the Spectrum of. *Paul W. Merrill* 481

HD 193576 = V 444 Cygni, On the Spectrum of. *Guido Münch* 540

Helium Atom, The Continuous Absorption Coefficient of the. *Su-Shu Huang* 354

Interstellar Gas, On the Density Distribution and Chemical Composition of the. *Bengt Strömgren* 242

Interstellar *Hα* Emission, The Purity of. *Thornton Page* 157

Interstellar Sodium, The Distribution of. *Lyman Spitzer, Jr.* 276

Iron Spectrum in Intermediate Coupling with Application to the Solar Curve of Growth, Line Strengths in the. *Winston M. Gottschalk* 326

AR Lacertae, An Attempt To Detect Polarization in the *Ca* II Emission Lines of. *Otto Struve* 155

Line-Absorption Coefficient Due to Doppler Effect and Damping, On the. *Daniel L. Harris III* 112

α Lyrae, On the Interpretation of the Continuous Spectrum of. *Anne B. Underhill* . . 83

RR Lyrae, The Radial Velocity of. *O. Struve and A. Blaauw* 60

Molecules in Late-Type Stars, Polyatomic. *P. Swings and A. McKellar* 458

Nebulae, Six-Color Photometry of Stars. VI. The Colors of Extragalactic. *Joel Stebbins and A. E. Whitford* 413

Ni I, Relative *gf*-Values for Lines of. *Robert B. King* 87

V 502 Ophiuchi, RV Corvi, and BF Virginis, Spectrographic Observations of the Eclipsing Binaries RZ Comae. *O. Struve and L. Gratton* 497

Oxygen Bands, Fine Structure of the Red System of Atmospheric. *Harold D. Babcock and Luise Herzberg* 167

γ Pegasi, The Spectrum of. II. *Anne B. Underhill* 476

Planetary Nebula NGC 2392, The Nuclear and Nebular Spectra of the. *O. C. Wilson* . 201

Planetary Nebulae, The Absorption-Line Spectra of the Central Stars of the. *Lawrence H. Aller* 462

Polarization in the *Ca* II Emission Lines of AR Lacertae, An Attempt To Detect. *Otto Struve* 155

Reviews:

BABCOCK, HAROLD D., and CHARLOTTE E. MOORE. *The Solar Spectrum* λ *6600 to* λ *13495* (P. C. Keenan) 546

MINEUR, HENRI. *L'Espace interstellaire* (H. C. van de Hulst) 162

MOORE, CHARLOTTE E. *Atomic Energy Levels* (Henry Norris Russell) 543

MOORE, CHARLOTTE E., and HAROLD D. BABCOCK. *The Solar Spectrum* λ *6600 to* λ *13495* (P. C. Keenan) 546

THOMPSON, ALLYN J. *Making Your Own Telescope* 547

Scattering of Sunlight in a Plane-stratified Atmosphere of Uniform Composition, The Primary and Secondary. *A. Hammad* 338

Sodium, The Distribution of Interstellar. *Lyman Spitzer, Jr.* 276

Spectra of the Central Stars of the Planetary Nebulae, The Absorption-Line. *Lawrence H. Aller* 462

Spectra of the Cool Carbon Stars, The Far Violet Region in the. *Andrew McKellar* . . 453

Spectra of the Planetary Nebula NGC 2392, The Nuclear and Nebular. *O. C. Wilson* . 201

Spectroscopic Binary, Spectroscopic and Photometric Observations of a Faint Wolf-Rayet. *W. A. Hiltner* 56

Spectroscopic Observations of 90 Stars. *Alfred H. Joy and S. A. Mitchell* 234

Spectrum of ζ Aurigae during Eclipses, Notes on the. *Dean B. McLaughlin* 237

Spectrum of 27 Canis Majoris, A Note on the. *O. Struve and Shu-Koo Kao* 537

Spectrum of ρ Cassiopeiae, Rapid Variations in the. *Jesse L. Greenstein* 78

Spectrum of Comet 1947n, The. *Jorge Sahade* 159

Spectrum of Comet 1947n, The. *P. Swings and Thornton Page* 526

Spectrum of the Eclipsing Binary UX Ursae Majoris, The. *Otto Struve* 153

Spectrum of HD 698 (J. A. Pearce's Star of Large Mass), A Note on the. *O. Struve and M. Rudkjøbing* 537

Spectrum of HD 45910, The Balmer Series in the. *Paul W. Merrill* 481

Spectrum of HD 193576 = V 444 Cygni, On the. *Guido Münch* 540

Spectrum of α Lyrae, On the Interpretation of the Continuous. *Anne B. Underhill* . . 83

Spectrum of γ Pegasi, The. II. *Anne B. Underhill* 476

Spectrum of α Virginis, Peculiar Features in the. *Otto Struve* 154

Stellar Atmosphere, On the Radiative Equilibrium of a. XXIV. *S. Chandrasekhar* . . 92

Stellar Atmospheres, Superthermic Phenomena in. I. Spicules and the Solar Chromosphere. *Richard N. Thomas* 130

Stellar Atmospheres, Superthermic Phenomena in. II. Departure from Thermodynamic Equilibrium in an Idealized Chromosphere. *Richard N. Thomas* 142

Stellar Model for Red Giants of High Central Temperature, A. *Robert S. Richardson and Martin Schwarzschild* 373

Sun from Its Internal Constitution, On the Chemical Composition of the. *Marjorie Hall Harrison* 310

Sun, On the Physical and Chemical Composition of the. *Geoffrey Keller* 347

Trumpler's Stars, The Luminosities of. *Mogens Rudkjøbing* 159

UX Ursae Majoris, The Spectrum of the Eclipsing Binary. *Otto Struve* 153

W Ursae Majoris Class, Radial Velocities of Two Stars of the. *Daniel M. Popper* . . 490

W Ursae Majoris Stars, Note on. *Gerard P. Kuiper* 541

α Virginis, Peculiar Features in the Spectrum of. *Otto Struve* 154

BF Virginis, Spectrographic Observations of the Eclipsing Binaries RZ Comae, V 502 Ophiuchi, RV Corvi, and. *O. Struve and L. Gratton* 497

INDEX TO AUTHORS

ADAMS, W. S., M. SCHWARZSCHILD, and B. SCHWARZSCHILD. On the Pulsation in the Atmosphere of η Aquilae 207

ALLER, LAWRENCE H. The Absorption-Line Spectra of the Central Stars of the Planetary Nebulae 462

BABCOCK, HAROLD D., and LUISE HERZBERG. Fine Structure of the Red System of Atmospheric Oxygen Bands 167

BABCOCK, HORACE W. The Magnetic Field of γ Equulei 191

BLAAUW, A., and O. STRUVE. The Radial Velocity of RR Lyrae 60

CHANDRASEKHAR, S. On the Radiative Equilibrium of a Stellar Atmosphere. XXIV . . 92

EGGEN, OLIN J. The System of Algol 1

EGGEN, OLIN J. The System of 44 i Bootis 15

GOTTSCHALK, WINSTON M. Line Strengths in the Iron Spectrum in Intermediate Coupling with Application to the Solar Curve of Growth 326

GRATTON, L., and O. STRUVE. Spectrographic Observations of the Eclipsing Binaries RZ Comae, V 502 Ophiuchi, RV Corvi, and BF Virginis 497

GREENSTEIN, JESSE L. Rapid Variations in the Spectrum of ρ Cassiopeiae 78

HAMMAD, A. The Primary and Secondary Scattering of Sunlight in a Plane-stratified Atmosphere of Uniform Composition 338

HARRIS, DANIEL L. III. On the Line-Absorption Coefficient Due to Doppler Effect and Damping 112

HARRISON, MARJORIE HALL. On the Chemical Composition of the Sun from Its Internal Constitution 310

HERZBERG, G., and J. G. PHILLIPS. Infrared *CN* Bands 163

HERZBERG, LUISE, and HAROLD D. BABCOCK. Fine Structure of the Red System of Atmospheric Oxygen Bands 167

HILTNER, W. A. Spectroscopic and Photometric Observations of a Faint Wolf-Rayet Spectroscopic Binary 56

HUANG, SU-SHU. The Continuous Absorption Coefficient of the Helium Atom . . . 354

JOY, ALFRED H., and S. A. MITCHELL. Spectroscopic Observations of 90 Stars . . . 234

KAO, SHU-KOO, and O. STRUVE. A Note on the Spectrum of 27 Canis Majoris . . . 537

KEENAN, P. C. Review of: *The Solar Spectrum, λ 6600 to λ 13495*, Harold D. Babcock and Charlotte E. Moore 546

KELLER, GEOFFREY. On the Physical and Chemical Composition of the Sun 347

KING, ROBERT B. Relative *gf*-Values for Lines of *Ni* I 87

KING, ROBERT B. Relative Transition Probabilities of the Swan Bands of Carbon . . 429

KOPAL, ZDENĚK. Remarks on the Determination of Intermediary Orbits of Eclipsing Binary Systems 46

KUIPER, GERARD P. A New Bright Double Star 542

KUIPER, GERARD P. Note on W Ursae Majoris Stars 541

MCKELLAR, A., and P. SWINGS. Polyatomic Molecules in Late-Type Stars 458

MCKELLAR, ANDREW. The Far Violet Region in the Spectra of the Cool Carbon Stars . 453

MCLAUGHLIN, DEAN B. Notes on the Spectrum of ζ Aurigae during Eclipses. 237

MERRILL, PAUL W. The Balmer Series in the Spectrum of HD 45910 481

MITCHELL, S. A., and ALFRED H. JOY. Spectroscopic Observations of 90 Stars . . . 234

MÜNCH, GUIDO. The Effect of Electron Scattering on the Line Spectrum of High-Temperature Stars 116

MÜNCH, GUIDO. On the Spectrum of HD 193576 = V 444 Cygni 540

PAGE, THORNTON. The Purity of Interstellar *Hα* Emission 157

PAGE, THORNTON, and P. SWINGS. The Spectrum of Comet 1947n 526

PHILLIPS, J. G., and G. HERZBERG. Infrared *CN* Bands 163

PHILLIPS, JOHN G. An Extension of the Swan System of the C_2 Molecule 434

PIOTROWSKI, S. L. An Analytical Method for the Determination of the Intermediary Orbit of an Eclipsing Variable 36

PIOTROWSKI, S. L. A Study of the Orbit of β Aurigae 510

POPPER, DANIEL M. Radial Velocities of Two Stars of the W Ursae Majoris Class . . 490

RICHARDSON, ROBERT S., and MARTIN SCHWARZSCHILD. A Stellar Model for Red Giants of High Central Temperature 373

ROBERTS, WALTER ORR. Association of Corona with Prominence 523

RUDKJØBING, M., and O. STRUVE. A Note on the Spectrum of HD 698 (J. A. Pearce's Star of Large Mass) 537

RUDKJØBING, MOGENS. The Luminosities of Trumpler's Stars 159

RUSSELL, HENRY NORRIS. Idealized Models and Rectified Light-Curves for Eclipsing Variables 388

RUSSELL, HENRY NORRIS. Preliminary Solutions for Eclipsing Binaries from Accurate Observations 53

RUSSELL, HENRY NORRIS. Review of: *Atomic Energy Levels*, Charlotte E. Moore . . 543

SAHADE, JORGE. The Spectrum of Comet 1947n 159

SCHWARZSCHILD, B., M. SCHWARZSCHILD, and W. S. ADAMS. On the Pulsation in the Atmosphere of η Aquilae 207

SCHWARZSCHILD, M., B. SCHWARZSCHILD, and W. S. ADAMS. On the Pulsation in the Atmosphere of η Aquilae 207

SCHWARZSCHILD, MARTIN, and ROBERT S. RICHARDSON. A Stellar Model for Red Giants of High Central Temperature 373

SLETTEBAK, ARNE. Three Be Stars Showing Bright Lines of *Fe* II 156

SMITH, BURKE. A Spectroscopic Study of β Aurigae 504

SPITZER, LYMAN, JR. The Distribution of Interstellar Sodium 276

STEBBINS, JOEL, and A. E. WHITFORD. Six-Color Photometry of Stars. VI. The Colors of Extragalactic Nebulae 413

STRÖMGREN, BENGT. On the Density Distribution and Chemical Composition of the Interstellar Gas 242

STRUVE, O., and A. BLAAUW. The Radial Velocity of RR Lyrae 60

STRUVE, O., and L. GRATTON. Spectrographic Observations of the Eclipsing Binaries RZ Comae, V 502 Ophiuchi, RV Corvi, and BF Virginis 497

STRUVE, O., and SHU-KOO KAO. A Note on the Spectrum of 27 Canis Majoris . . . 537

STRUVE, O., and M. RUDKJØBING. A Note on the Spectrum of HD 698 (J. A. Pearce's Star of Large Mass) 537

STRUVE, OTTO. An Attempt To Detect Polarization in the *Ca* II Emission Lines of AR Lacertae 155

STRUVE, OTTO. Peculiar Features in the Spectrum of α Virginis 154

STRUVE, OTTO. The Spectrum of the Eclipsing Binary UX Ursae Majoris 153

SWINGS, P., and A. MCKELLAR. Polyatomic Molecules in Late-Type Stars 458

SWINGS, P., and THORNTON PAGE. The Spectrum of Comet 1947n 526

THOMAS, RICHARD N. Superthermic Phenomena in Stellar Atmospheres. I. Spicules and the Solar Chromosphere 130

THOMAS, RICHARD N. Superthermic Phenomena in Stellar Atmospheres. II. Departure from Thermodynamic Equilibrium in an Idealized Chromosphere 142

UNDERHILL, ANNE B. On the Interpretation of the Continuous Spectrum of α Lyrae . . 83

UNDERHILL, ANNE B. The Spectrum of γ Pegasi. II 476

VAN DE HULST, H. C. Review of: *L'Espace interstellaire*, Henri Mineur 162

VAN HOOF, A. Emission Lines of *Ca* II in X Cygni 160

WHITFORD, A. E., and JOEL STEBBINS. Six-Color Photometry of Stars. VI. The Colors of Extragalactic Nebulae 413

WHITNEY, BALFOUR S. A Photored Study of the Eclipsing Variable QY Aquilae . . . 519

WILSON, O. C. The Nuclear and Nebular Spectra of the Planetary Nebula NGC 2392 . 201

WOOD, FRANK BRADSHAW. The Eclipsing Variable AO Cassiopeiae 28

POPULAR ASTRONOMY

A magazine now in its fifty-sixth year, devoted to the elementary aspects of Astronomy and allied sciences.

Published monthly, except July and September.

Yearly subscription rates: Domestic $4.00; Canadian $4.25; Foreign $4.50.

Address

POPULAR ASTRONOMY
CARLETON COLLEGE
NORTHFIELD, MINNESOTA, U.S.A.

Astronomical

LANTERN SLIDES

Since 1903, the Yerkes Observatory of the University of Chicago has been reproducing in lantern slides, transparencies, and prints the original astronomical photographs made at Williams Bay.

The lantern slides are uniformly 4×3¼ inches in size. The frequent call for small sets of slides for school and lecture purposes has led to the preparation of a list of 100 representative slides, a catalogue of which may be obtained upon request to the University of Chicago Press, 5750 Ellis Avenue, Chicago.

Prints as well as slides can be furnished, and for many subjects window transparencies are also supplied.

For catalogue and further information write

The University of Chicago Press
5750 Ellis Avenue, Chicago, Ill.

SCIENCE AT WAR

By **J. G. CROWTHER**
Chairman
Association of British Science Writers
and
R. WHIDDINGTON
Head, Dept. of Physics, University of Leeds

The first detailed account of science's contribution to the war effort, based on the official archives and documents assembled by the Scientific Advisory Committee to the British Cabinet. Because of the close and intimate collaboration between the American and British forces during World War II, this volume is of fundamental interest to the American scientist, as well as to the intelligent layman interested in science.

Although the use of science as an aid to war is a perversion from its proper purposes, we may find reassurance in recognizing that much of the discovery and invention which came to hand in response to the recent war demands will find immediate and beneficent uses in peace.

Among the basic topics dealt with in this book are: Radar, The Atomic Bomb, Operational Research, Science and the Sea, Submarine Detecting, Under Sea Observations, The Magnetic Mine, Underwater Explosions, War Diving, etc.

Illustrating the subject matter are almost one hundred graphs, drawings and photographs. $6.00

At Your Bookstore, or Use Order Coupon:

PHILOSOPHICAL LIBRARY, *Publishers*
15 E. 40th St., Dept. 269, New York 16, N.Y.

Please send me.....copy(ies) of SCIENCE AT WAR, @ $6.00 per copy. Enclosed is $.....

NAME.....

ADDRESS.....

(*Expedite shipment by enclosing remittance.*)

THE OBSERVATORY

FOUNDED 1877

* * *

A Magazine presenting current developments in Astronomy by means of Articles, Correspondence, Notes on discoveries and Reviews of important astronomical books. The papers read at the Meetings (Astronomical & Geophysical) of the Royal Astronomical Society and the discussions which follow are also fully reported.

* * *

Annual subscription for 6 issues, post free, 15/–
should be sent to

The Editors, ROYAL OBSERVATORY
Greenwich, London S.E., 10

What Are COSMIC RAYS?

"The best that has yet appeared for explaining cosmic rays to the general reader and to the physicist who wants a quick view of what has been done in this new field of specialization," says Professor ARTHUR H. COMPTON.

This book answers the question: "What are cosmic rays?" and traces the exciting adventures of their investigators from the discovery of cosmic rays to the latest stratospheric balloon flights.

$2.75

By **PIERRE AUGER**
noted French physicist, discoverer of Auger showers and Auger effect in X-rays

TRANSLATED BY
MAURICE M. SHAPIRO

☆

UNIVERSITY OF CHICAGO PRESS

ASTROPHYSICAL JOURNAL

VOL. 109, 1949
NOS 1-3
VOL. 110, 1949
NOS 1-3

PUB. 134

UNIVERSITY MICROFILMS
ANN ARBOR, MICHIGAN. 1950

THIS PUBLICATION IS REPRODUCED BY AGREEMENT WITH THE COPYRIGHT OWNER. EXTENSIVE DUPLICATION OR RESALE WITHOUT PERMISSION IS PROHIBITED.